frontiers | Research Topics

Understanding the role of the autonomic nervous system in health and disease

Edited by
Vitor Engracia Valenti, Moacir Fernandes Godoy
and Luiz Carlos Marques Vanderlei

Published in
Frontiers in Neuroscience
Frontiers in Physiology

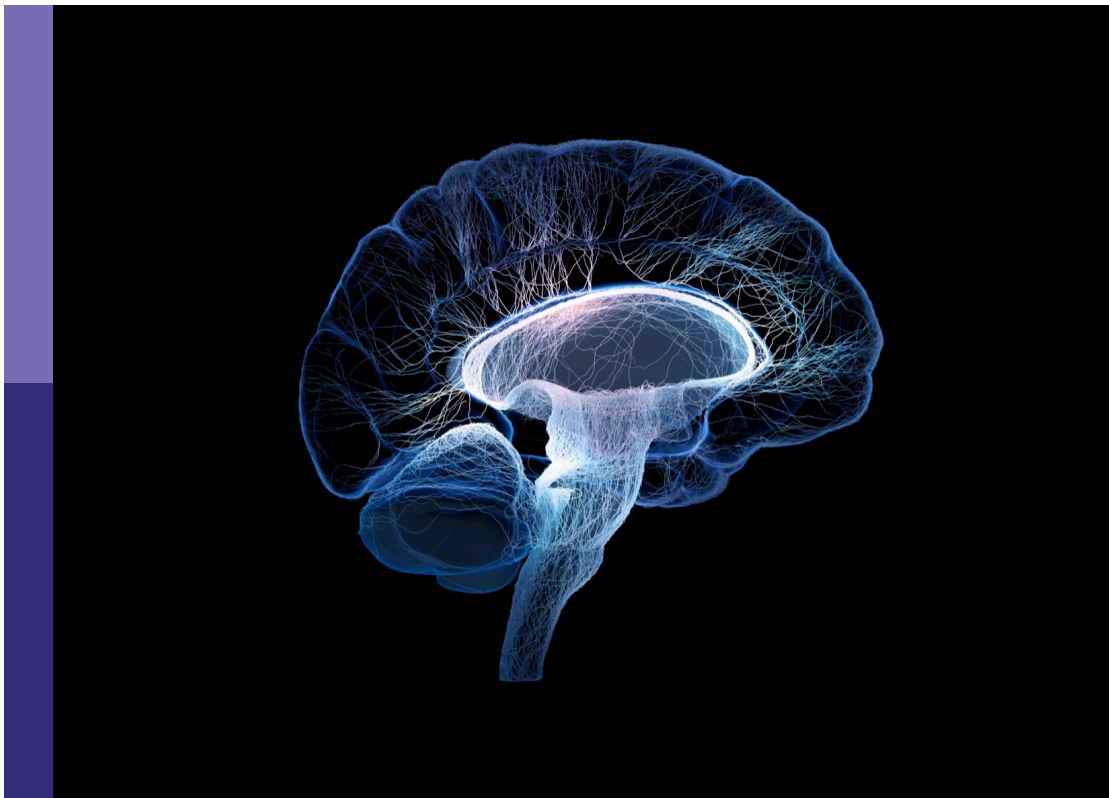

ISSN 1664-8714
ISBN 978-2-8325-5114-1
DOI 10.3389/978-2-8325-5114-1

About Frontiers

Frontiers is more than just an open access publisher of scholarly articles: it is a pioneering approach to the world of academia, radically improving the way scholarly research is managed. The grand vision of Frontiers is a world where all people have an equal opportunity to seek, share and generate knowledge. Frontiers provides immediate and permanent online open access to all its publications, but this alone is not enough to realize our grand goals.

Frontiers journal series

The Frontiers journal series is a multi-tier and interdisciplinary set of open-access, online journals, promising a paradigm shift from the current review, selection and dissemination processes in academic publishing. All Frontiers journals are driven by researchers for researchers; therefore, they constitute a service to the scholarly community. At the same time, the *Frontiers journal series* operates on a revolutionary invention, the tiered publishing system, initially addressing specific communities of scholars, and gradually climbing up to broader public understanding, thus serving the interests of the lay society, too.

Dedication to quality

Each Frontiers article is a landmark of the highest quality, thanks to genuinely collaborative interactions between authors and review editors, who include some of the world's best academicians. Research must be certified by peers before entering a stream of knowledge that may eventually reach the public - and shape society; therefore, Frontiers only applies the most rigorous and unbiased reviews. Frontiers revolutionizes research publishing by freely delivering the most outstanding research, evaluated with no bias from both the academic and social point of view. By applying the most advanced information technologies, Frontiers is catapulting scholarly publishing into a new generation.

What are Frontiers Research Topics?

Frontiers Research Topics are very popular trademarks of the *Frontiers journals series*: they are collections of at least ten articles, all centered on a particular subject. With their unique mix of varied contributions from Original Research to Review Articles, Frontiers Research Topics unify the most influential researchers, the latest key findings and historical advances in a hot research area.

Find out more on how to host your own Frontiers Research Topic or contribute to one as an author by contacting the Frontiers editorial office: frontiersin.org/about/contact

Understanding the role of the autonomic nervous system in health and disease

Topic editors

Vitor Engracia Valenti — São Paulo State University, Brazil

Moacir Fernandes Godoy — Faculdade de Medicina de São José do Rio Preto, Brazil

Luiz Carlos Marques Vanderlei — São Paulo State University, Brazil

Citation

Valenti, V. E., Godoy, M. F., Vanderlei, L. C. M., eds. (2024). *Understanding the role of the autonomic nervous system in health and disease*. Lausanne: Frontiers Media SA. doi: 10.3389/978-2-8325-5114-1

Table of contents

frontiers | Frontiers in Neuroscience

TYPE Editorial
PUBLISHED 26 June 2024
DOI 10.3389/fnins.2024.1446832

OPEN ACCESS

EDITED AND REVIEWED BY
Joel C. Bornstein,
The University of Melbourne, Australia

*CORRESPONDENCE
Vitor E. Valenti
✉ vitor.valenti@unesp.br

RECEIVED 10 June 2024
ACCEPTED 18 June 2024
PUBLISHED 26 June 2024

CITATION
Valenti VE, Vanderlei LCM and Godoy MF (2024) Editorial: Understanding the role of the autonomic nervous system in health and disease. *Front. Neurosci.* 18:1446832. doi: 10.3389/fnins.2024.1446832

Editorial: Understanding the role of the autonomic nervous system in health and disease

Vitor E. Valenti[1]*, Luiz Carlos M. Vanderlei[2] and Moacir F. Godoy[3]

[1]Autonomic Nervous System Center, School of Philosophy and Sciences, São Paulo State University, Marília, Brazil, [2]School of Technology and Sciences, São Paulo State University (Unesp), Presidente Prudente, Brazil, [3]Transdisciplinary Nucleus for the Study of Chaos and Complexity, NUTECC, São José do Rio Preto Medical School, FAMERP, São José do Rio Preto, Brazil

KEYWORDS

autonomic nervous system, heart rate variability, sympathetic nervous activity, parasympathetic, vagus nerve

Editorial on the Research Topic
Understanding the role of the autonomic nervous system in health and disease

Human life depends on the autonomic nervous system (ANS). This is because the ANS controls involuntary body functions, such as blood pressure, gastrointestinal function, heart rate and bladder activity. The ANS is composed of a network which controls physiological systems through combined inputs from the internal and external environment to keep human body homeostasis. The central autonomic nervous network, the sympathetic and parasympathetic nervous systems regulates body functions (Wehrwein et al., 2016). Previous studies have reported the involvement of the ANS in human disorders (Affoo et al., 2012; Figueiredo et al., 2020; Kłysz et al., 2021) and also in good physical condition (Shivkumar and Ardell, 2016; Speer et al., 2024). Considering its importance for the human organism, this Research Topic grouped 86 researchers, 13 studies and provides recent data related to the role of the ANS in disease and health.

One paper conducted by Laurino et al., performed a crossover clinical trial to investigate the effects of hydration on heart rate variability (HRV) during and after aerobic exercise in patients with coronary artery disease. HRV is a non-invasive method that estimates autonomic function through fluctuations of heart interbeat intervals. Reduced HRV is usually related to abnormal adaptation of the ANS, indicating physiological malfunction, while increased HRV indicates good adaptation and is associated with healthy individuals with appropriate autonomic function (Sassi et al., 2015). The authors evaluated 38 men who performed two moderate-intensity aerobic exercise protocols, control and hydration protocols. As main findings, it was demonstrated that intake of eight portions of mineral water in a total amount proportional to the loss, administered during and after physical exercise was able to accelerate the recovery of non-linear HRV and that the fluid lost volume during exercise did not impact non-linear HRV.

Kirby et al. explored traditional time and frequency domain indices of HRV during autonomic dysreflexia after spinal cord injury. This experimental study was conducted in male Sprague Dawley rats submitted to spinal cord surgery

to induce injury through a dorsal laminectomy at the T3 level. The results added integrated skin nerve activity as a biomarker that may be used for early detection and monitoring of autonomic dysreflexia.

HRV was also analyzed by Cheng W. et al. in 60 male inpatients with type 2 diabetes mellitus (T2DM) in sleep stages. The key questions asked whether HRV is more associated with metabolic function when sleep than during awake or the entire 24-h and if HRV changes during sleep cycles, inducing alterations in its interactivity with the metabolic system. Their data evidenced that metabolic function was associated with sleep quality, HRV differed between sleep and awake, indicating stronger and distinct interaction with metabolic function compared to 24-h and that HRV and its association with metabolic clinical indicators is altered during sleep cycles.

The heart rate rhythm autonomic control was investigated by Wu et al., who evaluated the acute effects of thoracic radiotherapy on HRV in 58 thoracic cancer patients. Participants were excluded in the presence of a pacemaker, those who previously received thoracic radiotherapy, patients with incomplete thoracic radiotherapy, and poor electrocardiogram quality. The main findings evidenced that thoracic radiotherapy significantly influenced the standard deviation of all normal RR intervals (SDNN), the root-mean square of differences between adjacent normal RR intervals (RMSSD), low frequency (LF), high frequency (HF) and total power HRV indices, suggesting reduced parasympathetic cardiac control and increased sympathetic cardiac regulation following this intervention.

The acute effects of an osteopathic technique were evaluated by Besson et al., who examined occipito-mastoid suture normalization intervention. The study examined 34 apparently healthy volunteers between 18 and 75 years old submitted to this passive and smooth osteopathic technique. The intervention led to higher RMSSD values compared to sham conditions, indicating increased parasympathetic cardiac control. However, the authors pointed to the short intervention period (10 min) applied in this study as a significant limitation, since conventional osteopathic technique interventions usually spend much more than 10 min.

The Poincaré plot was hypothesized by Yuan et al. as an index to predict the curative effect of metoprolol in pediatric postural orthostatic tachycardia syndrome. Based on their results, it was suggested that the longitudinal and transverse axis of the Poincaré plot can be used as an intuitive approach to anticipate the efficiency of metoprolol for postural orthostatic tachycardia syndrome. Nevertheless, the small sample size, the relatively basic graphic measurement methods and the single-center retrospective design were raised as relevant limitations.

In addition, Huang et al. examined traditional time and domain HRV indices in order to verify the effects of vagal nerve stimulation on esophageal motility and pharyngeal symptoms in patients with laryngopharyngeal reflux disease, which is a condition identified by stomach contents ejection into the larynx and pharynx, inducing inflammation in the throat (Mishra et al., 2020). As main results, it was found that acute transcutaneous auricular vagus nerve stimulation improved mental wellbeing and pharyngeal discomfort and increased upper esophageal sphincter pressures.

With this in mind, Wang et al. also investigated vagal nerve stimulation. The study evaluated the impact of transcutaneous auricular vagus nerve stimulation combined with task-oriented training on upper limbs activity in 20 subacute stroke patients compared to 20 participants in the sham group. The authors' data showed a positive effect of this intervention and suggested the modulation of cortical excitability as an explanation, since it may facilitate motor activity remodeling.

ANS function was investigated as a potential method for health complication prediction by Sharifi-Heris et al. The authors performed a prospective longitudinal observational study to analyze HRV during low risk pregnancy in healthy pregnant participants. The authors applied a hierarchical linear regression/mixed-effects model to understand the interaction between time as the independent variable and the root-mean square of differences between adjacent normal RR intervals (RMSSD) as the dependent variable to find out if the time could influence and estimate HRV. In conclusion, the study evidenced a distinction between healthy and complicated gestation according to the average HRV.

An interesting investigation of three cases published by Li et al. suggested a new treatment for restless leg syndrome. The study included a 47-years old male patient, a 57-years old male patient and a 24-years old female patient. Stellate ganglion block was proposed as a reliable method for treatment of symptoms, however, based on the small sample size, the authors recommended randomized controlled trials to provide further evidence regarding the effectiveness and safety.

The association between ANS and cognitive tasks was explored by Cheng S. et al. The study evaluated changes in ECG during distinct physical and cognitive loads during dynamic tasks in 35 healthy male volunteers. The n-back working memory task program was used as a cognitive load task and isotonic contraction of the left upper limb was used as a physical load procedure. Their main data pointed to the role of HRV during mental workload.

Another procedure explored in this Research Topic was acupuncture. Liu et al. tried to design a pain model by using HRV to comprehend the real-time changes in the ANS during acupuncture analgesia. This randomized, controlled, single-blind design evaluated 61 volunteers who received acupuncture intervention, 31 participants allocated to the sham group and 30 subjects in the model group. Interestingly, the authors found that acupuncture was related to increased heart rate vagal control. Moreover, the "needle sensation" presented positive correlation with both sympathetic and vagal heart rate regulation.

Finally, COVID was the focus of the study conducted by Barnden et al. The authors performed a pilot study to evaluate brain connectivity in post-COVID during cognitive tasks. The abovementioned cross-sectional investigation examined 10 long-COVID patients and 13 healthy control volunteers, which were submitted to functional MRI, cardiac and respiratory monitoring and the Stroop task. The data pointed to a number of differences in long COVID brain connectivity compared to healthy control participants. The differences related to the brainstem reticular activation system suggest that this structure may be crucial to long COVID sequel.

In summary, the articles published in this Research Topic present further elements related to HRV, hydration, sleep cycles, brain connectivity, metabolic function, cognitive function, long COVID, autonomic dysreflexia, spinal cord injury, restless leg syndrome, cognitive tasks and acupuncture. The data reported by this Research Topic provides valid evidence that adds relevant information to better understand the role of the ANS in disease and health.

Author contributions

VV: Conceptualization, Data curation, Formal analysis, Investigation, Project administration, Resources, Supervision, Validation, Visualization, Writing – original draft, Writing – review & editing. LV: Conceptualization, Data curation, Formal analysis, Investigation, Visualization, Writing – original draft, Writing – review & editing. MG: Conceptualization, Data curation, Formal analysis, Investigation, Validation, Visualization, Writing – original draft, Writing – review & editing.

Funding

The author(s) declare that financial support was received for the research, authorship, and/or publication of this article. VV, LV, and MG receive financial support from the National Council for Scientific and Technological Development, an entity linked to the Ministry of Science, Technology, Innovations and Communications from Brazil.

Conflict of interest

The authors declare that the research was conducted in the absence of any commercial or financial relationships that could be construed as a potential conflict of interest.

The author(s) declared that they were an editorial board member of Frontiers, at the time of submission. This had no impact on the peer review process and the final decision.

Publisher's note

References

Affoo, R. H., Foley, N., Rosenbek, J., Kevin Shoemaker, J., and Martin, R. E. (2012). Swallowing dysfunction and autonomic nervous system dysfunction in Alzheimer's disease: a scoping review of the evidence. *J. Am. Geriatr. Soc.* 61, 2203–2213. doi: 10.1111/jgs.12553

Figueiredo, T. G., de Souza, H. C. M., Neves, V. R., do Rêgo Barros, A. E. V., Dornelas de Andrade, A. F., and Brandão, D. C. (2020). Effects of physical exercise on the autonomic nervous system in patients with coronary artery disease: a systematic review. *Expert Rev. Cardiovasc. Ther.* 18, 749–759. doi: 10.1080/14779072.2020.1813568

Kłysz, B., Bembenek, J., Skowrońska, M., Członkowska, A., and Kurkowska-Jastrzebska, I. (2021). Autonomic nervous system dysfunction in Wilson's disease - a systematic literature review. *Auton. Neurosci.* 236:102890. doi: 10.1016/j.autneu.2021.102890

Mishra, P., Agrawal, D., and Artham, P. (2020). Screening test for LPRD: history versus video laryngoscopy. *Indian J. Otolaryngol. Head Neck Surg.* 72, 422–427. doi: 10.1007/s12070-020-01828-7

Sassi, R., Cerutti, S., Lombardi, F., Malik, M., Huikuri, H. V., Peng, C. K., et al. (2015). Advances in heart rate variability signal analysis: joint position statement by the e-Cardiology ESC Working Group and the European Heart Rhythm Association co-endorsed by the Asia Pacific Heart Rhythm Society. *Europace* 17, 1341–1353. doi: 10.1093/europace/euv015

Shivkumar, K., and Ardell, J. L. (2016). Cardiac autonomic control in health and disease. *J. Physiol.* 594, 3851–3852. doi: 10.1113/JP272580

Speer, K. E., Naumovski, N., and McKune, A. J. (2024). Heart rate variability to track autonomic nervous system health in young children: effects of physical activity and cardiometabolic risk factors. *Physiol. Behav.* 281:114576. doi: 10.1016/j.physbeh.2024.114576

Wehrwein, E. A., Orer, H. S., and Barman, S. M. (2016). Overview of the anatomy, physiology, and pharmacology of the autonomic nervous system. *Compr. Physiol.* 6, 1239–1278. doi: 10.1002/cphy.c150037

frontiers | Frontiers in Physiology

TYPE Original Research
PUBLISHED 14 April 2023
DOI 10.3389/fphys.2023.1157270

OPEN ACCESS

EDITED BY
Vitor Engracia Valenti,
São Paulo State University, Brazil

REVIEWED BY
Alberto Porta,
University of Milan, Italy
Szymon Siecinski,
Silesian University of Technology, Poland

*CORRESPONDENCE
Zhimin Ma,
mazhimin01@sina.com
Xingran Cui,
cuixr@seu.edu.cn

†These authors have contributed equally to this work and share first authorship

SPECIALTY SECTION
This article was submitted to Autonomic Neuroscience, a section of the journal Frontiers in Physiology

RECEIVED 02 February 2023
ACCEPTED 24 March 2023
PUBLISHED 14 April 2023

CITATION
Cheng W, Chen H, Tian L, Ma Z and Cui X (2023), Heart rate variability in different sleep stages is associated with metabolic function and glycemic control in type 2 diabetes mellitus.
Front. Physiol. 14:1157270.
doi: 10.3389/fphys.2023.1157270

Heart rate variability in different sleep stages is associated with metabolic function and glycemic control in type 2 diabetes mellitus

Wenquan Cheng[1†], Hongsen Chen[1†], Leirong Tian[1], Zhimin Ma[2*] and Xingran Cui[1,3*]

[1]State Key Laboratory of Bioelectronics, School of Biological Science and Medical Engineering, Southeast University, Nanjing, China, [2]Endocrinology Department, Suzhou Science and Technology Town Hospital, Suzhou, China, [3]Institute of Medical Devices (Suzhou), Southeast University, Suzhou, China

Introduction: Autonomic nervous system (ANS) plays an important role in the exchange of metabolic information between organs and regulation on peripheral metabolism with obvious circadian rhythm in a healthy state. Sleep, a vital brain phenomenon, significantly affects both ANS and metabolic function.

Objectives: This study investigated the relationships among sleep, ANS and metabolic function in type 2 diabetes mellitus (T2DM), to support the evaluation of ANS function through heart rate variability (HRV) metrics, and the determination of the correlated underlying autonomic pathways, and help optimize the early prevention, post-diagnosis and management of T2DM and its complications.

Materials and methods: A total of 64 volunteered inpatients with T2DM took part in this study. 24-h electrocardiogram (ECG), clinical indicators of metabolic function, sleep quality and sleep staging results of T2DM patients were monitored.

Results: The associations between sleep quality, 24-h/awake/sleep/sleep staging HRV and clinical indicators of metabolic function were analyzed. Significant correlations were found between sleep quality and metabolic function ($|r| = 0.386 \pm 0.062$, $p < 0.05$); HRV derived ANS function showed strengthened correlations with metabolic function during sleep period ($|r| = 0.474 \pm 0.100$, $p < 0.05$); HRV metrics during sleep stages coupled more tightly with clinical indicators of metabolic function [in unstable sleep: $|r| = 0.453 \pm 0.095$, $p < 0.05$; in stable sleep: $|r| = 0.463 \pm 0.100$, $p < 0.05$; in rapid eye movement (REM) sleep: $|r| = 0.453 \pm 0.082$, $p < 0.05$], and showed significant associations with glycemic control in non-linear analysis [fasting blood glucose within 24 h of admission (admission FBG), $|r| = 0.420 \pm 0.064$, $p < 0.05$; glycated hemoglobin (HbA1c), $|r| = 0.417 \pm 0.016$, $p < 0.05$].

Conclusions: HRV metrics during sleep period play more distinct role than during awake period in investigating ANS dysfunction and metabolism in T2DM patients, and sleep rhythm based HRV analysis should perform better in ANS and metabolic function assessment, especially for glycemic control in non-linear analysis among T2DM patients.

KEYWORDS

T2DM, heart rate variability (HRV), sleep, autonomic nervous system (ANS), metabolic function, nonlinear analysis, glycemic control

1 Introduction

Type 2 diabetes mellitus (T2DM) is a chronic hyperglycemia that causes physiological dysfunction and failure of various organs. Autonomic neuropathy is one of the most common complications of diabetes mellitus, which seriously affects the patients' life quality and brings about significant morbidity and mortality (Maser et al., 2003; Vinik et al., 2003; Ziegler et al., 2008). The dysfunction of autonomic nervous system (ANS) usually manifests first in vagal nerve (the longest parasympathetic nerve in the body, responsible for nearly three-quarters of parasympathetic activity), and damage to vagal nerve leads to resting tachycardia and an overall decrease in parasympathetic tone (Balcıoğlu and Müderrisoğlu, 2015).

Dysfunction of ANS, caused by T2DM, happens in any part of ANS from early stages of diabetes, which damages the cardiovascular, gastrointestinal, genitourinary and neurovascular systems (Pfeifer et al., 1982; Singh et al., 2000; Goit et al., 2012). The function of healthy ANS has obvious circadian rhythm (Cui et al., 2020), and the dysfunction of ANS can result in the loss of circadian rhythm to varying degrees (Liu et al., 2020). Consequently, diabetes is often followed by sleep disorders (Barone and Menna-Barreto, 2011). Meanwhile, sleep disorders accelerate the development of T2DM by worsening the metabolic control, which forms into a vicious spiral (Barone and Menna-Barreto, 2011). Researchers have found that poor sleep quality (Martyn-Nemeth et al., 2018), insufficient or excessive sleep duration, changes of sleep structure (Koren et al., 2011), decreasing sleep efficiency (Hur et al., 2020), increasing OSA severity (Kent et al., 2014), etc. are associated with poor diabetic control. Also, sleep disorders are strongly related to ANS function of T2DM patients (Jordan et al., 2014). The activation of the sympathetic nervous system (SNS) and the unbalance of ANS in patients with T2DM could be mediated through sleep impairments, including nocturnal breathing disturbances (Punjabi and Polotsky, 2005; López-Cano et al., 2019) and sleep curtailment (Leproult et al., 1997; Spiegel et al., 1999).

Heart rate variability (HRV) is considered to be an effective measure of heart-brain interaction and tension of ANS (Montano et al., 2009), and is widely used as a standard method for assessing autonomic function. Studies have found that T2DM patients' HRV differs significantly from normal people in time-domain, frequency-domain and non-linear analysis (Barone and Menna-Barreto, 2011; Faust et al., 2012; Martyn-Nemeth et al., 2018; Liu et al., 2020). Therefore, HRV analysis is considered an effective, non-invasive auxiliary detection method for T2DM patients' autonomic dysfunction. Cardiologists tend to analyze 24-h HRV, whereas internists tend to detect whether HRV is abnormal in different physiological states, known as Ewing test (Gerritsen et al., 2001).

Despite the full utilization in clinical fields, HRV analysis in current researches mainly focused on linear analysis of 24-h or 5–15 min electrocardiogram (ECG) collected in different physiological states, which fails to effectively extract the information in long-term signals and neglects the space-time complexity and fractal properties of heart rate time series. Meanwhile, it was a general problem that HRV metrics were accepted as measures of autonomic function without examination of the underlying physiological patterns (Stein and Pu, 2012) and autonomic pathways. Hence, controversial research results were presented. For example, researchers have found that low-frequency component of HRV was not predominantly influenced by SNS, but vagal nerve system (Reyes del Paso et al., 2013), and reflected multiple sources of variability (Martelli et al., 2014), which also challenged the usefulness of the ratio of low-frequency component to high-frequency component (LF/HF); higher HRV were related to disturbed sleep, such as in sleep disorders as negative feature (Stein and Pu, 2012); imparity of HRV metrics reflecting parasympathetic nervous system (PNS), such as high-frequency power (HF) and root mean square of successive of RR interval differences (RMSSD), occurred during different sleep stages (Glos et al., 2014; Zhang et al., 2020).

Therefore, based on the complex associations among sleep, ANS and T2DM, we monitored 24-h ECG, clinical metabolic indicators, sleep quality as well as sleep staging results of T2DM patients. Our objective was to help optimize the early prevention, post-diagnosis and management of T2DM and its complications. Our hypothesis included: 1) HRV derived ANS function is more associated with T2DM patients' metabolic function during sleep than during awake or the whole 24-h; 2) ANS function alters during sleep cycles, leading to changes on its interaction with metabolic system, thus we analyzed interaction between HRV derived ANS function with metabolic function in each sleep stage; finally, 3) non-linear HRV analysis during sleep cycles may discover more features of ANS function than conventionally used linear HRV analysis, leading to more extensive association with metabolic function and glycemic control.

2 Materials and methods

2.1 Patients

The study was conducted form July 2019 to January 2021. A total of 64 volunteered inpatients with T2DM from Suzhou Science & Technology Town Hospital took part in this study. Exclusion criteria were: type 1 diabetes mellitus, history of stroke, subacute myocardial infarction, kidney or liver transplant, other systemic disorders, current recreational drug or alcohol abuse and morbid obesity (body mass index >40). Because of the small number of female inpatients in the study (only 4), and considering that women in the same age group may be affected metabolically by perimenopausal syndrome, and decreasing the bias brought by sex (Nunan et al., 2010), data from only 60 male inpatients were included in the follow-up studies. This study was approved by the Institutional Review Board of Suzhou Science & Technology Town Hospital (No. IRB2019045). Prior to the study, all subjects were informed of the experimental protocol and precautions, and signed the written informed consent. Demographic characteristics of the subjects are demonstrated in Table 1. The Strengthening the Reporting of Observational Studies in Epidemiology (STROBE) guidelines for cross-sectional studies were followed for study reporting (Cuschieri, 2019).

2.2 Clinical indicators of metabolic function

During hospitalization, subjects underwent clinical examinations to obtain their metabolic function and assess their

TABLE 1 Characteristics of the study cohort. Data are presented as mean ± standard deviation (SD) if the variable is normally distributed, otherwise presented as median (p25, p75).

Parameters (Unit)	Data	Sample size
Demographics		
Age (years)	50 ± 16	60
Weight (kg)	77.5 ± 13.9	60
Height (cm)	172 ± 6	60
Clinical Indicators of Metabolic Function		
Admission FBG (mmol/L)	9.1 ± 3.1	52
Discharge FBG (mmol/L)	6.5 (5.2, 6.8)	37
HbA1c (%)	8.2 ± 1.7	40
SBP (mmHg)	136 ± 14	58
DBP (mmHg)	85 ± 11	58
WBC ($\times10^9$/L)	5.5 (5.0, 6.4)	56
N% (%)	62.8 ± 10.9	56
Hb (g/L)	146 ± 17	56
PLT ($\times10^9$/L)	203 ± 56	56
CRP (mg/L)	3 (1, 4)	51
ALT (U/L)	22 (11, 45)	56
AST (U/L)	19 (13, 23)	55
AST/ALT	0.867 (0.613, 1.188)	55
GGT (U/L)	25 (14, 49)	56
BUN (mmol/L)	5.6 ± 1.7	50
UA (μmol/L)	340 ± 102	51
TG (mmol/L)	1.14 (0.86, 1.64)	52
HDL-C (mmol/L)	1.02 ± 0.24	51
LDL-C (mmol/L)	2.50 ± 0.77	51
UMA (mg)	15.90 (6.05, 22.10)	49
UCr (g)	10.38 ± 5.90	47
UACR (mg/g)	1.097 (0.751, 1.853)	47
Diabetic Complications (n/total, n%)		
Diabetic nephropathy	6/58, 10.34%	
Diabetic retinopathy and cataract	16/58, 27.59%	
Diabetic peripheral neuropathy	4/58, 6.90%	
Coronary artery disease and cardiac insufficiency	3/58, 5.17%	
Lower extremity atherosclerosis or stenosis	4/58, 6.90%	
Carotid plaque	10/58, 17.24%	
Any of above complications	29/58, 50.00%	

Admission FBG, fasting blood glucose within 24 h of admission; Discharge FBG, fasting blood glucose within 24 h before discharge; HbA1c, glycated hemoglobin; SBP, systolic blood pressure; DBP, diastolic blood pressure; WBC, white blood cell; N%, percent of the number of neutrophils in the number of white blood cells; Hb, hemoglobin; PLT, platelet; CRP, c-reactive protein; ALT, alanine aminotransferase; AST, aspartate aminotransferase; AST/ALT, ratio of AST to ALT; GGT, gamma glutamyltransferase; BUN, blood urea nitrogen; UA, uric acid; TG, triglycerides; HDL-C, high-density lipoprotein-cholesterol; LDL-C, low-density lipoprotein-cholesterol; UMA, urine micro-albumin; UCr, urine creatinine; UACR, urine albumin-creatinine ratio.

health status. Upon admission, a fasting blood draw and urinary sample were obtained the next morning for routine glucose, lipid and renal panels. Subjects were also involved in investigation for diabetic complications. Clinical indicators of metabolic function analyzed in this study and diabetic complications statistics are demonstrated in Table 1.

Subsequently, clinical indicator outlier rejection was performed where box plot was utilized. The data were rearranged from largest to smallest, with the difference between the upper quartile U and the lower quartile L defined as IQR. The upper bound was set to U+1.5*IQR and the lower bound was set to L-1.5*IQR, and data exceeding the upper and lower bounds can be considered as outliers. Nevertheless, some data that did not appear to be gross errors, i.e., that were outside the range of normal values but might appear in patients who are in dysfunction states, were retained with the aim of reserving more information underneath the pathological data.

An HbA1c level greater than 9.0% indicates poor control of diabetes, which corresponds to a greater risk of complications and the need for more stringent treatment strategies (Inzucchi et al., 2015; Mosenzon et al., 2016; Ye et al., 2016; Garber et al., 2020). Subjects could be assigned to two groups according to the HbA1c level: one group had poor control of diabetes (HbA1c ≥ 9.0%) and the other did not (HbA1c < 9.0%).

2.3 ECG data recording

ECG recordings were collected by an FDA (U.S. Food and Drug Administration) approved ambulatory electrocardiogram monitor

(DynaDx Corporation, Mountainview, CA, United States) with a computer-based data-acquisition system. The ECG recording equipment was a single-lead Holter device that can record ECG for over 24 h. Sampling frequency of ECG monitoring was set to 250 Hz. All subjects were monitored in hospital for 24-h, starting at 10 p.m. on the second day of hospitalization. The 24-h ECG data was analyzed for HRV, which will be reported elsewhere. All ECG recordings were carefully checked with noise level, artifacts, and ectopic beats. Seventeen ECG recordings were discarded due to low data quality, too short recording time, or the fact that the inpatients had atrial fibrillation or server arrhythmia.

2.4 ECG data preprocessing

The band-pass Butterworth filter and zero-phase shift filter with a cut-off frequency of 5 Hz–35 Hz were first used to eliminate the baseline drift, power frequency interference, myoelectric interference, motion artifacts and equipment noise.

At present, plenty of R-peak detection methods have been proposed on ECG signal analysis. However, when applying these detectors on ECG signals collected in long-term recordings especially *via* wearable single-lead ECG devices, the R-peak detection accuracies were usually unsatisfying. To guarantee the accuracy of R-peak detection, a method for extracting high-quality RR intervals proposed in our previous study (Cui et al., 2020) was applied, which combing five commonly used R-peak detection methods including "Pan-Tompkins" (Pan and Tompkins, 1985; Hamilton and Tompkins, 1986), "jqrs" (Johnson et al., 2015), "mteo" (Solnik et al., 2008), "nqrs" (Li and Yang, 2013), and "sixth power" (Dohare et al., 2014). Outlier rejection for RR interval time series was performed, and box plot was utilized to find and reject outliers.

2.5 HRV analysis and metrics

In this study, we evaluated HRV based on the widely-used linear and non-linear HRV metrics (Task Force of the European Society of Cardiology the North American Society of Pacing Electrophysiology, 1996; Sassi et al., 2015).

2.5.1 Linear HRV analysis

Linear HRV metrics include time-domain metrics and frequency-domain metrics. Time-domain metrics quantify the amount of variability of the time period between successive heartbeats (RR intervals), and include HR-mean (mean of heart rate), SDNN (standard deviation of RR intervals), RMSSD (root mean square of successive RR intervals differences), SDSD (standard deviation of successive RR interval differences), SDANN (the standard deviation of the average value every 5 min in the RR interval) and pNN50 (the percentage of successive RR intervals that differ by more than 50 ms). Frequency-domain metrics estimate the distribution of absolute or relative power at different frequency bands. Generally, the whole frequency band (whose absolute power is noted as TP) is divided into three frequency bands: high-frequency band (0.15–0.40 Hz, whose absolute power is noted as HF), low-frequency band (0.04–0.15 Hz, whose absolute power is noted as LF) and very-low-frequency band (0.00–0.04 Hz, whose absolute power is noted as VLF). Other frequency-domain metrics include LFP (percentage of LF in TP), HFP (percentage of HF in TP) and LF/HF (ratio of LF-to-HF power). The widely used HRV analysis model for assessing ANS homeostasis includes three core statements (Pagani et al., 1986; Malliani et al., 1991; Montano et al., 2009): 1) the power of the high-frequency component reflects cardiac parasympathetic activity; 2) the power of low-frequency component reflects cardiac sympathetic activity; and 3) the LF-HF-ratio reflects sympathetic parasympathetic balance.

2.5.2 Non-linear HRV analysis

Non-linear analysis utilized in this study includes approximate entropy (ApEn) (Pincus, 1991), sample entropy (SampEn) (Chen et al., 2009), fuzzy entropy (FuzzyEn) (Richman and Moorman, 2000; Azami and Escudero, 2016), detrended fluctuation analysis (DFA, alpha1 and alpha2) (Peng et al., 1994), multi-scale entropy (MSE) (Costa et al., 2002) and multi-scale fuzzy entropy (MFE). Calculation steps are introduced in the supplementary material.

ApEn is a rather conventional measure to quantify irregularity and complexity and reflects the probability of new subsequences, and the more complex time series corresponds to larger ApEn. SampEn is a modification of ApEn, and is more accurate than ApEn in the case of less data. FuzzyEn is improved on the basis of SampEn, which is the entropy of a fuzzy set that contains vagueness and ambiguity uncertainties. When calculating ApEn, the embedding dimension m was set to 2, and the similar tolerance r was set to 0.25 times the SD of the sequence in order to find significant difference more clearly; in SampEn and FuzzyEn, r was set to 0.15 times the SD of the sequence.

MSE analyzes the complexity of time series from multiple time scales. The 25 coarse-grained time series are contracted from the original RR time series, in which we obtained 28 indices, including the SampEn value at each coarse-graining scale and 3 complexity metrics, MSEsum5, MSEsum10 and MSEsum20 (defined as the area of the MSE curve at scales 1–5, 1–10 and 1–20 respectively). The MSE curve usually rises rapidly at lower scales, peaks at scale 5, and then declines slowly, reaching a plateau after scale 20, therefore calculating the area of the MSE curve at scales 1–5 and 1–20 can portray the complexity characteristics of this curve at high and low resolutions. Similarly, MFE were calculated based on FuzzyEn.

DFA is a non-linear fractal analysis tool to discover potential self-similarity in the series and quantify the fractal scale of the time series. The α1 and α2 portray the short- and long-range correlation respectively.

2.6 Sleep quality assessment

Subjective sleep quality was assessed by Pittsburgh Sleep Quality Index (PSQI) and a brief sleep log was used to record sleep duration for the studied night. PSQI includes multiple sleep-related variables over the preceding month, using Likert and open-ended response formats (Spira et al., 2011). The PSQI yields seven component scores: subjective sleep quality, sleep latency, sleep duration, habitual sleep efficiency, sleep disturbances, sleep medication, and daytime dysfunction. Component scores range from 0 to 3 and are summed to obtain a global score, which ranges from 0 to 21. Higher

TABLE 2 Sleep quality metrics analyzed in this study. Data are presented as mean ± SD if the variable is normally distributed, otherwise presented as median (p25, p75).

Metrics (Unit)	Data	Sample size
PSQI	6 ± 3	53
AHI (event per hour)	21.2 (12.5, 38.8)	38
TST (hour)	7.8 ± 1.5	38
UST (hour)	3.8 ± 1.6	38
SST (hour)	2.5 ± 1.2	38
RST (hour)	1.6 ± 0.7	38
ALUS (min)	8.4 (6.4, 12.8)	38
ALSS (min)	11.2 ± 4.2	38
ALRS (min)	4.7 ± 1.1	38
USP (%)	47.53 ± 17.45	38
SSP (%)	32.22 ± 15.38	38
RSP (%)	20.45 ± 7.81	38

PSQI, Pittsburgh sleep quality index; AHI, apnea-hypopnea index; TST, total sleep time; UST, unstable sleep time; SST, stable sleep time; RST, rapid eye movement sleep time; ALUS, average length of unstable sleep segments; ALSS, average length of stable sleep segments; ALRS, average length of rapid eye movement sleep segments; USP, percentage of unstable sleep time in total sleep time; SSP, percentage of stable sleep time in total sleep time; RSP, percentage of rapid eye movement sleep time in total sleep time.

scores suggest greater sleep disturbance (Buysse et al., 1989). During 24-h ECG monitoring, 53 subjects filled in PSQI questionnaire.

Objective sleep quality and sleep staging were assessed by ECG-based cardiopulmonary coupling (CPC) analysis (Thomas et al., 2005), which has been cited in more than 260 publications (Yeh et al., 2008; Schramm et al., 2009; Thomas et al., 2010), and was introduced in the famous international sleep monograph "Principle and Practice of Medicine" (the sixth edition). The ECG recordings during sleep at night were extracted for sleep analysis in this study. CPC analysis is based on mathematical analysis of the coupling between HRV and the respiratory modulation of QRS waveform on a beat-to-beat basis. Major physiological sleep states derived from CPC analysis include stable sleep (indicated by high-frequency coupling, or HFC), unstable sleep (indicated by low frequency coupling, or LFC), and rapid eye movement (REM) or wakeful states (indicated by very low frequency coupling, or VLFC) (Thomas et al., 2005). In this study, 38 CPC sleep reports were available. Sleep quality metrics analyzed in this study are demonstrated in Table 2.

2.7 Statistical analysis

The data were analyzed by SPSS version 27.0 for Windows. The statistical analysis included significance analysis and correlation analysis. The normality of distribution of continuous variables was firstly tested by the Shaprio-Wilk test (significance level α = 0.05). For two normally distributed continuous variables, the Pearson correlation analysis was utilized to estimate the level of correlation, otherwise the Spearman analysis. Partial correlation analysis was also involved in the assessment of correlations between variables. For normally distributed variables, group differences were compared by independent sample *t*-test (2 groups) and one-way ANOVA (3 or more groups), otherwise Mann-Whitney U test (2 groups) or Kruskal-Wallis test (3 or more groups) were used. A value of $p < 0.05$ was considered significant. Missing data was completely at random, and pairwise deletion was conducted during the statistical analyses.

There are 25 scales and 3 complexity metrics for MSE and MFE respectively, and in order to demonstrate their overall correlations with clinical indicators in a straightforward way, we define the correlations between MSE and clinical indicators as mean ± SD of the correlations between SampEn at specific scales and clinical indicators. The coefficients of the same significant level ($p < 0.05$ or $p < 0.01$) between SampEn at certain scale and clinical indicators were selected to calculate the mean and SD. Similarly, the correlations between MFE and clinical indicators can be calculated. As for complexity metrics, the correlations between MSE complexity and clinical indicators are defined as mean ± SD of the correlations between specific complexity metrics (MSEsum5, MSEsum10 and MSEsum20) of the same significant level and clinical indicators, and similarly the correlations between MFE complexity and clinical indicators could be calculated.

3 Results

3.1 Correlations between sleep quality metrics and clinical indicators

Table 3 demonstrates the correlation coefficients between sleep quality metrics and clinical indicators. PSQI correlated rather weakly with DBP ($r = -0.296$, $p = 0.035$), Hb ($r = -0.291$, $p = 0.042$) and LDL-C ($r = -0.334$, $p = 0.023$), while sleep quality metrics calculated by CPC analysis were more significantly correlated with clinical indicators that were related to metabolic functions of T2DM patients. For example, liver function indicators AST/ALT was

TABLE 3 Correlation coefficients between sleep quality metrics and clinical metabolic indicators.

Sleep / Metabolic	PSQI	AHI	TST	UST	RST	ALUS	ALSS	ALRS	USP	SSP
Admission FBG			−0.383*ᵖ							
DBP	−0.296*ᵖ									
WBC							0.362*ˢ			
Hb	−0.291*ᵖ	−0.337*ˢ		−0.352*ᵖ		−0.385*ˢ			−0.347*ᵖ	
ALT			−0.371*ˢ	−0.334*ˢ						
AST/ALT			0.575**ˢ	0.424**ˢ						
BUN			0.488**ˢ	0.479**ˢ		0.442*ˢ			0.392*ˢ	
UA								−0.375*ᵖ		
TG			−0.405*ˢ							
HDL-C			0.386*ᵖ		0.348*ᵖ					
LDL-C	−0.334*ᵖ			−0.402*ᵖ					−0.363*ᵖ	0.357*ᵖ
UACR							0.423*ˢ			

Values in the table indicate the level of correlation, *$p < 0.05$, ** $p < 0.01$. ˢ represents Spearman correlation coefficient, and ᵖ represents Pearson correlation coefficient.

associated with TST ($r = -0.575$, $p < 0.001$) and UST ($r = 0.424$, $p = 0.009$), renal function indicator BUN was associated with TST ($r = 0.488$, $p = 0.005$), UST ($r = 0.479$, $p = 0.006$), ALUS ($r = 0.442$, $p = 0.011$) and USP ($r = 0.392$, $p = 0.027$). Moreover, TST and UST were significantly correlated with many clinical indicators, including admission FBG, Hb, ALT, AST/ALT, BUN, TG, HDL-C and LDL-C (e.g., TST & admission FBG, $r = -0.383$, $p = 0.025$; TST & TG, $r = -0.405$, $p = 0.019$; UST & LDL-C, $r = -0.400$, $p = 0.017$).

3.2 Significance of HRV metrics during sleep

Table 4 demonstrates the mean values of HRV metrics for 40 T2DM patients, which showed significant differences between sleep and awake periods, especially non-linear HRV metrics. During sleep period, subjects had smaller values of HR-mean, SDANN, TP, LF/HF and LFP, while their RMSSD, SDSD, SampEn, FuzzyEn, MSEsum5, MSEsum10, MSEsum20, MFEsum5, MFEsum10 and MFEsum20 were higher than those during awake period.

Table 5 demonstrates correlation coefficients between HRV metrics in 24-h/sleep/awake periods and clinical indicators. During 24-h period, significant correlations could be observed between liver function indicators ALT, AST/ALT and HRV metrics (e.g., ALT & HF, $r = 0.688$, $p < 0.001$; AST/ALT & LF, $r = -0.707$, $p < 0.001$; AST/ALT & HF, $r = -0.721$, $p < 0.001$), and between renal function indicator BUN and HRV metrics (e.g., RMSSD, $r = -0.482$, $p = 0.006$; pNN50, $r = -0.527$, $p = 0.002$; HF, $r = -0.517$, $p = 0.003$); as to HRV metrics, HFP was significantly correlated with many clinical indicators (ALT, $r = 0.466$, $p = 0.004$; AST/ALT, $r = -0.510$, $p = 0.001$; BUN, $r = -0.459$, $p = 0.007$), and since HF component mainly reflects PNS activity (Pagani et al., 1986; Malliani et al., 1991; Montano et al., 2009), it might suggest that PNS function is closely linked to physiological status in T2DM patients. During sleep period, significant correlations could be observed between many HRV metrics and DBP (e.g., SampEn, $r = 0.540$, $p < 0.001$; MSE complexity, $r = 0.571 \pm 0.054$, $p < 0.001$), Hb (e.g., MSE complexity, $r = 0.513 \pm 0.031$, $p = 0.001 \pm 0.001$; DFA-α2, $r = -0.524$, $p < 0.001$), ALT (e.g., HF, $r = 0.638$, $p < 0.001$; SampEn, $r = 0.645$, $p < 0.001$), AST/ALT (e.g., FuzzyEn, $r = -0.693$, $p < 0.001$; MFE complexity, $r = -0.711 \pm 0.021$, $p < 0.001$), and BUN (e.g., pNN50, $r = -0.556$, $p = 0.001$; SampEn, $r = -0.541$, $p = 0.002$); meanwhile, the significant correlations were observed between many clinical indicators and non-linear HRV metrics (e.g., ALT & SampEn, $r = 0.645$, $p < 0.001$; ALT & FuzzyEn, $r = 0.645$, $p < 0.001$; AST/ALT & MFE complexity, $r = -0.711 \pm 0.021$, $p < 0.001$). However, during awake period, the correlations between HRV metrics and clinical indicators decreased observably, and HRV metrics mainly correlated with liver function indicators ALT (e.g., LF, $r = 0.632$, $p < 0.001$; HF, $r = 0.628$, $p < 0.001$) and AST/ALT (e.g., LF, $r = -0.592$, $p < 0.001$; HF, $r = -0.606$, $p < 0.001$).

It could be seen that the overall level of correlation coefficients was significantly higher during sleep period than 24-h and awake periods. Correlations between variability-related HRV metrics (RMSSD and pNN50) and clinical indicators, including liver function (ALT, AST/ALT) and renal function (BUN), were more significant in sleep period than in 24-h and in awake period; significant correlations between complexity-related HRV metrics (SampEn, FuzzyEn, MSE complexity, MFE complexity) and clinical indicators were found mainly in sleep period.

3.3 HRV metrics in different sleep stages are more associated with T2DM clinical indicators

To investigate the relationship between HRV metrics (ANS function) in different sleep stages and the clinical indicators (metabolic function) of T2DM patients, the RR interval time

TABLE 4 HRV metrics for subjects during different recording period.

Metric (Unit)	24-h	Sleep	Awake	*p*-value
HR-mean (bpm)	78.99 ± 8.71	68.72 ± 8.24	83.57 ± 9.92	**<0.001†**
SDNN (ms)	114.66 (85.14, 147.21)	86.44 ± 29.33	90.41 ± 24.53	0.524
RMSSD (ms)	22.68 (14.97, 31.94)	23.87 (15.98, 39.39)	18.29 (14.37, 25.93)	**0.042†**
SDSD (ms)	22.68 (14.97, 31.94)	23.87 (15.98, 39.39)	18.29 (14.37, 25.93)	**0.042†**
SDANN (ms)	107.67 ± 34.20	57.51 (43.63, 71.61)	79.71 ± 23.38	**<0.001†**
pNN50 (%)	2.30 (0.63, 7.55)	3.59 (0.63, 17.81)	1.36 (0.56, 4.41)	0.061
TP ($\times 10^7$ ms^2)	4.49 ± 1.72	1.00 (0.71, 1.45)	1.38 (0.96, 1.87)	**0.038†**
VLF ($\times 10^4$ ms^2)	14.58 (9.02, 27.16)	6.19 (3.76, 9.68)	5.19 (2.44, 10.10)	0.473
LF ($\times 10^4$ ms^2)	3.92 (1.50, 6.97)	1.25 (0.61, 2.24)	1.51 (0.52, 2.71)	0.506
HF ($\times 10^3$ ms^2)	10.62 (5.56, 37.84)	4.50 (2.14, 15.49)	3.39 (1.38, 12.39)	0.383
LF/HF	2.58 (1.76, 3.29)	2.16 (1.39, 3.84)	3.73 ± 1.68	**0.006†**
LFP (%)	32.53 (32.07, 33.50)	32.46 (31.61, 33.17)	33.28 (32.58, 34.01)	**<0.001†**
HFP (%)	29.76 ± 1.55	29.53 ± 2.27	28.84 ± 1.42	0.117
DFA-α1	1.21 ± 0.18	1.20 ± 0.26	1.21 ± 0.17	0.848
DFA-α2	1.15 (1.10, 1.25)	1.20 ± 0.12	1.13 (1.06, 1.24)	0.071
ApEn	2.16 ± 0.31	2.21 (1.89, 2.31)	2.11 ± 0.31	0.771
SampEn	0.61 ± 0.23	1.14 ± 0.36	0.69 ± 0.23	**<0.001†**
FuzzyEn	1.41 ± 0.34	1.92 ± 0.47	1.43 ± 0.32	**<0.001†**
MSEsum5	3.43 ± 1.18	5.46 ± 1.55	3.99 ± 1.25	**<0.001†**
MSEsum10	7.75 ± 2.51	11.56 ± 3.00	9.08 ± 2.63	**<0.001†**
MSEsum20	16.88 ± 5.10	23.92 ± 5.75	19.95 ± 5.21	**0.002†**
MFEsum5	7.61 ± 1.85	9.55 ± 2.20	7.88 ± 1.83	**0.001†**
MFEsum10	16.52 ± 3.77	20.85 (18.06, 22.61)	17.23 ± 3.72	**0.007†**
MFEsum20	35.10 ± 7.25	42.22 (36.86, 46.05)	36.87 ± 7.06	**0.012†**

Data are presented as mean ± SD if the variable is normally distributed, otherwise presented as median (p25, p75). The bold font and † represent a significant difference between *Sleep* and *Awake*, i.e., $p < 0.05$.

series during sleep period were segmented according to sleep stages, including unstable sleep, stable sleep and REM sleep, and series from the same sleep stage were stitched together as a whole. Significant differences were observed among HRV metrics in different sleep stages. For example, the LF/HF reached its maxima in unstable sleep (4.04 ± 3.31), followed by REM sleep (3.36 ± 2.27) and its minima in stable sleep (1.45 ± 0.98). More details are shown in Supplementary Table S2.

The correlation coefficients between HRV metrics in different sleep stages and clinical indicators are demonstrated in Table 6. Linear HRV metrics, especially RMSSD, SDSD, pNN50, LF, HF and HFP were correlated significantly with Hb, ALT, AST/ALT and BUN (e.g., in unstable sleep: SDSD & ALT, $r = 0.665$, $p < 0.001$; RMSSD & AST/ALT, $r = -0.710$, $p < 0.001$; HF & AST/ALT, $r = -0.716$, $p < 0.001$; pNN50 & BUN, $r = -0.533$, $p = 0.002$; in stable sleep: HFP & AST/ALT, $r = -0.556$, $p < 0.001$; in REM sleep: LF & Hb, $r = 0.510$, $p = 0.001$). In non-linear HRV analysis, more metrics were tightly associated with clinical indicators, and the correlations were more significant with those in linear analysis (63 correlations with $|r|>0.5$, compared with 44 correlations with $|r|>0.5$ in linear analysis), especially the DFA metric α2 and the complexity metrics MSE and MFE (e.g., in unstable sleep: DFA-α2 & admission FBG, $r = -0.584$, $p < 0.001$; MFE & AST/ALT, $r = -0.614 \pm 0.052$, $p < 0.001$; MFE complexity & AST/ALT, $r = -0.680 \pm 0.014$, $p < 0.001$; in stable sleep: SampEn & ALT, $r = 0.786$, $p < 0.001$; MSE complexity & ALT, $r = 0.596 \pm 0.076$, $p < 0.001$; MSE & AST/ALT, $r = -0.571 \pm 0.132$, $p = 0.002 \pm 0.003$; FuzzyEn & AST/ALT, $r = -0.760$, $p < 0.001$). Compared with the correlation with linear HRV metrics, correlations between admission FBG, DBP, Hb, ALT, AST, AST/ALT, GGT, BUN and non-linear HRV metrics increased considerably (e.g., in unstable sleep: DFA-α2 & admission FBG, $r = -0.584$, $p < 0.001$; in stable sleep: SampEn & ALT, $r = 0.786$, $p < 0.001$; SampEn & AST, $r = 0.630$, $p < 0.001$; FuzzyEn & AST/ALT, $r = -0.760$, $p < 0.001$; SampEn & BUN, $r = -0.625$, $p < 0.001$; in REM sleep: MSE complexity & DBP, $r = 0.560 \pm 0.046$, $p < 0.001$; DFA-α2 & Hb,

TABLE 5 Correlation coefficients between HRV metrics during different recording period and clinical indicators.

HRV / Metabolic	RMSSD	pNN50	LF	HF	HFP	SampEn	MSE complexity	FuzzyEn	MFE complexity	DFA-α2
24-h										
Admission FBG			0.406^{**s}							−0.507^{**s}
Hb			0.471^{**s}	0.412^{*s}						−0.545^{**s}
ALT	0.602^{**s}	0.545^{**s}	0.658^{**s}	0.688^{**s}	0.466^{**s}					−0.519^{**s}
AST			0.457^{**s}	0.488^{**s}						−0.436^{**s}
AST/ALT	−0.572^{**s}	−0.650^{**s}	−0.707^{**s}	−0.721^{**s}	−0.510^{**s}					0.531^{**s}
BUN	−0.482^{**s}	−0.527^{**s}	−0.465^{**s}	−0.517^{**s}	−0.459^{**p}					0.430^{**s}
UACR						−0.458^{*s}	−0.492 ± 0.005^{**s}	−0.361^{*s}	−0.478 ± 0.008^{**s}	
Sleep										
Admission FBG							0.413 ± 0.034^{*p}		0.414 ± 0.010^{*s}	−0.575^{**p}
DBP			0.414^{**s}	0.483^{**s}		0.540^{**p}	0.571 ± 0.054^{**p}	0.528^{**p}	0.537 ± 0.015^{**s}	−0.458^{**p}
Hb	0.430^{**s}	0.418^{**s}	0.505^{**s}	0.430^{**s}		0.491^{**p}	0.513 ± 0.031^{**p}	0.495^{**p}	0.472^{**s}	−0.524^{**p}
ALT	0.629^{**s}	0.573^{**s}	0.624^{**s}	0.638^{**s}	0.449^{**s}	0.645^{**s}	0.574 ± 0.032^{**s}	0.645^{**s}	0.619 ± 0.028^{**s}	−0.435^{**s}
AST	0.440^{**s}		0.449^{**s}	0.434^{**s}		0.487^{**s}	0.449 ± 0.019^{**s}	0.449^{**s}	0.447 ± 0.001^{*s}	
AST/ALT	−0.692^{**s}	−0.657^{**s}	−0.660^{**s}	−0.691^{**s}	−0.496^{**s}	−0.641^{**s}	−0.593 ± 0.045^{**s}	−0.693^{**s}	−0.711 ± 0.021^{**s}	0.500^{**s}
GGT						0.489^{**s}	0.492 ± 0.011^{**s}	0.407^{*s}	0.454 ± 0.021^{**s}	
BUN	−0.535^{**s}	−0.556^{**s}	−0.436^{*s}	−0.522^{**s}	−0.409^{*p}	−0.541^{**p}	−0.525^{**p}	−0.521^{**p}	−0.533 ± 0.041^{**s}	
UACR							−0.400 ± 0.013^{**s}	−0.512^{**s}		
Awake										
Hb			0.438^{**s}							−0.662^{**s}
ALT	0.522^{**s}	0.498^{**s}	0.632^{**s}	0.628^{**s}	0.523^{**s}					−0.540^{**s}
AST			0.486^{**s}	0.461^{**s}						−0.439^{**s}
AST/ALT	−0.579^{**s}	−0.583^{**s}	−0.592^{**s}	−0.606^{**s}	−0.539^{**s}					0.554^{**s}
BUN	−0.441^{**s}	−0.491^{**s}	−0.455^{*s}	−0.466^{**s}	−0.431^{*p}		−0.403 ± 0.028^{*p}		−0.404 ± 0.029^{*s}	0.496^{**s}

Values in the table indicate the level of correlation, $^{*}p < 0.05$, $^{**}p < 0.01$. ^{s} represents Spearman correlation coefficient, and ^{p} represents Pearson correlation coefficient. Only metrics or indicators that had several significant correlations with others are selected, and only correlation coefficients whose absolute value were higher than 0.4 are presented here, while others are presented in Supplementary Table S1.

$r = -0.549$, $p < 0.001$; MSE complexity & GGT, $r = 0.494 \pm 0.009$, $p = 0.002 \pm 0.000$), and significant association between HbA1c, N%, PLT, HDL-C, LDL-C, UMA and HRV metrics were mainly observed in non-linear analysis (e.g., in unstable sleep: FuzzyEn & HbA1c, $r = 0.506$, $p = 0.001$; in stable sleep: MFE & N%, $r = -0.474$, $p = 0.003$; in REM sleep: MFE & PLT, $r = 0.515$, $p = 0.001$; DFA-α2 & LDL-C, $r = -0.495$, $p = 0.003$; MFE & UMA, $r = -0.512 \pm 0.008$, $p = 0.003 \pm 0.001$).

The findings hinted that HRV metrics in different sleep stages were more associated with T2DM clinical indicators. During each sleep stage, the correlation coefficients between HRV metrics and clinical indicators demonstrated a higher overall level compared with those during sleep period. Compared with linear HRV metrics, non-linear HRV metrics significantly correlated with more clinical indicators, including LDL-C and UACR.

3.4 Non-linear HRV metrics during sleep are associated with glycemic control

Interestingly, non-linear HRV metrics in different sleep stages were significantly associated with glycemic control, while few weak correlations were found between HRV metrics of 24-h and awake periods and glycemic control indicators. Table 7 demonstrates correlation coefficients between non-linear HRV metrics in three sleep stages and glycemic control indicators including admission FBG, discharge FBG and HbA1c. Most of non-linear HRV metrics were significantly correlated with admission FBG (e.g., in unstable sleep: DFA-α2, $r = -0.584$, $p < 0.001$; MSE, $r = 0.466$, $p = 0.006$; MSE complexity, $r = 0.440$, $p = 0.009$), yet had no or only weak correlation with discharge FBG. Both single- and multiple-scale sample entropies showed significant correlations with HbA1c (in unstable sleep: SampEn, $r = 0.438$, $p = 0.025$; MSE, $r = 0.411 \pm 0.016$, $p = 0.038 \pm 0.008$; MSE complexity, $r = 0.409 \pm 0.017$, $p = 0.039 \pm 0.009$; in stable sleep: MSE, $r = 0.389$, $p = 0.050$; in REM sleep: SampEn, $r = 0.424$, $p = 0.031$; MSE, $r = 0.418 \pm 0.022$, $p = 0.035 \pm 0.010$; MSE complexity, $r = 0.442 \pm 0.021$, $p = 0.024 \pm 0.007$).

Furthermore, the subjects were divided into two groups according to whether the subject had poor control of diabetes (HbA1c ≥ 9.0%, $n = 10$) or not (HbA1c < 9.0%, $n = 16$). Table 8 demonstrates between-group differences in non-linear HRV metrics. Significant differences were observed in non-linear metrics in unstable and stable sleep (in unstable sleep: DFA-alpha2, $p = 0.002$; MSEsum5, $p = 0.020$; MSEsum10, $p = 0.017$; MSEsum20, $p = 0.037$; in stable sleep: SampEn, $p = 0.020$; DFA-alpha2, $p = 0.026$; MSEsum5, $p = 0.002$; MSEsum10, $p = 0.004$; MSEsum20, $p = 0.024$).

TABLE 6 Correlation coefficients between HRV metrics in three sleep stages and clinical indicators.

(a) Correlation coefficients between linear HRV metrics and clinical indicators							
Linear HRV / Metabolic	Time-domain			Frequency-domain			
	RMSSD	SDSD	pNN50	VLF	LF	HF	HFP
Unstable sleep							
Hb	0.451**^{s}	0.451**^{s}	0.406*^{s}		0.472**^{s}	0.433**^{s}	
ALT	0.665**^{s}	0.665**^{s}	0.610**^{s}	0.436**^{s}	0.525**^{s}	0.682**^{s}	0.519**^{s}
AST	0.477**^{s}	0.477**^{s}	0.423*^{s}		0.410*^{s}	0.508**^{s}	
AST/ALT	−0.710**^{s}	−0.710**^{s}	−0.701**^{s}	−0.416*^{s}	−0.540**^{s}	−0.716**^{s}	−0.551**^{s}
BUN	−0.516**^{s}	−0.516**^{s}	−0.533**^{s}			−0.476**^{s}	
Stable Sleep							
ALT	0.568**^{s}	0.568**^{s}	0.525**^{s}		0.510**^{s}	0.581**^{s}	0.489**^{s}
AST	0.403*^{s}	0.403*^{s}				0.410*^{s}	
AST/ALT	−0.654**^{s}	−0.654**^{s}	−0.620**^{s}	−0.428**^{s}	−0.554**^{s}	−0.623**^{s}	−0.556**^{s}
BUN	−0.506**^{s}	−0.506**^{s}	−0.493**^{s}		−0.478**^{s}	−0.524**^{s}	−0.414*^{s}
REM Sleep							
Hb	0.410*^{s}	0.410*^{s}			0.510**^{s}	0.478*^{s}	
ALT	0.586**^{s}	0.586**^{s}	0.552**^{s}		0.475**^{s}	0.490*^{s}	0.430**^{s}
AST/ALT	−0.680**^{s}	−0.680**^{s}	−0.699**^{s}	−0.405*^{s}	−0.489**^{s}	−0.561**^{s}	−0.509**^{s}
BUN	−0.507**^{s}	−0.507**^{s}	−0.529**^{s}		−0.410*^{s}	−0.524**^{s}	−0.483**^{p}

(b) Correlation coefficients between non-linear HRV metrics and clinical indicators							
Non-linear HRV / Metabolic	DFA-α2	SampEn	MSE	MSE complexity	FuzzyEn	MFE	MFE complexity
Unstable Sleep							
Admission FBG	−0.584**^{p}	0.400*^{p}	0.466**^{s}	0.440**^{p}		0.436*^{s}	0.403 ± 0.003*^{p}
HbA1c	−0.412*^{p}	0.438*^{p}	0.411 ± 0.016*^{s}	0.409 ± 0.017*^{p}			
DBP		0.523**^{p}	0.488 ± 0.047**^{s}	0.545 ± 0.060**^{p}		0.457 ± 0.043**^{s}	0.543 ± 0.039**^{p}
Hb	−0.496**^{p}	0.483**^{p}	0.424 ± 0.001**^{s}	0.494 ± 0.031**^{p}	0.500**^{p}	0.435 ± 0.009**^{s}	0.490 ± 0.051**^{p}
ALT		0.572**^{s}	0.472 ± 0.047**^{s}	0.520 ± 0.029**^{p}	0.615**^{s}	0.538 ± 0.048**^{s}	0.590 ± 0.012**^{s}
AST			0.426**^{s}		0.440**^{s}	0.461 ± 0.043**^{s}	0.439**^{s}
AST/ALT	0.421*^{s}	−0.614**^{s}	−0.503 ± 0.063**^{s}	−0.583 ± 0.040**^{p}	−0.656**^{s}	−0.614 ± 0.052**^{s}	−0.680 ± 0.014**^{s}
GGT			0.455 ± 0.034**^{s}	0.452**^{p}		0.478 ± 0.048**^{s}	0.459**^{s}
BUN		−0.443*^{p}	−0.400 ± 0.035*^{s}	−0.408 ± 0.044*^{p}	−0.451*^{p}	−0.488 ± 0.032**^{s}	−0.463**^{p}
LDL-C		0.460**^{p}			0.428*^{s}		
Stable Sleep							
DBP		0.458**^{s}	0.463 ± 0.039**^{s}	0.447**^{s}	0.508**^{p}	0.456 ± 0.033**^{s}	0.474 ± 0.027**^{s}
N%			−0.462 ± 0.031**^{s}	−0.461 ± 0.035*^{s}		−0.474**^{s}	
Hb	−0.535**^{p}	0.498**^{s}	0.469 ± 0.037**^{s}	0.476 ± 0.070*^{s}	0.475**^{p}		0.431**^{s}
ALT	−0.419*^{s}	0.786**^{s}	0.553 ± 0.114**^{s}	0.596 ± 0.076**^{s}	0.721**^{s}	0.580 ± 0.070**^{s}	0.635 ± 0.042**^{s}
AST	−0.496**^{s}	0.630**^{s}	0.523 ± 0.058**^{s}	0.555 ± 0.051**^{s}	0.522**^{s}	0.488 ± 0.054**^{s}	0.491 ± 0.035**^{s}
AST/ALT	0.376*^{s}	−0.728**^{s}	−0.571 ± 0.132**^{s}	−0.516 ± 0.095**^{s}	−0.760**^{s}	−0.585 ± 0.075**^{s}	−0.667 ± 0.055**^{s}
GGT		0.441**^{s}	0.434 ± 0.011**^{s}		0.442*^{s}	0.482 ± 0.060**^{s}	0.447 ± 0.007*^{s}
BUN		−0.625*^{s}	−0.570 ± 0.078**^{s}		−0.576**^{p}	−0.545 ± 0.072**^{s}	−0.534 ± 0.047**^{s}
REM Sleep							
Admission FBG	−0.524**^{p}		0.403 ± 0.023*^{s}				
HbA1c		0.424*^{p}	0.418 ± 0.022*^{s}	0.442 ± 0.021*^{p}			
DBP	−0.507**^{p}	0.493**^{p}	0.502 ± 0.070**^{s}	0.560 ± 0.046**^{p}	0.496**^{p}	0.489 ± 0.049**^{s}	0.533 ± 0.029**^{s}
Hb	−0.549**^{p}	0.475**^{p}	0.479 ± 0.037**^{s}	0.524 ± 0.043**^{p}	0.504**^{p}	0.478 ± 0.054**^{s}	0.464 ± 0.040**^{s}
PLT						0.515**^{s}	
ALT	−0.402*^{s}	0.581**^{s}	0.512 ± 0.041**^{s}	0.552 ± 0.011**^{s}	0.591**^{s}	0.543 ± 0.061**^{s}	0.590 ± 0.007**^{s}
AST		0.416*^{s}	0.437 ± 0.019**^{s}	0.432 ± 0.003*^{s}	0.416*^{s}	0.476 ± 0.039**^{s}	0.402 ± 0.008*^{s}
AST/ALT	0.437**^{s}	−0.575**^{s}	−0.493 ± 0.042**^{s}	−0.518 ± 0.029**^{s}	−0.627**^{s}	−0.570 ± 0.070**^{s}	−0.649 ± 0.001**^{s}

(Continued on following page)

TABLE 6 (*Continued*) Correlation coefficients between HRV metrics in three sleep stages and clinical indicators.

(b) Correlation coefficients between non-linear HRV metrics and clinical indicators							
Non-linear HRV / Metabolic	DFA-α2	SampEn	MSE	MSE complexity	FuzzyEn	MFE	MFE complexity
GGT		0.478**S	0.462 ± 0.023**S	0.494 ± 0.009**S	0.400*S	0.468 ± 0.026**S	0.436**S
BUN		−0.472**P	−0.495 ± 0.030**S	−0.486**P	−0.496**P	−0.535 ± 0.043**S	−0.578 ± 0.010**S
LDL-C	−0.495**P	0.422*P		0.400 ± 0.010*P	0.400*P	0.484 ± 0.036**S	
UMA			−0.466*S			−0.512 ± 0.008**S	
UACR			−0.505 ± 0.027**S	−0.488 ± 0.004**S		−0.514 ± 0.046**S	−0.404 ± 0.003*S

Values in the table indicate the level of correlation, *$p < 0.05$, ** $p < 0.01$. S represents Spearman correlation coefficient, and P represents Pearson correlation coefficient. Only metrics or indicators that had several significant correlations with others are selected, and only correlation coefficients whose absolute value were higher than 0.4 are presented here, while others are presented in Supplementary Table S3.

TABLE 7 Correlation coefficients between non-linear HRV metrics in three sleep stages and clinical glycemic control indicators including admission FBG, discharge FBG and HbA1c.

Non-linear HRV / Glycemic control	DFA-α2	SampEn	MSE	MSE complexity	FuzzyEn	MFE	MFE complexity
Unstable Sleep							
Admission FBG	−0.584**P	0.400*P	0.466**S	0.440**P	0.378*P	0.436*S	0.403 ± 0.003*P
HbA1c	−0.412*P	0.438*P	0.411 ± 0.016*S	0.409 ± 0.017*P			
Stable Sleep							
Admission FBG		0.362*S	0.353 ± 0.015*S	0.364*S		0.377*S	
Discharge FBG			−0.423*S				
HbA1c			0.389*S				
REM Sleep							
Admission FBG	−0.524**P		0.403 ± 0.023*S			0.394 ± 0.024*S	
HbA1c		0.424*P	0.418 ± 0.022*S	0.442 ± 0.021*P			

Values in the table indicate the level of correlation, *$p < 0.05$, ** $p < 0.01$. S represents Spearman correlation coefficient, and P represents Pearson correlation coefficient.

TABLE 8 Difference in non-linear HRV metrics between the group had poor control of diabetes (HbA1c ≥ 9.0%) or did not (HbA1c < 9.0%). Data are presented as mean ± SD.

Sleep Stage	Non-linear HRV metric	HbA1c < 9.0% (n = 16)	HbA1c ≥ 9.0% (n = 10)	*p*-value
Unstable Sleep	DFA-α2	1.28 ± 0.09	1.15 ± 0.09	0.002
	MSEsum5	5.07 ± 1.20	6.19 ± 0.98	0.020
	MSEsum10	11.24 ± 2.47	13.63 ± 2.04	0.017
	MSEsum20	24.79 ± 5.03	29.03 ± 4.32	0.037
Stable Sleep	SampEn	1.42 ± 0.31	1.69 ± 0.18	0.020
	DFA-α2	1.11 ± 0.15	0.99 ± 0.08	0.026
	MSEsum5	6.54 ± 1.59	8.14 ± 0.69	0.002
	MSEsum10	13.33 ± 3.12	16.26 ± 1.48	0.004
	MSEsum20	26.31 ± 6.02	31.29 ± 3.12	0.024

TABLE 9 Partial correlation analysis between HbA1c and non-linear HRV metrics in unstable and REM sleep.

Non-linear HRV \ Glycemic control		HbA1c								
		Zero order	Nullified by AHI	Nullified by TST	Nullified by SST	Nullified by RST	Nullified by ALUS	Nullified by ALSS	Nullified by USP	Nullified by SSP
Unstable Sleep	SampEn	0.438*	0.474*		0.489*	0.453*	0.442*	0.527**	0.465*	0.532**
	MSEsum5	0.421*	0.428*		0.445*	0.457*	0.417*	0.469*	0.424*	0.468*
	MSEsum10	0.397*	0.396*		0.405*	0.458*	0.398*	0.422*		0.421*
REM Sleep	SampEn	0.424*	0.510**	0.402*	0.547**	0.411*	0.452*	0.549**	0.495*	0.569**
	MSEsum5	0.457*	0.505**	0.431*	0.552**	0.455*	0.470*	0.561**	0.499*	0.573**
	MSEsum10	0.428*	0.456*	0.400*	0.506**	0.438*	0.430*	0.534**	0.450*	0.524**

Values in the table indicate the level of correlation, *$p < 0.05$, ** $p < 0.01$.

TABLE 10 Partial correlation analysis between admission FBG and non-linear HRV metrics in 3 sleep stages.

Non-linear HRV \ Glycemic control		Admission FBG								
		Zero order	Nullified by AHI	Nullified by TST	Nullified by UST	Nullified by SST	Nullified by RST	Nullified by ALUS	Nullified by USP	Nullified by SSP
Unstable Sleep	DFA-α2	−0.584**	−0.585**	−0.549**	−0.569**	−0.595**	−0.580*	−0.594**	−0.582**	−0.586**
	SampEn	0.400*	0.435*		0.345*	0.464**	0.396*	0.398*	0.416*	0.437*
	MSEsum5	0.440**	0.448**	0.346*	0.397*	0.473**	0.433*	0.435*	0.440**	0.455**
	MSEsum10	0.425*	0.425*		0.393*	0.437*	0.419*	0.426**	0.422*	0.429*
	FuzzyEn	0.378*	0.413*			0.466**	0.375*	0.375*	0.403*	0.430*
	MFEsum5	0.405*	0.419*		0.353*	0.467**	0.399*	0.399*	0.413*	0.435*
	MFEsum10	0.401*	0.405*		0.353*	0.444**	0.393*	0.397*	0.400*	0.418*
Stable Sleep	MSEsum5	0.354*	0.353*			0.369*	0.354*	0.349*	0.350*	0.354*
REM Sleep	DFA-α2	−0.524**	−0.561**	−0.465**	−0.496**	−0.615**	−0.537**	−0.538**	−0.571**	−0.578**

Values in the table indicate the level of correlation, *$p < 0.05$, ** $p < 0.01$.

3.5 Association among glycemic control, non-linear HRV analysis and sleep

We also applied partial correlation analysis between HbA1c, admission FBG and non-linear HRV metrics in sleep stages as controlling the effect of sleep quality metrics, in order to briefly discover the interaction among glycemic control, non-linear HRV analysis and sleep.

Table 9 demonstrates partial correlations between HbA1c and non-linear HRV metrics in unstable and REM sleep. When nullifying the effect of SST, ALSS and SSP, the correlations between HbA1c and non-linear HRV metrics significantly strengthened (e.g., SampEn in REM sleep: zero order, $r = 0.424$, $p = 0.031$; nullified by SST, $r = 0.547$, $p = 0.005$; nullified by ALSS, $r = 0.549$, $p = 0.004$; nullified by SSP, $r = 0.569$, $p = 0.003$). However, the correlations between HbA1c and non-linear HRV metrics decreased and even were lost when corrected for TST (e.g., SampEn in REM sleep: zero order, $r = 0.424$, $p = 0.031$; nullified by TST, $r = 0.402$, $p = 0.046$; MSEsum10 in REM sleep: zero order, $r = 0.428$, $p = 0.029$; nullified by TST, $r = 0.400$, $p = 0.048$). The associations were mostly retained when corrected for other sleep metrics (e.g., MSEsum5 in unstable sleep: zero order, $r = 0.421$, $p = 0.032$; nullified by AHI, $r = 0.428$, $p = 0.033$; nullified by ALUS, $r = 0.417$, $p = 0.038$; nullified by USP, $r = 0.424$, $p = 0.035$).

Table 10 demonstrates partial correlations between admission FBG and non-linear HRV metrics in 3 sleep stages. When nullifying the effect of SST, the correlations between HbA1c and non-linear HRV metrics at sleep stages significantly strengthened (e.g., SampEn in unstable sleep: zero order, $r = 0.400$, $p = 0.019$; nullified by SST, $r = 0.464$, $p = 0.007$; FuzzyEn in unstable sleep: zero order, $r = 0.378$, $p = 0.027$; nullified by SST, $r = 0.466$, $p = 0.006$). When nullifying the effect of TST, the correlations between HbA1c and non-linear HRV metrics decreased and even were lost (e.g., MSEsum5 in unstable sleep: zero order, $r = 0.440$, $p = 0.009$; nullified by TST, $r = 0.346$, $p = 0.049$; DFA-α2 in REM sleep: zero order, $r = -0.524$, $p = 0.001$; nullified by TST, $r = -0.465$, $p = 0.006$). The associations between admission FBG and non-linear HRV metrics, especially DFA-α2, were retained when corrected for other sleep metrics (e.g., DFA-α2 in unstable sleep: zero order, $r = -0.584$, $p < 0.001$; nullified by AHI, $r = -0.585$, $p < 0.001$; nullified by USP, $r = -0.582$, $p < 0.001$; nullified

by SSP, $r = -0.586$, $p < 0.001$; DFA-α2 in REM sleep: zero order, $r = -0.524$, $p = 0.001$; nullified by RST, $r = -0.537$, $p = 0.001$; nullified by ALUS, $r = -0.538$, $p = 0.001$).

4 Discussion

This study focused on the relationships among sleep, HRV derived ANS function and metabolic function in T2DM, and the main findings were: 1) metabolic function was significantly correlated with sleep quality; 2) HRV derived ANS function was different between sleep and awake, showing strengthened and distinct distributions of correlations with metabolic function compared to 24-h analysis; 3) HRV derived ANS function and its correlation with clinical indicators of metabolic function altered during sleep cycles; 4) HRV analysis during sleep was strongly associated with clinical indicators of metabolic function, and this also applied to the glycemic control in patients with T2DM in non-linear analysis. These findings demonstrated that sleep rhythm based HRV analysis should be emphasized in ANS and metabolic function assessment and the rationality of non-linear HRV analysis for further application among T2DM patients and investigation of potential interactions among ANS, sleep and metabolic function (Lombardi, 2011; Perkiömäki, 2011).

In sleep quality assessment, PSQI had few and weak correlations with clinical indicators, while TST and UST correlated with more clinical indicators. The results suggest limitations of PSQI from its objectivity and indicate the important role of sleep in regulation of metabolic function. Researchers have found that circadian rhythms and sleep regulate hormones and lipids involved in energy metabolism (VanCauter et al., 1997; Scheer et al., 2009; Nguyen and Wright, 2010; Spiegel et al., 2011; Markwald et al., 2013), and disruption of sleep and circadian rhythms is progressively apparent as an influence factor to damaged physiological function, disease processes and metabolic dysregulation (Spiegel et al., 2005; Turek et al., 2005; Marcheva et al., 2010; Markwald and Wright, 2012).

The enhanced association between ANS and metabolic function during sleep is consistent with previously published results. Researchers have found that most of the biological functions changes during sleep compared to wake, such as heart rate, arterial blood pressure and etc., where ANS plays a vital role (Tobaldini et al., 2017). Results in Table 5, 6 showed that HRV metrics during sleep were associated with clinical indicators of metabolic function more significantly and broadly, compared to 24-h HRV, and there were significant differences between HRV metrics during sleep and awake. Thus, sleep might be a good model to investigate ANS activity and the fluctuation of ANS function caused by intrinsic factors, especially circadian rhythm, without influence factors of daytime activities such as eating behaviour, physical movement, etc. Meanwhile, studies have shown that HRV metrics are significantly influenced by routine life states and ECG recording time (morning, noon, evening), and the RR values are rather stable during night sleeping (Cui et al., 2020), so we analysed the RR interval time series during awake period (i.e., during daytime) as a whole, and at the same time the time of waking and sleeping of subjects was rather uniform, which may decrease bias brought by recording time.

Significant differences observed in many HRV metrics among different sleep stages suggest the dominance of SNS in unstable sleep and the dominance of PNS in stable sleep (Pagani et al., 1986; Malliani et al., 1991; Montano et al., 2009). Researchers have found that ANS tone and modulation are profoundly influenced by sleep related mechanisms (Somers et al., 1993; Trinder et al., 2001; Tobaldini et al., 2014; de Zambotti et al., 2018), while cardiovascular function within each sleep stage tends not to vary across the night (Silvani and Dampney, 2013). For ANS impose regulatory control over the cardiovascular system by SNS and PNS, which leads to HRV, the changes of HRV metrics in different sleep stages and their correlations with clinical indicators may associate more closely with the variability of ANS function during sleep cycles. Researchers have conducted HRV analysis during sleep to confirm different ANS function patterns at sleep stages (Scholz et al., 1997; Brandenberger et al., 2001; Trinder et al., 2001; Stein and Pu, 2012). Studies have shown that, since most of HRV metrics applied in this study were based on the assumption of stationary series (Akselrod et al., 1981; Pagani et al., 1986; Pincus et al., 1993; Task Force of the European Society of Cardiology the North American Society of Pacing Electrophysiology, 1996; Voss et al., 1996; Cooke et al., 1999; Porta et al., 2000b; Cysarz et al., 2000; Richman and Moorman, 2000; Wessel et al., 2000; Porta et al., 2001), non-stationarities of HRV sequences could have a great influence on the assessment of the balance of ANS by producing a bias toward a higher sympathetic modulation and a lower vagal modulation (Magagnin et al., 2011). We applied Augmented Dickey-Fuller test to all the HRV sequences for stationarity test, and found sequences during 24-h, daytime and sleep were mostly stationary. However, during sleep cycles, the sequences were mostly non-stationary. Hence, the distinct distribution pattern presented in analysis during sleep cycles may demonstrate the shift of sympathovagal balance toward sympathetic predominance since non-stationarities of the HRV sequences will highlight the shift (Magagnin et al., 2011). With enhanced and clarified interaction between ANS function and HRV analysis in each sleep stage, the underlying autonomic pathways (Stein and Pu, 2012) of different HRV metrics may be better distinguished from the remarkably strengthened correlations between clinical indicator of metabolic function and HRV metrics with distinct distribution patterns compared to traditional analysis of sleep quality and HRV, which is crucial to reveal the interaction among sleep, ANS and HRV.

Compared to linear analysis, non-linear HRV metrics in different sleep stages were associated with more T2DM clinical indicators. According to the development of chaotic theory and non-linear dynamics, it is now generally recognized that heart beat intervals (RR intervals) are non-linear and non-stationary time series, caused by complex interactions between physiological systems (Peng et al., 1995; Cerutti et al., 2007). Traditional methods in time- and frequency-domain may not be able to detect subtle but important changes in RR series (Costa et al., 2005). Currently, HRV frequency-domain metrics are extensively used to assess the function of ANS components, leading to controversial results (Stein and Pu, 2012; Reyes del Paso et al., 2013; Martelli et al., 2014). In this study, most comprehensive and strong correlations between HRV derived ANS function and metabolic function with distinct distribution patterns were observed in non-linear analysis, demonstrating the rationality of non-linear analysis in assessing ANS function.

However, a part of non-linear HRV metrics we chose are somehow influenced by some biases. ApEn is a biased statistic,

and the bias arises from two separate sources. First, in the calculation of the correlation integral $C_i^m(r)$, the vector $X(i)$ counts itself to ensure that the logarithms remain finite, which is defined as "self-matching," underestimating the calculation of conditional probabilities as a consequence of it and producing a bias towards regularity. If the number of matches between templates is low, the bias can be as high as 20% or 30%. Second, the concavity of the logarithm implies a bias in all the regularity statistics (Pincus and Huang, 1992; Delgado-Bonal and Marshak, 2019). On some occasions, ApEn failed to capture the sympathovagal balance (Porta et al., 2007a). The MSE method also has shortcomings. The course of the entropy-based complexity as a function of the time scale is partially linked to the reduction of variance inherent to the procedure for the elimination of the fast temporal scales, which confines more and more patterns inside phase space cells of constant dimension (Nikulin and Brismar, 2004). As a consequence, more and more patterns become indistinguishable, thus artificially reducing complexity with the scale factor τ. Obviously, this effect is more evident at large time scales when variance is importantly reduced, thus producing biased MSE courses especially at large time scales. Meanwhile, the procedure devised to eliminate fast time scales is suboptimal, thus producing uncontrolled effects on the assessment of complexity at any scale (Valencia et al., 2009).

It is likewise not negligible that the impact of the data length on the ability to predict the health status of ANS (Laborde et al., 2017). Long-term 24-h HRV recordings are acknowledged as the "gold standard" for clinical HRV assessment (Shaffer et al., 2014) and achieve greater predictive power than short-term measurements (Bigger et al., 1989; Fei et al., 1996; Nolan et al., 1998; Kleiger et al., 2005). However, increased HRV may correspond to longer recordings instead of the change of ANS function, and it is inappropriate to compare metrics like SDNN when they are calculated from epochs of different length (Saul et al., 1988; Task Force of the European Society of Cardiology the North American Society of Pacing Electrophysiology, 1996). Meanwhile, since mechanisms responsible for heart period modulations of a certain frequency, especially LF and HF power components, may not remain unchanged during long-term recording (Furlan et al., 1990), the interpretation of the results of frequency analysis is less well defined, and they may obscure the detailed information about autonomic modulation of RR intervals that is available in shorter recordings (Task Force of the European Society of Cardiology the North American Society of Pacing Electrophysiology, 1996).

In this study, surrogate tests (Porta et al., 2000a) was applied to all the HRV sequences analysed. The percentages of non-linear dynamics were: 1) 86.05% in 24-h HRV sequences; 2) 90.70% during awake period, and 39.53% during sleep period; 3) 52.63% during stable sleep, 55.26% during unstable sleep, and 68.42% during REM sleep. Therefore, non-linear dynamics in HRV sequences decreased during sleep, possibly due to the suppression of regulation of respiratory rhythm (Mador and Tobin, 1991; González et al., 2000; Francis et al., 2002; Jo et al., 2005), leading to stable patterns. And when HRV sequences were segmented based on sleep stages, the percentage of non-linear dynamics elevated, suggesting better manifestation of the non-linear components in HRV sequences during sleep cycles and demonstrating the effectiveness of non-linear analysis. Additionally, the distribution of non-linear features during different sleep stages, that the maximum of non-linear dynamics appeared during REM sleep, was consistent with non-linear respiratory dynamics (Sako et al., 2001).

However, researchers have found that in the analysis of short-term, stationary and successive HRV sequences, non-linear model-free and linear model-based conditional entropy correlate closely and have similar performance in the assessment of cardiac control (Porta et al., 2017). The conflicting conclusions may be a consequence of differences in stationary and non-linear features of HRV sequences utilized in analysis (Magagnin et al., 2011). Previous study has shown that short-term HRV in healthy young adults at rest is mainly linear (Porta et al., 2007b), while in this study HRV sequences during sleep cycles were mainly non-stationary and had non-linear features, demonstrating that the performance of non-linear analysis is related to the feature of HRV sequences.

Sleep rhythm based HRV analysis presents us significant correlations between ANS and metabolic function of T2DM patients covered by limitations of traditional measures, demonstrating its efficiency on distinguishing potential dynamic characteristics of ANS function and its correlation with metabolic function in different sleep stages. Hence, by analysing the correlation between ANS function patterns and metabolic function of T2DM patients, our findings propose a promising strategy for the evaluation of T2DM patients' metabolic function and physical condition to improve the early prevention, post-diagnosis and management of T2DM and its complications based on HRV analysis during sleep cycles.

Significant correlations were found among DBP and HRV metrics during sleep (see Table 5), and non-linear HRV metrics during sleep cycles significantly correlated with DBP with distinct distribution patterns (see Table 6), suggesting strong association between cardiac baroreflex control and the fluctuation of HRV metrics, especially non-linear ones, in T2DM patients. According to the SBP (136 ± 14 mmHg) and DBP (85 ± 11 mmHg) of the study cohort shown in Table 1 and "*Clinical practice guidelines for the management of hypertension in China*" (National Center for Cardiovascular Diseases et al., 2022), plenty of the subjects had hypertension of varying degrees, suggesting impairment of cardiac baroreflex control, associated with impairment of ANS and the presence of other neuropathies (Frattola et al., 1997; Tank et al., 2001; Ruiz et al., 2005; Vinik and Ziegler, 2007), which may be the effect of T2DM on baroreflex control through an impairment of vagal control (de Moura-Tonello et al., 2016), and the significant correlations support the finding that cardiovascular variability indexes are sensitive to autonomic dysfunction in T2DM patients in early stages (de Moura-Tonello et al., 2016). These findings demonstrate the effectiveness of non-linear HRV analysis and promising strategies for the early detection of autonomic dysfunction.

ANS plays an important role in the exchange of metabolic information between organs and regulation on peripheral metabolism (Yamada and Katagiri, 2007). In addition to affecting the activity of ANS, sleep also exerts a significant regulatory effect on glycemic control by influencing the balance and levels of hormones including leptin, growth hormone-releasing peptide, insulin and cortisol (Balbo et al., 2010), which enhances the association between HRV metrics during sleep and glycemic control of T2DM patients. Researchers have found that

24-h HRV metrics in time- and frequency-domain significantly decrease in T2DM patients with good glycemic control (HbA1c < 7.0%) and poor glycemic control (HbA1c > 7.0%), compared to healthy controls (Yu et al., 2020).

In this study, significant associations were only found between MSE complexity during sleep period and HbA1c, and significant group differences between subjects that had poor control of diabetes (HbA1c ≥ 9.0%, n = 10) and did not (HbA1c < 9.0%, n = 16) were observed in many non-linear metrics during unstable and stable sleep. Moreover, non-linear HRV metrics during sleep were significantly associated with FBG level, which is one of the important indicators for glycemic compliance (Association, 2013). The results indicates that non-linear HRV metrics during sleep may better manifest neuronal dysfunction caused by hyperglycemia, which induces oxidative stress and toxic glycosylation products (Pop-Busui, 2010), highlighting the importance of non-linear analysis during sleep.

Interestingly, higher HbA1c level was associated with higher entropy related metrics (see Table 8), the elevation of complexity may indicate worse metabolic function due to poor diabetic control (Costa et al., 2005). Additionally, in each sleep stage, the correlations between non-linear HRV metrics and FBG changed significantly before and after hospitalization, possibly due to the immediate impact of hospitalization on blood glucose control, reflecting the sensitivity of non-linear HRV assessment on glycemic control.

Due to the complex interaction among sleep, diabetic control and ANS function that sleep have a significant effect on both ANS and metabolic function, especially glycemic control of T2DM patients (Koren et al., 2011; Jordan et al., 2014; Kent et al., 2014; Martyn-Nemeth et al., 2018; Hur et al., 2020), partial correlation analysis was required to manifest the association between non-linear HRV metrics in sleep stages and glycemic control indicators clearly. With the nullification of sleep quality metrics, most of the correlations retained, which supported the significant correlations acquired by simple correlation analysis. Whereas the association significantly decreased or even vanished when TST was corrected, indicating the significant role of sleep quality in adjusting ANS and glycemic function of T2DM patients (Jordan et al., 2014; Martyn-Nemeth et al., 2018). Additionally, when stable sleep related metrics, especially SST, were nullified, the correlation between non-linear HRV metrics in sleep stages and glycemic control indicators significantly strengthened, demonstrating the functional significance of stable sleep stage. As well as stable sleep stage (slow wave sleep) is widely recognized as the most restorative of all sleep stages (Van Cauter et al., 2008) and when several important physiological activities occur specifically (Somers et al., 1993), researchers have found that stable sleep associates with brain glucose metabolism (Zoccoli et al., 2002) and suppression of stable sleep without any reduction in TST associates with poor diabetic control and increased risk of T2DM (Tasali et al., 2008).

In our original study, we also used RR interval time series from four time periods (late night, 3:00–4:00; dawn, 6:00–7:00; after lunch, 13:00–14:00; after dinner, 19:00–20:00) to perform HRV analysis and correlation analysis with metabolic indicators (see Supplementary Table S4–S7). Although distinct correlations were found between HRV metrics and metabolic functions during specific time periods, such as correlations between HRV and BUN, DBP or Hb at dawn, between HRV and HDL-C or LDL-C after lunch, and between metabolic indicators and LF/HF or LFP after dinner, the overall results were not satisfactory and systematic enough to be included in the main text. This may be due to the different physiological states of individuals at specific time periods and is influenced by meals and daytime activities.

To the best of our knowledge, few studies have applied time-, frequency-domain and non-linear analysis on HRV sequences in each sleep stage to inquire the association among ANS function, sleep cycle and metabolic function. We compared our results with those of using traditional methods in all-night sleep analysis and short-term linear HRV analysis. Representative results are shown in Table 11 in summary. In comparison with studies of correlations between all-night sleep and metabolic function, conducted among subjects without T2DM (Koren et al., 2011; Martyn-Nemeth et al., 2018; Feng et al., 2021), correlations found in this study were extensively stronger and broadened with a similar or notably smaller sample size. In comparison with studies of correlations between short-term linear HRV analysis and metabolic function, conducted among T2DM patients (Bhati et al., 2019), correlations found in this study were extensively stronger and broadened with a similar sample size, suggesting the potential of HRV analysis during sleep cycles in T2DM patients. However, when compared with a study with larger sample size (Balikai et al., 2022), correlations found in this study were more comprehensive but slightly weaker, which may be due to the limited sample size, exclusion of female subjects, differences in the physiological status of the subjects including duration and severity of diabetes since our subjects were all patients during hospitalization, the bias introduced by non-linear metrics including ApEn and MSE *via* the contamination of variance and suboptimal filtering procedure (Pincus and Huang, 1992; Nikulin and Brismar, 2004; Porta et al., 2007a; Valencia et al., 2009; Delgado-Bonal and Marshak, 2019) and the selection of long-term HRV sequences since metrics including LF, HF and SDNN would be affected by length of the sequences (Saul et al., 1988; Furlan et al., 1990; Task Force of the European Society of Cardiology the North American Society of Pacing Electrophysiology, 1996).

Therefore, this study provides new insights into research on the interaction among sleep, ANS and metabolic function, for T2DM patients, especially for diabetic control. Researchers have found that the dysfunction of T2DM patients' ANS manifests first in decreased parasympathetic activity (Pfeifer et al., 1982; Singh et al., 2000; Goit et al., 2012), even before clinical symptoms. The effective use of HRV analysis during sleep cycles to extract dynamic features of PNS and SNS in each sleep stage provides support for early detection of autonomic neuropathy. In addition, the extensively strong correlations between non-linear HRV metrics and glycemic control indicators including FBG and HbA1c demonstrates the validity of HRV analysis in each sleep stage, which can be another promising strategy for diabetic control and early diagnose of T2DM with less computational costs.

For further research, this study proposed to select HRV sequences based on physiological rhythms can locally reveal the dynamic features of HRV and magnify the potential biological origins and kinetic mechanisms of HRV under the influence of many external factors, such as respiration, circadian rhythm, sympathetic and vagal activity, as well as intrinsic factors, such as ion channel fluctuations and other molecular fluctuations, while

TABLE 11 Comparison of related studies on the interactions among sleep, HRV and metabolic function: subjects, methods, results and conclusion.

	Subjects	Method	Results	Conclusion
Martyn-Nemeth et al., (2018)	48 T1DM patients.	Group difference analysis on glycemic control according to the PSQI score (≤5 for good sleep quality and > 5 for poor sleep quality).	Poor sleep quality associated with greater nocturnal glycemic variability (p = 0.02). HbA1c did not vary between sleep quality groups.	Nocturnal glycemic variability associated with poor sleep quality.
Koren et al. (2011)	62 obese pubertal adolescents.	Analysis on the correlations between sleep architecture through overnight polysomnography, glucose and insulin homeostasis.	Significant associations between sleep duration and HbA1c (TST, r = −0.36, p < 0.01; REM duration, r = −0.35, p < 0.01) and fasting plasma glucose (N3 duration, r = −0.33, p < 0.01; REM duration, r = −0,31, p < 0.017).	There were significant relationships between sleep architecture and measures of glucose homeostasis and insulin secretion.
Feng et al. (2021)	2,308 suspected OSA patients.	Analysis on the correlations between sleep architecture through overnight polysomnography andclinical indicators (glucose, insulin, blood pressure, TG, HDL-C and LDL-C).	Significant weak correlations were found between SWS/TST ratio and BMI (r = −0.12, p < 0.01); between sleep efficiency and BMI (r = 0.11, p < 0.01); between MAI and BMI (r = 0.23, p < 0.01), glucose (r = 0.15, p < 0.01), insulin (r = 0.23, p < 0.01), DBP (r = 0.14, p < 0.01), TC (r = 0.13, p < 0.01), TG (r = 0.15, p < 0.01), LDL (r = 0.18, p < 0.01).	Only weak associations were observed between sleep and clinical indicators.
Bhati et al. (2019)	50 T2DM patients.	Analysis on the correlations between cardiac autonomic control evaluated by time-frequency domain HRV of 5-min ECG recorded after a rest period in the supine position and clinical indicators of inflammatory (IL-6, IL-18 and hsCRP) and endothelial function (NO, eNOS and ET-1).	Significant associations were found between IL-6 and TP (r = −0.34, p = 0.01), LF (r = −0.36, p < 0.01); between IL-18 and pNN50 (r = −0.53, p < 0.01), HF (r = −0.34, p < 0.05); between hsCRP and RMSSD (r = −0.40, p < 0.01), TP (r = −0.35, p = 0.01), LF (r = −0.31, p < 0.05), HF (r = −0.42, p < 0.01); between NO and RMSSD (r = 0.65, p < 0.001), TP (r = 0.30, p < 0.05), HF(r = 0.32, p < 0.05); between eNOS and RMSSD (r = 0.43, p < 0.01). Whereas, ET-1 is not associated with any HRV indices.	Clinical indicators of inflammation and endothelial function are associated with global HRV, suggesting pathophysiological link between subclinical inflammation, endothelial dysfunction and cardiac autonomic dysfunction in T2DM.
Balikai et al. (2022)	120 T2DM patients.	Analysis on the correlations between one-minute HRV time-frequency domain indices during forced deep breathing and fasting serum HDL levels.	Significant correlations were observed between HDL and Mean HR (r = 0.74, p < 0.001), LFnu (relative power in normal units, r = −0.62, p < 0.001) and ratio of LF/HF (r = 0.53, p < 0.001); between HDL and HFnu (relative power in normal units, r = 0.64, p < 0.001), SDNN (r = 0.75, p < 0.001), RMSSD (r = 0.63, p < 0.001) and pNN50 (r = 0.82, p < 0.001).	HDL-C level and all other HRV indices are dependent on each other in patients with T2DM. And most of the patients with low HDL-C level might be associated with autonomic imbalance.
Our study	64 T2DM patients	Analysis on the correlations between sleep quality, 24-h/awake/sleep/sleep staging HRV and clinical indicators of metabolic function.	Significant correlations were found between sleep quality and metabolic function (admission FBG, DBP, WBC, Hb, ALT, AST/ALT, BUN, UA, TG, HDL-C, LDL-C, UACR, $\|r\|$ = 0.386 ± 0.062, p < 0.05); HRV derived ANS function showed strengthened correlations with metabolic function during sleep period (admission FBG, DBP, Hb, ALT, AST/ALT, GGT, BUN, UACR, $\|r\|$ = 0.474 ± 0.100, p < 0.05); non-linear HRV metrics during sleep stages coupled more tightly with clinical indicators of metabolic function than linear analysis (HbA1c, DBP, N%, Hb, ALT, AST, AST/ALT, GGT, BUN, LDL-C, UMA, UACR, $\|r\|$ = 0.462 ± 0.086, p < 0.05), and showed significant association with glycemic control.	HRV metrics during sleep period plays more distinct role than during awake period in investigating ANS dysfunction and metabolism in T2DM patients, and sleep rhythm based HRV analysis should perform better in ANS and metabolic function assessment, especially for glycemic control in non-linear analysis among T2DM patients.

reducing the computational cost and elevating local resolution of long term signals, providing new insights into long term physiological signal processing.

There are several potential limitations of this study. Mainly middle-aged male inpatients were included in the analysis, who do not represent the whole spectrum of T2DM patients, to eliminate the influence of climacterium on metabolic function. Although we did a further outlier rejection to reduce the influences of specific situations, there are still diversities between people with different physiological factors (age, gender, health status, course of disease, etc.) that were not included in this study, requiring further studies. Despite of the non-linear dynamics in HRV sequences appeared in our study, researchers have found that short-term heart period variability in healthy young adults at rest is mainly linear (Porta et al., 2007b). Since there weren't thorough restrictions on subjects' daily behaviour during hospitalization, further studies are required to investigate the production of non-linear components in long-term HRV sequences by applying forcing input to subjects. Lastly, due to the limited sample size, we did not build more accurate statistical models of HRV, ANS, sleep and metabolic function to further investigate their potential biological origins and kinetic mechanisms.

Data availability statement

The raw data supporting the conclusion of this article will be made available by the authors, without undue reservation.

Ethics statement

The studies involving human participants were reviewed and approved by the Institutional Review Board of Suzhou Science & Technology Town Hospital (No. IRB2019045). The patients/participants provided their written informed consent to participate in this study.

Author contributions

WC, LT, and XC conceived and designed the study. WC and HC performed the experiment and analyzed the data. WC and HC drafted the manuscript. XC and ZM supervised the analysis, reviewed and editing the manuscript. All authors contributed to the article and approved the submitted version.

Funding

This work was supported in part by National Key Research and Development Program of China under Grant 2018YFC2001100, in part by the National Natural Science Foundation of China under Grant 82274631, 61807007.

Acknowledgments

The authors thank all the subjects participated in this study, and the members from Suzhou Science & Technology Town Hospital for helping with data collection.

Conflict of interest

The authors declare that the research was conducted in the absence of any commercial or financial relationships that could be construed as a potential conflict of interest.

Publisher's note

Supplementary material

The Supplementary Material for this article can be found online at: https://www.frontiersin.org/articles/10.3389/fphys.2023.1157270/full#supplementary-material

References

Akselrod, S., Gordon, D., Ubel, F. A., Shannon, D. C., Berger, A. C., and Cohen, R. J. (1981). Power spectrum analysis of heart rate fluctuation: A quantitative probe of beat-to-beat cardiovascular control. *Science* 213(4504), 220–222. doi:10.1126/science.6166045

Association, A. D. (2013). Diagnosis and classification of diabetes mellitus. *Diabetes Care* 37 (1), S81–S90. doi:10.2337/dc14-S081

Azami, H., and Escudero, J. (2016). *Matlab codes for "refined multiscale fuzzy entropy based on standard deviation for biomedical signal analysis*. University of Edinburgh, School of Engineering, Institute for Digital Communications.

Balbo, M., Leproult, R., and Van Cauter, E. (2010). Impact of sleep and its disturbances on hypothalamo-pituitary-adrenal Axis activity. *Int. J. Endocrinol.* 2010, 759234. doi:10.1155/2010/759234

Balcıoğlu, A. S., and Müderrisoğlu, H. (2015). Diabetes and cardiac autonomic neuropathy: Clinical manifestations, cardiovascular consequences, diagnosis and treatment. *World J. Diabetes* 6 (1), 80–91. doi:10.4239/wjd.v6.i1.80

Balikai, F. A., Javali, S. B., Shindhe, V. M., Deshpande, N., Benni, J. M., Shetty, D. P., et al. (2022). Correlation of serum HDL level with HRV indices using multiple linear regression analysis in patients with type 2 diabetes mellitus. *Diabetes Res. Clin. Pract.* 190, 109988. doi:10.1016/j.diabres.2022.109988

Barone, M. T. U., and Menna-Barreto, L. (2011). Diabetes and sleep: A complex cause-and-effect relationship. *Diabetes Res. Clin. Pract.* 91 (2), 129–137. doi:10.1016/j.diabres.2010.07.011

Bhati, P., Alam, R., Moiz, J. A., and Hussain, M. E. (2019). Subclinical inflammation and endothelial dysfunction are linked to cardiac autonomic neuropathy in type 2 diabetes. *J. Diabetes & Metabolic Disord.* 18 (2), 419–428. doi:10.1007/s40200-019-00435-w

Bigger, J. T., Jr., Albrecht, P., Steinman, R. C., Rolnitzky, L. M., Fleiss, J. L., and Cohen, R. J. (1989). Comparison of time- and frequency domain-based measures of cardiac parasympathetic activity in Holter recordings after myocardial infarction. *Am. J. Cardiol.* 64 (8), 536–538. doi:10.1016/0002-9149(89)90436-0

Brandenberger, G., Ehrhart, J., Piquard, F., and Simon, C. (2001). Inverse coupling between ultradian oscillations in delta wave activity and heart rate variability during sleep. *Clin. Neurophysiol.* 112 (6), 992–996. doi:10.1016/S1388-2457(01)00507-7

Buysse, D. J., Reynolds, C. F., Monk, T. H., Berman, S. R., and Kupfer, D. J. (1989). The Pittsburgh sleep quality index: A new instrument for psychiatric practice and research. *Psychiatry Res.* 28 (2), 193–213. doi:10.1016/0165-1781(89)90047-4

Cerutti, S., Esposti, F., Ferrario, M., Sassi, R., and Signorini, M. G. (2007). Long-term invariant parameters obtained from 24-h holter recordings: A comparison between different analysis techniques. *Chaos An Interdiscip. J. Nonlinear Sci.* 17 (1), 015108. doi:10.1063/1.2437155

Chen, W., Zhuang, J., Yu, W., and Wang, Z. (2009). Measuring complexity using FuzzyEn, ApEn, and SampEn. *Med. Eng. Phys.* 31 (1), 61–68. doi:10.1016/j.medengphy.2008.04.005

Cooke, W. H., Hoag, J. B., Crossman, A. A., Kuusela, T. A., Tahvanainen, K. U. O., and Eckberg, D. L. (1999). Human responses to upright tilt: A window on central autonomic integration. *J. Physiology* 517 (2), 617–628. doi:10.1111/j.1469-7793.1999.0617t.x

Costa, M., Goldberger, A. L., and Peng, C. K. (2005). Multiscale entropy analysis of biological signals. *Phys. Rev. E* 71 (2), 021906. doi:10.1103/PhysRevE.71.021906

Costa, M., Goldberger, A. L., and Peng, C. K. (2002). Multiscale entropy analysis of complex physiologic time series. *Phys. Rev. Lett.* 89 (6), 068102. doi:10.1103/PhysRevLett.89.068102

Cui, X., Tian, L., Li, Z., Ren, Z., Zha, K., Wei, X., et al. (2020). On the variability of heart rate variability—evidence from prospective study of healthy young college students. *Entropy* 22 (11), 1302. doi:10.3390/e22111302

Cuschieri, S. (2019). The STROBE guidelines. *Saudi J. Anaesth.* 13 (1), S31–s34. doi:10.4103/sja.SJA_543_18

Cysarz, D., Bettermann, H., and Leeuwen, P. v. (2000). Entropies of short binary sequences in heart period dynamics. *Am. J. Physiology-Heart Circulatory Physiology* 278 (6), H2163–H2172. doi:10.1152/ajpheart.2000.278.6.H2163

de Moura-Tonello, S. C. G., Porta, A., Marchi, A., de Almeida Fagundes, A., Francisco, C. d. O., Rehder-Santos, P., et al. (2016). Cardiovascular variability analysis and baroreflex estimation in patients with type 2 diabetes in absence of any manifest neuropathy. *PLOS ONE* 11 (3), e0148903. doi:10.1371/journal.pone.0148903

de Zambotti, M., Trinder, J., Silvani, A., Colrain, I. M., and Baker, F. C. (2018). Dynamic coupling between the central and autonomic nervous systems during sleep: A review. *Neurosci. Biobehav. Rev.* 90, 84–103. doi:10.1016/j.neubiorev.2018.03.027

Delgado-Bonal, A., and Marshak, A. (2019). Approximate entropy and sample entropy: A comprehensive tutorial. *Entropy* 21 (6), 541. doi:10.3390/e21060541

Dohare, A. K., Kumar, V., and Kumar, R. (2014). An efficient new method for the detection of QRS in electrocardiogram. *Comput. Electr. Eng.* 40 (5), 1717–1730. doi:10.1016/j.compeleceng.2013.11.004

Faust, O., Acharya, U. R., Molinari, F., Chattopadhyay, S., and Tamura, T. (2012). Linear and non-linear analysis of cardiac health in diabetic subjects. *Biomed. Signal Process. Control* 7 (3), 295–302. doi:10.1016/j.bspc.2011.06.002

Fei, L., Copie, X., Malik, M., and Camm, A. J. (1996). Short- and long-term assessment of heart rate variability for risk stratification after acute myocardial infarction. *Am. J. Cardiol.* 77 (9), 681–684. doi:10.1016/S0002-9149(97)89199-0

Feng, N., Yang, J., Xu, H., Zhang, C., Wang, F., Wu, X., et al. (2021). The associations between sleep architecture and metabolic parameters in patients with obstructive sleep apnea: A hospital-based cohort study. *Front. Neurology* 12, 606031. doi:10.3389/fneur.2021.606031

Francis, D. P., Willson, K., Georgiadou, P., Wensel, R., Davies, L. C., Coats, A., et al. (2002). Physiological basis of fractal complexity properties of heart rate variability in man. *J. Physiology* 542 (2), 619–629. doi:10.1113/jphysiol.2001.013389

Frattola, A., Parati, G., Gamba, P., Paleari, F., Mauri, G., Di Rienzo, M., et al. (1997). Time and frequency domain estimates of spontaneous baroreflex sensitivity provide early detection of autonomic dysfunction in diabetes mellitus. *Diabetologia* 40 (12), 1470–1475. doi:10.1007/s001250050851

Furlan, R., Guzzetti, S., Crivellaro, W., Dassi, S., Tinelli, M., Baselli, G., et al. (1990). Continuous 24-hour assessment of the neural regulation of systemic arterial pressure and RR variabilities in ambulant subjects. *Circulation* 81(2), 537–547. doi:10.1161/01.CIR.81.2.537

Garber, A. J., Handelsman, Y., Grunberger, G., Einhorn, D., Abrahamson, M. J., Barzilay, J. I., et al. (2020). Consensus statement by the American association of clinical endocrinologists and American college of endocrinology on the comprehensive type 2 diabetes management algorithm – 2020 executive summary. *Endocr. Pract.* 26 (1), 107–139. doi:10.4158/CS-2019-0472

Gerritsen, J., Dekker, J. M., TenVoorde, B. J., Kostense, P. J., Heine, R. J., Bouter, L. M., et al. (2001). Impaired autonomic function is associated with increased mortality, especially in subjects with diabetes, hypertension, or a history of cardiovascular disease: The hoorn study. *Diabetes Care* 24 (10), 1793–1798. doi:10.2337/diacare.24.10.1793

Glos, M., Fietze, I., Blau, A., Baumann, G., and Penzel, T. (2014). Cardiac autonomic modulation and sleepiness: Physiological consequences of sleep deprivation due to 40h of prolonged wakefulness. *Physiology Behav.* 125, 45–53. doi:10.1016/j.physbeh.2013.11.011

Goit, R. K., Khadka, R., Sharma, S. K., Limbu, N., and Paudel, B. H. (2012). Cardiovascular autonomic function and vibration perception threshold in type 2 diabetes mellitus. *J. Diabetes its Complicat.* 26 (4), 339–342. doi:10.1016/j.jdiacomp.2012.03.026

González, J. J., Cordero, J. J., Feria, M., and Pereda, E. (2000). Detection and sources of nonlinearity in the variability of cardiac R-R intervals and blood pressure in rats. *Am. J. Physiology-Heart Circulatory Physiology* 279 (6), H3040–H3046. doi:10.1152/ajpheart.2000.279.6.H3040

Hamilton, P. S., and Tompkins, W. J. (1986). Quantitative investigation of QRS detection rules using the MIT/BIH arrhythmia database. *Ieee Trans. Biomed. Eng.* 33 (12), 1157–1165. doi:10.1109/tbme.1986.325695

Hur, M. H., Lee, M. K., Seong, K., and Hong, J. H. (2020). Deterioration of sleep quality according to glycemic status. *Diabetes & Metabolism J.* 44 (5), 679–686. doi:10.4093/dmj.2019.0125

Inzucchi, S. E., Bergenstal, R. M., Buse, J. B., Diamant, M., Ferrannini, E., Nauck, M., et al. (2015). Management of hyperglycemia in type 2 diabetes, 2015: A patient-centered approach: Update to a position statement of the American diabetes association and the European association for the study of diabetes. *Diabetes Care* 38 (1), 140–149. doi:10.2337/dc14-2441

Jo, J. A., Blasi, A., Valladares, E., Juarez, R., Baydur, A., and Khoo, M. C. K. (2005). Determinants of heart rate variability in obstructive sleep apnea syndrome during wakefulness and sleep. *Am. J. Physiology-Heart Circulatory Physiology* 288 (3), H1103–H1112. doi:10.1152/ajpheart.01065.2003

Johnson, A. E. W., Behar, J., Andreotti, F., Clifford, G. D., and Oster, J. (2015). Multimodal heart beat detection using signal quality indices. *Physiol. Meas.* 36 (8), 1665–1677. doi:10.1088/0967-3334/36/8/1665

Jordan, A. S., McSharry, D. G., and Malhotra, A. (2014). Adult obstructive sleep apnoea. *Lancet* 383 (9918), 736–747. doi:10.1016/s0140-6736(13)60734-5

Kent, B. D., Grote, L., Ryan, S., Pépin, J. L., Bonsignore, M. R., Tkacova, R., et al. (2014). Diabetes mellitus prevalence and control in sleep-disordered breathing: The European sleep apnea cohort (ESADA) study. *Chest* 146 (4), 982–990. doi:10.1378/chest.13-2403

Kleiger, R. E., Stein, P. K., and Bigger, J. T., Jr. (2005). Heart rate variability: Measurement and clinical utility. *Ann. Noninvasive Electrocardiol.* 10 (1), 88–101. doi:10.1111/j.1542-474X.2005.10101.x

Koren, D., Levitt Katz, L. E., Brar, P. C., Gallagher, P. R., Berkowitz, R. I., and Brooks, L. J. (2011). Sleep architecture and glucose and insulin homeostasis in obese adolescents. *Diabetes Care* 34 (11), 2442–2447. doi:10.2337/dc11-1093

Laborde, S., Mosley, E., and Thayer, J. F. (2017). Heart rate variability and cardiac vagal tone in psychophysiological research – recommendations for experiment planning, data analysis, and data reporting. *Front. Psychol.* 8, 213. doi:10.3389/fpsyg.2017.00213

Leproult, R., Copinschi, G., Buxton, O., and Van Cauter, E. (1997). Sleep loss results in an elevation of cortisol levels the next evening. *Sleep* 20 (10), 865–870. doi:10.1093/sleep/20.10.865

Li, F., and Yang, H. (2013). A real-time QRS complex detection algorithm based on composite filter and curve feature point extraction. *Comput. Appl. Softw.* 30 (11).

Liu, S.-H., Lo, L.-W., Tsai, T.-Y., Cheng, W.-H., Lin, Y.-J., Chang, S.-L., et al. (2020). Circadian rhythm dynamics on multiscale entropy identifies autonomic dysfunction associated with risk of ventricular arrhythmias and near syncope in chronic kidney disease. *J. Cardiol.* 76 (6), 542–548. doi:10.1016/j.jjcc.2020.05.017

Lombardi, F., and Stein, P. K. (2011). Origin of heart rate variability and turbulence: An appraisal of autonomic modulation of cardiovascular function. *Front. Physiology* 2, 95. doi:10.3389/fphys.2011.00095

López-Cano, C., Gutiérrez-Carrasquilla, L., Sánchez, E., González, J., Yeramian, A., Martí, R., et al. (2019). Sympathetic hyperactivity and sleep disorders in individuals with type 2 diabetes. *Front. Endocrinol.* 10, 752. doi:10.3389/fendo.2019.00752

Mador, M. J., and Tobin, M. J. (1991). Effect of alterations in mental activity on the breathing pattern in healthy subjects. *Am. Rev. Respir. Dis.* 144 (3), 481–487. doi:10.1164/ajrccm/144.3_Pt_1.481

Magagnin, V., Bassani, T., Bari, V., Turiel, M., Maestri, R., Pinna, G. D., et al. (2011). Non-stationarities significantly distort short-term spectral, symbolic and entropy heart rate variability indices. *Physiol. Meas.* 32 (11), 1775–1786. doi:10.1088/0967-3334/32/11/S05

Malliani, A., Pagani, M., Lombardi, F., and Cerutti, S. (1991). Cardiovascular neural regulation explored in the frequency domain. *Circulation* 84(2), 482–492. doi:10.1161/01.CIR.84.2.482

Marcheva, B., Ramsey, K. M., Buhr, E. D., Kobayashi, Y., Su, H., Ko, C. H., et al. (2010). Disruption of the clock components CLOCK and BMAL1 leads to hypoinsulinaemia and diabetes. *Nature* 466 (7306), 627–631. doi:10.1038/nature09253

Markwald, R. R., Melanson, E. L., Smith, M. R., Higgins, J., Perreault, L., Eckel, R. H., et al. (2013). Impact of insufficient sleep on total daily energy expenditure, food intake, and weight gain. *Proc. Natl. Acad. Sci.* 110(14), 5695–5700. doi:10.1073/pnas.1216951110

Markwald, R. R., and Wright, K. P. (2012). "Circadian misalignment and sleep disruption in shift work: Implications for fatigue and risk of weight gain and obesity," in *Sleep loss and obesity: Intersecting epidemics*. Editors P. Shiromani, T. Horvath, S. Redline, and E. Van Cauter (New York, NY: Springer New York), 101–118.

Martelli, D., Silvani, A., McAllen, R. M., May, C. N., and Ramchandra, R. (2014). The low frequency power of heart rate variability is neither a measure of cardiac sympathetic tone nor of baroreflex sensitivity. *Am. J. Physiology-Heart Circulatory Physiology* 307 (7), H1005–H1012. doi:10.1152/ajpheart.00361.2014

Martyn-Nemeth, P., Phillips, S. A., Mihailescu, D., Farabi, S. S., Park, C., Lipton, R., et al. (2018). Poor sleep quality is associated with nocturnal glycaemic variability and fear of hypoglycaemia in adults with type 1 diabetes. *J. Adv. Nurs.* 74 (10), 2373–2380. doi:10.1111/jan.13765

Maser, R. E., Mitchell, B. D., Vinik, A. I., and Freeman, R. (2003). The association between cardiovascular autonomic neuropathy and mortality in individuals with diabetes: A meta-analysis. *Diabetes Care* 26 (6), 1895–1901. doi:10.2337/diacare.26.6.1895

Montano, N., Porta, A., Cogliati, C., Costantino, G., Tobaldini, E., Casali, K. R., et al. (2009). Heart rate variability explored in the frequency domain: A tool to investigate the link between heart and behavior. *Neurosci. Biobehav. Rev.* 33 (2), 71–80. doi:10.1016/j.neubiorev.2008.07.006

Mosenzon, O., Pollack, R., and Raz, I. (2016). Treatment of type 2 diabetes: From "guidelines" to "position statements" and back: Recommendations of the Israel national diabetes council. *Diabetes Care* 39 (2), S146–S153. doi:10.2337/dcS15-3003

National Center for Cardiovascular Diseases, Chinese medical doctor association, hypertension committee of Chinese medical doctor association, Chinese society of Cardiology, Chinese medical association,, and hypertension committee of cross-straits medical exchanges association (2022). clinical practice guidelines for the management of hypertension in China. *Chin. J. Cardiol.* 50, 1050–1095. doi:10.3760/cma.j.cn112148-20220809-00613

Nguyen, J., and Wright, K. P., Jr. (2010). Influence of weeks of circadian misalignment on leptin levels. *Nat. Sci. Sleep.* 2, 9–18. doi:10.2147/nss.s7624

Nikulin, V. V., and Brismar, T. (2004). Comment on "Multiscale entropy analysis of complex physiologic time series". *Phys. Rev. Lett.* 92 (8), 089803. author reply 089804. doi:10.1103/PhysRevLett.92.089803

Nolan, J., Batin, P. D., Andrews, R., Lindsay, S. J., Brooksby, P., Mullen, M., et al. (1998). Prospective study of heart rate variability and mortality in chronic heart failure: Results of the United Kingdom heart failure evaluation and assessment of risk trial (UK-heart). *Circulation* 98(15), 1510–1516. doi:10.1161/01.CIR.98.15.1510

Nunan, D., Sandercock, G. R. H., and Brodie, D. A. (2010). A quantitative systematic review of normal values for short-term heart rate variability in healthy adults. *Pacing Clin. Electrophysiol.* 33 (11), 1407–1417. doi:10.1111/j.1540-8159.2010.02841.x

Pagani, M., Lombardi, F., Guzzetti, S., Rimoldi, O., Furlan, R., Pizzinelli, P., et al. (1986). Power spectral analysis of heart rate and arterial pressure variabilities as a marker of sympatho-vagal interaction in man and conscious dog. *Circulation Res.* 59(2), 178–193. doi:10.1161/01.RES.59.2.178

Pan, J., and Tompkins, W. J. (1985). A real-time QRS detection algorithm. *Ieee Trans. Biomed. Eng.* 32 (3), 230–236. doi:10.1109/tbme.1985.325532

Peng, C. K., Buldyrev, S. V., Havlin, S., Simons, M., Stanley, H. E., and Goldberger, A. L. (1994). Mosaic organization of DNA nucleotides. *Phys. Rev. E* 49 (2), 1685–1689. doi:10.1103/PhysRevE.49.1685

Peng, C. K., Havlin, S., Stanley, H. E., and Goldberger, A. L. (1995). Quantification of scaling exponents and crossover phenomena in nonstationary heartbeat time series. *Chaos An Interdiscip. J. Nonlinear Sci.* 5 (1), 82–87. doi:10.1063/1.166141

Perkiömäki, J. (2011). Heart rate variability and non-linear dynamics in risk stratification. *Front. Physiology* 2, 81. doi:10.3389/fphys.2011.00081

Pfeifer, M. A., Cook, D., Brodsky, J., Tice, D., Reenan, A., Swedine, S., et al. (1982). Quantitative evaluation of cardiac parasympathetic activity in normal and diabetic man. *Diabetes* 31 (4), 339–345. doi:10.2337/diab.31.4.339

Pincus, S. M. (1991). Approximate entropy as a measure of system complexity. *Proc. Natl. Acad. Sci.* 88(6), 2297–2301. doi:10.1073/pnas.88.6.2297

Pincus, S. M., Cummins, T. R., and Haddad, G. G. (1993). Heart rate control in normal and aborted-SIDS infants. *Am. J. Physiology-Regulatory, Integr. Comp. Physiology* 264 (3), R638–R646. doi:10.1152/ajpregu.1993.264.3.R638

Pincus, S. M., and Huang, W.-M. (1992). Approximate entropy: Statistical properties and applications. *Commun. Statistics - Theory Methods* 21 (11), 3061–3077. doi:10.1080/03610929208830963

Pop-Busui, R. (2010). Cardiac autonomic neuropathy in diabetes: A clinical perspective. *Diabetes Care* 33 (2), 434–441. doi:10.2337/dc09-1294

Porta, A., Baselli, G., Guzzetti, S., Pagani, M., Malliani, A., and Cerutti, S. (2000a). Prediction of short cardiovascular variability signals based on conditional distribution. *IEEE Trans. Biomed. Eng.* 47 (12), 1555–1564. doi:10.1109/10.887936

Porta, A., Gnecchi-Ruscone, T., Tobaldini, E., Guzzetti, S., Furlan, R., and Montano, N. (2007a). Progressive decrease of heart period variability entropy-based complexity during graded head-up tilt. *J. Appl. Physiology* 103 (4), 1143–1149. doi:10.1152/japplphysiol.00293.2007

Porta, A., Guzzetti, S., Furlan, R., Gnecchi-Ruscone, T., Montano, N., and Malliani, A. (2007b). Complexity and nonlinearity in short-term heart period variability: Comparison of methods based on local nonlinear prediction. *IEEE Trans. Biomed. Eng.* 54 (1), 94–106. doi:10.1109/TBME.2006.883789

Porta, A., Guzzetti, S., Montano, N., Furlan, R., Pagani, M., Malliani, A., et al. (2001). Entropy, entropy rate, and pattern classification as tools to typify complexity in short heart period variability series. *IEEE Trans. Biomed. Eng.* 48 (11), 1282–1291. doi:10.1109/10.959324

Porta, A., Guzzetti, S., Montano, N., Pagani, M., Somers, V., Malliani, A., et al. (2000b). Information domain analysis of cardiovascular variability signals: Evaluation of regularity, synchronisation and co-ordination. *Med. Biol. Eng. Comput.* 38 (2), 180–188. doi:10.1007/bf02344774

Porta, A., Maria, B. D., Bari, V., Marchi, A., and Faes, L. (2017). Are nonlinear model-free conditional entropy approaches for the assessment of cardiac control complexity superior to the linear model-based one? *IEEE Trans. Biomed. Eng.* 64 (6), 1287–1296. doi:10.1109/TBME.2016.2600160

Punjabi, N. M., and Polotsky, V. Y. (2005). Disorders of glucose metabolism in sleep apnea. *J. Appl. Physiology* 99 (5), 1998–2007. doi:10.1152/japplphysiol.00695.2005

Reyes del Paso, G. A., Langewitz, W., Mulder, L. J. M., van Roon, A., and Duschek, S. (2013). The utility of low frequency heart rate variability as an index of sympathetic cardiac tone: A review with emphasis on a reanalysis of previous studies. *Psychophysiology* 50 (5), 477–487. doi:10.1111/psyp.12027

Richman, J. S., and Moorman, J. R. (2000). Physiological time-series analysis using approximate entropy and sample entropy. *Am. J. Physiology-Heart Circulatory Physiology* 278 (6), H2039–H2049. doi:10.1152/ajpheart.2000.278.6.H2039

Ruiz, J., Monbaron, D., Parati, G., Perret, S., Haesler, E., Danzeisen, C., et al. (2005). Diabetic neuropathy is a more important determinant of baroreflex sensitivity than carotid elasticity in type 2 diabetes. *Hypertension* 46(1), 162–167. doi:10.1161/01.HYP.0000169053.14440.7d

Sako, T., Burioka, N., Suyama, H., Nomura, T., Takeshima, T., and Shimizu, E. (2001). Nonlinear behavior of human respiratory movement during different sleep stages. *Chronobiology Int.* 18 (1), 71–83. doi:10.1081/CBI-100001172

Sassi, R., Cerutti, S., Lombardi, F., Malik, M., Huikuri, H. V., Peng, C.-K., et al. (2015). Advances in heart rate variability signal analysis: Joint position statement by the e-cardiology ESC working group and the European heart rhythm association co-endorsed by the Asia pacific heart rhythm society. *EP Eur.* 17 (9), 1341–1353. doi:10.1093/europace/euv015

Saul, J. P., Albrecht, P., Berger, R. D., and Cohen, R. J. (1988). Analysis of long term heart rate variability: Methods, 1/f scaling and implications. *Comput. Cardiol.* 14, 419–422.

Scheer, F. A. J. L., Hilton, M. F., Mantzoros, C. S., and Shea, S. A. (2009). Adverse metabolic and cardiovascular consequences of circadian misalignment. *Proc. Natl. Acad. Sci.* 106(11), 4453–4458. doi:10.1073/pnas.0808180106

Scholz, U. J., Bianchi, A. M., Cerutti, S., and Kubicki, S. (1997). Vegetative background of sleep: Spectral analysis of the heart rate variability. *Physiology Behav.* 62 (5), 1037–1043. doi:10.1016/S0031-9384(97)00234-5

Schramm, P., Neville, A. G., Madison, S., Thomas, R. J., and Baker, D. N. (2009). Cardio-pulmonary coupling (CPC) measures correlate to standard sleep variables in a random clinical sample of patients suspected with sleep disordered breathing (SDB). *Sleep* 32, A189.

Shaffer, F., McCraty, R., and Zerr, C. L. (2014). A healthy heart is not a metronome: An integrative review of the heart's anatomy and heart rate variability. *Front. Psychol.* 5, 1040. doi:10.3389/fpsyg.2014.01040

Silvani, A., and Dampney, R. A. L. (2013). Central control of cardiovascular function during sleep. *Am. J. Physiology-Heart Circulatory Physiology* 305 (12), H1683–H1692. doi:10.1152/ajpheart.00554.2013

Singh, J. P., Larson, M. G., O'Donnell, C. J., Wilson, P. F., Tsuji, H., Lloyd-Jones, D. M., et al. (2000). Association of hyperglycemia with reduced heart rate variability (The Framingham Heart Study). *Am. J. Cardiol.* 86 (3), 309–312. doi:10.1016/s0002-9149(00)00920-6

Solnik, S., DeVita, P., Rider, P., Long, B., and Hortobágyi, T. (2008). Teager-Kaiser Operator improves the accuracy of EMG onset detection independent of signal-to-noise ratio. *Acta Bioeng. Biomech.* 10 (2), 65–68.

Somers, V. K., Dyken, M. E., Mark, A. L., and Abboud, F. M. (1993). Sympathetic-nerve activity during sleep in normal subjects. *N. Engl. J. Med.* 328 (5), 303–307. doi:10.1056/nejm199302043280502

Spiegel, K., Knutson, K., Leproult, R., Tasali, E., and Cauter, E. V. (2005). Sleep loss: A novel risk factor for insulin resistance and type 2 diabetes. *J. Appl. Physiology* 99 (5), 2008–2019. doi:10.1152/japplphysiol.00660.2005

Spiegel, K., Leproult, R., and Van Cauter, E. (1999). Impact of sleep debt on metabolic and endocrine function. *Lancet* 354 (9188), 1435–1439. doi:10.1016/S0140-6736(99)01376-8

Spiegel, K., Tasali, E., Leproult, R., Scherberg, N., and Van Cauter, E. (2011). Twenty-four-Hour profiles of acylated and total ghrelin: Relationship with glucose levels and impact of time of day and sleep. *J. Clin. Endocrinol. Metabolism* 96 (2), 486–493. doi:10.1210/jc.2010-1978

Spira, A. P., Beaudreau, S. A., Stone, K. L., Kezirian, E. J., Lui, L.-Y., Redline, S., et al. (2011). Reliability and validity of the Pittsburgh sleep quality index and the epworth sleepiness scale in older men. *Journals Gerontology Ser. A* 67A (4), 433–439. doi:10.1093/gerona/glr172

Stein, P. K., and Pu, Y. (2012). Heart rate variability, sleep and sleep disorders. *Sleep. Med. Rev.* 16 (1), 47–66. doi:10.1016/j.smrv.2011.02.005

Tank, J., Jordan, J., Neuke, A., Mölle, A., and Weck, M. (2001). Spontaneous baroreflex sensitivity and heart rate variability are not superior to classic autonomic testing in older patients with type 2 diabetes. *Am. J. Med. Sci.* 322 (1), 24–30. doi:10.1097/00000441-200107000-00005

Tasali, E., Leproult, R., Ehrmann, D. A., and Van Cauter, E. (2008). Slow-wave sleep and the risk of type 2 diabetes in humans. *Proc. Natl. Acad. Sci.* 105(3), 1044–1049. doi:10.1073/pnas.0706446105

Task Force of the European Society of Cardiology the North American Society of Pacing Electrophysiology (1996). Heart rate variability. *Circulation* 93(5), 1043–1065. doi:10.1161/01.CIR.93.5.1043

Thomas, R. J., Mietus, J. E., Peng, C.-K., and Goldberger, A. L. (2005). An electrocardiogram-based technique to assess cardiopulmonary coupling during sleep. *Sleep* 28 (9), 1151–1161. doi:10.1093/sleep/28.9.1151

Thomas, R. J., Mietus, J. E., Peng, C.-K., Goldberger, A. L., Crofford, L. J., and Chervin, R. D. (2010). Impaired sleep quality in fibromyalgia: Detection and quantification with ECG-based cardiopulmonary coupling spectrograms. *Sleep. Med.* 11 (5), 497–498. doi:10.1016/j.sleep.2009.09.003

Tobaldini, E., Costantino, G., Solbiati, M., Cogliati, C., Kara, T., Nobili, L., et al. (2017). Sleep, sleep deprivation, autonomic nervous system and cardiovascular diseases. *Neurosci. Biobehav. Rev.* 74, 321–329. doi:10.1016/j.neubiorev.2016.07.004

Tobaldini, E., Pecis, M., and Montano, N. (2014). Effects of acute and chronic sleep deprivation on cardiovascular regulation. *Arch. Ital. De. Biol.* 152 (2-3), 103–110. doi:10.12871/000298292014235

Trinder, J., Kleiman, J., Carrington, M., Smith, S., Breen, S., Tan, N., et al. (2001). Autonomic activity during human sleep as a function of time and sleep stage. *J. Sleep Res.* 10 (4), 253–264. doi:10.1046/j.1365-2869.2001.00263.x

Turek, F. W., Joshu, C., Kohsaka, A., Lin, E., Ivanova, G., McDearmon, E., et al. (2005). Obesity and metabolic syndrome in circadian *clock* mutant mice. *Science* 308(5724), 1043–1045. doi:10.1126/science.1108750

Valencia, J. F., Porta, A., Vallverdu, M., Claria, F., Baranowski, R., Orlowska-Baranowska, E., et al. (2009). Refined multiscale entropy: Application to 24-h holter recordings of heart period variability in healthy and aortic stenosis subjects. *IEEE Trans. Biomed. Eng.* 56 (9), 2202–2213. doi:10.1109/TBME.2009.2021986

Van Cauter, E., Spiegel, K., Tasali, E., and Leproult, R. (2008). Metabolic consequences of sleep and sleep loss. *Sleep. Med.* 9, S23–S28. doi:10.1016/S1389-9457(08)70013-3

VanCauter, E., Polonsky, K. S., and Scheen, A. J. (1997). Roles of circadian rhythmicity and sleep in human glucose regulation. *Endocr. Rev.* 18 (5), 716–738. doi:10.1210/er.18.5.716

Vinik, A. I., Maser, R. E., Mitchell, B. D., and Freeman, R. (2003). Diabetic autonomic neuropathy. *Diabetes Care* 26 (5), 1553–1579. doi:10.2337/diacare.26.5.1553

Vinik, A. I., and Ziegler, D. (2007). Diabetic cardiovascular autonomic neuropathy. *Circulation* 115(3), 387–397. doi:10.1161/CIRCULATIONAHA.106.634949

Voss, A., Kurths, J., Kleiner, H. J., Witt, A., Wessel, N., Saparin, P., et al. (1996). The application of methods of non-linear dynamics for the improved and predictive recognition of patients threatened by sudden cardiac death. *Cardiovasc Res.* 31 (3), 419–433. doi:10.1016/0008-6363(96)00008-9

Wessel, N., Ziehmann, C., Kurths, J., Meyerfeldt, U., Schirdewan, A., and Voss, A. (2000). Short-term forecasting of life-threatening cardiac arrhythmias based on symbolic dynamics and finite-time growth rates. *Phys. Rev. E* 61 (1), 733–739. doi:10.1103/PhysRevE.61.733

Yamada, T., and Katagiri, H. (2007). Avenues of communication between the brain and tissues/organs involved in energy homeostasis. *Endocr. J.* 54 (4), 497–505. doi:10.1507/endocrj.KR-106

Ye, S., Ruan, P., Yong, J., Shen, H., Liao, Z., and Dong, X. (2016). The impact of the HbA1c level of type 2 diabetics on the structure of haemoglobin. *Sci. Rep.* 6 (1), 33352. doi:10.1038/srep33352

Yeh, G. Y., Mietus, J. E., Peng, C.-K., Phillips, R. S., Davis, R. B., Wayne, P. M., et al. (2008). Enhancement of sleep stability with Tai Chi exercise in chronic heart failure: Preliminary findings using an ECG-based spectrogram method. *Sleep. Med.* 9 (5), 527–536. doi:10.1016/j.sleep.2007.06.003

Yu, Y., Hu, L., Xu, Y., Wu, S., Chen, Y., Zou, W., et al. (2020). Impact of blood glucose control on sympathetic and vagus nerve functional status in patients with type 2 diabetes mellitus. *Acta Diabetol.* 57 (2), 141–150. doi:10.1007/s00592-019-01393-8

Zhang, L., Wu, H., Zhang, X., Wei, X., Hou, F., and Ma, Y. (2020). Sleep heart rate variability assists the automatic prediction of long-term cardiovascular outcomes. *Sleep. Med.* 67, 217–224. doi:10.1016/j.sleep.2019.11.1259

Ziegler, D., Zentai, C. P., Perz, S., Rathmann, W., Haastert, B., Döring, A., et al. (2008). Prediction of mortality using measures of cardiac autonomic dysfunction in the diabetic and nondiabetic population: The MONICA/KORA augsburg cohort study. *Diabetes Care* 31 (3), 556–561. doi:10.2337/dc07-1615

Zoccoli, G., Walker, A. M., Lenzi, P., and Franzini, C. (2002). The cerebral circulation during sleep: Regulation mechanisms and functional implications. *Sleep. Med. Rev.* 6 (6), 443–455. doi:10.1053/smrv.2001.0194

frontiers | Frontiers in Neuroscience

TYPE Original Research
PUBLISHED 22 June 2023
DOI 10.3389/fnins.2023.1182607

OPEN ACCESS

EDITED BY
Vitor Engracia Valenti,
São Paulo State University, Brazil

REVIEWED BY
Neysa Aparecida Tinoco Regattieri,
University of Brasilia, Brazil
Mark Bolding,
University of Alabama at Birmingham,
United States

*CORRESPONDENCE
Leighton Barnden
l.barnden@griffith.edu.au

RECEIVED 09 March 2023
ACCEPTED 06 June 2023
PUBLISHED 22 June 2023

CITATION
Barnden L, Thapaliya K, Eaton-Fitch N, Barth M and Marshall-Gradisnik S (2023) Altered brain connectivity in Long Covid during cognitive exertion: a pilot study.
Front. Neurosci. 17:1182607.
doi: 10.3389/fnins.2023.1182607

Altered brain connectivity in Long Covid during cognitive exertion: a pilot study

Leighton Barnden[1]*, Kiran Thapaliya[1,2], Natalie Eaton-Fitch[1], Markus Barth[2,3] and Sonya Marshall-Gradisnik[1]

[1]National Centre for Neuroimmunology and Emerging Diseases, Menzies Health Institute Queensland, Griffith University, Southport, QLD, Australia, [2]Centre for Advanced Imaging, The University of Queensland, Brisbane, QLD, Australia, [3]School of Information Technology and Electrical Engineering, The University of Queensland, Brisbane, QLD, Australia

Introduction: Debilitating Long-Covid symptoms occur frequently after SARS-COVID-19 infection.

Methods: Functional MRI was acquired in 10 Long Covid (LCov) and 13 healthy controls (HC) with a 7 Tesla scanner during a cognitive (Stroop color-word) task. BOLD time series were computed for 7 salience and 4 default-mode network hubs, 2 hippocampus and 7 brainstem regions (ROIs). Connectivity was characterized by the correlation coefficient between each pair of ROI BOLD time series. We tested for HC versus LCov differences in connectivity between each pair of the 20 regions (ROI-to-ROI) and between each ROI and the rest of the brain (ROI-to-voxel). For LCov, we also performed regressions of ROI-to-ROI connectivity with clinical scores.

Results: Two ROI-to-ROI connectivities differed between HC and LCov. Both involved the brainstem rostral medulla, one connection to the midbrain, another to a DM network hub. Both were stronger in LCov than HC. ROI-to-voxel analysis detected multiple other regions where LCov connectivity differed from HC located in all major lobes. Most, but not all connections, were weaker in LCov than HC. LCov, but not HC connectivity, was correlated with clinical scores for disability and autonomic function and involved brainstem ROI.

Discussion: Multiple connectivity differences and clinical correlations involved brainstem ROIs. Stronger connectivity in LCov between the medulla and midbrain may reflect a compensatory response. This brainstem circuit regulates cortical arousal, autonomic function and the sleep–wake cycle. In contrast, this circuit exhibited weaker connectivity in ME/CFS. LCov connectivity regressions with disability and autonomic scores were consistent with altered brainstem connectivity in LCov.

KEYWORDS

Long Covid, fMRI, connectivity, brainstem, medulla, midbrain, upregulation

1. Introduction

Subjects suffering 'Ongoing Symptomatic COVID-19' (National Institute for Health and Care Excellence, 2020) complain of persisting fatigue, shortness of breath, and cognitive dysfunction (Soriano et al., 2022). In common with much of the literature we here label this condition long-COVID (LCov). The symptom characteristics of long-COVID resemble those of myalgic encephalomyelitis/chronic fatigue syndrome (ME/CFS) (Wong and Weitzer, 2021) and it has been suggested that LCov symptomatology is consistent with brainstem dysfunction (Yong, 2021).

While we were acquiring advanced brain MRI data for a new ME/CFS study we took the opportunity to select a sample of LCov subjects, using criteria in ME/CFS questionnaires, to perform the same MRI protocol.

Quantitative brain MRI studies in long-Covid are sparse, especially studies designed to detect differences in brain connectivity which underlies normal behavior and cognition. Functional MRI (fMRI) acquires several hundred MRI images that are blood oxygen level dependent (BOLD), either during resting state or a cognitive task. Correlations between the BOLD time series from different locations characterize connectivity between them. The most basic analysis derives connectivity between pairs of *a-priori* regions-of-interest (ROIs), e.g., hubs of intrinsic networks, and compares patient and healthy control (HC) populations. The risk of missing affected brain locations with limited *a-priori* ROIs can be mitigated by also computing connectivity between each ROI and all voxels in the rest of the brain to locate clusters of voxels where connectivity differs from HC. Further insights can be gained by seeking correlations between connectivity and disease severity. Sensitivity to changes in brain function is enhanced by acquiring fMRI while the subject is performing a cognitive task.

In ME/CFS, fMRI studies have been performed with disparate methodology to localize regions with altered connectivity. Hubs of brain intrinsic networks were a natural focus. The tri-network model proposed by Menon (2011) integrates 3 key intrinsic brain networks — the central executive network (CEN), salience network (SA), and the default mode network (DM), into a single cohesive model underlying normal behavior and cognition. This model predicts that the levels of *internally*-directed cognition of the DM and *externally*-directed cognition of the CEN networks are anti-correlated and under the control of the SA, such that if the brain engages one of the two, the SA inhibits the activation of the other (Shaw et al., 2021). Such a reciprocal relationship implies that if SA to DMN connectivity is different to HC in LCov, then SA to CEN connectivity will also differ (with opposite sign).

Most ME/CFS fMRI studies analyzed resting state fMRI and reported varied results mostly involving hubs of the salience (SA) and default mode (DM) networks (Boissoneault et al., 2016; Gay et al., 2016; Wortinger et al., 2017; Manca et al., 2021), although altered SA right insula connectivity was a finding in all studies. Two fMRI studies have been performed during a cognitive task. The first (Baraniuk et al., 2022) examined only the BOLD signal amplitude and reported diminished BOLD in the midbrain (before physical exercise). The second (Shan et al., 2018a; Barnden et al., 2019; Su et al., 2022) evaluated BOLD correlations (connectivity) between the brain's default mode (DM) and salience (SA) network hubs and hippocampal and brainstem nuclei and detected altered DM connectivity (Shan et al., 2018b), weaker connectivity within the brainstem (Barnden et al., 2019) and altered connectivity between SA and DMN hubs (Su et al., 2022). Compromised SA and brainstem regulatory function will have consequences for cognitive and autonomic function (Hall, 2011) and leads to our hypothesis, based on overlapping symptoms, that LCov would also exhibit altered intrinsic brain connectivity.

Here we test the hypothesis that intrinsic brain connectivity in LCov is different to HC. For 10 LCov and 13 HC subjects fMRI was acquired on a 7T research MRI scanner which yields superior quality (signal to noise ratio) images relative to conventional 3T scanners, particularly in the brainstem (Colizoli et al., 2020). Patient selection and data analysis was informed by our experience with ME/CFS which shares many LCov symptoms. During the scan, subjects performed the Stroop color-word cognitive task which challenges conflict monitoring/cognitive control between task relevant and task-irrelevant stimuli (Egner and Hirsch, 2005).

Abbreviations: LCov, Long Covid; HC, Healthy Control; ROI, Region of Interest; ME/CFS, Myalgic Encephalomyelitis/Chronic Fatigue Syndrome; SA, Salience Network; DM, Default Mode Network; RAS, Reticular Activation System.

2. Methods and materials

2.1. Subjects

The study was approved by Griffith University Human Research Ethics Committee (2022/666) and written informed consent was obtained from all individuals. This cross-sectional investigation was conducted at the National Centre for Neuroimmunology and Emerging Diseases (NCNED) on the Gold Coast, Queensland, Australia. Eligible participants were medical-practitioner referred and assessed using the NCNED research questionnaire for fatigue affected subjects, which recorded severity of post-exertional malaise, cognitive disturbances, immune manifestations, thermoregulatory complaints, gastrointestinal symptoms, urinary frequency, body pain, and sleep disturbances. Long-COVID participants were selected with one or more of these symptoms, with moderate or worse severity, with onset less than 3 months following COVID-19 infection and persisting for at least 3 months, according to the WHO working case definition (Soriano et al., 2022). Healthy controls reported no chronic health condition or evidence of underlying illness. Participants were aged between 18- and 65-years. Medical history was requested to identify comorbid manifestations or exclusionary diagnoses including mental illness, malignancies, autoimmune, neurological, or cardiovascular diseases. Female participants were not pregnant or breastfeeding. Finally, 10 Long-COVID (7F, 3M) who met the WHO clinical case definition and 13 healthy control subjects (7F, 6M) were included in this study.

2.2. MRI acquisition

Two 7.5 min fMRI acquisitions separated by 90 s were acquired sagitally for each subject during the cognitive task. In this work we confine ourselves to analysis of the first fMRI acquisition. The fMRI image volumes were acquired on a 7T whole-body MRI research scanner (Siemens Healthcare, Erlangen, Germany) with a 32-channel head coil (Nova Medical Wilmington, United States). For each fMRI, 225 volumes of fMRI data were acquired using a multiband echo-planar imaging (EPI) pulse sequence developed at the University of Minnesota (Auerbach et al., 2013), with 80 sagittal slices, multiband factor = 3, TR = 2000 ms, TE = 22.4 ms, flip angle = 70°, acquisition matrix 192 × 192 and voxel size 1.25 mm^3. The 225 fMRI volumes were acquired while the subject responded to a sequence of Stroop color-word tests (Leung et al., 2000).

An anatomical image was acquired using Siemens T2 'SPACE' optimized 3D fast spin-echo (T2wSE) TR = 3200 ms, TE = 563 ms, scans on an adjacent 3T scanner on the same day. Acquisition time was 5:44 (min:sec). These scans employed an optimized variable flip

angle sequence (Siemens SPACE) to yield a 'true 3D' acquisition in a shortened time. Their 'contrast equivalent' TE compares with standard T2wSE TE (Busse et al., 2006) although the signal is also influenced by T1 relaxation (Mugler, 2014), possibly more than for T2wSE. These T2 'SPACE' images were sagittal with pixel size 0.88 × 0.88 × 0.9 mm. T2 'SPACE' were chosen for the anatomical scan because their spin-echo sequence renders them resistant to the magnetic field induced distortions of the conventional gradient-echo MPRAGE sequences (Bushberg et al., 2002), particularly in the brainstem.

2.3. Cardiac and respiratory monitoring

Physiological noise in the fMRI BOLD time series was modeled using 200 Hz time-series from pulse oximeter and respiratory strap sensors recorded during the scan. The cardiac and respiratory time series interactions were computed using the TAPAS toolbox (Kasper et al., 2017) and used as covariates to correct physiological noise.

2.4. The Stroop task

For each task fMRI, the Stroop task was used to investigate the attention and concentration difficulties reported by Long COVID patients (Leung et al., 2000). Each Stroop task displayed two colored words. The upper word, either RED, BLUE, YELLOW, or XXXX, was colored either red, blue, or yellow on a black background. The lower word was either RED, BLUE, or YELLOW colored white on a black background. The subject was asked to decide whether the *color* of the upper word agreed with the *meaning* of the lower word and press one of two buttons on a handpiece to respond 'yes' or 'no.' The Stroop task fMRI was divided into four conditions, three were trials: either *neutral* (upper word is XXXX), *incongruent* (the upper word is in a color different to the lower word meaning), or *congruent* (upper word is in the color of the lower word meaning). The incongruent task is considered more challenging because of the inhibitory element required to overcome the natural impulse to read the top word rather than only inspect its color, and so decide meaning vs. meaning of the lower word rather than color vs. meaning. The fourth condition, *rest*, was the period between a trial response and the next trial onset. During this 'rest' condition a fixed stationary cross appeared on the screen for a period randomized between 3 and 12 s.

In each task fMRI, a total of 60 Stroop trials were randomly distributed over each 7.5 min acquisition with average inter-stimulus time of 10.5 s. 40% of trials were incongruent, 30% were congruent, and 30% were neutral. For each trial type, the stimulus-onset and response times were recorded. Their difference was reaction time. For each trial type, mean reaction time and accuracy = correct/total responses were evaluated for each fMRI run for each group.

2.5. Clinical scores

Clinical Scores used in regressions with LCov connectivity were SF36physical, SF36mental, Disability, Life (domestic) Activity, Heart rate (HR) and Heart rate Variability (HRV) and Respiration Rate (Resp) and Variability (RespV). HR, HRV, Resp and RespV were extracted from the power spectra of the pulse oximeter and respiration strap time series recorded during the 7.5 min scan (peak frequency and full width of peak at half maximum). Symptom scores were extracted from the Research Registry questionnaire developed by NCNED with the Centres for Disease Control and Prevention (CDC) and accessed online through Lime survey. Symptom severity was scored on a 0–5 scale (0: none, 1:very mild, 2:mild, 3: moderate, 4:severe, 5: very severe). The SF36 scores (Ware et al., 1995) were the average of Physical Functioning (10 items) and Mental Health (5 items) domains. Disability was the Bell Disability scale (Bell, 1995) and Life Activities was from the WHODAS assessment (Ustun et al., 2010).

2.6. Regions of interest

Table 1 lists the 20 MNI space ROIs that were assessed: 7 in SA hubs, 4 in DMN hubs, 5 reticular activation system (RAS) nuclei, periacqueductal gray matter (PAG) in the midbrain, the left culmen of cerebellum, and bilateral hippocampus nuclei. SA and DMN regions were supplied with the CONN package (Whitfield-Gabrieli and Nieto-Castanon, 2012). The 9 subcortical regions outside of the SA and DMN were selected because of their involvement in ME/CFS reported in an earlier MRI study (Barnden et al., 2016) or their rich connections (hippocampus subiculum) to brainstem RAS nuclei

TABLE 1 The 20 ROIs between which connectivity was assessed.

ROI location	Laterality	Abbreviation	Voxels
Salience network (7)			
Anterior insula	L&R	SA.AI_L, SA.AI_R	446, 388
Supramarginal gyrus (BA40)	L&R	SA.SMG_L, SA.SMG_R	233, 284
Rostral prefrontal cortex	L&R	SA.rPFC_L, SA.rPFC_R	1166, 581
Anterior cingulate cortex	Midline	SA.ACC	1063
Default mode network (4)			
Inferior lateral parietal	L&R	DM.LP_L, DM.LP_R	1041, 1326
Medial prefrontal cortex	Midline	DM.mPFC	1346
Posterior cingulate cortex	Midline	DM.PCC	4833
Brainstem (6)			
Rostral medulla	L&R	Mdul_L, Mdul_R	123
Midbrain: cuneiform nucleus	L&R	CnF_L, CnF_R	125
Midbrain: dorsal raphe nucleus	Midline	DoRph	129
Midbrain: periaqueductal gray	Midline	PAG	66
Subcortical (3)			
Culmen of cerebellum	L	Culm_L	123
Hippocampus: subiculum	L&R	Hippo_L, Hippo_R	377, 377

Salience (SA) and default mode (DM) network hubs were provided in the CONN package. L is Left, R is Right. Voxel volume was 1.95 mm^3.

(Edlow et al., 2016). See (Barnden et al., 2019) for details of subcortical ROI creation.

2.7. MRI processing

The fMRI data was pre-processed using the default preprocessing pipeline in the CONN toolbox (Whitfield-Gabrieli and Nieto-Castanon, 2012; Nieto-Castanon, 2020) dedicated to connectivity evaluation and statistical comparisons. Motion was computed during the series of 225 volumes. After omitting the first 5 volumes while the magnetic field reached a steady state, the average of the motion corrected volumes was spatially normalized to a template image in MNI space and the deformation applied to all motion corrected volumes. The 1.25 mm voxel size of the original 7T fMRI was retained throughout. The anatomical image was segmented into gray matter, white matter, and CSF for calculation of their volumes for use as denoising covariates. See the CONN handbook (Nieto-Castanon, 2020) for details. Time series of the 6 rigid-body motion parameters, cardiac and respiratory time series and their interactions, and a binary covariate identifying outlier intra-fMRI movements were used in denoising of fMRI mean ROI BOLD or voxel BOLD time-series.

For each fMRI voxel, BOLD time-series were computed. ROI time series were the average of their voxel time series. Denoising of the ROI (and voxel) BOLD time-series incorporated physiological noise, motion parameters, and total white matter and CSF volumes as nuisance covariates. After denoising, a temporal bandpass filter was used to remove frequencies from the BOLD time series below 0.008 Hz and above 0.15 Hz (Sasai et al., 2021).

For each subject, after denoising and filtering the BOLD time-series for each voxel, the mean BOLD time-series in each of the 20 ROIs (seeds) was computed. For each pair of ROIs, correlation between their BOLD time-series yielded a correlation coefficient, used here to characterize their functional connectivity (FC). Differences between FC of the 13 HC and 10 LCov were tested using CONN's ROI-to-ROI approach. Regressions between the 10 LCov FC and clinical measures were also tested. Then for each ROI, its mean BOLD time series was correlated with the BOLD time series for each voxel in the brain using CONN's 'Seed-to-voxel' utility to yield a 3D image of correlation coefficients. For each voxel a test for ROI connectivity differences between the 13 HC and 10 LCov was performed and then significant voxel clusters were reported. Clusters were defined by the conventional *uncorrected* p threshold of 0.001, and because we retained a very small voxel size (1.25 mm compared to the conventional 2 mm) with higher noise levels we also assessed clusters defined by an *uncorrected* 0.005 threshold. We reported clusters with p-FDR < 0.05. Functional Connectivity values were computed for the entire set of 180 connection pairs between the 20 ROIs. The terms connectivity and 'correlation coefficient' are used interchangeably here.

2.8. General linear model

To compare the LCov and HC groups, 'second-level' CONN analysis applied a multivariate parametric General Linear Model (GLM) for all correlation coefficients (connectivity values). Age was included as a covariate. The GLM model here was

$$Y_i = \beta_1.X_{i1} + \beta_2.X_{i2} + \beta_3.X_{i3} + \varepsilon_i$$

where, for a given pair of ROIs (seeds), Y_i are the FC connectivity values (i = 1 to 23 subjects), X_{i1}, X_{i2}, are binary vectors that specify group membership (for X_{i1} 1 is HC, 0 is LCov; for X_{i2} 0 is HC and 1 is LCov). X_{i3} is the vector of ages for the 23 subjects. Solving the GLM equation yields β_1, β_2 and β_3 the relative contribution of group and age to the observed variation in Y_i. ε_i is the residual variation not explained by group membership or age, which has zero mean and variance σ^2, and is used to estimate statistical inference of β_1 and β_2. Group differences were tested with contrast [1–1 0].

For the seed-to-voxel analysis, Y_i is the vector of connectivity *images* for each subject. That is, for a particular ROI, Y_i is the 3D image in which each voxel value is the correlation coefficient between the ROI mean BOLD time-series and that voxel's BOLD time-series. The significance of clusters of voxels was derived using random field theory (Friston et al., 1994). Clusters with $p < 0.05$ are reported here with locations from CONN's internal atlas.

A similar model was used to test for correlations between LCov ROI-to-ROI connectivity and LCov clinical scores, with X_{i1} for LCov group membership, X_{i2} for LCov clinical score and X_{i3} for age, and contrast [0 1 0].

2.9. Statistical inference

Results were reported by CONN as the T statistic for connectivity difference for each ROI pair and a false discovery rate (FDR) corrected value of p (Benjamini and Hochberg, 1995) defined as the expected proportion of false discoveries among all ROI pairs with similar or larger effects across the entire set of 180 pairs. Each ROI pair with an FDR corrected value of p <0.05 for difference between LCov and HC is reported below.

The seed-to-voxel tests for significant clusters were 1-sided with clusters defined by an uncorrected threshold voxel P (uvP) = 0.001 and 0.005. Clusters with p-FDR < 0.05 are reported here.

3. Results

3.1. Subject symptoms

The symptoms scored by each of the 10 LCov subjects and their age, gender and severities are given in Table 2. All 10 subjects reported moderate to very severe fatigue, muscle aches and unrefreshing and/or disturbed sleep. 7/10 subjects reported cognitive (concentration and/or memory) problems. Age mean (standard deviation) was 44 (15) for LCov and 39 (13) for HC. Gender was F/M = 7/3.

3.2. Stroop task accuracies and reaction times

Table 3 shows that, for the three categories of the Stroop task, LCov accuracies were lower than for HC, although the difference was only significant (p = 0.026) for the Neutral task. Similarly, LCov Reaction Times were slower than HC but were not significant (p > 0.05).

TABLE 2 Symptoms (left column) that were scored by each subject, and subject gender, age and symptom severity scores.

Subject	1	2	3	4	5	6	7	8	9	10
Gender	F	M	F	F	M	F	F	M	F	F
Age	49	64	46	30	40	59	43	61	32	19
Fatigue	4	3	3	3	3	3	4	4	4	3
Concentration	3	3	3		4	3	4	4		
Memory					3		4	3		
Muscle aches	4	3	3	4	4	3	3	4	3	3
Joint pain	3	3	3			3	3			4
Headaches	3	3			4	3	3	3	3	3
Sensitivity to light	3	3			4	3	3			
Sensitivity to noise/vibration	3	3								
Odor/taste							3	3		
Unrefreshing sleep	3	4	3		4	3	4	3	5	4
Sleep disturbances	3	3	3	3	4		3	3		5
Muscle weakness				4		4	3	4		
Lymph						4	3	4	3	
Throat										4
Fever							5	3		
Nausea					3		5			5
Abdominal pain	3				3		5		3	5
Bloating		3		3			4		4	4
Bowel							5			4
Urinary frequency										4
Breathing	3			3			4			
Light headed	3		3		4				3	3
Arrythmia										4
Sweating							4	3		
Cold extremities				3			4		3	

Severity scores relevant to LCov selection were 3: moderate, 4: severe, 5: very severe.

3.3. LCov vs. HC connectivity

Altered LCov connectivity was detected with three statistical tests:

A. The test for different LCov connectivity to HC between pairs of 20 ROIs was positive for two ROI pairs (Table 4 and Figure 1). The brainstem medulla was involved in both, one connecting with the midbrain, the other with a DM hub. Both connections were *stronger* in LCov than HC.
B. The test of connections between each of the 20 brain ROIs and all voxels in the rest of the brain identified clusters of voxels for which ROI correlations were different in LCov from HC. Table 5 lists the ROI seeds and cluster locations. Voxel clusters with different connectivity in LCov were detected for five SA and three DM network hubs (seeds). Most, but not all, cluster correlations were weaker in LCov than HC. Seven clusters were significant with p-FDR < 0.0001. The strongest statistical inference was seen for the SA.AI_L seed (p-FDR < 1e-6) for two clusters, one in the left temporal and one in the left frontal lobe (see Figure 2A). A cluster in the right operculum also correlated with the SA.AI_L region (Figure 2B) but with stronger connectivity in LCov than HC.
C. The test for regressions in LCov between ROI-to-ROI connectivity and clinical scores revealed LC connectivity correlated with the disability score and two autonomic scores (Table 6 and Figure 3). A brainstem ROI (Mdul_R, PAG) was involved in two of the four significant correlations, and three involved salience network hubs (ACC, rPFC_L and rPFC_R). Because HC regressions with these clinical scores were insignificant, the LCov correlations can be regarded as abnormal. Two of the three clinical scores, HRV and RespV from data acquired during the scan, related to autonomic regulation.

4. Discussion

In this pilot study we derived BOLD time series for 10 Long Covid and 13 Healthy Controls in 20 brain ROIS. Correlations between pairs of BOLD time series quantified connectivity between their ROIs. The ROIs included Salience (SA) and Default Mode (DM) Network hubs

TABLE 3 Healthy control (HC) and long Covid (LCov), Stroop task accuracies and reaction times for each of the three categories of Stroop task (incongruent, congruent and neutral).

Cohort	*N*	Accuracy			Reaction time (seconds)			Stroop
		Incongruent	Congruent	Neutral	Incongruent	Congruent	Neutral	Effect
HC	13	0.940	0.982	0.995	1.413	1.221	1.230	0.139
LCov	10	0.923	0.973	0.901*	2.094	1.826	1.685	0.162

Stroop Effect = (Incongruent Reaction Time – Congruent Reaction Time) / Mean Reaction Time.
*Significantly lower than HC ($p = 0.026$).

TABLE 4 Two ROI pairs with reduced connectivity in 13 HC versus 10 LCov.

ROI1	ROI2	T(20)	p-FDR
Mdul_L	CnF_R	−4.22	0.0080
Mdul_L	DM.LP_R	−3.17	0.046

T is the T statistic. Negative T indicates weaker connectivity in HC. p-FDR is false discovery rate corrected statistical inference. ROI names are expanded in Table 1.

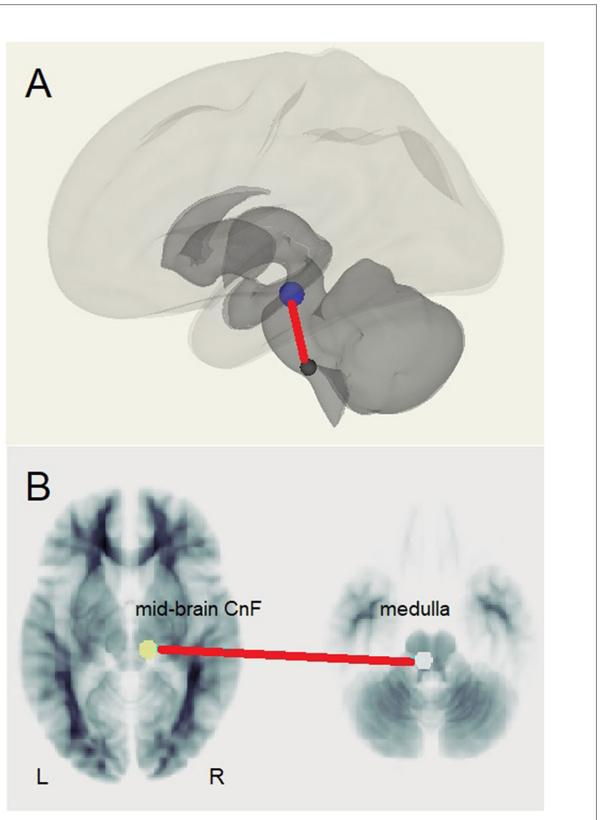

FIGURE 1
The brainstem connection between the midbrain right cuneiform nucleus and left rostral medulla that was stronger in LCov than HC. **(A)** Medulla (lower) to Cuneiform Nucleus (upper) connection shown relative to surface images of subcortical (dark) and cortical (light) white matter. **(B)** Left medulla and right cuneiform nucleus (CnF) shown on reference white matter transaxial sections.

and subcortical ROIs (Table 1). Despite the small subject numbers, we showed several differences in LCov intrinsic brain connectivity relative to HC. Differences involving nuclei of the brainstem reticular activation system (RAS) suggest this regulatory structure may be pivotal to LCov symptoms.

4.1. LCov vs. HC comparisons – ROI to ROI connectivity

The principal finding was *increased* LCov connectivity relative to HC in the brainstem between the rostral medulla (Mdul_L) and midbrain cuneiform nucleus (CnF_R). There was also an increase from the Mdul_L to a DM hub (DM.LP_R). The first result is consistent with a brainstem volume study (Thapaliya et al., 2023) of the same subjects that reported *larger* volumes in LCov than HC. Both Mdul_L and CnF_R ROIs contain nuclei of the reticular activation system (RAS), an interconnected complex of small regulatory nuclei in the brainstem that influence cortical activity by both neurotransmitter release and oscillatory electrical stimulation. The midbrain CnF is located in the brainstem excitatory area and the rostral medulla in the brainstem inhibitory area (Hall, 2011). The 'circuit' between the two determines cortical excitation and sleep. In concert with the hypothalamus this circuit also controls autonomic function (Hall, 2011).

The excitatory CnF nuclei receive feedback via sensory signals from the periphery and signals from the cortex dependent on levels of brain thought or motor processes. Increases in physical or cortical activity then stimulate the excitatory area to maintain or enhance cortical activity (Hall, 2011). The connection from the medulla inhibitory area reduces excitatory output to facilitate the sleep–wake cycle.

Increased LCov connectivity in this circuit is perhaps counter-intuitive, and may be interpretated as an upregulation in RAS BOLD activity

- as a response to viral damage in the brainstem. Reported reactive gliosis and microglial activation (Pajo et al., 2021) may represent an injury that requires enhanced BOLD levels for normal brainstem connectivity.
- to compensate for broadly compromised cortical dysfunction (Fisher et al., 2021) and consequent reduced cortical feedback. The mechanism for this is unknown but may resemble the recently discovered regulatory process that maintains somatosensory performance in HC (Barnden et al., 2022).

The complexity of the RAS makes it difficult to exactly specify the RAS nuclei that generate the Mdul and CnF BOLD activity, although the Mdul ROI encompasses median raphe, gigantocellular and hypoglossal nuclei (Naidich et al., 2009), while the CnF involves in-part the midbrain reticular formation (MRF), pedunculotegmental nucleus and the pontis oralis (Athinoula, n.d.). The pedunculotegmental, also known as pedunculopontine (PPN), nucleus has been identified as the principal brainstem nucleus for activation of higher cortical regions (Garcia-Rill et al., 2016a,b, 2019).

TABLE 5 ROI to voxel-cluster pairs with LCov connectivity different to HC.

ROI seed	LCov	Cluster location*	x y z	Cluster p-FDR and size (k)			
			(MNI)	0.001	k	0.005†	k
SA.AI_L	↓	infTemp/(occip part) L	−58 −38 −16	<1e-6	142	<1e-6	327
	↓	midFron L	−40 + 6 + 46	0.0060	34	<1e-6	311
	↓	precentral WM L	−32 0 + 36	0.0060	34	^	^
	↓	midFron L	−38 + 26 + 36	0.0060	34	^	^
	↑	Central Operculum R	+46–4 + 11			0.0001	152
SA.AI_R	↓	midTemp L	−54 −46 −14			0.00042	139
	↓	inf/midTemp Occip R	+56–44 −12			0.00072	118
SA.rPFC_R	↓	postCentral L	−38 −40 + 60	0.0081	40	0.000004	211
	↓	supraMarginal L	−44 −36 + 40	0.022	30	^	^
	↓	postCentral, SMG R	+40–26 + 36			0.0044	102
SA.SMG_L	↓	midtemp L	−64 −54 + 4	0.034	32	0.021	71
	↓	centralOperculum R	+58–6 + 12			0.021	76
	↓	midFron R	+34 + 4 + 58	0.034	25	0.047	58
SA.SMG_R	↑	latOccipInf&sup L	−38 −86 + 16			0.00007	158
	↑	supPar L	−28 −52 + 58			0.040	62
DM.PCC	↓	Angular L	−50 −56 + 28	0.00046	59	0.00009	158
	↓	midFron R	+36 + 14 + 42			0.036	66
DM.LP_L	↓	preCentral R	+48–18 + 58	0.0031	45	0.000002	227
	↑	midFron L	−42 + 36 + 26	0.0085	35	0.0069	88
DM.LP_R	↓	latOccip sup L	−38 −64 + 48	0.041	32	0.000002	237
	↓	Fron pole L	−42 + 54 + 4			0.0046	94
Mdul_R	↑	latOccip pole L	−28 −84 + 8			0.0035	89
HippoL	↓	Fron pole	+10 + 68 + 14	0.020	35	0.020	73
HippoR	↓	ParietalOperculum L	−42 −30 + 20	0.0099	36	0.020	65
	↓	paraCing supFron R	+4 + 46 + 20			0.0014	107
	↓	infTemp L	−60 −22 −26			0.020	62
Average 7	↓	midFron R	+56 + 14 + 40			0.011	78
Brainstem	↑	midFron / Fron pole R	+30 + 34 + 46			0.0060	85
Average 7SA	↓	Temp (occip part) L	−56 −48 −12			0.00056	138
Average 4DM	↓	Angular gyrus L	−50 −56 + 28			0.00015	158

ROI names are expanded in Table 1. The 'LCov' column indicates LCov connectivity is weaker (↓) or stronger (↑) than HC. Cluster statistics (p-FDR) and size (k voxels) for uncorrected voxel thresholds uvP < 0.001, and uvP < 0.005 are listed. Voxels were 1.25 mm isotropic.

* Temp, temporal; Occip, occipital; Fron, frontal; Cing, cingulate; ant, anterior; inf, inferior; mid, middle.

† Clusters separated with threshold uvP = 0.001 which merged with threshold 0.005 are indicated by '^' below their parent cluster.

The stronger Mdul_L to DM.LP_R connection in LCov is consistent with a relationship whereby increased Mdul_L activity in LCov decreases DM activity to facilitate executive network activity (Menon, 2011).

4.2. LCOV vs. HC comparisons – ROI to voxel connectivity

Involvement of brain regions beyond the 20 *a-priori* ROIs can be detected by tests for different LCov and HC connectivity between each ROI and the whole brain using voxel-based analysis. Table 5 lists multiple new regions thus detected. Differences were found brain areas connecting to 5 SA and 3 DM hubs, most but not all with HC > LCov. The middle frontal gyrus (bilaterally) and inferior and middle temporal lobes (left only) showed different LCov connectivity with SA hubs. Cluster defining thresholds of both uncorrected voxel $p = 0.001$ and 0.005 were examined. We felt the more liberal 0.005 threshold was justified because of the small voxel size and corresponding increase in BOLD time-series noise.

4.3. Connectivity regressions with LCov clinical scores

Regressions with disability and the autonomic measures of respiration rate variability and heart rate variability were significant for the brainstem Mdul_R and PAG in LCov but not HC, suggesting abnormal function of the RAS nuclei in those locations.

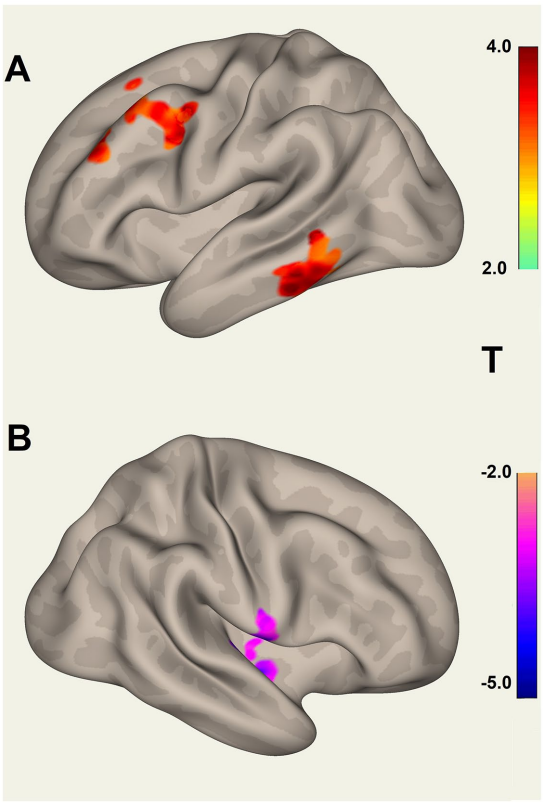

FIGURE 2
Voxel clusters that connect to the Salience Network left Anterior Insula seed, where connectivity for HC differs from LCov. **(A)** Two clusters for HC>LCov connectivity in left inferior temporal area (lower) and left middle frontal and pre-central areas (upper), and **(B)** for HC<LCov connectivity in the right central operculum. The clusters are contiguous above and/or beneath the reference white matter surface. Refer to Table 5 (SA.AI_L) for details.

TABLE 6 ROI pairs for which Long Covid connectivity correlated with the clinical scores: bell disability, heart rate variability and respiration rate variability.

ROI1	ROI2	T(19)	p-FDR
Bell disability			
SA.ACC	SA.rPFC_L	+5.86	0.039
Heart rate variability			
PAG	Hippo_R	+4.87	0.034
Respiration rate variability			
Mdul_R	SA.rPFC_R	+5.64	0.015
DM.LP_L	SA.SMG_R	−5.59	0.016

T is the T statistic, p-FDR is the false discovery rate corrected statistical inference. The sign of T indicates whether the correlation was positive (+) or negative (−). ROI names are expanded in Table 1.

4.4. Stroop task performance

Long-Covid subjects performed the Stroop task with lower accuracy and slower reaction times than HC. Accuracy for the 3 categories of task was highest for the 'neutral' task in HC but lowest in LCov. This may indicate failure of the LCov subjects to understand or remember the instructions given for this category.

4.5. Comparison with ME/CFS

An ME/CFS fMRI study optimized for the brainstem (Barnden et al., 2019) reported *weaker* connectivity between the medulla and midbrain during a Stroop task. Here in LCov during the same task, medulla to midbrain connectivity was *stronger*. Thus, increased brainstem connectivity in LCov discriminates LCov from ME/CFS, although brainstem involvement is important in both. Larger sample sizes are required to clarify this. Duration of illness may be an important determinant for connectivity. The relatively acute (<2 years) symptoms of LCov compared to several years or decades for ME/CFS may be relevant. Longitudinal studies of LCov are needed to test for an evolution of brain pathology that may yield a pattern more like ME/CFS.

4.6. Potential biological mechanism

A recent investigation of impaired cell membrane calcium transport and transient receptor potential melastatin 3 (TRPM3) reported dysfunction in both ME/CFS and LCov (Cabanas et al., 2018; Sasso et al., 2022). These TRPM3 ion channels are widely expressed in the cerebellum, dorsal midbrain, amygdala and medulla (Allen Institute, 2022) and are believed to be involved in a range of biological processes including memory formation and consolidation, thermoregulation, pain, inflammation, and coordination (Oberwinkler and Philipp, 2014). Further, the prevalence of TRPM receptors in microglia could result in increased recruitment with neurotoxic potential (Bezzi et al., 2001; Ifuku et al., 2014). Microglial density is 10 times greater in the medulla than in the cortex (Mittelbron et al., 2001) and may account for medulla involvement in both ME/CFS and LCov.

4.7. ROI selection

To avoid excessive multiple-comparison corrections for statistical inference, we limited our analysis to 20 regions: 7 SA hubs, 4 DM hubs, 6 brainstem regions, two hippocampus and a cerebellum region (Table 1). This choice was informed by ME/CFS experience (Barnden et al., 2016, 2019). Independent Component Analysis (ICA) may provide a more comprehensive survey of altered intra-brain connectivity in LCov.

4.8. Limitations

The limited number of subjects in this pilot study required a corresponding limit of the number of brain regions between which connectivity was assessed. These preliminary results must be confirmed with more subjects. Future analysis of connectivity changes within and between the sequential 7.5 min runs in larger LCov cohorts will permit evaluation of more regions and may

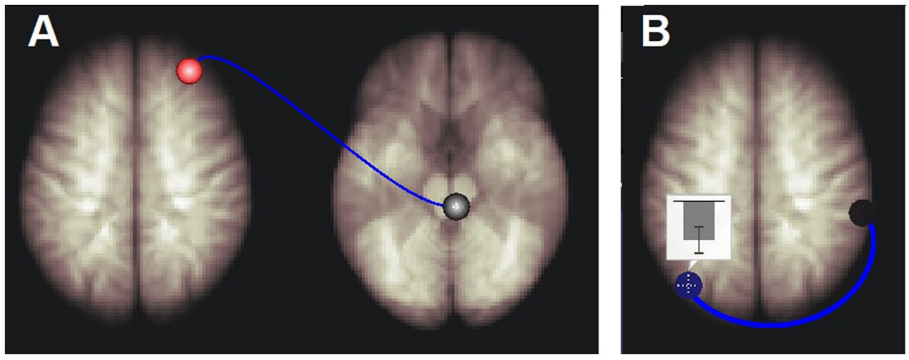

FIGURE 3
Long Covid connections that correlated with respiration rate variability. **(A)** Right medulla to right rostral prefrontal cortex connectivity was positively correlated with respiration rate variability. **(B)** Left default mode network inferior lateral parietal hub (DM.LP_L) to right salience network supra marginal gyrus hub (SA.SMG_R) connectivity was negatively correlated with respiration rate variability. The inset shows the mean and standard deviation of correlation coefficients (connectivity) between the BOLD time series of the DM.LP_L and SA.SMG_R regions. See Table 6 for details.

provide further insights into the rate of development of cognitive fatigue.

5. Conclusion

In this pilot study of brain connectivity in Long Covid, despite limited subject numbers, we have detected significant differences from HC, mostly in brainstem and salience network connections that are important for the regulation of brain function. Altered regulatory connections can have complex consequences that may manifest as the symptoms of LCov. In the brainstem during the same cognitive exertion, *enhanced* connectivity in LCov was opposite to the *impaired* connectivity in ME/CFS.

Data availability statement

The datasets presented in this article are not readily available because datasets analyzed and/or generated during the current study are not publicly available due to confidentiality agreements. Requests to access the datasets should be directed to ncned@griffith.edu.au.

Ethics statement

The studies involving human participants were reviewed and approved by the Griffith University Human Research Ethics Committee (2022/666). The patients/participants provided their written informed consent to participate in this study.

Author contributions

LB: conceptualization and formal analysis. LB, KT, NE-F, and MB: methodology. LB and NE-F: writing of original draft. KT and SM-G: writing – review and editing. All authors contributed to the article and approved the submitted version.

Funding

This research was funded by ME Research UK (MERUK, https://www.meresearch.org.uk/). Other funding bodies include: the Stafford Fox Medical Research Foundation (489798), the National Health and Medical Research Council (1199502), McCusker Charitable Foundation (49979), Ian and Talei Stewart, Buxton Foundation (4676), Henty Community (4879), Henty Lions Club (4880), Mason Foundation (47107), Mr. Douglas Stutt, Blake Beckett Trust Foundation (4579), Alison Hunter Memorial Foundation (4570), and the Change for ME Charity (4575).

Acknowledgments

We are thankful to Tania Manning and Kay Schwarz for recruiting participants for this study, radiographers (Nicole Atcheson, Aiman Al-Najjar, Jillian Richardson, and Sarah Daniel) at the Centre for Advanced Imaging of The University of Queensland for helping us to acquire MRI data, and all the patients and healthy controls who donated their time and energy to participate. We thank James Baraniuk for useful discussions on this work.

Conflict of interest

The authors declare that the research was conducted in the absence of any commercial or financial relationships that could be construed as a potential conflict of interest.

Publisher's note

References

Allen Institute. (2022). Genotype frequencies of transient receptor potential melastatin M3 ion chan…: EBSCOhost. Available at: https://web-b-ebscohost-com.libraryproxy.griffith.edu.au/ehost/detail/detail?vid=2&sid=d53b80f2-49aa-4d4a-94fe-ee2fcd4a8d5d%40sessionmgr103&bdata=JnNpdGU9ZWhvc3QtbGl2ZSZzY29wZT1zaXRl (Accessed August 19, 2021).

Athinoula, A. Harvard Ascending Arousal Network Atlas | MGH/HST Martinos Center for Biomedical Imaging. Available at: https://www.nmr.mgh.harvard.edu/resources/aan-atlas (Accessed May 3, 2023).

Auerbach, E. J., Xu, J., Yacoub, E., Moeller, S., and Ugurbil, K. (2013). Multiband accelerated spin-echo echo planar imaging with reduced peak RF power using time-shifted RF pulses. *Magnetic Resonance in Medicine* 69, 1261–7.

Baraniuk, J. N., Amar, A., Pepermitwala, H., and Washington, S. D. (2022). Differential effects of exercise on fMRI of the midbrain ascending arousal network nuclei in myalgic encephalomyelitis/chronic fatigue syndrome (ME/CFS) and gulf war illness (GWI) in a model of postexertional malaise (PEM). *Brain Sci.* 12:78. doi: 10.3390/brainsci12010078

Barnden, L., Crouch, B., Kwiatek, R., Shan, Z., Thapaliya, K., Staines, D., et al. (2022). Anti-correlated myelin-sensitive MRI levels in humans consistent with a subcortical to sensorimotor regulatory process—multi-cohort multi-modal evidence. *Brain Sci.* 12:1693. doi: 10.3390/brainsci12121693

Barnden, L. R., Kwiatek, R., Crouch, B., Burnet, R., and Del Fante, P. (2016). Autonomic correlations with MRI are abnormal in the brainstem vasomotor Centre in chronic fatigue syndrome. *Neuroimage* 11, 530–537. doi: 10.1016/j.nicl.2016.03.017

Barnden, L. R., Shan, Z. Y., Staines, D. R., Marshall-Gradisnik, S., Finegan, K., Ireland, T., et al. (2019). Intra brainstem connectivity is impaired in chronic fatigue syndrome. *Neuroimage* 24:102045. doi: 10.1016/j.nicl.2019.102045

Bell, DS. *The doctor's guide to chronic fatigue syndrome*. Reading, Massachusetts: Addison Wesley; (1995), *1*, 9–33.

Benjamini, Y., and Hochberg, Y. (1995). Controlling the false discovery rate: a practical and powerful approach to multiple testing. *J. R. Stat. Soc Ser. B* 57, 289–300. doi: 10.1111/j.2517-6161.1995.tb02031.x

Bezzi, P., Domercq, M., Brambilla, L., Galli, L., Schols, D., De Clercq, E., et al. (2001). CXCR4-activated astrocyte glutamate release via TNFα: amplification by microglia triggers neurotoxicity. *Nat. Neurosci.* 4, 702–710. doi: 10.1038/89490

Boissoneault, J., Letzen, J., Lai, S., O'Shea, A., Craggs, J., Robinson, M. E., et al. (2016). Abnormal resting state functional connectivity in patients with chronic fatigue syndrome: an arterial spin-labeling fMRI study. *Magn. Reson. Imaging* 34, 603–608. doi: 10.1016/j.mri.2015.12.008

Bushberg, JT, Seibert, JA, Leidholdt, EM, and Boone, JM. *The essential physics of medical imaging. 2nd* Philadelphia: Lippincott, Williams and Wilkins; (2002).

Busse, R. F., Hariharan, H., Vu, A., and Brittain, J. H. (2006). Fast spin echo sequences with very long echo trains: design of variable refocusing flip angle schedules and generation of clinical T2 contrast. *Magn. Reson. Med.* 55, 1030–1037. doi: 10.1002/mrm.20863

Cabanas, H., Muraki, K., Eaton, N., Balinas, C., Staines, D., and Marshall-Gradisnik, S. (2018). Loss of transient receptor potential melastatin 3 ion channel function in natural killer cells from chronic fatigue syndrome/myalgic encephalomyelitis patients. *Mol. Med.* 24:44. doi: 10.1186/s10020-018-0046-1

Colizoli, O., de Gee, J. W., van der Zwaag, W., and Donner, T. H. (2020). Comparing fMRI responses measured at 3 versus 7 tesla across human cortex, striatum, and brainstem. *bioRxiv*. doi: 10.1101/2020.05.12.090175

Edlow, B. L., McNab, J. A., Witzel, T., and Kinney, H. C. (2016). The structural connectome of the human central homeostatic network. *Brain Connect.* 6, 187–200. doi: 10.1089/brain.2015.0378

Egner, T., and Hirsch, J. (2005). The neural correlates and functional integration of cognitive control in a stroop task. *NeuroImage* 24, 539–547. doi: 10.1016/j.neuroimage.2004.09.007

Fisher, K. M., Zaaimi, B., Edgley, S. A., and Baker, S. N. (2021). Extensive cortical convergence to primate reticulospinal pathways. *J. Neurosci.* 41, 1005–1018. doi: 10.1523/JNEUROSCI.1379-20.2020

Friston, K. J., Worsley, K. J., Frackowiak, R. S. J., Mazziotta, J. C., and Evans, A. C. (1994). Assessing the significance of focal activations using their spatial extent. *Hum. Brain Mapp.* 1, 210–220. doi: 10.1002/hbm.460010306

Garcia-Rill, E., D'Onofrio, S., and Mahaffey, S. (2016a). Bottom-up gamma: the pedunculopontine nucleus and reticular activating system. *Transl. Brain Rhythm.* 1, 49–53. doi: 10.15761/TBR.1000109

Garcia-Rill, E., Saper, C. B., Rye, D. B., Kofler, M., Nonnekes, J., Lozano, A., et al. (2019). Focus on the pedunculopontine nucleus consensus review from the May 2018 brainstem society meeting in Washington, DC. *Clin. Neurophysiol.* 130, 925–940. doi: 10.1016/j.clinph.2019.03.008

Garcia-Rill, E., Virmani, T., Hyde, J. R., D'Onofrio, S., and Mahaffey, S. (2016b). Arousal and the control of perception and movement. *Curr. Trends Neurol.* 10, 53–64.

Gay, C. W., Robinson, M. E., Lai, S., O'Shea, A., Craggs, J. G., Price, D. D., et al. (2016). Abnormal resting-state functional connectivity in patients with chronic fatigue syndrome: results of seed and data-driven analyses. *Brain Connect.* 6, 48–56. doi: 10.1089/brain.2015.0366

Hall, JE. *Guyton and hall textbook of physiology*. Philadelphia: Saunders Elsevier; (2011).

Ifuku, M., Hossain, S. M., Noda, M., and Katafuchi, T. (2014). Induction of interleukin-1β by activated microglia is a prerequisite for immunologically induced fatigue. *Eur. J. Neurosci.* 40, 3253–3263. doi: 10.1111/ejn.12668

Kasper, L., Bollmann, S., Diaconescu, A. O., Hutton, C., Heinzle, J., Iglesias, S., et al. (2017). The PhysIO Toolbox for Modeling Physiological Noise in fMRI Data. *J Neurosci Methods* 30, 56–72.

Leung, H. C., Skudlarski, P., Gatenby, J. C., Peterson, B. S., and Gore, J. C. (2000). An event-related functional MRI study of the stroop color word interference task. *Cerebral Cortex* 10, 552–560. doi: 10.1093/cercor/10.6.552

Manca, R., Khan, K., Mitolo, M., De Marco, M., Grieveson, L., Varley, R., et al. (2021). Modulatory effects of cognitive exertion on regional functional connectivity of the salience network in women with ME/CFS: a pilot study. *J. Neurol. Sci.* 422:117326. doi: 10.1016/j.jns.2021.117326

Menon, V. (2011). Large-scale brain networks and psychopathology: a unifying triple network model. *Trends Cogn. Sci.* 15, 483–506. doi: 10.1016/j.tics.2011.08.003

Mittelbron, M., Dietz, K., Schluesener, H. J., and Meyermann, R. (2001). Local distribution of microglia in the normal adult human central nervous system differs by up to one order of magnitude. *Acta Neuropathol.* 101, 249–255. doi: 10.1007/s004010000284

Mugler, J. P. (2014). Optimized three-dimensional fast-spin-echo MRI. *J. Magn. Reson. Imaging* 39, 745–767. doi: 10.1002/jmri.24542

Naidich, TP, Duvernoy, HM, Delman, BN, Sorenson, AG, Kollias, SS, and Haacke, EM. *Duvernoy's atlas of the brainstem and cerebellum. High-field MRI: surface anatomy, internal structure, vascularisation and 3D anatomy*. Wien, NewYork: Springer. (2009).

National Institute for Health and Care Excellence. *COVID-19 rapid guideline: managing the long-term effects of COVID-19*. London: National Institute for Health and Care Excellence (NICE). (2020)

Nieto-Castanon, A. *Handbook of functional connectivity magnetic resonance imaging methods in CONN*. Boston, MA: Hilbert Press; (2020)

Oberwinkler, J., and Philipp, S. E. (2014). TRPM3. *Handb. Exp. Pharmacol.* 222, 427–459. doi: 10.1007/978-3-642-54215-2_17

Pajo, A. T., Espiritu, A. I., Apor, A. D. A. O., and Jamora, R. D. G. (2021). Neuropathologic findings of patients with COVID-19: a systematic review. *Neurol. Sci.* 42, 1255–1266. doi: 10.1007/s10072-021-05068-7

Sasai, S., Koike, T., Sugawara, S. K., Hamano, Y. H., Sumiya, M., Okazaki, S., et al. (2021). Frequency-specific task modulation of human brain functional networks: a fast fMRI study. *Neuroimage* 224:117375. doi: 10.1016/j.neuroimage.2020.117375

Sasso, E. M., Muraki, K., Eaton-Fitch, N., Smith, P., Lesslar, O. L., Deed, G., et al. (2022). Transient receptor potential melastatin 3 dysfunction in post COVID-19 condition and myalgic encephalomyelitis/chronic fatigue syndrome patients. *Mol. Med.* 28:98. doi: 10.1186/s10020-022-00528-y

Shan, Z. Y., Finegan, K., Bhuta, S., Ireland, T., Staines, D. R., Marshall-Gradisnik, S. M., et al. (2018a). Brain function characteristics of chronic fatigue syndrome: a task fMRI study. *Neuroimage* 19, 279–286. doi: 10.1016/j.nicl.2018.04.025

Shan, Z. Y., Finegan, K., Bhuta, S., Ireland, T., Staines, D. R., Marshall-Gradisnik, S. M., et al. (2018b). Decreased connectivity and increased blood oxygenation level dependent complexity in the default mode network in individuals with chronic fatigue syndrome. *Brain Connect.* 8, 33–39. doi: 10.1089/brain.2017.0549

Shaw, S. B., McKinnon, M. C., Heisz, J., and Becker, S. (2021). Dynamic task-linked switching between brain networks - a tri-network perspective. *Brain Cogn.* 151:105725. doi: 10.1016/j.bandc.2021.105725

Soriano, J. B., Murthy, S., Marshall, J. C., Relan, P., and Diaz, J. V. (2022). A clinical case definition of post-COVID-19 condition by a Delphi consensus. *Lancet Infect. Dis.* 22, e102–e107. doi: 10.1016/S1473-3099(21)00703-9

Su, J., Thapaliya, K., Eaton-Fitch, N., Marshall-Gradisnik, S. M., and Barnden, L. R. (2022). Connectivity between salience and default mode networks and subcortical nodes distinguishes between two classes of ME/CFS. *Brain Connect* 13, 164–173. doi: 10.1089/brain.2022.0049

Thapaliya, K., Marshall-Gradisnik, S., Barth, M., Eaton-Fitch, N., and Barnden, L. (2023). Brainstem volume changes in myalgic encephalomyelitis/chronic fatigue syndrome and long COVID patients. *Front. Neurosci.* 17:1125208. doi: 10.3389/fnins.2023.1125208

Ustun, TB, Kostanjesek, N, Chatterji, S, and Rehm, JWorld Health Organization. (2010). Measuring health and disability: manual for WHO disability assessment

schedule (WHODAS 2.0). World Health Organization. Available at: https://apps.who.int/iris/handle/10665/43974 (Accessed November 24, 2022).

Ware, J. E., Kosinski, M., Bayliss, M. S., McHorney, C. A., Rogers, W. H., and Raczek, A. (1995). Comparison of methods for the scoring and statistical analysis of SF-36 health profile and summary measures: summary of results from the medical outcomes study. *Med. Care* 33, AS264–AS279.

Whitfield-Gabrieli, S., and Nieto-Castanon, A. (2012). Conn: a functional connectivity toolbox for correlated and anticorrelated brain networks. *Brain Connect.* 2, 125–141. doi: 10.1089/brain.2012.0073

Wong, T. L., and Weitzer, D. J. (2021). Long COVID and myalgic encephalomyelitis/chronic fatigue syndrome (ME/CFS)-a systemic review and comparison of clinical presentation and symptomatology. *Medicina* 57:418. doi: 10.3390/medicina57050418

Wortinger, L. A., Glenne Oie, M., Endestad, T., and Bruun, W. V. (2017). Altered right anterior insular connectivity and loss of associated functions in adolescent chronic fatigue syndrome. *PLoS One* 12:e0184325. doi: 10.1371/journal.pone.0184325

Yong, S. J. (2021). Persistent brainstem dysfunction in long-COVID: a hypothesis. *ACS Chem. Neurosci.* 12, 573–580. doi: 10.1021/acschemneuro.0c00793

frontiers | Frontiers in Neuroscience

TYPE Original Research
PUBLISHED 22 June 2023
DOI 10.3389/fnins.2023.1147299

OPEN ACCESS

EDITED BY
Phyllis Kravet Stein,
Washington University in St. Louis, United States

REVIEWED BY
Rita Polito,
University of Foggia, Italy
Ines Villano,
University of Campania Luigi Vanvitelli, Italy

*CORRESPONDENCE
Maria Júlia Lopez Laurino
✉ majulaurino@hotmail.com

RECEIVED 18 January 2023
ACCEPTED 31 May 2023
PUBLISHED 22 June 2023

CITATION
Laurino MJL, Silva AKF, Santos LA and Vanderlei LCM (2023) Water drinking during aerobic exercise improves the recovery of non-linear heart rate dynamics in coronary artery disease: crossover clinical trial. *Front. Neurosci.* 17:1147299. doi: 10.3389/fnins.2023.1147299

Water drinking during aerobic exercise improves the recovery of non-linear heart rate dynamics in coronary artery disease: crossover clinical trial

Maria Júlia Lopez Laurino*, Anne Kastelianne França da Silva, Lorena Altafin Santos and Luiz Carlos Marques Vanderlei

Laboratory of Stress Physiology, Department of Physiotherapy, São Paulo State University (UNESP), Faculty of Science and Technology, Presidente Prudente, Brazil

Introduction: The post-exercise recovery is a period of vulnerability of the cardiovascular system in which autonomic nervous system plays a key role in cardiovascular deceleration. It is already known that individuals with coronary artery disease (CAD) are at greater risk due to delayed vagal reactivation in this period. Water ingestion has been studied as a strategy to improve autonomic recovery and mitigate the risks during recovery. However, the results are preliminary and need further confirmation. Therefore, our aim was to investigate the influence of individualized water drinking on the non-linear dynamics of heart rate during and after aerobic exercise in CAD subjects.

Methods: 30 males with CAD were submitted to a control protocol composed of initial rest, warming up, treadmill exercise, and passive recovery (60 min). After 48 hours they performed the hydration protocol, composed of the same activities, however, with individualized water drinking proportional to the body mass lost in the control protocol. The non-linear dynamics of heart rate were assessed by indices of heart rate variability extracted from the recurrence plot, detrended fluctuation analysis, and symbolic analysis.

Results and discussion: During exercise, the responses were physiological and similar in both protocols, indicating high sympathetic activity and reduced complexity. During recovery, the responses were also physiological, indicating the rise of parasympathetic activity and the return to a more complex state. However, during hydration protocol, the return to a more complex physiologic state occurred sooner and non-linear HRV indices returned to resting values between the 5th and 20th minutes of recovery. In contrast, during the control protocol, only a few indices returned to resting values within 60 minutes. Despite that, differences between protocols were not found. We conclude that the water drinking strategy accelerated the recovery of non-linear dynamics of heart rate in CAD subjects but did not influence responses during exercise. This is the first study to characterize the non-linear responses during and after exercise in CAD subjects.

KEYWORDS

autonomic nervous system, cardiac rehabilitation, complexity, fluid replacement, post-exercise recovery, coronary artery disease

1. Introduction

Coronary artery disease (CAD) is associated with autonomic imbalance (Floras and Ponikowski, 2015), which delays the post-exercise recovery of the cardiovascular and autonomic nervous systems (ANS) (Ushijima et al., 2009). The recovery efficiency of these systems has a significant prognostic value (Qiu et al., 2017) and is related to the risk of occurrence of acute cardiovascular events after exercises, such as ischemia and arrhythmias (Thompson et al., 2007).

Among the strategies that can accelerate post-exercise recovery, a fluid replacement strategy can be easily implemented in exercise-based cardiac rehabilitation programs. However, despite the important role that the autonomic nervous system (ANS) plays in cardiovascular deceleration after exercise (Fisher et al., 2015) and the risks related to the autonomic impairment and delayed recovery of CAD subjects (Ushijima et al., 2009; Floras and Ponikowski, 2015), only two studies investigated the effects of water drinking in the autonomic recovery in this population (Laurino et al., 2021; Silva et al., 2022).

Results from these studies were based on heart rate variability (HRV) analysis that evaluated the autonomic recovery. HRV analysis evaluates the ANS through the variation of consecutive NN intervals. HRV can be analyzed by linear methods, such as the time and frequency domains (Shaffer and Ginsberg, 2017), and by non-linear methods, which give information regarding the level of complexity of the ANS, which reflects the parasympathetic and sympathetic interaction/competition to modulate the HR (Henriques et al., 2020).

Therefore, using the HRV indices extracted from the Poincaré plot, Silva et al. (2022) evaluated the effects of water drinking in the 1-h autonomic recovery after a 40-min moderate-intensity session of exercise and found that water drinking promoted a faster and more efficient parasympathetic recovery. Corroborating with this finding, Laurino et al. (2021) reported a small effect of water drinking in the fast recovery phase from the same exercise session, recording a higher vagal response at the first minute of recovery.

Although both studies had positive results, they considered only linear indices of HRV, and the effect found for water drinking was mild to moderate. Thus, a new investigation is needed to determine whether these results can be reproduced using other HRV metrics, which will add further evidence to the benefits of water intake in exercise recovery. In this scenario, the use of non-linear metrics appears reasonable, because ANS control over the HR works as a non-linear and complex biological system (Porta et al., 2009). Also, Figueiredo et al. (2018) have suggested that the non-linear methods are more sensitive for detecting the physiological acute modifications following a high-intensity training session.

Nevertheless, studies that evaluated autonomic modulation during and after exercise through non-linear methods are just beginning, and most have considered only one method of non-linear analysis and evaluated only healthy young men and athletes (Henriques et al., 2020).

Thus, this study aimed to investigate the influence of a programmed water drinking protocol in CAD subjects, performed during and after moderate aerobic exercise, on the non-linear dynamics of heart rate during the periods of exercise and recovery from a cardiac rehabilitation session. We hypothesized that water drinking would be able to accelerate autonomic recovery and reduce the responses of non-linear dynamics of HR during exercise.

2. Materials and methods

2.1. Trial design

The trial was a crossover design. However, randomization was not possible once the hydration strategy adopted was individualized and based on the amount of fluid lost in the control session. Although the carryover effect was not expected in this study, a 48-h washout period was adopted. All procedures were prospectively registered at ClinicalTrials.gov (NCT03198806) and described in detail by Silva et al. (2020). We followed the Consolidated Standards of Reporting Clinical Trials extension to randomized crossover trials (Dwan et al., 2019).

2.2. Participants

This study recruited 38 men with the main diagnosis of CAD and left ventricle ejection fraction of above 50%, who did or did not have acute myocardial infarction and belong to functional classes I and II according to the New York Heart Association (Harvey et al., 1994). The volunteers were recruited as per convenience in two cardiac rehabilitation centers located in Presidente Prudente—São Paulo, Brazil, through a previous analysis of their medical records regarding the inclusion and exclusion criteria by an independent researcher. The eligible subjects were invited to participate in the study.

Individuals who were participating in an exercise-based cardiac rehabilitation for at least 3 months without contraindications to exercise (unstable angina, significant valvular disease, respiratory diseases, non-controlled hypertension and diabetes mellitus, renal and hepatic disorders, myocarditis, electrolyte disorders, abnormal hemodynamic responses during the cardiopulmonary exercise test, and neurological and/or orthopedics disorders that could preclude the protocol performance) were included in the study. To ensure the reliability of the HRV data, individuals who were smokers, classified with "low-risk drinking or abstinence" by the Alcohol Use Disorders Identification Test (AUDIT), Lima et al. (2005) were not included (Catai et al., 2019). Individuals who did not participate in all phases of the study protocol and those who presented errors >5% in the HRV data were excluded from the final analysis (Catai et al., 2019).

The study was approved by the Committee for Ethics and Research of the Faculty of Science and Technology—UNESP (CAAE: 54864716.8.0000.5402) and followed the Declaration of Helsinki. All volunteers signed the consent form after agreeing to participate in the study.

2.3. Experimental procedure

The experimental procedure (Figure 1) was divided into three phases scheduled with an interval of at least 48 h (washout) to allow

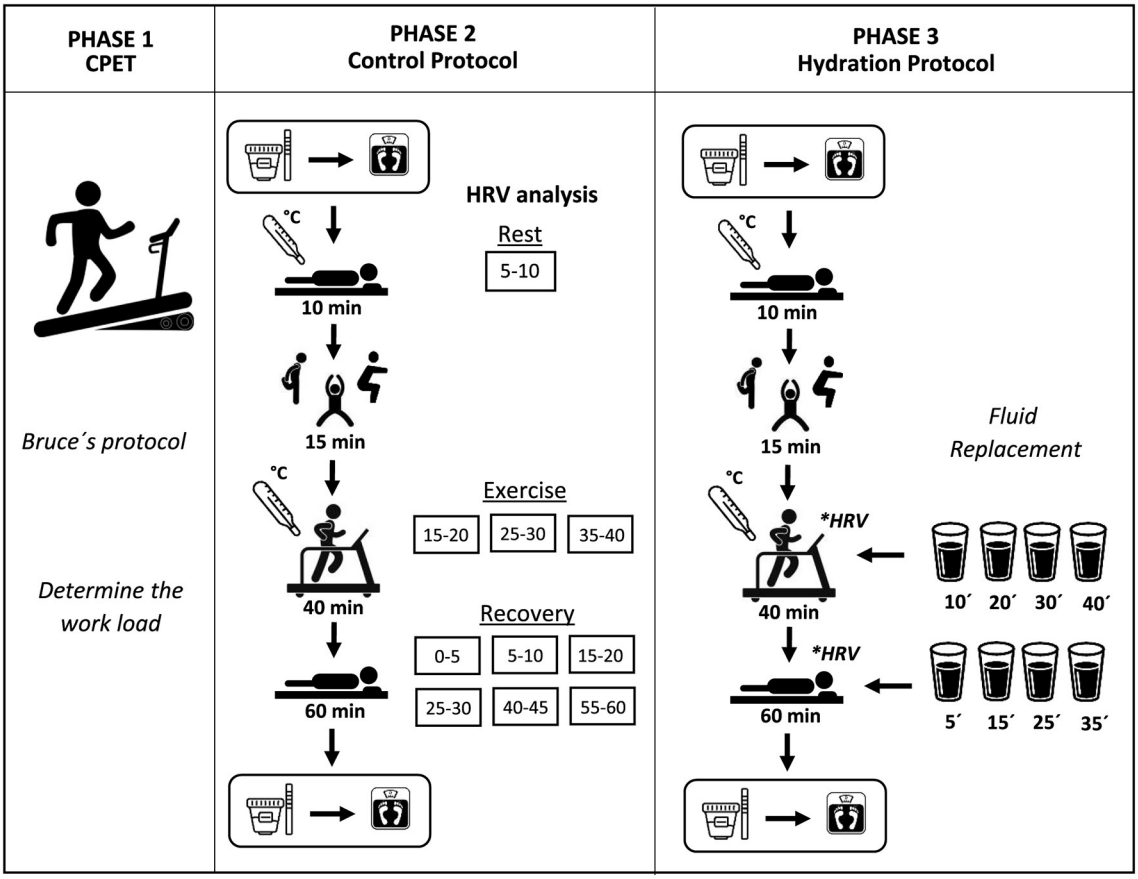

FIGURE 1
Experimental procedure.

the complete recovery of the participants and minimize the acute effects of the exercise. All procedures are described in detail in the article published by Silva et al. (2020).

In the first stage, a cardiopulmonary exercise test (CPET) was performed by a physician, according to Bruce's protocol (Meneghelo et al., 2011), to evaluate the hemodynamic responses and guide the exercise intensity prescription. It was set as 60 to 80% of the HR reached at the anaerobic threshold, determined by the analysis of the expiration gases, analyzed by the commercial system Quark PFT (Cosmed, Rome, Italy) (Cabral-Santos et al., 2015). The test was interrupted by voluntary physical exertion or according to the interruption criteria for the CPET (Meneghelo et al., 2011).

In the second stage, the control protocol (CON) was performed. It was composed of activities similar to those that usually constitute a session in exercise-based cardiac rehabilitation programs: initial rest in the supine position for 10 min; warm-up (stretching and free active exercises for arms and legs) for 15 min; aerobic exercise on a treadmill for 40 min; cooldown performed for 5 min with half the load used during exercise; and passive recovery in the supine position for 60 min.

In the third stage, the hydration protocol (HYD) was performed. It was composed of the same activities and procedures as the CON except that, during exercise and recovery, all volunteers drank 8 equal portions of mineral water (Bonafont, Brazil) at room temperature, which were offered every 10 min, starting at the 10th min of the exercise (Sawka et al., 2007). The amount of water ingested by each volunteer was calculated based on the body mass variation during the CON, considering that 1 gram lost is equal to 1 milliliter of fluid lost (Von Duvillard et al., 2004). This method had the aim of matching the fluid losses during the whole protocol and avoiding hypohydration. During recovery, participants used a straw to drink the water maintaining the supine position to avoid any interference in the HRV data.

In both protocols, before the initial rest and after the passive recovery, a urine sample was collected and analyzed (Combur 10 M teste, Roche®, Brazil) to determine the urine-specific gravity, which is considered a marker of the hydration level (Armstrong, 2005). Values above 1.020 classified the volunteer as dehydrated (Sawka et al., 2007). After the urine collection, the body mass was measured with a precision of 5 g (Balmak, Premium Bk−200Fa, Brazil). At the end of the initial rest and cooldown, the axillar temperature was measured through a thermometer (G-Tech). To record the RR intervals used to calculate the HRV indices, the Polar RS800CX HR monitor (Polar Electro, Kempele, Finland) (Rezende Barbosa et al., 2016) was placed on the volunteer's chest.

To ensure the HRV data reliability, all volunteers were oriented to not perform vigorous physical activity and to not consume stimulant substances during the 24 h previous to each phase (Catai et al., 2019). To ensure an initial hydrated state, they were oriented to ingest 500 ml of water 2 h before CON and HYD (Sawka et al.,

2007). To avoid circadian variation, all phases were performed between 1:00 and 6:00 pm, and the room temperature and humidity were controlled (21°-23°C and 40–60%) (Catai et al., 2019).

2.4. Outcomes

The ANS was evaluated through the HRV non-linear methods considering the following epochs for analysis: 5–10 min of initial rest; 15–20, 25–30, and 35–40 min of exercise; 0–5, 5–10, 15–20, 25–30, 40–45, and 55–60 min of recovery (Peçanha et al., 2017). We ensured that each RR series contained at least 256 consecutive RR intervals (Catai et al., 2019).

The RR series were submitted to a digital filtration (Polar Precision Performance SW version 5.0) (Nunan et al., 2009) followed by a visual inspection to eliminate premature ectopic beats and artifacts. Only series with more than 95% of sinus heartbeats were included in the study (Catai et al., 2019). The data filtering was performed by an experienced and blinded researcher.

The HRV methods considered for the ANS evaluation were as follows:

I) Detrended fluctuation analysis (DFA) is defined as the root-mean-square fluctuation of the integrated and detrended RR series. The DFA-total, the short-term alpha correlations (alpha-1), considering correlations from 4 to 11 RR intervals, and the long-term alpha correlations (alpha-2), considering the rest of the series (11 to 64 RR intervals), were calculated. This analysis classifies the RR series as linear, fractal, or random, with values ranging from 0.5 to 1.5. A resting physiological state is characterized by fractal correlation, with values closer to 1 (Peng et al., 1994). During moderate-intensity exercise, the tendency is for the RR series to become linear, with values closer to 1.5 (Gronwald et al., 2018).

II) Recurrence plot corresponds to the graph reconstruction of the spatial trajectory of the RR series (Eckmann et al., 1987). From the graph, the following indices were extracted: recurrence rate (REC—defined as the ratio of all recurrence states to all possible states), determinism (DET—defined as the ratio of recurrence points forming diagonal to all recurrence points), both of which indicate how predictable the RR series is. An RR series with higher values of REC and DET is associated with reduced parasympathetic activity, as demonstrated in animal models (Dabiré et al., 1998). For these analyses, the embedding dimension was set as $m = 10$, lag was fixed at $\tau = 1$, and the threshold distance was determined by $r = \sqrt{m}SD$, where SD represents the standard deviation of the RR intervals in the time series.

III) Sample entropy (SampEn) is defined as the conditional probability that two sequences similar for n points remain similar at the next point, which indicates the RR series complexity, which is reduced during exercise (Javorka et al., 2002). For this calculation, the embedding dimension was set as $m = 2$, and the tolerance was set as $r = 0.2SD$ (Richman and Moorman, 2000).

IV) Symbolic analysis indicates the quantity and type of variation between three consecutive RR intervals, classifying them into the following families: 0V (no variation, representing sympathetic modulation), 1V (one variation, representing global modulation), 2LV (two equal variations), and 2LV (two different variations), both representing parasympathetic modulation (Porta et al., 2007).

The DFA indices were calculated using the software "Detrended fluctuation analysis" available in the PhysioNet repository (Goldberger et al., 2000). The recurrence plot indices were calculated using the Kubios HRV software version 2.0 (Tarvainen et al., 2014). The symbolic analysis was performed using the software Symbolic Analysis fast version 4.0 (University of Milano, Italy).

As a secondary outcome, systolic (SBP) and diastolic (DBP) blood pressures were measured to provide additional information about the effect of water drinking on the cardiovascular and autonomic responses throughout the experimental procedure. The arterial blood pressure was measured indirectly using a stethoscope (Littmann, Saint Paul, USA) and an aneroid sphygmomanometer (Welch Allyn Tycos, New York, USA) at the following times: 10th min of initial rest; 15th and 35th min of treadmill exercise; and 5th, 10th, 20th, 30th, 40th, 50th, and 60th min of recovery. From these data, the mean arterial blood pressure (MBP) was calculated.

2.5. Sample size

The sample size was defined based on the results obtained in a pilot project for the sample entropy data. We adopted the magnitude of the significant difference of 0.2575 and considered a standard deviation of 0.3545, a significance level of 5%, and a power of 80%. Thus, the sample size resulted in 30 subjects.

2.6. Statistical analysis

The normality of the data was evaluated by the Shapiro–Wilk test. The comparison between the initial and final measures of body mass, axillar temperature, and urine-specific gravity was performed by Student's t-test for paired data or the Wilcoxon test. For the between-protocol comparison, the Student's t-test for unpaired data or the Mann–Whitney test was used. Cohen's d effect size was calculated (Maher et al., 2013). The HRV indices and arterial blood pressure were analyzed through the two-way ANOVA for repeated measures followed by Bonferroni or Dunnett's post-hoc test. The sphericity was checked by Mauchly's test, and, when violated, the Greenhouse–Geisser correction was considered. The partial eta-squared effect size was calculated (Maher et al., 2013).

This model was not adjusted by the daily use of beta-blockers and antihypertensive drugs due to the crossover design; thus, the effect of the medication is expected to not interfere with the analysis.

Statistical significance was set at 5%. The analyses were performed by a blinded researcher using a coded datasheet. All analyses were performed using the IBM SPSS Statistics software version 22.0 (IBM Corp, Armonk, New York).

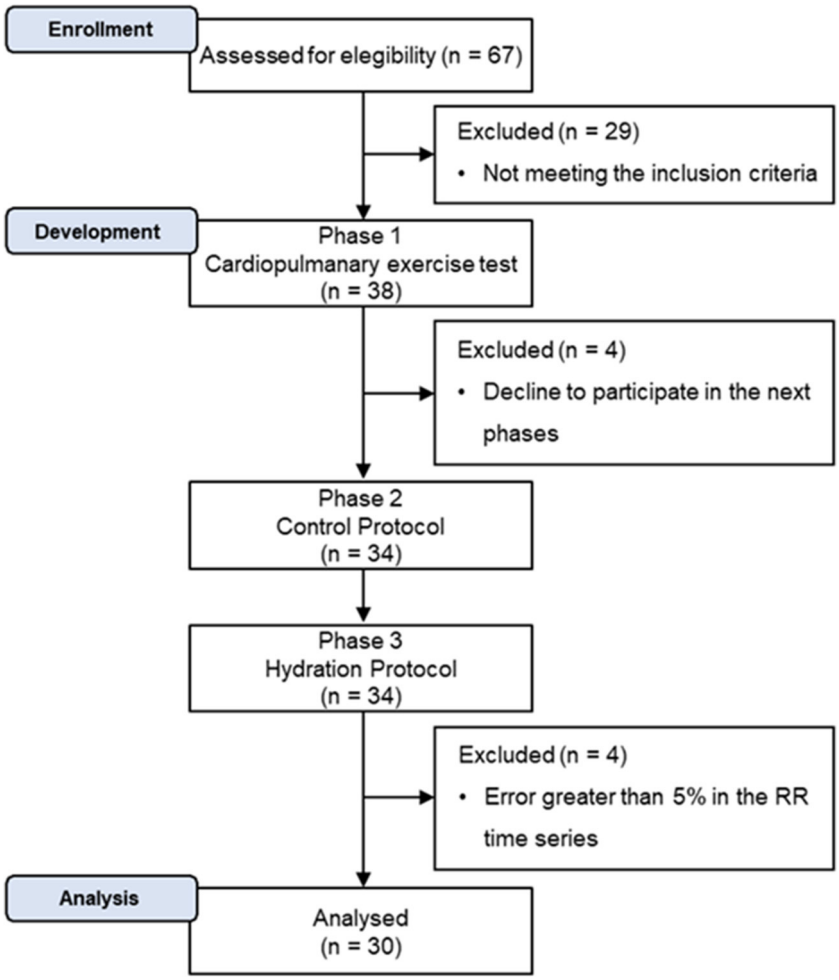

FIGURE 2
Participation flow diagram.

3. Results

In this study, we initially recruited 38 men, but four subjects dropped out before CON. Thus, the outcome assessment was not possible, making it unfeasible to consider the analysis of the intention to treat. After HYD, four subjects were excluded due to equipment error at the RR interval time series record. However, the data imputation was not considered due to the repeated measures design and the great HRV variation between subjects and epochs. After sample losses, 30 subjects were analyzed (Figure 2), whose characterization is shown in Table 1.

Of the 30 men analyzed, seven (23.30%) did not reach the anaerobic threshold during the test, so the VO2peak value of these subjects (24.64 ± 8.28 ml/Kg/min) was considered for the exercise prescription (American College of Sports Medicine., 2014).

The fluid loss was assessed through participants' body mass measurements. Our results revealed body mass reduction after the CON protocol. The average fluid loss (600 ± 180 ml) represented a reduction of 0.7% in body mass. A small reduction in body mass was also observed after the HYD protocol. The average fluid loss (170 ± 188 ml) represented a 0.2% reduction in body mass (Table 2).

The dynamic hydration condition was assessed through urine-specific gravity. Our results revealed that the hydration level was maintained after the CON protocol. A significantly lower hydration level was observed after the HYD protocol, with a large size effect. Although no significant differences were observed, there was a reduction in the axillary temperature after the HYD protocol. No change in the axillary temperature was observed after the CON protocol (Table 2).

The non-linear HRV indices analyzed during exercise are shown in Table 3. There were no significant differences between protocols and for the time vs. protocol interaction. However, there were differences between epochs (P-value < 0.05) for all indices, except for SampEn, Alpha-1, and 2ULV.

During exercise, in both protocols, the indices REC, DFA-total, and Alpha-2 increased and the 2LV index decreased. The 0V index increased only in CON, and the DET index increased only during HYD.

The non-linear HRV indices analyzed during recovery are shown in Figure 3. For all indices, there were no significant

TABLE 1 Sample characteristics ($N = 30$).

Variable	Mean ± SD	Minimum	Maximum
Age (years)	63.7 ± 8.4	45.0	83.0
Weight (Kg)	80.9 ± 12.8	58.0	108.5
Height (m)	1.7 ± 0.1	1.6	1.8
BMI (Kg/m²)	27.7 ± 4.1	20.6	39.4
Period of treatment (years)	3.4 ± 4.2	0.2	17.8
Resting HR (bpm)	63.3 ± 8.2	49.0	78.0
SBP (mmHg)	116.3 ± 8.9	100.0	140.0
DBP (mmHg)	76.0 ± 7.7	60.0	90.0
VO_2peak (ml/Kg/min)	27.1 ± 6.6	14.3	38.8
Maximum HR (bpm)	138.5 ± 22.4	98.0	173.0
Treadmill workload (Km/h)	4.8 ± 0.8	3.2	6.0
Amount of water ingested (ml)	600.0 ± 180.0	200.0	1000.0
Cardiac risk factors	**N (%)**		
Previous myocardial infarction	4 (13.3)		
Diabetes	14 (46.7)		
Dyslipidemia	21 (70.0)		
Hypertension	26 (86.7)		
Obesity	7 (23.3)		
Family history	20 (66.7)		
Ex-smoker	13 (43.3)		
Medicines of daily use	**N (%)**		
Anticoagulant	23 (76.7)		
Beta-blockers	21 (70.0)		
ARA II	10 (33.3)		
Ca^{2+} channel blockers	8 (26.7)		
K^{+} channel blockers	1 (3.3)		
ACE inhibitor	6 (20.0)		
Diuretics	9 (30.0)		
Vasodilator	3 (10.0)		
Statins	24 (80.0)		
Other	11 (36.7)		

Kg, kilogram; m, meters; Kg/m², kilogram/meter²; mmHg, millimeters of mercury; bpm, beats per minute; ml/min/kg, milliliter/minute/kilogram; km/h, kilometer/hour; BMI, body mass index; SBP, systolic blood pressure; DBP, diastolic blood pressure; HR, heart rate; VO2peak, peak oxygen consumption; ARA II, angiotensin II receptor antagonists; ACE, angiotensin-converting enzyme; Ca+, Calcium; K+ = Potassium.

differences between protocols. However, significant time vs. protocol interaction was found for REC, DFA-total, and Alpha-1 indices (P-value < 0.05). There were significant differences between epochs (P-value < 0.05) for all indices.

TABLE 2 Values of body mass, axillary temperature, and urine-specific gravity before and after each protocol ($N = 30$).

	Initial	Final	P-value (Cohen's d–effect magnitude)
Body mass (Kg)			
Control	81.5 ± 12.6	**80.9 ± 12.6**	<0.001 (0.05–null)
Hydration	81.4 ± 12.5	**81.3 ± 12.6**	0.026 (0.01–null)
Axillary temperature (°C)			
Control	35.1 ± 0.8	35.1 ± 1.0	0.328 (0.15–small)
Hydration	35.3 ± 1.0	**34.8 ± 1.1**	0.042 (0.43–small)
Urine-specific gravity			
Control	1.015 ± 0.005	1.014 ± 0.005	0.135 (0.20–small)
Hydration	1.016 ± 0.004	**1.012 ± 0.004**	<0.001 (1.00–large)

Mean ± standard deviation. Values in bold: significant difference ($p < 0.05$) from the initial measure. Kg, kilogram; °C, degrees Celsius.

Figure 3 shows that, during recovery, a gradual re-establishment of the indices to values close to those recorded at rest was observed in both protocols. There was a progressive increase of SampEn, 1V, 2LV, and 2ULV indices and a decrease of REC, DET, Alpha-1, Alpha-2, DFA-total, and 0V indices. However, the epoch in which this re-establishment occurred was different between protocols, happening earlier in HYD for most indices. Only the 1V index recovered at the same time in both protocols.

Table 4 displays results for SBP, DBP, and MBP. During exercise, there was no difference between protocols (SBP: $p = 0.94$; DBP: 0.91; MBP: 0.92) and no time vs. protocol interaction (SBP: $p = 0.24$; DBP: 0.47; MBP: 0.37). However, a large effect size was observed for SBP ($p = 0.00$; $\eta^2P = 0.62$), DBP ($p = 0.00$; $\eta^2P = 0.24$), and MBP ($p = 0.00$; $\eta^2P = 0.45$). Similarly, analysis of the recovery showed no difference between protocols (SBP: $p = 0.37$; DBP: $p = 0.56$; MBP: 0.45) and no interaction (SBP: $p = 0.63$; DBP: $p = 0.67$; MBP: 0.63); however, a medium/large time effect was observed (SBP: $p = 0.00$; $\eta^2P = 0.08$/DBP: $p = 0.01$; $\eta^2P = 0.05$/MBP: 0.00; $\eta^2P = 0.47$).

4. Discussion

Our main results showed that the water intake strategy could accelerate the recovery of the non-linear dynamic of HR of CAD subjects after an exercise-based cardiac rehabilitation session. However, during the exercise phase, the fluid lost and replaced did not influence the responses of the non-linear dynamics of HR in this period, corroborating with the previous studies of Silva et al. and Laurino et al.

The exercise protocol used in this study is similar to those commonly adopted in cardiac rehabilitation programs. The 0.7% reduction in body mass at the end of the CON showed that, although no significant changes were observed in the urine-specific gravity, the fluid loss registered approached a state of mild hypohydration, defined as a reduction of more than 1% in body

TABLE 3 Comparison between rest and exercise epochs for control and hydration protocols ($N = 30$).

	Rest	Exercise Epochs			ANOVA P-value (η^2_p-effect magnitude)
	5°-10° min	15°-20° min	25°-30° min	35°-40° min	
REC (%)					
Control	34.5 ± 8.9	41.5 ± 7.0	**42.9 ± 7.8**	**43.5 ± 6.8**	Epochs: 0.00 (0.28–large) Interaction: 0.55 (0.01–small)
Hydration	36.0 ± 9.5	**44.5 ± 8.0**	**44.3 ± 8.4**	**43.1 ± 5.1**	
DET (%)					
Control	98.0 ± 1.7	98.9 ± 1.1	99.0 ± 1.1	99.2 ± 0.9	Epochs: 0.00 (0.25–large) Interaction: 0.78 (0.00–null)
Hydration	98.2 ± 1.4	**99.2 ± 0.9**	**99.1 ± 1.0**	**99.3 ± 0.5**	
SampEn					
Control	1.5 ± 0.4	1.4 ± 0.3	1.4 ± 0.3	**1.3 ± 0.3**	Epochs: 0.01 (0.07–medium) Interaction: 0.79 (0.00–null)
Hydration	1.4 ± 0.4	1.4 ± 0.3	1.4 ± 0.3	1.3 ± 0.2	
DFA-total					
Control	1.01 ± 0.11	**1.11 ± 0.14**	**1.12 ± 0.13**	**1.15 ± 0.16**	Epochs: 0.00 (0.18–large) Interaction: 0.95 (0.00–null)
Hydration	1.05 ± 0.16	**1.14 ± 0.11**	**1.14 ± 0.15**	**1.14 ± 0.12**	
Alpha-1					
Control	0.98 ± 0.31	0.96 ± 0.25	1.01 ± 0.23	1.01 ± 0.23	Epochs: 0.54 (0.01–small) Interaction: 0.69 (0.00–null)
Hydration	1.04 ± 0.25	1.02 ± 0.21	1.02 ± 0.20	1.05 ± 0.20	
Alpha-2					
Control	1.01 ± 0.12	**1.10 ± 0.18**	**1.10 ± 0.15**	**1.10 ± 0.20**	Epochs: 0.00 (0.15–large) Interaction: 0.94 (0.00–null)
Hydration	1.01 ± 0.20	**1.14 ± 0.15**	**1.12 ± 0.20**	**1.12 ± 0.15**	
0V (%)					
Control	26.1 ± 16.3	32.9 ± 14.3	**34.4 ± 13.7**	**38.9 ± 14.6**	Epochs: 0.00 (0.14–large) Interaction: 0.24 (0.02–small)
Hydration	27.1 ± 17.5	**36.6 ± 13.1**	**37.2 ± 13.8**	34.9 ± 11.8	
1V (%)					
Control	44.1 ± 5.9	42.2 ± 6.9	42.5 ± 6.6	40.0 ± 6.9	Epochs: 0.00 (0.08–medium) Interaction: 0.32 (0.02–small)
Hydration	44.3 ± 6.8	41.1 ± 6.7	41.5 ± 6.8	41.4 ± 4.8	
2LV (%)					
Control	7.6 ± 4.1	**3.9 ± 3.0**	**3.5 ± 3.0**	**3.2 ± 2.9**	Epochs: 0.00 (0.36–large) Interaction: 0.47 (0.01–small)
Hydration	7.6 ± 5.2	**2.8 ± 3.6**	**2.9 ± 2.3**	**3.4 ± 2.4**	
2ULV (%)					
Control	22.2 ± 14.8	21.0 ± 8.6	19.6 ± 6.9	17.9 ± 6.9	Epochs: 0.27 (0.02–small) Interaction: 0.39 (0.01–small)
Hydration	21.0 ± 12.8	19.4 ± 10.1	18.9 ± 7.6	20.2 ± 7.5	

Mean ± standard deviation. Values in bold: significant difference ($p < 0.05$) from rest. REC, recurrence rate; DET, determinism; SampEn, sample entropy; DFA, analysis of detrended fluctuations; 0V, no variation; 1V, one variation; 2LV, two equal variations; 2ULV, two different variations; η^2_p, partial eta-squared.

mass (Mcdermott et al., 2017). It did not promote changes in the non-linear dynamics of HR during exercise, but it was able to delay the recovery of CAD subjects after a cardiac rehabilitation session.

The ANS is important in the regulation of acute hemodynamic responses to exercise. Parasympathetic withdrawal increases the HR in low-intensity exercise, and the activation of the sympathetic nervous system increases the HR at a level that will supply the body's demands in high-intensity exercise (Fisher et al., 2015). This scenario was observed in our study, as the non-linear autonomic responses observed were characterized by increased sympathetic and reduced parasympathetic modulation (evidenced by an increased 0V and a reduced 2LV and 2ULV, respectively). Also, a decreased complexity and fractal characteristic of the RR series is expected during exercise (evidenced by the decreased SampEn and increased REC, DET, DFA-total, and Alpha-2) (Casties et al., 2005; Floras and Ponikowski, 2015; Gronwald et al., 2018).

The same non-linear autonomic changes were observed in athletes during light and moderate aerobic exercise (Gronwald et al., 2018). These changes are explained by the sympathetic branch predominance, which reduces the variation between consecutive

RR intervals, increasing the linearity and predictability and reducing the complexity of the series (Fisher et al., 2015; Gronwald et al., 2018).

The magnitude of autonomic responses to exercise is mediated by a complex pathway that includes central command, exercise pressor response, and arterial baroreflex modifications, all of which are associated with exercise intensity and environmental conditions (Fisher et al., 2015). The sympathetic overactivity observed in CAD (Ushijima et al., 2009) is related to chronotropic incompetence, fatigue, and diminished coronary blood flow during exercise (Fisher et al., 2015), augmenting the risk of chest pain and arrhythmias (Thompson et al., 2007). However, given the non-significant differences between the CON and HYD protocols, we can conclude that the water drinking was not able to change or enhance the autonomic profile of CAD during exercise by maintaining the hydration status.

It is important to highlight that the negative effects of fluid loss during exercise in heart rate, cardiac output, and arterial blood pressure are usually registered above ∼2% of body mass reduction induced by higher exercise intensities and hot environments (Trangmar and González-Alonso, 2019), which were not part of our study. Also, the fluid loss occurred throughout the periods of exercise and recovery, so the amount of fluid lost only during exercise may not be sufficient to influence non-linear responses during this period.

Immediately after exercise, the HR rapidly decreases, mainly due to parasympathetic reactivation, mediated by the interruption of central command and the mechanoreflex (evidenced by the increase in 2LV and 2ULV). After this fast reduction, the HR remains slightly elevated due to the slow sympathetic activity reduction in the face of the gradual reestablishment of body temperature and reduction of metaboreflexes (evidenced by the decrease in 0V) (Peçanha et al., 2014). This residual sympathetic overactivity is important to maintain a slightly elevated cardiac output to preserve the perfusion pressure against peripheral vasodilatation (Fisher et al., 2015). During recovery, the complexity and fractal characteristics of the RR series are reestablished (evidenced by the increase in SampEn, the decrease in REC and DET, and the return of DFA-total and Alpha-1 to values closer to 1.00) (Godoy, 2016).

The ANS recovery in the CON protocol was delayed, and some indices did not achieve complete recovery after the 60-min evaluation. This delay, especially for CAD individuals, represents an increased risk, once the maintenance of a high sympathetic modulation induces ischemic and arrhythmic events during recovery (Thompson et al., 2007). Also, in the CON protocol, the REC, DET, SampEn, DFA-total, and 2ULV indices reached the recovery between the 10th and 30th min post-exercise. However, after 40 min, they returned to an unrecovered state, suggesting that maintaining a state of hypohydration after exercise may retard the long-term recovery of the ANS, which should be further investigated in future studies. However, when the water drinking strategy was used, all indices achieved complete recovery between the 5th and 20th min. These results are in accordance with previous studies (Laurino et al., 2021; Silva et al., 2022), reinforcing the positive effects of water drinking in the post-exercise autonomic recovery of CAD individuals.

The beneficial effects of water drinking on autonomic recovery in CAD are yet to be fully elucidated. However, based on previous observations, we may hypothesize that the sympathetic-mediated acute pressor response may be involved in this response. It is known that, at the level of portal circulation, small changes in blood osmolality toward hypoosmolality produce a spinal reflex-like mechanism that activates the postganglionic sympathetic neurons, leading to a rise in blood pressure. This pressor response was observed only in populations with an altered baroreflex sensitivity, as found in the elderly (May and Jordan, 2011), the population of our study. The results found for arterial blood pressure confirm this hypothesis; once in the HYD protocol, the post-exercise hypotension observed in the CON protocol was attenuated.

Although, due to the complexity of the neuronal pathways regulating cardiovascular function, a rise in sympathetic activity at the spinal level does not produce cardiac responses (May and Jordan, 2011). Our data confirm this mechanism, despite the high blood pressure during the recovery of the non-linear response, which indicated a more preserved parasympathetic modulation during the HYD protocol. In line with this theory, a recent study showed that the acute ingestion of at least 200 mL of water produced a bradycardia response related to an increased vagal tone at the sinus node. However, the physiological mechanism responsible for this response is not wellestablished in the literature (Grasser, 2020). It is important to point out that all these mechanisms were previously investigated in a rest condition in response to a single bout of water ingestion; thus, the post-exercise response to a fractioned dose drinking strategy may include different pathways.

The fluid replacement protocol proposed in this study is classified as "programmed or planned drinking," in which a predetermined and individualized amount of fluid is ingested to prevent dehydration by matching the sweat losses. This method considers the variation in the sweating rate between individuals (Kenefick, 2018). Also, most of the individuals enrolled in cardiac rehabilitation are elderly and may have an impaired sense of thirst (Kenney and Chiu, 2001), which could preclude adequate fluid replacement if it is performed *ad libitum*, which is the method commonly used when the patient brings his water bottle to the rehabilitation session and drinks it during or at the end of the exercise.

In the clinical practice scenario, these results have important implications, as they raise the potential importance of the implementation of planned drinking protocols during exercise-based cardiac rehabilitation sessions. Also, this strategy is low-cost and easy to implement and could increase the safety of these programs (Thompson et al., 2007; Qiu et al., 2017). Also, we highlight the importance of controlling the temperature of the cardiac rehabilitation room and orienting the patients regarding the importance of fluid replacement and the place and time of day to perform unsupervised activities. This is because high temperatures can promote even more significant fluid losses that, when not adequately replaced, may significantly impair autonomic recovery, increasing the risks of sudden events. Furthermore, this study adds new information to the literature regarding the characteristics and physiology of the non-linear dynamics of HR of CAD subjects during the periods of exercise and recovery. To our knowledge, this

10.3389/fnins.2023.1147299

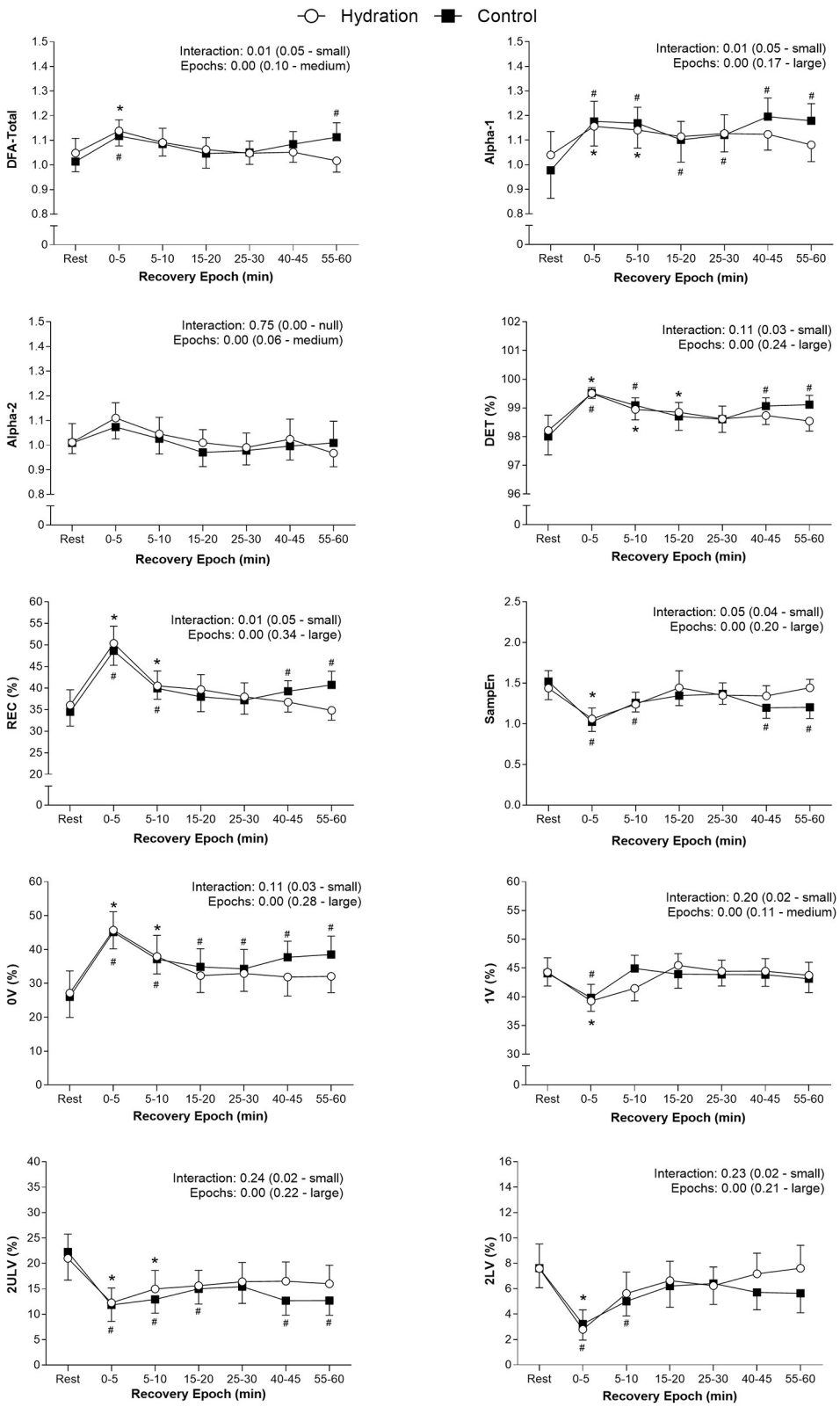

FIGURE 3
Differences between rest and recovery epochs for all indices analyzed in both protocols. Values are plotted as mean and 95% confidence intervals. The ANOVA effects found for epochs and interaction are presented as the p-value (effect size—effect magnitude). #Significant difference ($p < 0.05$) from rest in CON; *Significant difference ($p < 0.05$) from rest in HYD; REC, Recurrence rate; DET, Determinism; SampEn, Sample entropy; DFA, detrended fluctuations analysis; 0V, no variation; 1V, one variation; 2LV, two equal variations; 2ULV, two different variations.

TABLE 4 Values of systolic, diastolic, and mean arterial blood pressure throughout control and hydration protocols ($N = 30$).

	Rest	Exercise		Recovery						
	10° min	15° min	35° min	5° min	10° min	20° min	30° min	40° min	50° min	60° min
SBP (mmHg)										
Control	116.3 ± 8.9	**132.1 ± 12.0**	**132.1 ± 11.1**	114.3 ± 10.1	112.3 ± 9.3	**110.0 ± 9.8**	**108.3 ± 9.8**	**109.3 ± 9.8**	**111.3 ± 14.8**	112.3 ± 13.8
	–	–	–	[−2.0 ± 9.6]	[−4.0 ± 8.1]	[−6.3 ± 9.3]	[−8.0 ± 9.6]	[−7.0 ± 9.1]	[−5.0 ± 14.6]	[−4.0 ± 13.8]
Hydration	118.0 ± 11.6	**132.3 ± 9.3**	**129.7 ± 10.3**	114.3 ± 13.8	113.3 ± 12.4	112.3 ± 12.5	112.3 ± 11.0	113.7 ± 14.0	114.3 ± 14.5	114.7 ± 14.3
	–	–	–	[−3.7 ± 11.6]	[−4.7 ± 10.7]	[−5.7 ± 11.6]	[−5.7 ± 12.2]	[−4.3 ± 11.9]	[−3.7 ± 11.9]	[−3.3 ± 12.9]
DBP (mmHg)										
Control	76.0 ± 7.7	**83.0 ± 6.5**	79.0 ± 7.1	74.3 ± 8.2	71.7 ± 10.2	71.3 ± 9.4	71.3 ± 8.6	72.3 ± 9.7	72.7 ± 11.1	73.3 ± 12.1
	–	–	–	[−1.7 ± 7.5]	[−4.3 ± 8.6]	[−4.7 ± 8.6]	[−4.7 ± 7.7]	[−3.7 ± 8.1]	[3.3 ± 10.6]	[−2.7 ± 11.1]
Hydration	77.0 ± 11.5	**81.7 ± 10.8**	78.7 ± 9.4	74.0 ± 10.0	73.0 ± 9.5	74.0 ± 10.4	74.0 ± 9.3	74.3 ± 10.1	73.0 ± 9.5	73.7 ± 9.6
	–	–	–	[−3.0 ± 7.9]	[−4.0 ± 8.9]	[−3.0 ± 9.9]	[−3.0 ± 11.8]	[−2.7 ± 9.8]	[−4.0 ± 10.4]	[−3.3 ± 9.9]
MBP (mmHg)										
Control	89.4 ± 7.5	**99.4 ± 7.2**	**96.7 ± 7.3**	87.7 ± 8.6	85.2 ± 9.5	**84.2 ± 9.1**	**83.7 ± 8.5**	**84.7 ± 9.3**	**85.5 ± 11.7**	86.3 ± 12.3
	–	–	–	[−1.8 ± 7.7]	[−4.2 ± 7.7]	[−5.2 ± 7.3]	[−5.8 ± 7.5]	[−4.8 ± 7.8]	[−3.9 ± 11.2]	[−3.1 ± 11.4]
Hydration	90.7 ± 10.5	**98.6 ± 9.3**	**95.7 ± 9.0**	87.4 ± 9.5	86.4 ± 9.0	86.8 ± 9.9	86.8 ± 8.9	87.4 ± 10.3	86.8 ± 10.6	87.3 ± 10.1
	–	–	–	[−3.2 ± 7.3]	[−4.2 ± 7.9]	[−3.9 ± 8.7]	[−3.9 ± 10.8]	[−3.2 ± 9.2]	[−3.9 ± 10.1]	[−3.3 ± 9.5]

Mean ± standard deviation [ΔRecovery–Rest]. Values in bold: significant difference ($p < 0.05$) from rest. SBP, systolic blood pressure; DBP, diastolic blood pressure; MBP, mean arterial blood pressure; mmHg, millimeters of mercury.

10.3389/fnins.2023.1147299

is the first study to address it and consider the effects of fluid loss as well as its replacement in these periods.

Despite these promising results, the limitation regarding the lack of randomization needs to be pointed out. Thus, to minimize this potential bias, only individuals familiar with and attending cardiac rehabilitation were included to eliminate the possible acute effects of exercise.

New studies addressing this topic are needed to better understand the physiological effects of fluid loss and replacement in subjects with CAD, the effects of using other fluid replacement strategies, and the use of other types of beverages. The effect of water drinking when active recovery is performed needs to be investigated. As we included only males in our study, new research on the female population is needed as well.

Given these results, we conclude that the proposed water drinking protocol was able to accelerate the recovery of non-linear dynamics of HR after moderate-intensity aerobic exercise performed in the models of a cardiac rehabilitation session and that the volume of fluid lost during exercise did not influence autonomic responses in this period.

Data availability statement

The raw data supporting the conclusions of this article will be made available by the authors, without undue reservation.

Ethics statement

The studies involving human participants were reviewed and approved by Committee for Ethics and Research of the Faculty of Science and Technology—UNESP (CAAE: 54864716.8.0000.5402). The patients/participants provided their written informed consent to participate in this study.

Author contributions

AS and LV conceived and designed the study. ML, AS, and LS carried out the experiment and data collection. ML and AS performed the data analysis. ML, AS, and LV contributed to the data interpretation and manuscript writing. LV supervised the project. All authors discussed and contributed to the final manuscript version.

Funding

This work was supported by the Conselho Nacional de Desenvolvimento Científico e Tecnológico (CNPq) [Grant Number 401258/2016-5] and the Coordenação de Aperfeiçoamento de Pessoal de Nível Superior—Brazil (CAPES) [finance code 001].

Acknowledgments

We would like to thank the Conselho Nacional de Desenvolvimento Científico e Tecnológico (CNPq), the Coordenação de Aperfeiçoamento de Pessoal de Nível Superior—Brazil (CAPES) for supporting this work, and the Laboratory of Cell Physiology of Exercise (LAFICE) for having provided the space and equipment.

Conflict of interest

The authors declare that the research was conducted in the absence of any commercial or financial relationships that could be construed as a potential conflict of interest.

Publisher's note

References

American College of Sports Medicine. (2014). *ACSM's Guidelines for Exercise Testing and Prescription*. 9 ed. Baltimore: Wolters Kluwer.

Armstrong, L. E. (2005). Hydration assessment techniques. *Nutr. Rev.* 63, S40–S54. doi: 10.1301/nr.2005.jun.S40-S54

Cabral-Santos, C., Gerosa-Neto, J., Inoue, D. S., Panissa, V. L. G., Gobbo, L. A., Zagatto, A. M., et al. (2015). Similar anti-inflammatory acute responses from moderate-intensity continuous and high-intensity intermittent exercise. *J. Sport Sci. Med.* 14, 849–856.

Casties, J., Mottet, D., and Le Gallais, D. (2005). Non-Linear analyses of heart rate variability during heavy exercise and recovery in cyclists. *Int. J. Sports Med.* 26, 1–6. doi: 10.1055/s-2005-872968

Catai, A. M., Pastre, C. M., Godoy, M. F., de Silva, E., Takahashi, A. C., de Siva, M., et al. (2019). Heart rate variability: are you using it properly? Standardization checklist of procedures. *Braz. J. Phys. Ther.* 20, 215. doi: 10.1016/j.bjpt.2019.02.006

Dabiré, H., Mestivier, D., Jarnet, J., Safar, M. E., and Chau, N. P. (1998). Quantification of sympathetic and parasympathetic tones by non-linear indexes in normotensive rats. *Am. J. Physiol. Heart. Circ. Physiol.* 275, 1290–1297. doi: 10.1152/ajpheart.1998.275.4.H1290

Dwan, K., Li, T., Altman, D. G., and Elbourne, D. (2019). CONSORT 2010 statement: extension to randomized crossover trials. *Bmj* 366, l4378. doi: 10.1136/bmj.l4378

Eckmann, J. P., Kamphorst, S. O., and Ruelle, D. (1987). Recurrence plots of dynamical systems. *Europhys. Lett.* 4, 973–977. doi: 10.1209/0295-5075/4/9/004

Figueiredo, R., Pereira, R., and Neto, O. P. (2018). Non-linear analysis is the most suitable method to detect changes in heart autonomic control after exercise of different durations. *Comput. Biol. Med.* 97, 83–88. doi: 10.1016/j.compbiomed.2018.04.011

Fisher, J. P., Young, C. N., and Fadel, P. J. (2015). Autonomic adjustments to exercise in humans. *Compr. Physiol.* 5, 475–512. doi: 10.1002/cphy.c140022

Floras, J. S., and Ponikowski, P. (2015). The sympathetic/parasympathetic imbalance in heart failure with reduced ejection fraction. *Eur. Heart J.* 36, 1974–1982. doi: 10.1093/eurheartj/ehv087

Godoy, M. F. (2016). Non-linear analysis of heart rate variability: a comprehensive review. *J. Cardiol. Therapy* 3, 528–533. doi: 10.17554/j.issn.2309-6861.2016.03.101-4

Goldberger, A. L., Amaral, L. A., Glass, L., Hausdorff, J. M., Ivanov, P. C., and Mark, R. G. (2000). PhysioBank, PhysioToolkit and PhysioNet: Components of a new research resource for complex physiologic signals. *Circulation*. 101, E215–E220. doi: 10.1161/01.CIR.101.23.e215

Grasser, E. K. (2020). Dose-dependent heart rate responses to drinking water: a randomized crossover study in young, non-obese males. *Clinic. Autonom. Res.* 30, 567–570. doi: 10.1007/s10286-020-00673-6

Gronwald, T., Hoos, O., Ludyga, S., and Hottenrott, K. (2018). Non-linear dynamics of heart rate variability during incremental cycling exercise. *Res. Sports Med.* 8, 1–11. doi: 10.1080/15438627.2018.1502182

Harvey, R., Dolgin, R., and Leom, T. (1994). "New York Heart Association Criteria Committe," in *Nomenclature and Criteria for Diagnosis of Diseases of the Heart and Great Vessels* (Boston: Little. Brown). p. 286.

Henriques, T., Ribeiro, M., Teixeira, A., Castro, L., Antunes, L., and Costa-Santos, C. (2020). Non-linear methods most applied to heart-rate time series: a review. *Entropy* 22, 309. doi: 10.3390/e22030309

Javorka, M., Zila, I., Balharek, T., and Javorka, K. (2002). Heart rate recovery after exercise: relations to heart rate variability and complexity. *Brazil. J. Med. Biologic. Res.* 35, 991–1000. doi: 10.1590/S0100-879X2002000800018

Kenefick, R. W. (2018). Drinking strategies: planned drinking vs. drinking to thirst. *Sports Med.* 48, 31–37. doi: 10.1007/s40279-017-0844-6

Kenney, W. L., and Chiu, P. (2001). Influence of age on thirst and fluid intake. *Med. Sci. Sports Exerc.* 33, 1524–1532. doi: 10.1097/00005768-200109000-00016

Laurino, M. J. L., da Silva, A. K. F., Santos, L. A., Ribeiro, F., Vanzella, L. M., Corazza, D. A. G., et al. (2021). Vagal reactivation after a cardiac rehabilitation session associated with hydration in coronary artery disease patients: crossover clinical trial. *Sci. Rep.* 11, 40. doi: 10.1038/s41598-021-89840-x

Lima, C. T., Freire, A. C., Silva, A. P., Teixeira, R. M., Farrell, M., and Prince, M. (2005). Concurrent and construct validity of the audit in an urban brazilian sample. *Alcohol Alcohol* 40, 584–589. doi: 10.1093/alcalc/agh202

Maher, J. M., Markey, J. C., and Ebert-May, D. (2013). The other half of the story: Effect size analysis in quantitative research. *CBE Life Sci. Educ.* 12, 345–351. doi: 10.1187/cbe.13-04-0082

May, M., and Jordan, J. (2011). The osmopressor response to water drinking. *Am. J. Physiol. Regul. Integr. Comp. Physiol.* 300, 40–46. doi: 10.1152/ajpregu.00544.2010

Mcdermott, B. P., Anderson, S. A., Lawrence, E., Casa, D. J., Samuel, N., Cooper, L., et al. (2017). National athletic trainers' association position statement: fluid replacement for the physically active. *J. Athl. Train.* 52, 877–895. doi: 10.4085/1062-6050-52.9.02

Meneghelo, R. S., Araújo, C. G. S., Stein, R., Mastrocolla, L. E., Albuquerque, P. F., and Serra, S. M. (2011). III Diretrizes da Sociedade Brasileira de Cardiologia Sobre Teste Ergométrico. *Rev. Bras. Fisioter.* 95, 1–26. doi: 10.1590/S0066-782X2010002400001

Nunan, D., Gay, D., Jakovljevic, D. G., Hodges, L. D., Sandercock, G. R. H., and Brodie, D. A. (2009). Validity and reliability of short-term heart-rate variability from the Polar S810. *Med. Sci. Sports Exer.* 41, 243–250. doi: 10.1249/MSS.0b013e318184a4b1

Peçanha, T., Bartels, R., Brito, L. C., Paula-Ribeiro, M., Oliveira, R. S., and Goldberger, J. J. (2017). Methods of assessment of the post-exercise cardiac autonomic recovery: a methodological review. *Int. J. Cardiol.* 227, 795–802. doi: 10.1016/j.ijcard.2016.10.057

Peçanha, T., Silva-Júnior, N. D., and Forjaz, C. L., de M. (2014). Heart rate recovery: autonomic determinants, methods of assessment and association with mortality and cardiovascular diseases. *Clin. Physiol. Funct. Imag.* 34, 327–339. doi: 10.1111/cpf.12102

Peng, C. K., Havlin, S., Stanley, H. E., and Goldberger, A. L. (1994). Quantification of scaling exponents and crossover phenomena in non-stationary heartbeat time series. *CHAOS* 5, 82–87. doi: 10.1063/1.166141

Porta, A., Rienzo, M., di, Wessel, N., and Kurths, J. (2009). Addressing the complexity of cardiovascular regulation. *Philosophic. Transact. Royal Soc. Mathematic. Physic. Eng. Sci.* 367, 1215–1218. doi: 10.1098/rsta.2008.0292

Porta, A., Tobaldini, E., Guzzetti, S., Furlan, R., Montano, N., and Gnecchi-ruscone, T. (2007). Assessment of cardiac autonomic modulation during graded head-up tilt by symbolic analysis of heart rate variability. *Am. J. Physiol. Heart Circ. Physiol.* 293, 702–708. doi: 10.1152/ajpheart.00006.2007

Qiu, S., Cai, X., Sun, Z., Li, L., Zuegel, M., Steinacker, J. M., et al. (2017). Heart rate recovery and risk of cardiovascular events and all-cause. *J. Am. Heart Assoc.* 6, 1–12. doi: 10.1161/JAHA.117.005505

Rezende Barbosa, M. P. C., Silva, N. T., Azevedo, F. M., Pastre, C. M., and Vanderlei, L. C. M. (2016). Comparison of Polar® RS800G3TM heart rate monitor with Polar® S810iTM and electrocardiogram to obtain the series of RR intervals and analysis of heart rate variability at rest. *Clin. Physiol. Funct. Imag.* 36, 112–117. doi: 10.1111/cpf.12203

Richman, J. S., and Moorman, J. R. (2000). Physiological time-series analysis using approximate entropy and sample entropy. *Am. J. Physiol. Heart Circ. Physiol.* 278, 2039–2049. doi: 10.1152/ajpheart.2000.278.6.H2039

Sawka, M. N., Burke, L. M., Eichner, E. R., Maughan, R. J., Montain, S. J., and Stachenfeld, N. S. (2007). Exercise and fluid replacement. *Med. Sci. Sport Exer.* 39, 377–390. doi: 10.1249/mss.0b013e31802ca597

Shaffer, F., and Ginsberg, J. P. (2017). An Overview of heart rate variability metrics and norms. *Front. Public Health* 5, 258. doi: 10.3389/fpubh.2017.00258

Silva, A. K. F., Laurino, M. J. L., Vanzella, L. M., Santos, L. A., Ribeiro, F., Corazza, D. A. G., et al. (2020). Influence of the hydration on autonomic modulation and cardiorespiratory parameters of coronary heart disease patients submitted to a cardiovascular rehabilitation session: Crossover clinical trial protocol. *Motriz. Revista de Educacao Fisica* 26, 2210. doi: 10.1590/s1980-6574202000010022

Silva, A. K. F., Santos, L. A., Laurino, M. J. L., Vanzella, L. M., Ribeiro, F., Rozan, G. B., et al. (2022). Hydration influence on the autonomic recovery of the coronary diseases patient: geometric indices analysis. *Res. Q. Exerc. Sport* 93, 230–239. doi: 10.1080/02701367.2020.1818672

Tarvainen, M. P., Niskanen, J. P., Lipponen, J. A., Ranta-aho, P. O., and Karjalainen, P. A. (2014). Kubios HRV—heart rate variability analysis software. *Comput. Meth. Prog. Bio.* 113, 210–220. doi: 10.1016/j.cmpb.2013.07.024

Thompson, P. D., Franklin, B. A., Balady, G. J., Blair, S. N., Corrado, D., Estes, N. A. M., et al. (2007). Exercise and acute cardiovascular events: Placing the risks into perspective a scientific statement from the american heart association council on nutrition, physical activity, and metabolism and the council on clinical cardiology. *Circulation* 115, 2358–2368. doi: 10.1161/CIRCULATIONAHA.107.181485

Trangmar, S. J., and González-Alonso, J. (2019). Heat, hydration and the human brain, heart and skeletal muscles. *Sports Med.* 49, S69–S85. doi: 10.1007/s40279-018-1033-y

Ushijima, A., Fukuma, N., Kato, Y., Aisu, N., and Mizuno, K. (2009). Sympathetic excitation during exercise as a cause of attenuated heart rate recovery in patients with myocardial infarction. *J. Nippon Med. Sch.* 76, 76–83. doi: 10.1272/jnms.76.76

Von Duvillard, S. P., Braun, W. A., Markofski, M., Beneke, R., and Leithäuser, R. (2004). Fluids and hydration in prolonged endurance performance. *Nutrition* 20, 651–656. doi: 10.1016/j.nut.2004.04.011

frontiers | Frontiers in Neuroscience

TYPE Original Research
PUBLISHED 28 August 2023
DOI 10.3389/fnins.2023.1210815

OPEN ACCESS

EDITED BY
Luiz Carlos Marques Vanderlei,
São Paulo State University, Brazil

REVIEWED BY
James W. Grau,
Texas A & M University, United States
Zeljka Minic,
Wayne State University, United States

*CORRESPONDENCE
Bradley S. Duerstock
✉ bsd@purdue.edu

RECEIVED 23 April 2023
ACCEPTED 02 August 2023
PUBLISHED 28 August 2023

CITATION
Kirby AK, Pancholi S, Anderson Z, Chesler C, Everett TH IV and Duerstock BS (2023) Time and frequency domain analysis of physiological features during autonomic dysreflexia after spinal cord injury.
Front. Neurosci. 17:1210815.
doi: 10.3389/fnins.2023.1210815

Time and frequency domain analysis of physiological features during autonomic dysreflexia after spinal cord injury

Ana Karina Kirby[1], Sidharth Pancholi[1], Zada Anderson[1], Caroline Chesler[1], Thomas H. Everett IV[2] and Bradley S. Duerstock[1,3]*

[1]Weldon School of Biomedical Engineering, Purdue University, West Lafayette, IN, United States, [2]Krannert Cardiovascular Research Center, Division of Cardiovascular Medicine, School of Medicine, Indiana University, Indianapolis, IN, United States, [3]School of Industrial Engineering, Purdue University, West Lafayette, IN, United States

Introduction: Autonomic dysreflexia (AD) affects about 70% of individuals with spinal cord injury (SCI) and can have severe consequences, including death if not promptly detected and managed. The current gold standard for AD detection involves continuous blood pressure monitoring, which can be inconvenient. Therefore, a non-invasive detection device would be valuable for rapid and continuous AD detection.

Methods: Implanted rodent models were used to analyze autonomic dysreflexia after spinal cord injury. Skin nerve activity (SKNA) features were extracted from ECG signals recorded non-invasively, using ECG electrodes. At the same time, blood pressure and ECG data sampled was collected using an implanted telemetry device. Heart rate variability (HRV) features were extracted from these ECG signals. SKNA and HRV parameters were analyzed in both the time and frequency domain.

Results: We found that SKNA features showed an increase approximately 18 seconds before the typical rise in systolic blood pressure, indicating the onset of AD in a rat model with upper thoracic SCI. Additionally, low-frequency components of SKNA in the frequency domain were dominant during AD, suggesting their potential inclusion in an AD detection system for improved accuracy.

Discussion: Utilizing SKNA measurements could enable early alerts to individuals with SCI, allowing timely intervention and mitigation of the adverse effects of AD, thereby enhancing their overall well-being and safety.

KEYWORDS

spinal cord injury, autonomic dysreflexia, sympathetic nerve activity, autonomic functions, heart rate variability

1. Introduction

There are approximately 17,810 new SCI cases each year in the United States (National Spinal Cord Injury Statistical Center, 2016). SCI is not only devastating because of paralysis, but secondary complications also impede one's overall well-being (Ahuja et al., 2017). One of the most severe secondary complications arising from autonomic nervous system dysfunction (ANS) in high-level SCI is AD, which is characterized by uncontrolled sympathetic nerve hyperactivity. Approximately 70% of individuals with an SCI at or above the T6 level experience AD, which is typically triggered by noxious stimulation below the level of injury (Bycroft et al., 2005). Common causes or triggers of AD include bladder dilation, bowel distention, and restrictive clothing (Murray et al., 2019). These

triggers cause nerve impulses to be sent to the spinal cord, activating the sympathetic nervous system, constricting blood vessels, and increasing blood pressure. The increase in blood pressure is detected by baroreceptors, which send signals to the brain to oppose the rise in blood pressure by slowing the heart and opening blood vessels. This compensatory control is accomplished through the parasympathetic vagus nerve activation of the heart and the blood vessels above the level of injury. However, this parasympathetic response cannot overcome the constricted vessels below the level of injury, resulting in prolonged hypertension (Karlsson, 2006). If not treated promptly, AD can cause damage to major organs and can be fatal (Eldahan and Rabchevsky, 2018).

Being familiar with triggers and symptoms is necessary to identify AD, which can be problematic for newly injured patients. A survey of individuals with an SCI and their families revealed 41% had never heard of AD (McGillivray et al., 2009). Clinically, the gold standard for AD detection is an increase of 20 mmHg or more in systolic blood pressure (SBP), but constantly monitoring a patient's blood pressure is burdensome and impedes daily activities (D. W. Popok et al., 2017). Currently, no noninvasive monitoring system is available to aid with the detection of AD. Therefore, AD is not typically monitored outside of the clinical setting. Current technological advances in noninvasive electronic sensors in the biomedical domain allow for the development of a wearable AD detection system for continuous monitoring. Noninvasive AD detection requires two components: an array of noninvasive physiological sensors and a machine learning model trained using participant data to determine the onset of an AD event.

An AD detection system was previously created for persons with SCI using a Microsoft Band™ smartwatch device, galvanic skin response (GSR), skin temperature, and heart rate. A machine learning model was trained using data from persons with SCI and was based on their presentation of symptoms, such as sweating, headaches, and cold and clammy skin. This system detected the onset of AD with 94.1% accuracy and a 4.9% false negative rate in participants performing regular daily activities (Suresh and Duerstock, 2018, 2020). A comprehensive evaluation of other noninvasive physiological features that may be superior to these smartwatch-based sensors was assessed, particularly through time domain analysis of SKNA. Temporal measures of sympathetic and parasympathetic activity including ISKNA (integrated skin nerve activity), number of bursts, percentage of the number of normal-to-normal values (medianNN), and root mean square of successive differences (RMSSD) were shown to optimally form machine learning models with high accuracy of AD detection (93.4%; Suresh et al., 2022a,b). In another study (Sagastibeltza et al., 2022), the occurrence of AD in patients with SCI was investigated using clinical and physiological data. The study successfully developed a classification system that could identify patients at risk of AD with an 80% accuracy rate, indicating the promising potential of these techniques for diagnosing AD in SCI patients.

In previous studies conducted on rats, the frequency domain of both SKNA and HR have been examined in the context of SCI. These investigations have revealed notable differences in the frequency patterns exhibited by these signals before and after SCI. Specifically, it has been observed that during episodes of AD, the very low frequency (VLF) and low frequency (LF) components of HRV are dominant, while the high frequency (HF) components are more prominent in the baseline state (Carnevali et al., 2013; Silva et al., 2017). In human and large animal models, the commonly used frequency ranges for LF and HF bands are 0.04–0.15 Hz and 0.15–0.40 Hz, respectively (Cívicos Sánchez et al., 2021). However, in the rat model, the frequency bands differ slightly. The specific frequency ranges used for LF and HF bands in the rat model are as follows: LF (0.2–0.75 Hz) and HF (0.75–2.5 Hz; Zajączkowski et al., 2014; Silva et al., 2017). Furthermore, research involving rats and bats has extensively explored a wide range of frequencies, spanning from 0 to 10 Hz. Interestingly, the findings reveal that both rat and bat species exhibit dominance exceeding 2 Hz (Morrison, 1999; Reynolds et al., 2019). This intriguing observation suggests the presence of distinct and significant frequency patterns in these animals, highlighting the relevance and importance of investigating frequency responses beyond the conventional HF range. These ranges have been established through research and studies conducted on rats.

The prompt detection of AD is of utmost importance. A quick and noninvasive AD detection system capable of providing advance warning, even if within a range of seconds to minutes, would be highly valuable in anticipating a rise in SBP. Such a system would allow individuals to take immediate action, such as raising the head of the bed and seeking assistance to address the AD trigger, thereby potentially mitigating the onset of hypertension.

Using a rat model of SCI, the timing of SKNA was compared to the increase in blood pressure, monitored in real-time through implanted telemetry and non-invasive ECG electrodes, establishing a correlation. Further characterization of AD events was investigated using frequency domain analysis of HRV and ISKNA. Previous frequency domain analyses have determined disease or ill health states compared to normal states based on the emergence of dominant frequencies (Physick-Sheard et al., 2000). In addition, selecting dominant frequency bands as potential features in creating machine-learning models could lead to more accurate AD detection (Suresh et al., 2022b).

One of the key contributions of this work is the estimation of the onset time of SKNA features in comparison to other HRV features when AD occurs. By examining the timing of SKNA activity alongside other HRV measures, a further understanding of the temporal relationships and potential associations between these physiological markers was gained. This analysis provides a deeper understanding of the interplay between SKNA and other HRV features. Secondly, the study focuses on analyzing the features in both the time domain and frequency domain, allowing for a comprehensive assessment of the significant differences between AD events and baseline conditions. By examining these domains, the research provides valuable insights into the distinct characteristics and patterns associated with AD and baseline state.

2. Methods

2.1. Animal model

Male Sprague Dawley rats ($n = 9$), purchased from Envigo (Indianapolis, IN), were used in this study. Before arriving at the research facility, four-month-old rats weighing 350–400 grams were implanted with a single-pressure biopotential implant (HD-S11 Implant, Data Sciences International, USA). The entire telemetry implantation surgery was conducted at Envigo, Indianapolis. Male rats were selected exclusively for the study due to the high incidence of SCI in men, who account for around 80% of all cases and tend to sustain injuries at an earlier age (Raguindin et al., 2021). All animals were

individually housed in plexiglass cages with straw bedding and had access to food and water. The rats were acclimated to the experimental setup, which included electrodes, a restraining jacket, and a plastic holder with air holes (HLD-RL model, Kent Scientific, USA), over a four-week period using a previously published protocol (Kirby et al., 2023). Acclimation was necessary to measure ANS parameters in conscious animals without undue stress.

2.2. Experimental procedures

2.2.1. SCI surgery and post-surgery care

A dorsal laminectomy was performed at the T3 level in each rat, exposing the spinal cord. Using specially made forceps, the spinal cord was compressed for 15 s to induce injury. The compression at the T4 level caused ischemia, replicating common clinical injuries as described by Blight (1991). Following the SCI, the rats experienced hindleg motor function loss, which was assessed through a toe pinch test, while retaining the ability to use their forelimbs.

Post-surgery, the rats' bladders were manually expressed, and they received 15 mL of lactated Ringer's solution subcutaneously. The rats were closely monitored and kept on a heating pad until fully awake and alert. They were then placed in cages with ALPHA-dri® bedding to prevent abdominal irritation caused by movement. Meloxicam and Baytril were administered once a day for 3 days post-surgery to prevent infection and alleviate pain. During the first week after surgery, the rats' bladders were expressed three times a day to prevent urinary tract infections. Trained personnel monitored and weighed the rats daily. To encourage eating, Ensure® nutrition, peanut butter, and apple sauce were provided since weight loss is commonly observed after SCI. If the animals lost more than 20% of their initial body weight prior to the SCI surgery, they were euthanized. A 5-day recovery period was provided after surgery before commencing the experiments.

2.2.2. CRD procedure

The experimental setup for the CRD protocol involved anesthetizing the rats with 4% isoflurane and inserting a lubricated balloon-inflated catheter 2 cm into their rectums (Rabchevsky et al., 2011; Sachdeva et al., 2021). Non-invasive electrodes and alligator clips were placed on the rats before they were wrapped in a jacket. Then the rats were placed in a restraint tube. The rats were given time to wake up and given a 20-min acclimation period before the balloon was inflated with 2 mL of air. To mark the beginning and end of each CRD event, invasive ECG recordings were made simultaneously with non-invasive recordings as shown in Figure 1. The start of a CRD event was identified by a sharp increase in voltage generated by a single square pulse from a stimulator (GRASS s48 Stimulator). The stimulator was connected to the rat using a coax cable and alligator clamps, with one clamp positioned under a front limb and the other attached to the leg on the opposite side. The pulse from the stimulator not only marked the start of the CRD event but also initiated the inflation of the balloon. To ensure consistent force and timing, a 3D-printed syringe holder with a small motor was used. The motor was programmed to inflate the catheter balloon with 2 mL of air for 1 min. This process was repeated three times during the experiment, with 10-min intervals between each inflation. The CRD protocol was conducted on specific post-surgery days, which included days 5, 7, 9, 11, 14, 16, 19, and 21 (Kramer and Kinter, 2003; Krassioukov et al., 2009; Popok et al., 2016).

The entire experimental procedure was approved by the Purdue Animal Care and Use Committee (PACUC). The approval number associated with our project is 1810001814.

2.3. Data collection and analysis

During the non-invasive data collection, ECG electrodes were connected to a bio-amplifier on the Power Lab 26T system (AD Instruments, USA) at a sampling rate of 10 kHz. The recorded ECG signal underwent downsampling to 2 kHz and was then high-pass filtered using a cutoff frequency of 500 Hz, following the methodology described by Everett IV et al. in 2017. From the filtered signal, the integrated skin nerve activity (ISKNA) was obtained by integrating the absolute value over a 100 ms period using LabChart 8 software (AD Instruments, USA).

The occurrence of the AD event was identified by observing the rise in blood pressure, specifically an increase of more than 15 mmHg, prior to the onset of bradycardia, which was visually confirmed. This distinct pattern, as illustrated in Figure 2, is characterized by an initial elevation in blood pressure followed by a subsequent decrease in heart rate (Suresh et al., 2022a).

To detect burst activity, a dual threshold algorithm was applied. This algorithm calculated the amplitude at each time point within the frequency range of 500 to 995 Hz. The computed amplitudes were normalized by the average amplitude of the entire series. Two thresholds, based on normalized amplitudes, were established: a higher threshold for burst onset detection and a lower threshold for burst termination. A burst was considered to occur when the signal's amplitude crossed the higher threshold and lasted until the amplitude fell below the lower threshold. The analysis of SKNA and burst activity was performed using the "neurodsp" library in Python, as described by Cole et al. (2019). Parameters such as the number of bursts per second and burst duration were also calculated.

For HRV and SKNA features, normalization was conducted per rat per experiment day. Data from 1 min before, during, and after each AD event were exported into Origin Pro for further analysis. Peak detection was achieved using a local maximum method, with the baseline defined as the mean of 180-s windows. Peaks exceeding 20% of the threshold were considered significant. The time delay between the onset of AD and the increase in SKNA activity, root mean square of RMSSD, and HR were calculated.

Simultaneously, ECG recordings were obtained from implanted telemetry devices throughout each experiment day, with a duration of 50 min. This allowed data collection during both the baseline and adverse event periods. The Lomb periodogram within LabChart 8 software (AD Instruments Inc., Colorado Springs, CO) was utilized to calculate the power spectrum of frequencies present in the HRV, derived from the RR-interval variation. The Lomb periodogram, employing the method of least squares, facilitated the fitting of sine waves and the computation of power spectra at specified frequencies, following the methodology described by Li et al. (2019). Prior to the Lomb periodogram, the filtered ECG signal underwent windowing and linear detrending. Power spectrum plots were generated and categorized into three bands: VLF, LF, and HF. In the rat model, the

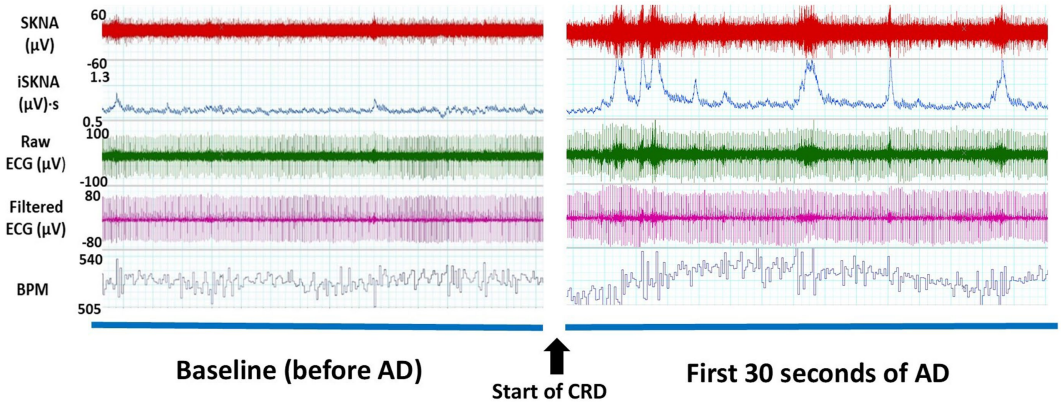

FIGURE 1
Thirty-second windows of electrocardiography (ECG) signals collected from a representative subject for one autonomic dysreflexia (AD) event from non-invasive electrodes. An increase in skin nerve activity (SKNA) and integrated skin nerve activity (ISKNA) is seen within the first 30 s of the onset of AD.

VLF band ranged from 0 to 0.2 Hz, the LF band ranged from 0.2 to 0.75 Hz, and the HF band ranged from 0.75 to 2.5 Hz.

The integrated SKNA data were also analyzed in these frequency bands. Furthermore, in our study, we utilized the entire frequency band ranging from 0 to 10 Hz to comprehensively analyze the frequency components of interest. Specifically, we focused on frequencies beyond the conventional 2 Hz range to investigate HRV and gain insights into the autonomic nervous system's influence on cardiac regulation. These frequency bands were selected to assess the impact of the autonomic nervous system on bodily functions, as established by Silva et al. (2017) and Zajączkowski et al. (2014).

Specific sections of data collected during the baseline and CRD events that led to AD were extracted and subjected to analysis. The dominant frequencies were detected using a 128,000-point fast Fourier transform size with 93.75% overlap, following the approach outlined by Liu et al. (2021).

3. Results

In this study, we employed min-max normalization to rescale the features of each day for every rat. This normalization method allows for fair comparison and combination of features across different days by transforming the data to a common scale. Data analysis was conducted per trial, enabling a detailed examination of the collected data for each specific day of the experiment. These meticulous steps were taken to ensure precise and reliable analysis while mitigating potential confounding factors.

3.1. Time delay analysis

Both HRV features, including medianNN and RMSSD, were significantly higher during AD compared to baseline. Similarly, average ISKNA and the number of bursts per second were significantly higher during AD as seen in Figure 2. The study found that SKNA bursts and ISKNA activity increased before SBP increased, indicating the onset of AD. The average time delay between the onset of CRD and the increase in ISKNA and SKNA bursts was 5.6 ± 4.5 s and 5.3 ± 5.2 s, respectively. An illustration showcasing this phenomenon can be found in Figure 3.

The increase in SBP occurred, on average, 23.4 ± 18.0 s after the inflation of the balloon catheter, which inducted AD ≈ 70% of the time. Changes in RMSSD, an indicator of HRV, were observed at 9.4 ± 9.3 s after the onset of AD. The decrease in heart rate was detected at 35.8 ± 34.4 s after the beginning of the AD event. Additionally, the variation between the HR parameters is larger compared to the SKNA parameters (Figure 4).

The ANOVA (analysis of variance) revealed significant differences in the physiological parameters between the baseline and AD groups. Specifically, ISKNA ($p = 0.04$) and bursts per second ($p = 0.01$) exhibited distinct patterns, indicating substantial disparities between the baseline and AD states. Additionally, medianNN showed a significant difference ($p < 0.001$), highlighting contrasting characteristics between the baseline and AD groups. These findings provide valuable insights into the unique physiological responses associated with ISKNA, burst per second, and medianNN, underscoring the distinctive features of the baseline and AD states.

Furthermore, the Tukey Kramer Post-hoc Test indicated significant differences ($p < 0.05$) in the time delay from the start of CRD to the increase in various features, including ISKNA vs. SBP, bursts per second vs. SBP, RMSSD vs. SBP, bursts per second vs. HR, and ISKNA vs. HR. These results highlight the significant distinctions in the temporal relationships between ISKNA and the other variables.

3.2. Frequency domain analysis

3.2.1. SKNA and ISKNA (0 to 10 Hz band)

During the baseline measurement, the SKNA signal exhibited a dominant frequency of approximately 8.23 ± 0.67 Hz. However, when an AD event occurred, there were distinct changes in the frequency profile. Two notable peaks emerged during this period: the first peak was observed at around 7.23 ± 0.78 Hz, and a dominant peak was also evident at 0.001 Hz as shown in Figures 5A,B.

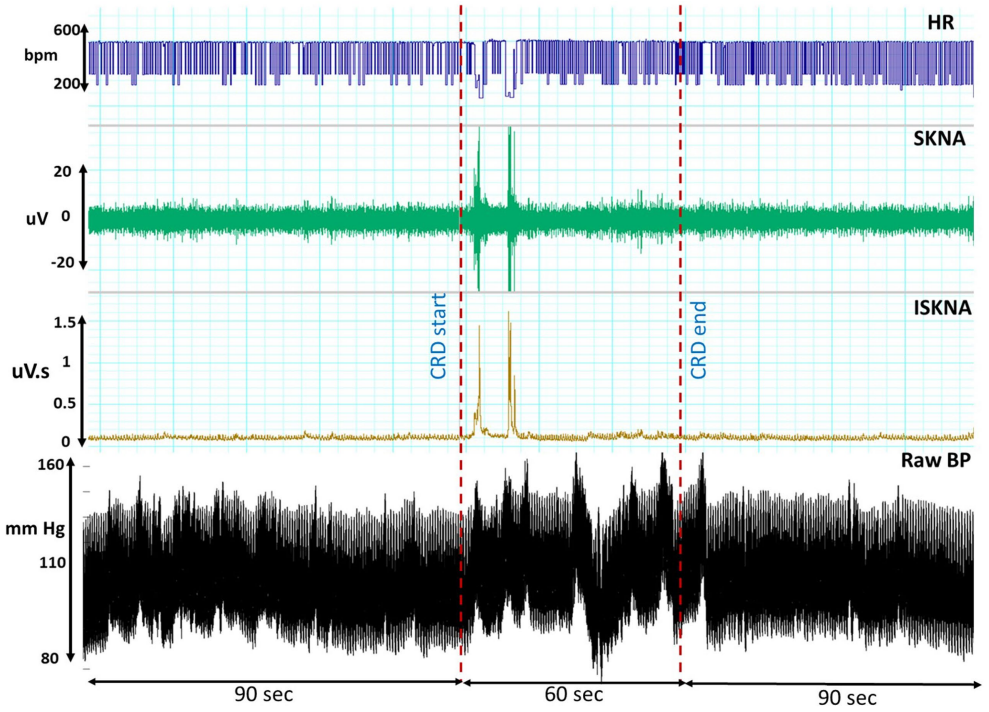

FIGURE 2
This illustrates the temporal profiles of raw blood pressure, heart rate (HR), skin nerve activity (SKNA), and integrated skin nerve activity (ISKNA) recorded during the colorectal distension (CRD) procedure that led to autonomic dysreflexia (AD).

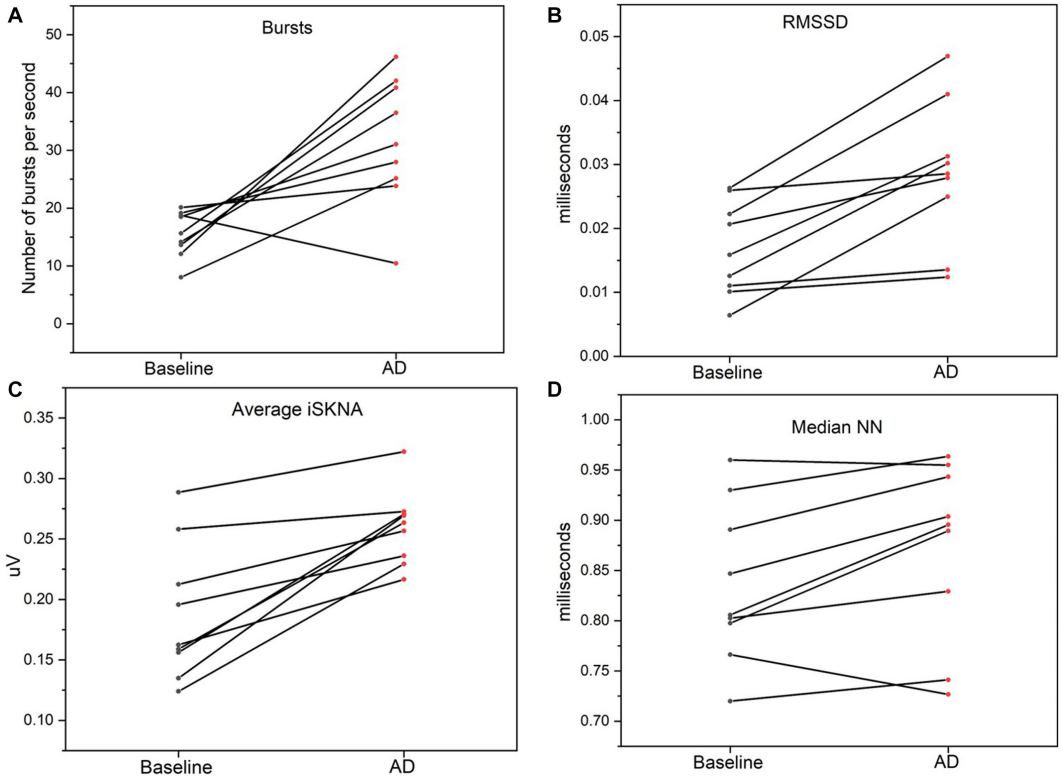

FIGURE 3
(A) Bursts per second was significantly higher during autonomic dysreflexia (AD) compared to baseline. **(B)** Average integrated skin nerve activity (ISKNA) during baseline was significantly increased during AD compared to baseline. **(C)** Root mean square of successive differences (RMSSD) was significantly higher during AD compared to baseline. **(D)** Median NN was significantly higher during AD compared to baseline.

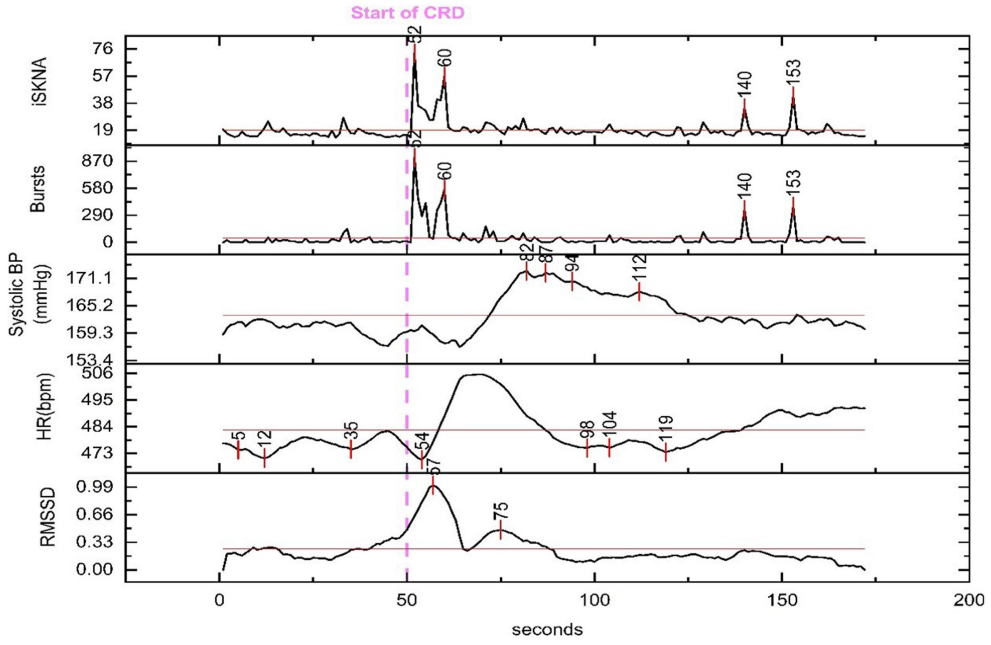

FIGURE 4
Physiological features extracted for time delay analysis from a representative animal. The dashed line marks the beginning of the colorectal distention (CRD) event that led to autonomic dysreflexia (AD) and the time for each peak is marked throughout the recording. An increase in skin nerve activity (SKNA) features and root mean square of successive differences (RMSSD) along with a decrease in heart rate (HR) is seen shortly after the onset of CRD.

Conversely, the baseline analysis of the ISKNA signal revealed a dominant frequency of approximately 1.4 ± 0.23 Hz. Interestingly, when an AD event took place, a significant shift in the dominant frequency occurred. The dominant frequency moved to a lower value, approximately 0.076 ± 0.12 Hz shown in Figures 5C,D.

3.2.2. ISKNA (VLF, LF, and HF bands)

The dominant ISKNA frequency during AD was observed to be in the LF band. This was supported by a significant difference ($p < 0.05$) between the average dominant frequency during baseline (0.19 ± 0.11 Hz), typically associated with the HF band, and the average dominant frequency during AD (0.07 ± 0.01 Hz), indicating a shift towards the LF band. The PSD plots in Figure 6 depict the power spectral density of AD and baseline.

3.2.3. Heart rate variability

Dominant frequencies of RR intervals were analyzed and normalized for all nine subjects. The average VLF power during baseline was 37.8%, while the average VLF power during AD was 44.2%. LF power was the lowest for both baseline (11.7%) and AD (12.0%). Average HF power was 39.0% during baseline and 24.3% during AD. The dominant frequencies for each subject are summarized in Table 1.

An ANOVA was performed to compare the measurements between the baseline and AD conditions for each frequency band and LF/HF ratio. The results revealed no significant difference between baseline and AD for VLF power ($p = 0.38$) and LF power ($p = 0.13$). However, there was a significant decrease in HF power ($p = 0.017$) during AD compared to baseline. Furthermore, the LF/HF ratio was significantly higher ($p = 0.0328$) during AD compared to the baseline. The time-frequency plot in Figure 7 displayed the dominance of VLF during AD in contrast to the baseline.

These findings indicate that while VLF and LF power did not differ significantly between the baseline and AD conditions, HF power was significantly lower and the LF/HF ratio was significantly higher during AD. The time-frequency plot further supports the observation of increased VLF dominance during AD.

Further MANOVA (Multivariate Analysis of Variance) analyses were performed to explore these differences in more detail for the time domain (ISKNA, bursts per second, RMSSD, medianNN) and frequency domain (VLF, LF, HF, LF/HF) features separately. The time domain features showed a highly significant distinction (p-value = 0.0002), indicating a clear dissimilarity between the AD and baseline groups in this domain. Similarly, the frequency domain features exhibited an even more pronounced significance (p-value = 1.07634e-07), indicating a substantial and statistically significant differentiation between the AD and baseline groups in this specific domain. These findings provide robust evidence of significant variations between the AD and baseline groups across both the time domain and frequency domain features, as evidenced by the separate MANOVA analyses.

4. Discussion

SKNA features were detected noninvasively and before the typical rise in SBP as measured through telemetry implants during AD events. This study focused on further understanding changes in sympathetic and parasympathetic activity in response to AD in both time and frequency domains. Using implanted telemetry ECG, we compared the timing of ISKNA and nerve bursts to the resultant increase of SBP during AD. We anticipated that activation of the stellate ganglion, as measured through SKNA, would precede the

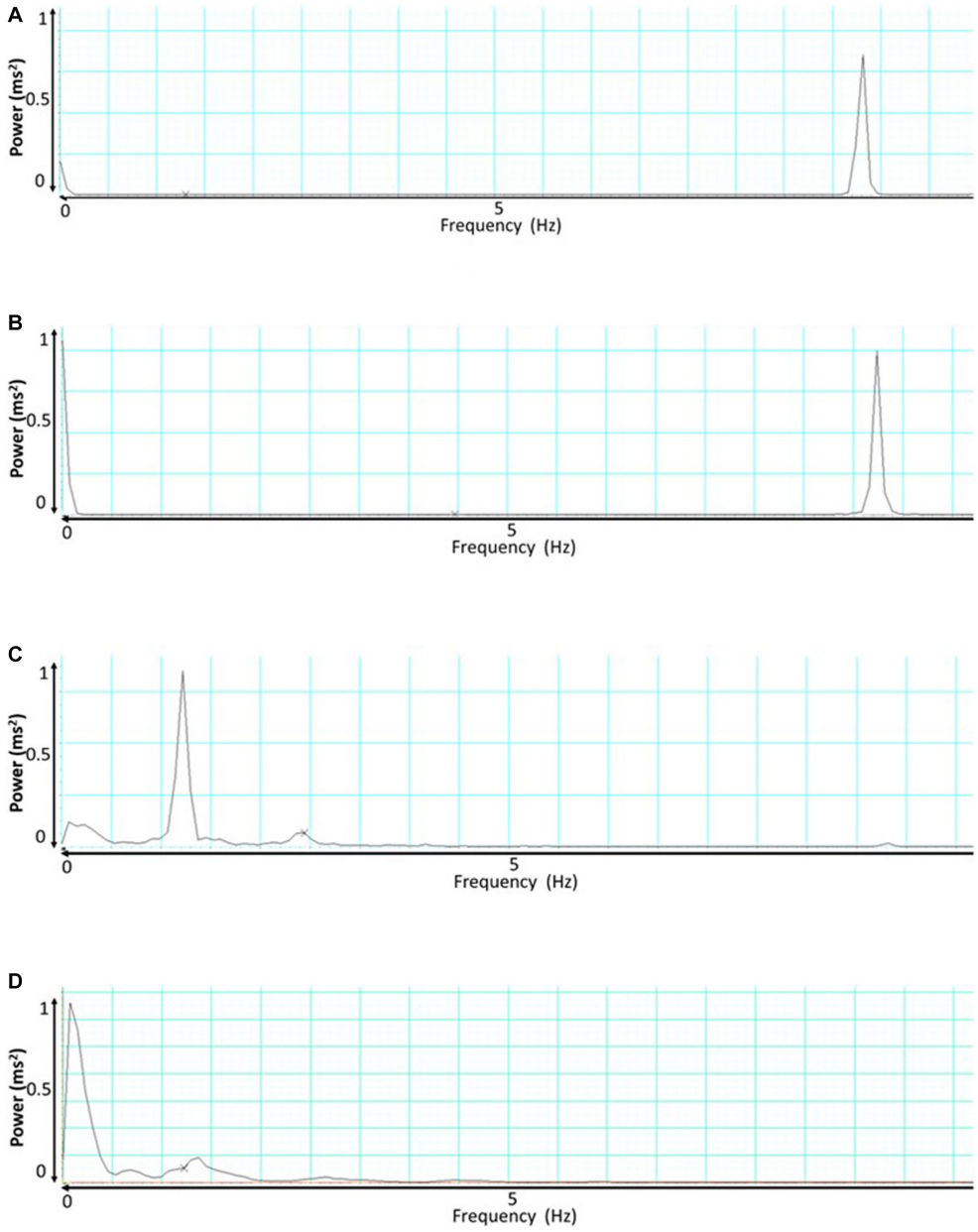

FIGURE 5
This presents the frequency analysis of skin nerve activity (SKNA) and integrated skin nerve activity (ISKNA) signals during baseline and autonomic dysreflexia (AD). **(A)** Shows the SKNA signal during baseline, while **(B)** displays the SKNA signal during AD. Similarly, **(C,D)** exhibit the ISKNA signal during baseline and AD, respectively.

increase of SBP through baroreflexes. For newly spinal cord injured individuals it takes time to learn their telltale symptoms of AD and then determine what the source or trigger of this episode may be, such as a lack of voiding of the urinary bladder, noxious stimuli not felt below the injury, or bowel impaction. Thus, there may be medical benefits of such an AD detection system.

4.1. Time domain analysis

AD is characterized by a large increase in sympathetic activity that leads to an increase in blood pressure. The sympathetic activity was detected through a significant increase in SKNA features, including average ISKNA and the number of bursts per second during AD. The parasympathetic activity was also detected during AD through the increase in median NN and RMSSD.

The gold standard of AD detection is an increase in SBP, but this study exposed activation of the sympathetic nervous system was first detected through SKNA. Burst activity was detected using a noninvasive ECG recording, which encourages the development of wearable solutions for persons with SCI that suffer from AD. Therefore, burst activity and ISKNA has the potential to detect AD prior to the symptomatic manifestation of paroxysmal hypertension that is currently used by persons with SCI to detect the occurrence of an AD

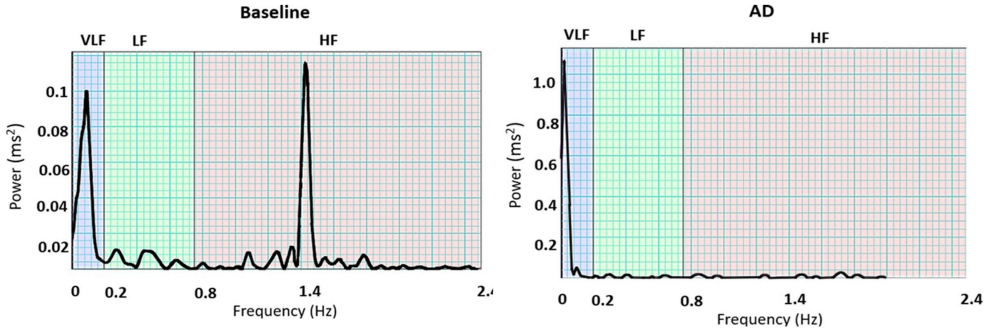

FIGURE 6
PSD plots during baseline and autonomic dysreflexia (AD) for one subject: Dominant frequencies during baseline were seen in both the very low frequency (VLF) and high frequency (HF) bands, while VLF is dominant during AD.

TABLE 1 Dominant frequencies for each subject.

	VLF (%)		LF (%)		HF (%)		LF/HF	
Sub	Baseline	AD	Baseline	AD	Baseline	AD	Baseline	AD
1	30.3	36.8	15.2	15.8	46.2	38.5	0.354	0.443
2	56.3	39.1	4.1	10.8	34.3	32.9	0.186	0.355
3	45.1	47.1	11.0	12.6	32.6	28.3	0.345	0.564
4	49.8	48.7	9.9	8.7	28.9	31.9	0.492	0.309
5	31.7	62.5	8.7	10.6	25.4	25.3	0.432	0.395
6	46.4	78.4	19.2	6.6	30.9	13.5	0.656	0.498
7	12.9	16.1	13.2	14.8	58.7	54.6	0.225	0.270
8	27.9	34.7	16.3	17.5	47.0	40.2	0.368	0.499
9	39.6	34.4	7.3	10.9	47.1	43.3	0.196	0.316
Aver-age	37.8	44.2	11.7	12.0	39.0	34.3	0.362	0.405
	(12.8–56.3)	(16.1–78.4)	(4.1–19.2)	(6.5–17.4)	(25.3–58.7)	(13.5–54.6)	(0.27–0.56)	(0.18–0.36)

event. Throughout the study, the bursts per second count, which reflects the burst activity of the SKNA signal, exhibited distinct patterns. On day 5, the bursts per second count was recorded at 84.76 bursts/s, indicating a high level of burst activity at the onset of AD. It is important to note that on this particular day, there were only a small number of reported AD events, which was less than half of the count observed on other experimental days. This suggests that the burst detection algorithm may have captured low-amplitude spikes as bursts during the recovery period.

From day 7 to day 16, the burst per second count gradually decreased, reaching an average value of 20.19 bursts/s on day 16. This decline in burst activity indicates a reduction in the occurrence of AD-related bursts during this period. However, starting from day 19, there was a notable increase in the burst per second count. On day 19, the average burst per second count rose to 37.57 bursts/s, and on day 21, it further increased to 41.35 bursts/s. This upward trend in burst activity suggests a resurgence of AD-related bursts in the later stages of the study.

The larger variation within HR parameters showed that parasympathetic activity did not activate at a uniform rate after the onset of AD. Instead, parasympathetic activity occurs in response to the increase of systolic blood pressure and is likely activated through changes in baroreceptors in the cardiovascular system. Therefore, using SKNA activity to detect the onset of AD would be more accurate. Providing early detection of AD before symptoms arise would provide persons with SCI additional time to identify and eliminate AD triggers to prevent the onset of major symptoms and outcomes associated with AD. Although the onset of SKNA spikes averaged only 18 s prior to the anticipated increase in SBP in this rat study, this may have clinical value for paralyzed persons.

4.2. Frequency domain analysis

The ISKNA frequency domain analysis revealed LF dominance during AD and HF dominance during baseline, which follows the literature, which has found LF to be dominant during disease states (Meng et al., 2022). The use of SKNA has been shown to be predictive of increased cardiac sympathetic tone, such as heart failure, resulting in a significant decrease in LF components. SKNA was shown to be more accurate compared to HRV in assessing cardiac sympathetic activity in canines with myocardial infarction (Zajączkowski et al., 2014). Because

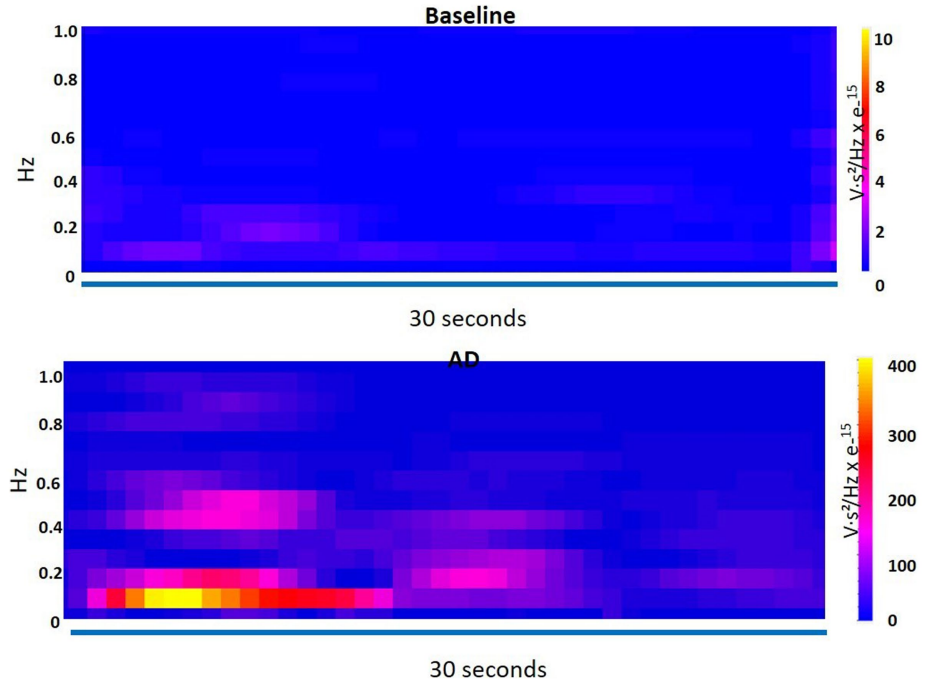

FIGURE 7
Time-frequency plot shows the dominance of very low frequency (VLF) during autonomic dysreflexia (AD) as compared to the baseline.

cardiac and skin sympathetic innervations are linked, sympathetic nerves from both structures activate at the same time. HF dominance during baseline indicated parasympathetic activity as confirmed through HRV frequency domain analysis. LF dominance during AD clearly exhibited sympathetic hyperactivity using ISKNA analysis, which was not defined during power spectral HRV analysis due to loss of sympathetic nervous tone in patients with SCI.

In our frequency analysis of the SKNA signal within the 0 to 10 Hz range, we observed a distinct frequency component around 8 Hz. Notably, during the occurrence of AD, we observed a subtle shift in this frequency component, moving towards approximately 7 Hz. This frequency shift implies the presence of bradycardia, a reduction in heart rate, during AD episodes. These findings highlight the potential association between changes in HRV and cardiovascular responses during AD.

Our HRV frequency domain analysis detected parasympathetic activity during baseline with a significant increase in HF, and a difference in LF/HF ratio that revealed a shift of sympathovagal balance toward sympathetic dominance during AD. There was no significant difference in VLF between baseline and AD, which could be because of the SCI, which disconnects the communication of the sympathetic nervous system between the lungs and the heart. LF power also was not significantly different between baseline and AD, which could be explained by the sympathetic and parasympathetic activity fluctuations during AD. Our data suggest HRV frequency domain analysis, which emphasized the detection of parasympathetic parameters, may not be optimal for AD studies due to the lack of differences in LF and VLF components. In contrast, subcutaneous nerve activity has been shown to be more effective in estimating cardiac sympathetic tone.

5. Conclusion

We determined that certain SKNA parameters can be detected noninvasively before the gold standard increase in blood pressure. The frequency domain analysis of ISKNA has been found to be a useful technique in the identification of biomarkers for detecting AD in rats, with a specific emphasis on the LF band during the progression of the disease. These biomarkers can aid in the development of a universally applicable approach for the early detection and monitoring of AD, which may have significant clinical implications. SKNA frequency domain features can noninvasively detect the early onset of AD in paralyzed humans. Such a system would advantageously alert SCI individuals of impending AD events prior to severe symptoms, preventing long-term cardiovascular complications. Identifying these parameters provides insights into autonomic function during AD events, which can inform targeted interventions for AD patients with SCI.

Data availability statement

The datasets used and/or analyzed during the current study available from the corresponding author upon reasonable request.

Ethics statement

The animal studies were approved by Purdue Animal Care and Use Committee (PACUC). The studies were conducted in accordance with the local legislation and institutional requirements. Written informed consent was obtained from the owners for the participation of their animals in this study.

Author contributions

AK designed and carried out the experiments, analysis, and drafted the manuscript. SP provided guidance with data analysis and edited the manuscript. ZA and CC provided invaluable support while conducting experiments. THE provided guidance using skin nerve activity physiological recording. BSD conceived, coordinated, and facilitated this research.

Funding

We would like to thank the Indiana State Department of Health through the Indiana Spinal Cord and Brain Injury Research Fund (PI: BSD) and the Department of Defense Congressionally Directed Medical Research Programs Spinal Cord Injury Research Program (SC190164 W81XWH-20-1-0725) for supporting this research. We would like to express our gratitude to the National Institutes of Health (NIH) for their support of our research through the NIH R01HL158952 grant (PI: Everett).

Acknowledgments

The authors are grateful to the Purdue University Center for Paralysis Research for assistance with animal care and management.

Conflict of interest

The authors declare that the research was conducted in the absence of any commercial or financial relationships that could be construed as a potential conflict of interest.

Publisher's note

References

Ahuja, C. S., Wilson, J. R., Nori, S., Kotter, M. R. N., Druschel, C., Curt, A., et al. (2017). Traumatic spinal cord injury. *Nat. Rev. Dis. Primers* 3:17018. doi: 10.1038/nrdp.2017.18

Blight, A. R. (1991). Morphometric analysis of a model of spinal cord injury in Guinea pigs, with behavioral evidence of delayed secondary pathology. *J. Neurol. Sci.* 103, 156–171. doi: 10.1016/0022-510X(91)90159-5

Bycroft, J., Shergill, I. S., Choong, E. A. L., Arya, N., and Shah, P. J. R. (2005). Autonomic Dysreflexia: a medical emergency. *Postgrad. Med. J.* 81, 232–235. doi: 10.1136/pgmj.2004.024463

Carnevali, L., Trombini, M., Porta, A., Montano, N., de Boer, S. F., and Sgoifo, A. (2013). Vagal withdrawal and susceptibility to cardiac arrhythmias in rats with high trait aggressiveness. *PLoS One* 8:e68316. doi: 10.1371/journal.pone.0068316

National Spinal Cord Injury Statistical Center (2016). '*Facts and figures at a glance*'. Birmingham, AL: University of Alabama at Birmingham *10*.

Cívicos Sánchez, N., Acera, M., Murueta-Goyena, A., Sagastibeltza, N., Martínez, R., Cuadrado, M., et al. (2021). Quantitative analysis of Dysautonomia in patients with autonomic Dysreflexia. *J. Neurol.* 268, 2985–2994. doi: 10.1007/s00415-021-10478-w

Cole, S., Donoghue, T., Gao, R., and Voytek, B. (2019). Neuro DSP: a package for neural digital signal processing. *J. Open Source Softw.* 4:1272. doi: 10.21105/joss.01272

Eldahan, Khalid C., and Rabchevsky, Alexander G. (2018). 'Autonomic dysreflexia after spinal cord injury: systemic pathophysiology and methods of management'. Autonomic neuroscience: basic and clinical. Elsevier B.V.

Karlsson, A.-K. (2006). Overview: autonomic dysfunction in spinal cord injury: clinical presentation of symptoms and signs. *Prog. Brain Res.* 152, 1–8. doi: 10.1016/S0079-6123(05)52034-X

Kirby, A., Pancholi, S., Suresh, S., Anderson, Z., Chesler, C., Everett, T. H., et al. (2023). Acclimation protocol for spinal cord injured rats to minimize stress during non-invasive multimodal sensing of the autonomic nervous system. *J. Military Med.*

Kramer, K., and Kinter, L. B. (2003). Evaluation and applications of radiotelemetry in small laboratory animals. *Physiol. Genomics* 13, 197–205. doi: 10.1152/physiolgenomics.00164.2002

Krassioukov, A., Warburton, D. E., Teasell, R., and Eng, J. J.Spinal Cord Injury Rehabilitation Evidence Research Team (2009). A systematic review of the management of autonomic dysreflexia after spinal cord injury. *Arch. Phys. Med. Rehabil.* 90, 682–695. doi: 10.1016/j.apmr.2008.10.017

Li, K., Rüdiger, H., and Ziemssen, T. (2019). Spectral analysis of heart rate variability: time window matters. *Front. Neurol.* 10:545. doi: 10.3389/fneur.2019.00545

Liu, X., Yuan, Y., Wong, J., Meng, G., Ueoka, A., Woiewodski, L. M., et al. (2021). The frequency Spectrum of sympathetic nerve activity and Arrhythmogenicity in ambulatory dogs. *Heart Rhythm.* 18, 465–472. doi: 10.1016/j.hrthm.2020.11.023

McGillivray, C. F., Hitzig, S. L., Cathy Craven, B., Tonack, M. I., and Krassioukov, A. V. (2009). Evaluating knowledge of autonomic Dysreflexia among individuals with spinal cord injury and their families. *J. Spinal Cord Med.* 32, 54–62. doi: 10.1080/10790268.2009.11760753

Meng, G., He, W., Wong, J., Li, X., Mitscher, G. A., Straka, S., et al. (2022). Successful continuous positive airway pressure treatment reduces skin sympathetic nerve activity in patients with obstructive sleep apnea. *Heart Rhythm.* 19, 127–136. doi: 10.1016/j.hrthm.2021.09.018

Morrison, S. F. (1999). RVLM and raphe differentially regulate sympathetic outflows to splanchnic and Brown adipose tissue. *Am. J. Phys. Regul. Integr. Comp. Phys.* 276, R962–R973. doi: 10.1152/ajpregu.1999.276.4.R962

Murray, T. E., Krassioukov, A. V., Pang, E. H. T., Zwirewich, C. V., and Chang, S. D. (2019). Autonomic Dysreflexia in patients with spinal cord injury: what the radiologist needs to know. *Am. J. Roentgenol.* 212, 1182–1186. doi: 10.2214/AJR.18.20798

Physick-Sheard, P. W., Marlin, D. J., Thornhill, R., and Schroter, R. C. (2000). Frequency domain analysis of heart rate variability in horses at rest and during exercise. *Equine Vet. J.* 32, 253–262. doi: 10.2746/042516400776563572

Popok, D., West, C., Frias, B., and Krassioukov, A. V. (2016). Development of an algorithm to perform a comprehensive study of autonomic dysreflexia in animals with high spinal cord injury using a telemetry device. *J. Vis. Exp.* 113:e52809. doi: 10.3791/52809

Popok, D. W., West, C. R., Hubli, M., Currie, K. D., and Krassioukov, A. V. (2017). Characterizing the severity of autonomic cardiovascular dysfunction after spinal cord injury using a novel 24 hour ambulatory blood pressure analysis software. *J. Neurotrauma* 34, 559–566. doi: 10.1089/neu.2016.4573

Rabchevsky, A. G., Patel, S. P., Duale, H., Lyttle, T. S., O'Dell, C. R., and Kitzman, P. H. (2011). Gabapentin for spasticity and autonomic dysreflexia after severe spinal cord injury. *Spinal Cord* 49, 99–105. doi: 10.1038/sc.2010.67

Raguindin, P. F., Muka, T., and Glisic, M. (2021). Sex and gender gap in spinal cord injury research: focus on Cardiometabolic diseases. A Mini review. *Maturitas* 147, 14–18. doi: 10.1016/j.maturitas.2021.03.004

Reynolds, C. A., O'Leary, D. S., Ly, C., Smith, S. A., and Minic, Z. (2019). Development of a Decerebrate model for investigating mechanisms mediating Viscero-sympathetic reflexes in the Spinalized rat. *Am. J. Phys. Heart Circ. Phys.* 316, H1332–H1340. doi: 10.1152/ajpheart.00724.2018

Sachdeva, R., Nightingale, T. E., Pawar, K., Kalimullina, T., Mesa, A., Marwaha, A., et al. (2021). Noninvasive Neuroprosthesis promotes cardiovascular recovery after spinal cord injury. *Neurotherapeutics* 18, 1244–1256. doi: 10.1007/s13311-021-01034-5

Sagastibeltza, Nagore, Salazar-Ramirez, Asier, Yera, Ainhoa, Martinez, Raquel, Muguerza, Javier, Sanchez, Nora Civicos, et al. (2022). 'Preliminary study on the detection of autonomic Dysreflexia using machine learning techniques'. Advances and Applications in Computer Science, Electronics, and Industrial Engineering: Proceedings of the Conference on Computer Science, Electronics and Industrial Engineering (CSEI 2021), 433.

Silva, L. E. V., Geraldini, V. R., de Oliveira, B. P., Silva, C. A. A., Porta, A., and Fazan, R. (2017). Comparison between spectral analysis and symbolic dynamics for heart rate variability analysis in the rat. *Sci. Rep.* 7:8428. doi: 10.1038/s41598-017-08888-w

Suresh, Shruthi, and Duerstock, Bradley. (2018). Optimal feature selection for the detection of autonomic Dysreflexia in individuals with tetraplegia. IEEE International Symposium on Signal Processing and Information Technology (ISSPIT).

Suresh, S., and Duerstock, B. S. (2020). Automated detection of symptomatic autonomic Dysreflexia through multimodal sensing. *IEEE J. Trans. Eng. Health Med.* 8, 1–8. doi: 10.1109/JTEHM.2019.2955947

Suresh, S., Everett IV, T. H., Shi, R., and Duerstock, B. S. (2022a). Automatic detection and characterization of autonomic Dysreflexia using multi-modal non-invasive sensing and neural networks. *Neurot. Rep.* 3, 501–510. doi: 10.1089/neur.2022.0041

Suresh, S., Newton, D. T., Everett IV, T. H., Lin, G., and Duerstock, B. S. (2022b). Feature selection techniques for a machine learning model to detect autonomic Dysreflexia. *Front. Neuroinform.* 16:901428. doi: 10.3389/fninf.2022.901428

Zajączkowski, Stanisław, Smolińska, Maria, Badtke, Piotr, and Wierzba, Tomasz H. (2014). 'Time-domain and spectral analysis of heart rate variability in rats challenged with hypoxia'. In Computing in cardiology 2014, 785–788. IEEE.

frontiers | Frontiers in Neuroscience

TYPE Original Research
PUBLISHED 04 September 2023
DOI 10.3389/fnins.2023.1256067

OPEN ACCESS

EDITED BY
Vitor Engracia Valenti,
São Paulo State University, Brazil

REVIEWED BY
Felipe Ribeiro,
São Paulo State University, Brazil
Szymon Siecinski,
University of Lübeck, Germany

*CORRESPONDENCE
Xiaochun Zhang
✉ ceiq@sina.com
Bo Shi
✉ shibo@bbmc.edu.cn

RECEIVED 10 July 2023
ACCEPTED 22 August 2023
PUBLISHED 04 September 2023

CITATION
Wu S, Guan W, Zhao H, Li G, Zhou Y, Shi B and Zhang X (2023) Assessment of short-term effects of thoracic radiotherapy on the cardiovascular parasympathetic and sympathetic nervous systems. *Front. Neurosci.* 17:1256067. doi: 10.3389/fnins.2023.1256067

Assessment of short-term effects of thoracic radiotherapy on the cardiovascular parasympathetic and sympathetic nervous systems

Shuang Wu[1,2], Weizheng Guan[3,4], Huan Zhao[3,4], Guangqiao Li[3,4], Yufu Zhou[2], Bo Shi[3,4]* and Xiaochun Zhang[1,5]*

[1]School of Medicine, Yangzhou University, Yangzhou, China, [2]Department of Radiation Oncology, First Affiliated Hospital, Bengbu Medical College, Bengbu, China, [3]School of Medical Imaging, Bengbu Medical College, Bengbu, China, [4]Anhui Key Laboratory of Computational Medicine and Intelligent Health, Bengbu Medical College, Bengbu, China, [5]Department of Oncology, Yangzhou Hospital of Traditional Chinese Medicine, Yangzhou, China

Background: Prior research suggests that cardiovascular autonomic dysfunction might be an early marker of cardiotoxicity induced by antitumor treatment and act as an early predictor of cardiovascular disease-related morbidity and mortality. The impact of thoracic radiotherapy on the parasympathetic and sympathetic nervous systems, however, remains unclear. Therefore, this study aimed to evaluate the short-term effects of thoracic radiotherapy on the autonomic nervous system, using deceleration capacity (DC), acceleration capacity (AC) of heart rate, and heart rate variability (HRV) as assessment tools.

Methods: A 5 min electrocardiogram was collected from 58 thoracic cancer patients before and after thoracic radiotherapy for DC, AC, and HRV analysis. HRV parameters employed included the standard deviation of the normal-normal interval (SDNN), root mean square of successive interval differences (RMSSD), low frequency power (LF), high frequency power (HF), total power (TP), and the LF to HF ratio. Some patients also received systemic therapies alongside radiotherapy; thus, patients were subdivided into a radiotherapy-only group (28 cases) and a combined radiotherapy and systemic therapies group (30 cases) for additional subgroup analysis.

Results: Thoracic radiotherapy resulted in a significant reduction in DC (8.5 [5.0, 14.2] vs. 5.3 [3.5, 9.4], $p = 0.002$) and HRV parameters SDNN (9.9 [7.03, 16.0] vs. 8.2 [6.0, 12.4], $p = 0.003$), RMSSD (9.9 [6.9, 17.5] vs. 7.7 [4.8, 14.3], $p = 0.009$), LF (29 [10, 135] vs. 24 [15, 50], $p = 0.005$), HF (35 [12, 101] vs. 16 [9, 46], $p = 0.002$), TP (74 [41, 273] vs. 50 [33, 118], $p < 0.001$), and a significant increase in AC (−8.2 [−14.8, −4.9] vs. -5.8 [−10.1, −3.3], $p = 0.003$) and mean heart rate (79.8 ± 12.6 vs. 83.9 ± 13.6, $p = 0.010$). Subgroup analysis indicated similar trends in mean heart rate, DC, AC, and HRV parameters (SDNN, RMSSD, LF, HF, TP) in both the radiotherapy group and the combined treatment group post-radiotherapy. No statistically significant difference was noted in the changes observed in DC, AC, and HRV between the two groups pre- and post-radiotherapy.

Conclusion: Thoracic radiotherapy may induce cardiovascular autonomic dysfunction by reducing parasympathetic activity and enhancing sympathetic activity. Importantly, the study found that the concurrent use of systemic therapies did not significantly amplify or contribute to the alterations in autonomic function in the short-term following thoracic radiotherapy. DC, AC and HRV are promising

and feasible biomarkers for evaluating autonomic dysfunction caused by thoracic radiotherapy.

KEYWORDS

autonomic modulation, cardiovascular toxicity, deceleration/acceleration capacities of heart rate, heart rate variability, thoracic radiotherapy

Introduction

Thoracic radiotherapy serves as a pivotal element in the treatment of thoracic cancer (TC), including breast cancer, esophageal cancer, lung cancer, and other thoracic malignancies (Raghunathan et al., 2017). Existing research has indicated that thoracic radiotherapy can precipitate vascular endothelial dysfunction, leading to accelerated atherosclerosis and inflammatory activation (Sylvester et al., 2018; Venkatesulu et al., 2018; Baselet et al., 2019). Numerous studies have investigated the amplified risk resulting from thoracic radiotherapy, implicating myocardial, coronary, valvular, and pericardial diseases, along with arrhythmias, as factors contributing to increased mortality (Jacob et al., 2016; Armanious et al., 2018). In this context, the cardiovascular autonomic nervous system (ANS)—a key regulator of heart rate, myocardial function, and myocardial blood flow—assumes significant importance. The initiation of cardiovascular toxicity, as well as early indications of diastolic/systolic dysfunction and disease severity, may stem from cardiovascular autonomic dysfunction (AD) caused by radiation and chemotherapy (Tjeerdsma et al., 1999; Guimarães et al., 2015; Teng et al., 2021). Therefore, examining the impact of thoracic radiotherapy on ANS could provide substantial insights into both short and long-term cardiovascular adversities associated with radiotherapy.

The cardiovascular ANS is constituted by the sympathetic nervous system (SNS) and the parasympathetic nervous system (PNS) (Schwartz and De Ferrari, 2011). ANS functionality can be assessed through several clinically viable measures, such as deceleration capacity (DC), acceleration capacity (AC) of heart rate, and heart rate variability (HRV) (Bauer et al., 2006a; Lombardi and Stein, 2011; Zou et al., 2016). Previous research has underscored the prognostic value of DC, AC, and HRV in the early detection of cardiovascular disease onset and sudden cardiac death rates in patients with conditions like myocardial infarction, heart failure, dilated cardiomyopathy, or coronary artery disease (Arsenos et al., 2016; Zou et al., 2016; Wang et al., 2017; Rizas et al., 2018; Fang et al., 2020). More recent observational studies have established that DC is a potent predictor of cardiovascular toxicity stemming from treatments like epirubicin or trastuzumab in breast cancer patients (Feng and Yang, 2015; Feng et al., 2021). Hence, the incorporation of DC, AC, and HRV in clinical studies investigating potential cardiovascular toxicity resulting from antitumor therapy could prove beneficial.

Earlier studies have provided preliminary insights into the effects of antitumor treatment on cardiovascular ANS in patients with malignant tumors (Ekholm et al., 2000; Groarke et al., 2015; Stachowiak et al., 2018; Caru et al., 2019). Early identification of cardiovascular AD has the potential to enhance preventative strategies to mitigate clinically significant cardiac toxicity subsequent to thoracic radiotherapy. It may be necessary to identify novel biomarkers in order to facilitate the early detection of heart damage resulting from radiation exposure. Therefore, the objective of this study is to elucidate the alterations in DC, AC, and HRV before and after thoracic radiotherapy in TC patients, contributing novel insights into the short-term radiotherapy effects on cardiovascular ANS.

Materials and methods

Participants

This study included TC patients who underwent thoracic radiotherapy at the Department of Tumor Radiotherapy, the First Affiliated Hospital of Bengbu Medical College. Exclusion criteria were as follows: (1) presence of a pacemaker, (2) prior receipt of thoracic radiotherapy, (3) incomplete thoracic radiotherapy, and (4) poor electrocardiogram (ECG) quality. The study was approved by the local hospital's Clinical Medical Research Ethics Board (registration number: 2019KY031). All participants were voluntary contributors who provided informed consent.

Patients were administered thoracic radiotherapy via a linear accelerator (Siemens or Elekta Synergy Platform) using 6-MV photon beams. The median cumulative radiation dose was 50 Gray, while the median individual radiation dose was 2 Gray. Certain patients also received potentially cardiotoxic systemic therapies, such as taxanes, platinum compounds, or trastuzumab, which may instigate variations in the cardiovascular ANS (Coumbe and Groarke, 2018; Teng et al., 2021). Consequently, we partitioned TC patients into two groups: the radiotherapy-only group, and the combined radiotherapy and systemic therapies group.

Data collection

An ECG was captured before and after radiotherapy using an ECG recorder (HeaLink-R211B; HeaLink Ltd., Bengbu, China). A V6-lead was employed, and ECGs were collected at a sampling rate of 400 Hz. Participants remained in a supine position, motionless for 5 min during ECG collection. The same operator conducted measurements both pre- and post-radiotherapy.

Deceleration/acceleration capacities of heart rate and heart rate variability analysis

The Pan-Tompkins algorithm was employed in this study to extract the R-peaks from the ECG readings (Pan and Tompkins, 1985). The Kubios software's threshold-based automatic artifact

correction algorithm was used to rectify both technical and physiological artifacts (Niskanen et al., 2004). The mean heart rate (HR) was defined as the average resting heart rate over a period of 5 min. The phase-rectified signal averaging technique was utilized for the computation of the DC and AC. Initially, the R-R intervals time series were examined to detect the decelerating and accelerating anchors that were characterized by a longer or shorter value than the preceding value, respectively. Subsequently, R-R intervals segments surrounding the decelerating and accelerating anchors were evaluated. Lastly, the aforementioned segments were aligned at the decelerating and accelerating anchors, and the signals of segments were averaged to derive the phase-rectified signal averaging signals (Bauer et al., 2006a,b; Nasario-Junior et al., 2014). Several commonly used HRV parameters were engaged in this study: the standard deviation of the normal-normal intervals (SDNN), root mean square of successive interval differences (RMSSD), low frequency power (LF, 0.04–0.15 Hz), high frequency power (HF, 0.15–0.4 Hz), total power (TP, 0–0.4 Hz), and the ratio of LF to HF (LF/HF). For the frequency domain HRV analysis, R-R interval sequences were transformed into evenly sampled time series using a 4 Hz resampling rate, with the aid of a cubic spline interpolation method. The fast Fourier transform algorithm was applied in tandem with Welch's periodogram method (150 s window width and 50% overlap window) to calculate HRV spectra.

DC is a quantitative metric of the PNS regulatory ability, while AC symbolizes the SNS tone. SDNN represents the overall variability of HRV, reflecting the combined activity of the PNS and SNS. RMSSD is indicative of vagus nerve activity, LF is influenced by both PNS and SNS, and HF corresponds to the PNS tone. TP is representative of the activities of the PNS and SNS, while the LF/HF ratio indicates the interplay between the SNS and PNS (Bauer et al., 2006a; Vanderlei et al., 2009; Lombardi and Stein, 2011; Zou et al., 2016; Thomas et al., 2019).

All DC, AC, and HRV indicators were analyzed using Kubios HRV Premium software (version 3.5, Magi Kubios Oy, Kuopio, Finland[1]) (Niskanen et al., 2004).

Statistical analysis

The Shapiro–Wilk test was applied to verify the normality of the data. The independent sample *t*-test or Mann–Whitney *U* test was utilized to compare the differences in each continuous variable, and the Chi-square test was employed to compare the differences in each counting variable among the subgroups before thoracic radiotherapy. The differences in DC, AC, and HRV before and after radiotherapy were analyzed by the Paired Sample *t*-test or Wilcoxon sign-rank test. Cohen's *d* value characterized the effect sizes of the differences in DC, AC, and HRV before and after radiotherapy in the subgroups. The independent sample *t*-test or Mann–Whitney *U* test was used to compare the differences in DC, AC, and HRV before and after radiotherapy among the subgroups. All of these statistical analyses were conducted using SPSS Statistics 25.0 (IBM Corp., Chicago, Illinois, United States of America). All tests were two-tailed, with p values of <0.05 considered statistically significant.

Results

A total of 58 patients diagnosed with TC were considered, consisting of 25 males and 33 females, with an average age of 58.6 ± 12.1 years. The prevalence of specific cancer types varied among the participants, with esophageal cancer being the most common (20/58), followed by breast (19/58), lung (16/58), Hodgkin's lymphoma (1/58), thymic cancer (1/58), and lung metastasis (1/58). The patients were categorized into two cohorts based on their treatment regimen during thoracic radiotherapy: one received solely radiotherapy (28 patients) while the other received a combination of radiotherapy and systemic therapies (30 patients). The overall patient characteristics and a comparison of variables for subgroups pre-radiotherapy are detailed in Table 1.

Our statistical analysis revealed significant variations in mean HR, DC, AC, SDNN, RMSSD, LF, HF, and TP across all patients when data prior to radiotherapy were compared. Specific changes included a significant decrease in DC ($p = 0.002$), SDNN ($p = 0.003$), RMSSD ($p = 0.009$), LF ($p = 0.005$), HF ($p = 0.002$), and TP ($p < 0.001$) when compared with pre-radiotherapy data. Contrastingly, AC ($p = 0.003$) and mean HR ($p = 0.010$) increased post-radiotherapy. A higher LF/HF ratio was observed post-radiotherapy, although this difference was not statistically significant (Table 2).

The subgroup analysis demonstrated that mean HR, DC, AC, as well as HRV parameters SDNN, RMSSD, LF, HF, and TP followed a consistent trend of increase or decrease post-thoracic radiotherapy in both the radiotherapy and combined therapy groups (Figure 1). The effect sizes of DC, AC, and HRV within subgroups are illustrated in Figure 2.

To examine whether the short-term effects of combined thoracic radiotherapy and systemic therapies on the cardiovascular ANS were either synergistic or additive, we analyzed the variations in DC, AC, and HRV before and after radiotherapy for subgroup patients. However, no statistically significant differences were found in the changes of DC, AC, and HRV between the two groups pre- and post-radiotherapy (Figure 3).

Discussion

This study evaluated the immediate effects of thoracic radiotherapy on DC, AC, and HRV in TC patients. Our findings demonstrated that thoracic radiotherapy could lead to significant alterations in mean HR, DC, AC, and HRV parameters including SDNN, RMSSD, LF, HF, and TP. Additionally, a subgroup analysis was performed, taking into account patients who were also receiving systemic therapies concurrently with radiotherapy. The outcomes implied that mean HR, DC, AC, SDNN, RMSSD, LF, HF, and TP demonstrated identical trends of increase or decrease post-radiotherapy, in both the radiotherapy-only group and the combined radiotherapy and systemic therapies group. Importantly, there was no substantial difference observed in the alterations of DC, AC, and HRV between the two groups before and after the radiotherapy.

1 https://www.kubios.com

TABLE 1 General characteristics of patients with comparisons of variables for subgroups prior to radiotherapy.

Variables	All ($N = 58$)	Radiotherapy group ($N = 28$)	Radiotherapy with systemic therapies group ($N = 30$)	p
Gender (Male/Female)	25/33	10/18	15/15	0.272
Age (years)	58.6 ± 12.1	56.1 ± 11.3	60.9 ± 12.6	0.130
BMI (kg/m^2)	23.3 ± 3.6	23.9 ± 3.3	22.7 ± 3.8	0.188
Hypertension (yes/no)	14/44	6/22	8/22	0.641
Diabetes (yes/no)	5/53	2/26	3/27	1.000
Diagnosis (BC/EC/LC/others)	19/20/16/3	13/5/8/2	6/15/8/1	**0.049**
Mean HR (bpm)	79.8 ± 12.6	82.9 ± 10.6	76.9 ± 13.7	0.070
DC (ms)	8.5 [5.0, 14.2]	7.8 [5.3, 16.8]	9.8 [3.5, 14.2]	0.767
AC (ms)	−8.2 [−14.8, −4.9]	−7.6 [−17.3, −5.1]	−9.0 [−14.8, −4.0]	0.744
SDNN (ms)	9.9 [7.0, 16.0]	9.9 [6.9, 17.7]	9.8 [7.0, 16.0]	0.950
RMSSD (ms)	9.9 [6.9, 17.5]	9.8 [6.6, 15.9]	9.9 [7.2, 18.0]	0.889
LF (ms^2)	29 [10, 135]	44 [13, 133]	25 [9, 140]	0.455
HF (ms^2)	35 [12, 101]	34 [13, 119]	44 [10, 101]	0.913
TP (ms^2)	74 [41, 273]	72 [40, 301]	74 [41, 273]	0.852
LF/HF	0.936 [0.379, 2.618]	0.905 [0.463, 2.506]	1.051 [0.303, 2.948]	0.630

Values are expressed as the number of patients or mean ± standard deviation or median [1st quartile, 3rd quartile].
Bold p values indicate statistical significance (p-value < 0.05).
N, number of individuals; BMI, body mass index; BC, breast cancer; EC, esophageal cancer; LC, lung cancer.

TABLE 2 Comparison of variables for all patients before and after radiotherapy.

Variables	Pre-values	Post-values	p
Mean HR (bpm)	79.8 ± 12.6	83.9 ± 13.6	**0.010**
DC (ms)	8.5 [5.0, 14.2]	5.3 [3.5, 9.4]	**0.002**
AC (ms)	−8.2 [−14.8, −4.9]	−5.8 [−10.1, −3.3]	**0.003**
Time-domain indices of HRV			
SDNN (ms)	9.9 [7.03, 16.0]	8.2 [6.0, 12.4]	**0.003**
RMSSD (ms)	9.9 [6.9, 17.5]	7.7 [4.8, 14.3]	**0.009**
Frequency-domain indices of HRV			
LF (ms^2)	29 [10, 135]	24 [15, 50]	**0.005**
HF (ms^2)	35 [12, 101]	16 [9, 46]	**0.002**
TP (ms^2)	74 [41, 273]	50 [33, 118]	**< 0.001**
LF/HF	0.936 [0.379, 2.618]	1.281 [0.631, 2.395]	0.559

Values are expressed as mean ± standard deviation or median [1st quartile, 3rd quartile].
Bold p values indicate statistical significance (p-value < 0.05).

The pathophysiology of cardiovascular AD induced by thoracic radiotherapy and systemic therapies is multifaceted and complex. The primary mechanisms underlying thoracic radiotherapy-associated AD encompass direct neural damage caused by radiation and the pro-inflammatory state inherent in malignancies (Teng et al., 2021). The direct radiation exposure to the vagal nerve and carotid regions may instigate inflammation and subsequent fibrosis, leading to potential damage to the vagal nerve and carotid sinus baroreflexes (Sharabi et al., 2003; Goodman and Schrader, 2009; Kong et al., 2011). An alternate explanation for the incidence of cardiovascular AD in cancer survivors could be the modification of the ANS as a consequence of a pro-inflammatory state, as opposed to intrinsic neural damage. This inflammatory state is frequently observed in cancer settings, particularly at the initiation of radiotherapy, triggering an overproduction of inflammatory cytokines such as interleukin-1, interleukin-6, and tumor necrosis factor-alpha. These factors may suppress vagal nerve activity, which in turn results in an elevation of the resting heart rate and a shift in the balance between the PNS and SNS toward SNS predominance (Thayer and Lane, 2007). Systemic therapies, such as chemotherapy or targeted therapy, may also affect the ANS during and after cancer treatment. The etiology of chemotherapy-induced AD, involving agents like anthracyclines, taxanes, and platinum compounds, may involve inflammatory pathways,

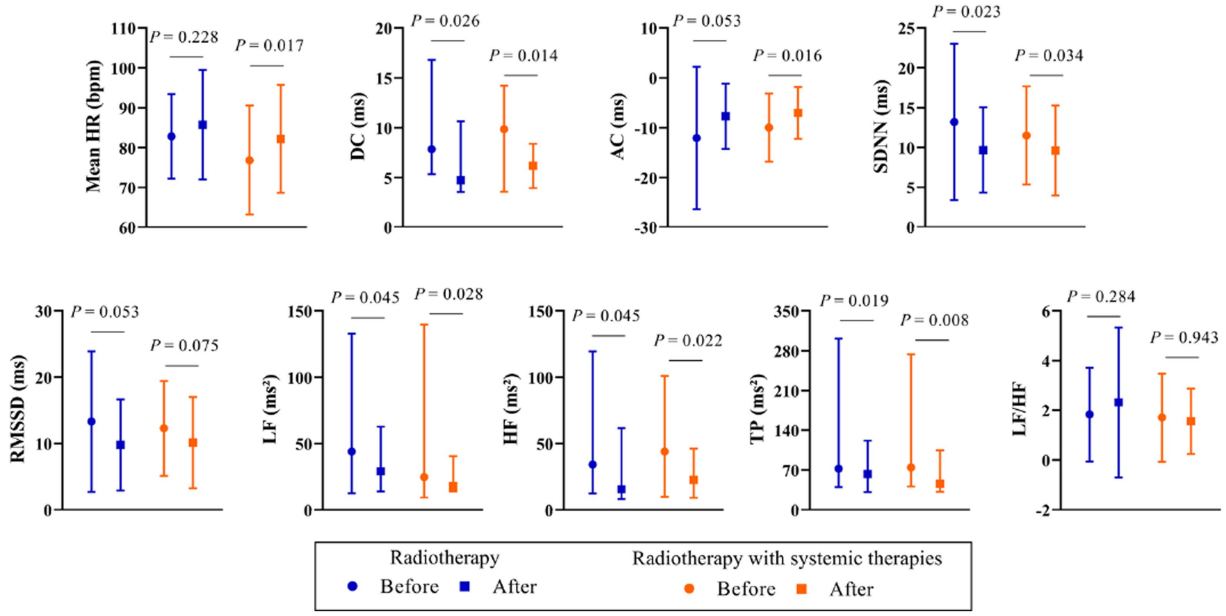

FIGURE 1
Differences in parameters for subgroups of patients pre- and post-radiotherapy.

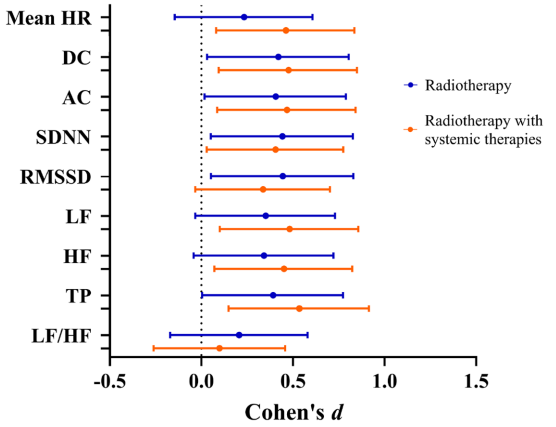

FIGURE 2
Effect size of variables for subgroups pre- and post-radiotherapy.

cellular injury, and oxidative stress (Coumbe and Groarke, 2018; Teng et al., 2021).

The stability of heart rhythm is primarily determined by the combined effects of the PNS and SNS (Lahiri et al., 2008). Recent research demonstrated that patients with Hodgkin's lymphoma who underwent thoracic radiotherapy presented a higher mean HR in contrast to those who did not undergo such treatment (Groarke et al., 2015). Moreover, previous findings strongly correlated an elevated mean HR with increased morbidity and mortality rates of cardiovascular diseases (Cooney et al., 2010; Anker et al., 2016; Lee et al., 2016). In this study, thoracic radiotherapy was found to increase the mean HR of all TC patients. A subgroup analysis revealed that patients who underwent radiotherapy demonstrated a higher mean HR post-treatment, although the difference was not statistically significant. This observation suggests that an elevated mean HR could be an efficient, albeit not entirely accurate, indicator for a rapid assessment of cardiovascular AD.

Numerous studies have emphasized the close correlation between neck or chest irradiation and cardiovascular AD (Hoca et al., 2012; Huang et al., 2013; Goyal et al., 2017). For instance, an investigation involving 14 TC patients discovered that mediastinal radiotherapy resulted in a decrease in HF values and an increase in the LF/HF in HRV frequency domain parameters (Hoca et al., 2012). Our research corroborated that thoracic radiotherapy negatively impacts HRV indicators, including SDNN, RMSSD, LF, HF, and TP. These findings suggest that thoracic radiotherapy may contribute to AD by diminishing PNS activity. Nevertheless, our study found no statistically significant difference in LF/HF values pre- and post-radiotherapy, which might be attributable to the complex physiological basis of LF/HF. Pagani et al. (1984) proposed the use of LF/HF to measure cardiac sympatho-vagal balance. However, several studies have contested this approach, asserting that LF/HF fails to accurately quantify the dynamic relationship between SNS and PNS activities and cannot confidently depict the physiological basis of LF/HF (Billman, 2011; Billman, 2013). DC and AC represent emerging noninvasive techniques for evaluating autonomic modulation (Bauer et al., 2006a; Zou et al., 2016). Recent observational studies have shown that DC was an effective predictor of epirubicin-related or trastuzumab-related cardiotoxicity development in patients with breast cancer (Feng and Yang, 2015; Feng et al., 2021). Our study determined that thoracic radiotherapy can significantly decrease DC while simultaneously increasing AC. This indicates that thoracic radiotherapy may lead to a reduction in PNS tone, as reflected by DC, and an increase in SNS activity, as assessed by AC, in TC patients. The changes in DC and AC precipitated by thoracic radiotherapy may correlate with the incidence of cardiovascular disease and sudden cardiac death rates

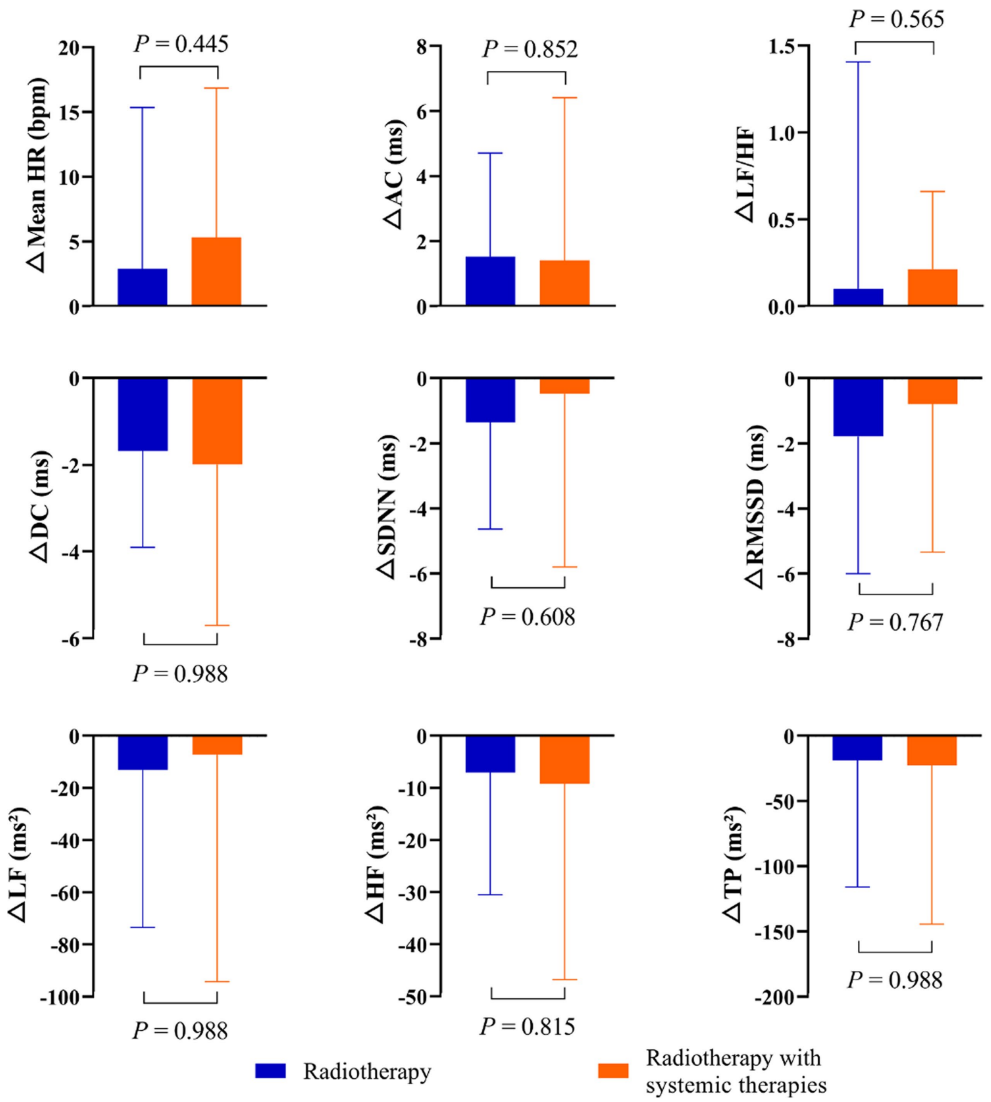

FIGURE 3
Change in DC, AC, and HRV, calculated as post-radiotherapy value minus pre-radiotherapy value for subgroups of patients.

in TC patients post-radiotherapy. However, these potential relationships warrant verification through long-term follow-up studies.

Prior research has established the potential cardiovascular toxicity of taxanes, platinum compounds, anthracyclines, and trastuzumab (Jain et al., 2017; Coumbe and Groarke, 2018; Dong and Chen, 2018). For instance, Dermitzakis et al. (2016) found that concurrent paclitaxel and carboplatin chemotherapy significantly influenced the PNS and SNS in ovarian cancer patients, predominantly affecting parasympathetic heart innervation. Liu et al. (2023) showed that the combination of taxane and carboplatin chemotherapy could impact early ANS status in patients with cervical cancer. Meinardi et al. (2001) discovered that even moderate doses of epirubicin were not associated with persistent alterations in HRV for breast cancer patients, suggesting a possible dose–response relationship for anthracycline-induced ANS damage. Our findings revealed no statistically significant difference in the alterations of DC, AC, and HRV pre- and post-radiotherapy between the radiotherapy-only group and the combined radiotherapy and systemic therapies group. This implies that, in the short term, thoracic radiotherapy coupled with systemic therapies does not significantly exacerbate or add to ANS changes. Currently, while radiotherapy and systemic therapies may exert cardiac toxic effects, the precise mechanism of their interaction remains elusive.

Emerging evidence has shown that patients receiving thoracic radiotherapy have an increased risk for developing cardiovascular disease (Groarke et al., 2015; Jacob et al., 2016; Armanious et al., 2018). According to the American Society of Clinical Oncology's clinical practice guideline, baseline assessment of the left ventricular ejection fraction could feasibly stratify risk in patients potentially susceptible to cardiovascular toxicity (Armenian et al., 2017). However, relying solely on left ventricular ejection fraction as an indicator of cardiac performance has faced substantial criticism (Konstam and Abboud, 2017; Marwick, 2018). Prior research has demonstrated that cardiovascular ANS

function may be a more accurate mortality predictor following myocardial infarction than left ventricular ejection fraction (Bauer et al., 2006a). Additional studies have emphasized the significance of alterations in serum biomarkers, notably cardiac troponin, for forecasting cardiovascular toxicity (Cardinale et al., 2010; Pavo et al., 2015). Therefore, we propose a baseline assessment encompassing ANS function, left ventricular ejection fraction, and troponin measurement for cardiovascular toxicity risk stratification, with subsequent combined measurements for longitudinal cardiac monitoring.

Limitations

Our study's primary limitation is the heterogeneity of the study population. Given our limited sample size, it was unattainable to discern the distinct performance of DC, AC, and HRV in patients with varying types of TC. We strongly advocate for future studies to augment the sample size and prioritize these differences (e.g., tumor type, chemotherapy drugs and doses). Furthermore, due to limited statistical power, some background variables potentially influencing cardiovascular ANS, such as physical activity, were omitted.

Conclusion

Our study elucidates the modifications of DC, AC, and HRV pre- and post-thoracic radiotherapy in patients diagnosed with TC. These results suggest that thoracic radiotherapy prompts cardiovascular AD by diminishing PNS activity and augmenting SNS tone. Additionally, the data implies that combining radiotherapy with systemic therapies may not yield a substantial synergetic or additive impact on the ANS in the short term. We hypothesize that the simultaneous measurement of DC, AC, and HRV could be helpful in developing an integrated biomarker for identifying both short- and long-term radiotherapy-induced cardiac autonomic modulation impairments.

Data availability statement

The raw data supporting the conclusions of this article will be made available by the authors, without undue reservation.

Ethics statement

The studies involving humans were approved by the Medical Ethics Committee of the First Affiliated Hospital of Bengbu Medical College. The studies were conducted in accordance with the local legislation and institutional requirements. The participants provided their written informed consent to participate in this study.

Author contributions

SW: Data curation, Writing – original draft. WG: Formal analysis, Writing – original draft. HZ: Writing – original draft. GL: Writing – original draft. YZ: Resources, Supervision, Writing – review & editing. BS: Conceptualization, Methodology, Resources, Writing – review & editing, XZ: Resources, Supervision, Writing – review & editing.

Funding

This research was funded by the "512" Outstanding Talents Fostering Project of Bengbu Medical College (grant number BY51201312), the Natural Science Research Project of Anhui Educational Committee (grant number KJ2021A0803), and the Scientific Research Innovation Project of Bengbu Medical College (grant number BYKC201905).

Conflict of interest

An immediate family member of BS owns stock in HeaLink Ltd., Bengbu, China.

The remaining authors declare that the research was conducted in the absence of any commercial or financial relationships that could be construed as a potential conflict of interest.

Publisher's note

References

Anker, M. S., Ebner, N., Hildebrandt, B., Springer, J., Sinn, M., Riess, H., et al. (2016). Resting heart rate is an independent predictor of death in patients with colorectal, pancreatic, and non-small cell lung cancer: results of a prospective cardiovascular long-term study. *Eur. J. Heart Fail.* 18, 1524–1534. doi: 10.1002/ejhf.670

Armanious, M. A., Mohammadi, H., Khodor, S., Oliver, D. E., Johnstone, P. A., and Fradley, M. G. (2018). Cardiovascular effects of radiation therapy. *Curr. Probl. Cancer* 42, 433–442. doi: 10.1016/j.currproblcancer.2018.05.008

Armenian, S. H., Lacchetti, C., Barac, A., Carver, J., Constine, L. S., Denduluri, N., et al. (2017). Prevention and monitoring of cardiac dysfunction in survivors of adult cancers: American Society of Clinical Oncology clinical practice guideline. *J. Clin. Oncol.* 35, 893–911. doi: 10.1200/JCO.2016.70.5400

Arsenos, P., Manis, G., Gatzoulis, K. A., Dilaveris, P., Gialernios, T., Angelis, A., et al. (2016). Deceleration capacity of heart rate predicts arrhythmic and total mortality in heart failure patients. *Ann. Noninvasive Electrocardiol.* 21, 508–518. doi: 10.1111/anec.12343

Baselet, B., Sonveaux, P., Baatout, S., and Aerts, A. (2019). Pathological effects of ionizing radiation: endothelial activation and dysfunction. *Cell. Mol. Life Sci.* 76, 699–728. doi: 10.1007/s00018-018-2956-z

Bauer, A., Kantelhardt, J. W., Barthel, P., Schneider, R., Mäkikallio, T., Ulm, K., et al. (2006a). Deceleration capacity of heart rate as a predictor of mortality after myocardial infarction: cohort study. *Lancet* 367, 1674–1681. doi: 10.1016/S0140-6736(06)68735-7

Bauer, A., Kantelhardt, J. W., Bunde, A., Barthel, P., Schneider, R., Malik, M., et al. (2006b). Phase-rectified signal averaging detects quasi-periodicities in non-stationary data. *Physica A.* 364, 423–434. doi: 10.1016/j.physa.2005.08.080

Billman, G. E. (2011). Heart rate variability – a historical perspective. *Front. Physiol.* 2:86. doi: 10.3389/fphys.2011.00086

Billman, G. E. (2013). The LF/HF ratio does not accurately measure cardiac sympatho-vagal balance. *Front. Physiol.* 4:26. doi: 10.3389/fphys.2013.00026

Cardinale, D., Colombo, A., Torrisi, R., Sandri, M. T., Civelli, M., Salvatici, M., et al. (2010). Trastuzumab-induced cardiotoxicity: clinical and prognostic implications of troponin I evaluation. *J. Clin. Oncol.* 28, 3910–3916. doi: 10.1200/JCO.2009.27.3615

Caru, M., Corbin, D., Périé, D., Lemay, V., Delfrate, J., Drouin, S., et al. (2019). Doxorubicin treatments induce significant changes on the cardiac autonomic nervous system in childhood acute lymphoblastic leukemia long-term survivors. *Clin. Res. Cardiol.* 108, 1000–1008. doi: 10.1007/s00392-019-01427-9

Cooney, M. T., Vartiainen, E., Laatikainen, T., Juolevi, A., Dudina, A., and Graham, I. M. (2010). Elevated resting heart rate is an independent risk factor for cardiovascular disease in healthy men and women. *Am. Heart J.* 159, 612–619.e3. doi: 10.1016/j.ahj.2009.12.029

Coumbe, B. G. T., and Groarke, J. D. (2018). Cardiovascular autonomic dysfunction in patients with cancer. *Curr. Cardiol. Rep.* 20:69. doi: 10.1007/s11886-018-1010-y

Dermitzakis, E. V., Kimiskidis, V. K., Lazaridis, G., Alexopoulou, Z., Timotheadou, E., Papanikolaou, A., et al. (2016). The impact of paclitaxel and carboplatin chemotherapy on the autonomous nervous system of patients with ovarian cancer. *BMC Neurol.* 16:190. doi: 10.1186/s12883-016-0710-4

Dong, J., and Chen, H. (2018). Cardiotoxicity of anticancer therapeutics. *Front. Cardiovasc. Med.* 5:9. doi: 10.3389/fcvm.2018.00009

Ekholm, E. M., Salminen, E. K., Huikuri, H. V., Jalonen, J., Antila, K. J., Salmi, T. A., et al. (2000). Impairment of heart rate variability during paclitaxel therapy. *Cancer* 88, 2149–2153. doi: 10.1002/(sici)1097-0142(20000501)88:9<2149::aid-cncr22>3.0.co;2-z

Fang, S. C., Wu, Y. L., and Tsai, P. S. (2020). Heart rate variability and risk of all-cause death and cardiovascular events in patients with cardiovascular disease: a meta-analysis of cohort studies. *Biol. Res. Nurs.* 22, 45–56. doi: 10.1177/1099800419877442

Feng, Y., Qin, Z., and Yang, Z. (2021). Deceleration capacity of heart rate predicts trastuzumab-related cardiotoxicity in patients with HER2-positive breast cancer: a prospective observational study. *J. Clin. Pharm. Ther.* 46, 93–98. doi: 10.1111/jcpt.13258

Feng, Y. Y., and Yang, Z. J. (2015). Clinical application of the heart rate deceleration capacity test to predict Epirubicin-induced cardiotoxicity. *J. Cardiovasc. Pharmacol.* 66, 371–375. doi: 10.1097/FJC.0000000000000289

Goodman, B. P., and Schrader, S. L. (2009). Radiation-induced cranial neuropathies manifesting as baroreflex failure and progressive bulbar impairment. *Neurologist* 15, 102–104. doi: 10.1097/NRL.0b013e31817ba3a6

Goyal, M., Shukla, P., Gupta, D., Bisht, S., Verma, N. S., Tiwari, S., et al. (2017). Cardiovascular sequel of neck irradiation in head and neck cancer patients. *Int. J. Radiat. Biol.* 93, 711–716. doi: 10.1080/09553002.2017.1303217

Groarke, J. D., Tanguturi, V. K., Hainer, J., Klein, J., Moslehi, J. J., Ng, A., et al. (2015). Abnormal exercise response in long-term survivors of hodgkin lymphoma treated with thoracic irradiation: evidence of cardiac autonomic dysfunction and impact on outcomes. *J. Am. Coll. Cardiol.* 65, 573–583. doi: 10.1016/j.jacc.2014.11.035

Guimarães, S. L., Brandão, S. C., Andrade, L. R., Maia, R. J., and Markman Filho, B. (2015). Cardiac sympathetic hyperactivity after chemotherapy: early sign of cardiotoxicity? *Arq. Bras. Cardiol.* 105, 228–234. doi: 10.5935/abc.20150075

Hoca, A., Yildiz, M., and Ozyigit, G. (2012). Evaluation of the effects of mediastinal radiation therapy on autonomic nervous system. *Med. Oncol.* 29, 3581–3586. doi: 10.1007/s12032-012-0237-5

Huang, C. C., Huang, T. L., Hsu, H. C., Chen, H. C., Lin, H. C., Chien, C. Y., et al. (2013). Long-term effects of neck irradiation on cardiovascular autonomic function: a study in nasopharyngeal carcinoma patients after radiotherapy. *Muscle Nerve* 47, 344–350. doi: 10.1002/mus.23530

Jacob, S., Pathak, A., Franck, D., Latorzeff, I., Jimenez, G., Fondard, O., et al. (2016). Early detection and prediction of cardiotoxicity after radiation therapy for breast cancer: the BACCARAT prospective cohort study. *Radiat. Oncol.* 11:54. doi: 10.1186/s13014-016-0627-5

Jain, D., Russell, R. R., Schwartz, R. G., Panjrath, G. S., and Aronow, W. (2017). Cardiac complications of cancer therapy: pathophysiology, identification, prevention, treatment, and future directions. *Curr. Cardiol. Rep.* 19:36. doi: 10.1007/s11886-017-0846-x

Kong, L., Lu, J. J., Liss, A. L., Hu, C., Guo, X., Wu, Y., et al. (2011). Radiation-induced cranial nerve palsy: a cross-sectional study of nasopharyngeal cancer patients after definitive radiotherapy. *Int. J. Radiat. Oncol. Biol. Phys.* 79, 1421–1427. doi: 10.1016/j.ijrobp.2010.01.002

Konstam, M. A., and Abboud, F. M. (2017). Ejection fraction: misunderstood and overrated (changing the paradigm in categorizing heart failure). *Circulation* 135, 717–719. doi: 10.1161/CIRCULATIONAHA.116.025795

Lahiri, M. K., Kannankeril, P. J., and Goldberger, J. J. (2008). Assessment of autonomic function in cardiovascular disease: physiological basis and prognostic implications. *J. Am. Coll. Cardiol.* 51, 1725–1733. doi: 10.1016/j.jacc.2008.01.038

Lee, D. H., Park, S., Lim, S. M., Lee, M. K., Giovannucci, E. L., Kim, J. H., et al. (2016). Resting heart rate as a prognostic factor for mortality in patients with breast cancer. *Breast Cancer Res. Treat.* 159, 375–384. doi: 10.1007/s10549-016-3938-1

Liu, J., Guan, W., Sun, Y., Wang, Y., Li, G., Zhang, S., et al. (2023). Early detection of the impact of combined taxane and carboplatin treatment on autonomic nerves in patients with cervical cancer: measurement of heart rate variability. *Front. Physiol.* 14:1126057. doi: 10.3389/fphys.2023.1126057

Lombardi, F., and Stein, P. K. (2011). Origin of heart rate variability and turbulence: an appraisal of autonomic modulation of cardiovascular function. *Front. Physiol.* 2:95. doi: 10.3389/fphys.2011.00095

Marwick, T. H. (2018). Ejection fraction pros and cons: JACC state-of-the-art review. *J. Am. Coll. Cardiol.* 72, 2360–2379. doi: 10.1016/j.jacc.2018.08.2162

Meinardi, M. T., van Veldhuisen, D. J., Gietema, J. A., Dolsma, W. V., Boomsma, F., van den Berg, M. P., et al. (2001). Prospective evaluation of early cardiac damage induced by epirubicin-containing adjuvant chemotherapy and locoregional radiotherapy in breast cancer patients. *J. Clin. Oncol.* 19, 2746–2753. doi: 10.1200/JCO.2001.19.10.2746

Nasario-Junior, O., Benchimol-Barbosa, P. R., and Nadal, J. (2014). Refining the deceleration capacity index in phase-rectified signal averaging to assess physical conditioning level. *J. Electrocardiol.* 47, 306–310. doi: 10.1016/j.jelectrocard.2013.12.006

Niskanen, J. P., Tarvainen, M. P., Ranta-Aho, P. O., and Karjalainen, P. A. (2004). Software for advanced HRV analysis. *Comput. Methods Progr. Biomed.* 76, 73–81. doi: 10.1016/j.cmpb.2004.03.004

Pagani, M., Lombardi, F., Guzzetti, S., Sandrone, G., Rimoldi, O., Malfatto, G., et al. (1984). Power spectral density of heart rate variability as an index of sympatho-vagal interaction in normal and hypertensive subjects. *J. Hypertens. Suppl.* 2, S383–S385.

Pan, J., and Tompkins, W. J. (1985). A real-time QRS detection algorithm. *IEEE Trans. Biomed. Eng.* BME-32, 230–236. doi: 10.1109/TBME.1985.325532

Pavo, N., Raderer, M., Hülsmann, M., Neuhold, S., Adlbrecht, C., Strunk, G., et al. (2015). Cardiovascular biomarkers in patients with cancer and their association with all-cause mortality. *Heart* 101, 1874–1880. doi: 10.1136/heartjnl-2015-307848

Raghunathan, D., Khilji, M. I., Hassan, S. A., and Yusuf, S. W. (2017). Radiation-induced cardiovascular disease. *Curr. Atheroscler. Rep.* 19:22. doi: 10.1007/s11883-017-0658-x

Rizas, K. D., Eick, C., Doller, A. J., Hamm, W., von Stuelpnagel, L., Zuern, C. S., et al. (2018). Bedside autonomic risk stratification after myocardial infarction by means of short-term deceleration capacity of heart rate. *Europace* 20, f129–f136. doi: 10.1093/europace/eux167

Schwartz, P. J., and De Ferrari, G. M. (2011). Sympathetic-parasympathetic interaction in health and disease: abnormalities and relevance in heart failure. *Heart Fail. Rev.* 16, 101–107. doi: 10.1007/s10741-010-9179-1

Sharabi, Y., Dendi, R., Holmes, C., and Goldstein, D. S. (2003). Baroreflex failure as a late sequela of neck irradiation. *Hypertension* 42, 110–116. doi: 10.1161/01.HYP.0000077441.45309.08

Stachowiak, P., Milchert-Leszczyńska, M., Falco, M., Wojtarowicz, A., Kaliszczak, R., Safranow, K., et al. (2018). Heart rate variability during and after chemotherapy with anthracycline in patients with breast cancer. *Kardiol. Pol.* 76, 914–916. doi: 10.5603/KP.2018.0098

Sylvester, C. B., Abe, J. I., Patel, Z. S., and Grande-Allen, K. J. (2018). Radiation-induced cardiovascular disease: mechanisms and importance of linear energy transfer. *Front. Cardiovasc. Med.* 5:5. doi: 10.3389/fcvm.2018.00005

Teng, A. E., Noor, B., Ajijola, O. A., and Yang, E. H. (2021). Chemotherapy and radiation-associated cardiac autonomic dysfunction. *Curr. Oncol. Rep.* 23:14. doi: 10.1007/s11912-020-01013-7

Thayer, J. F., and Lane, R. D. (2007). The role of vagal function in the risk for cardiovascular disease and mortality. *Biol. Psychol.* 74, 224–242. doi: 10.1016/j.biopsycho.2005.11.013

Thomas, B. L., Claassen, N., Becker, P., and Viljoen, M. (2019). Validity of commonly used heart rate variability markers of autonomic nervous system function. *Neuropsychobiology* 78, 14–26. doi: 10.1159/000495519

Tjeerdsma, G., Meinardi, M. T., van Der Graaf, W. T., van Den Berg, M. P., Mulder, N. H., Crijns, H. J., et al. (1999). Early detection of anthracycline induced cardiotoxicity in asymptomatic patients with normal left ventricular systolic function: autonomic versus echocardiographic variables. *Heart* 81, 419–423. doi: 10.1136/hrt.81.4.419

Vanderlei, L. C., Pastre, C. M., Hoshi, R. A., Carvalho, T. D., and Godoy, M. F. (2009). Basic notions of heart rate variability and its clinical applicability. *Rev. Bras. Cir. Cardiovasc.* 24, 205–217. doi: 10.1590/s0102-76382009000200018

Venkatesulu, B. P., Mahadevan, L. S., Aliru, M. L., Yang, X., Bodd, M. H., Singh, P. K., et al. (2018). Radiation-induced endothelial vascular injury: a review of possible mechanisms. *JACC Basic Transl. Sci.* 3, 563–572. doi: 10.1016/j.jacbts.2018.01.014

Wang, C. G., Luo, X. C., Yao, T., Liu, Y. Y., Zhao, S. H., Cheng, J. Y., et al. (2017). Clinical value of DC and DRs in warning sudden cardiac death of patients with coronary artery disease. *Zhongguo Ying Yong Sheng Li Xue Za Zhi* 33, 244–247. doi: 10.12047/j.cjap.5509.2017.060

Zou, C., Dong, H., Wang, F., Gao, M., Huang, X., Jin, J., et al. (2016). Heart acceleration and deceleration capacities associated with dilated cardiomyopathy. *Eur. J. Clin. Investig.* 46, 312–320. doi: 10.1111/eci.12594

frontiers | Frontiers in Neuroscience

TYPE Original Research
PUBLISHED 25 September 2023
DOI 10.3389/fnins.2023.1271461

OPEN ACCESS

EDITED BY
Vitor Engracia Valenti,
São Paulo State University, Brazil

REVIEWED BY
Patrick William Chambers,
Torrance Memorial Medical Center,
United States
Anatoliy Gozhenko,
Ministry of Health of Ukraine, Ukraine

*CORRESPONDENCE
Cyril Besson
✉ Cyril.besson@chuv.ch

RECEIVED 02 August 2023
ACCEPTED 01 September 2023
PUBLISHED 25 September 2023

CITATION
Besson C, Mur T, Benaim C, Schmitt L and Gremeaux V (2023) Short-term effects on heart rate variability of occipito-mastoid suture normalization in healthy subjects.
Front. Neurosci. 17:1271461.
doi: 10.3389/fnins.2023.1271461

Short-term effects on heart rate variability of occipito-mastoid suture normalization in healthy subjects

Cyril Besson[1,2]*, Thierry Mur[3], Charles Benaim[4], Laurent Schmitt[5] and Vincent Gremeaux[1,2]

[1]Department of Sports Medicine, Swiss Olympic Medical Center, Lausanne University Hospital, Lausanne, Switzerland, [2]Institute of Sports Sciences, University of Lausanne, Lausanne, Switzerland, [3]Department of Physiotherapy, Aquamed Center, Montreux, Switzerland, [4]Department of Physical Medicine and Rehabilitation, Lausanne University Hospital, Lausanne, Switzerland, [5]National School of Mountain Sports/National Ski-Nordic Centre, Premanon, France

Occipito-mastoid structure normalization (OMSN) is an osteopathic manipulative treatment aimed at reducing tension around the jugular foramen, where cranial nerves IX, X, and XI exit the skull. The purpose of this study was to observe how heart rate variability (HRV), a marker of autonomic cardiac regulation, was modulated after an OMSN vs. a sham technique (SHAM). Pre- and post-intervention HRV was analyzed in two randomly chosen groups of 15 participants (OMSN vs. SHAM group). HRV was collected in the supine position 5 min before and 5 min after a 10-min application of either OMSN or SHAM. The time and group effect was analyzed using a two-way ANOVA. Independently from group intervention, a significant time effect induced increased HRV. No group effect differences were observed. Multiple comparisons for time and group interaction showed that the root mean square of successive differences (RMSSD), a vagally mediated HRV variable, increased to a greater extent for the OMSN group ($p = 0.03$) than for the SHAM group. However, both OMSN and SHAM techniques had a significant effect on HRV. Compared to a SHAM technique, OMSN had a significant effect on HRV vagally related metric RMSSD in the short term. We conclude that 10 min of OMSN may be used to induce a short-term influence on parasympathetic autonomic nervous system modulations.

KEYWORDS

osteopathy manual therapy, vagal modulation, cardiac autonomic control, skull, SHAM

1. Introduction

Osteopathy promotes health *via* a patient-centered holistic approach. The term osteopathic manipulative treatment (OMT) encompasses non-invasive forms of manual therapy using palpation and manual techniques to influence body-tissue interconnection and to maintain or restore health (Carnevali et al., 2020). Among the assumed outcomes, OMT is believed to influence the autonomic nervous system (ANS), which in turn is essential to general health (Rees, 2014; Rechberger et al., 2019; Carnevali et al., 2020). The ANS regulates physiological functions, maintaining body homeostasis according to internal and external variations. It is composed of two main branches: (1) the parasympathetic system (PS) has a craniosacral anatomical organization, which predominates in periods of calm, in particular, to regenerate the body and (2) the orthosympathetic system (OS) has a predominant dorsolumbar organization, which produces "fight or flight" reactions

in the face of an impending threat (McCorry, 2007; Wehrwein et al., 2016). An imbalance in the ANS is called dysautonomia and has numerous causes (Reichgott, 1990). They can be functional, for instance, a structural alteration of functional ANS anatomy (e.g., compression or inflammation) and can be affected by different stressful stimuli (Grossman and Taylor, 2007; Porges, 2009; Thayer and Lane, 2009). Osteopathy is among the different treatments available for dysautonomia (Rechberger et al., 2019). A meta-analysis that found 23 studies on osteopathy efficacy on ANS, which incorporated three main techniques [high-velocity low-amplitude techniques (HVLAT); cranial OMT techniques; mobilization techniques in the thoracic and cervical spine], highlighted those as follows: (1) Significant changes in ANS activity may happen with HVLAT, (2) no conclusion could be drawn from studies on cranial osteopathy due to lack of methodological quality, (3) significant changes in ANS activity may happen in suboccipital region treatments, (4) no conclusion could be drawn from studies on cervical and thoracic mobilization, (5) whether activations happen in the sympathetic or parasympathetic part of ANS is unclear, and (6) thorough methodological research must be conducted (Rechberger et al., 2019). The authors concluded that OMT can positively influence ANS. However, they highlighted that different OMTs were performed using different techniques, regions, and ways of evaluating the ANS activity.

Heart rate variability (HRV) is used to interpret ANS cardiac control with the advantage of being non-invasive and easy to collect (Grossman and Taylor, 2007; Porges, 2009; Thayer and Lane, 2009). It is employed as a quantitative and qualitative stress assessment, especially by measuring cardiac vagal tone activity (Malik, 1996; Laborde et al., 2017). Literature has recently focused on the osteopathic effects on the ANS using different techniques and treatment locations. However, an improved organization of research protocols is required (Steel et al., 2017; Rechberger et al., 2019; Carnevali et al., 2020). In a recent perspective article, Carnevali et al. considered that heart rate variability (HRV) analysis can be used to evaluate the effectiveness of OMT. Indeed, some HRV variables may reliably be interpreted as reflecting cardiac vagal tone using measures such as the root mean square of successive beat-to-beat interval differences (RMSSD) or the high-frequency (HF) power spectrum (Laborde et al., 2017; Shaffer and Ginsberg, 2017). Among studies cited by Rechberger's meta-analysis, Giles et al. showed an increase in the HF power spectrum after suboccipital decompression (Giles et al., 2013). Another study showed a decrease in sympathetic activity after a suboccipital manipulation (Purdy et al., 1996).

Cranial nerves IX, X, and XI [glossopharyngeal, vagus, and accessory (or spinal accessory)] pass through the jugular foramen between the occiput and the temporal bone of the skull. Dysfunction of the jugular foramen may cause dysautonomia, and thus, OMT techniques may be adopted in certain cases. As the vagus nerve is one of the main parasympathetic nerves (Gerritsen and Band, 2018) and its activity is closely related to homeostasis, treatments targeting the jugular foramen area may have a certain relevance in ANS balance. Sergueef described the occipito-mastoid suture normalization (OMSN) to be effective in normalizing tensions between the occiput and the temporal bone (Sergueef, 2018). Its purpose is to achieve a state of equilibrium of tensions in the treated area, favorable to mechanical, circulatory, and neurological harmonization. However, there is a scarcity of related research in this area and even if this technique may be used for treating an imbalance, no current research exists on possible effects in healthy participants. To the best of our knowledge, no study has investigated the objective non-invasive measurement of stress *via* HRV after an OMSN OMT neither in patients nor in healthy participants. This study aimed to describe whether a cranial technique of normalization of the occipito-mastoid suture may influence cardiac vagal activity HRV-related indexes in a priori asymptomatic participants. We hypothesized that parasympathetic nervous system (PNS) HRV markers will increase to a greater extent compared to a sham technique (SHAM) following an OMSN OMT session in healthy subjects.

2. Materials and methods

2.1. Participants and study design

The criteria for inclusion were to be generally healthy and be aged between 18 and 75 years old. The exclusion criteria included primary or secondary dysautonomia, head trauma-induced dysautonomia, and treatment influencing cardiorespiratory function. Thirty-four people participated voluntarily in the study. which was approved by the Canton de Vaud ethics committee (#2020-02867) in accordance with the ethical standards of the Helsinki Declaration. All participants signed an informed consent form.

A prospective, interventional study, single-blinded, randomized control trial design was used to compare HRV pre- and post-OMSN or SHAM techniques. Participants were included for a single visit to the physiotherapy center Aquamed Malley in Lausanne. They were equipped with a heart rate monitor and were then randomly assigned to either the OMSN or SHAM group (single blinded). Participants were installed in a supine position on a physical therapy table, with their eyes closed, and were asked not to think about anything in particular. After ensuring that there was no discomfort (e.g., excessive belt tension or feeling of cold), participants remained in that position for 3 min before R-R intervals were recorded for a period of 5 min. Once this first R-R interval measurement period was over, the investigator applied either OMSN or SHAM treatments for 10 min. R-R intervals were then collected again during a 5-min period following the intervention.

2.2. Heart rate variability

To minimize confounding factors on HRV, participants were asked to attend the laboratory under standardized conditions: no training or intense physical activity in the 24 h preceding the visit, no muscle soreness, fasted or to have finished their last meal at least 3 h before the beginning of the protocol,

no alcohol, tea or caffeine ingestion or smoking during the last 12 h. They were asked not to attend if they showed signs of illness. It is known that data obtained for a short-term intra-individual HRV analysis remain interpretable as being less impacted by external factors (Quintana and Heathers, 2014). However, we standardized experimental conditions according to the following criteria: indirect and equal intensity lighting, constant and comfortable temperature, no particular noise or smell, communication limited to set-up, and protocol presentation instructions. The participants were asked not to move or engage in conversation unless they needed to communicate important information or experienced discomfort.

Participants were equipped with a Polar H10 heart rate monitor paired with a Polar V800 watch (Polar Electro Oy, Kempele, Finland) to collect R-R intervals. R-R intervals were extracted from the Polar online platform and visually inspected for artifacts and ectopic beats, which were automatically and manually corrected using Kubios Premium (Kubios, Finland) (Tarvainen et al., 2014). An experienced exercise physiologist blinded to which group participants belonged to performed the analysis. The final 4 min of each 5 min samples were analyzed as it allowed a reliable frequency-domain analysis (Bourdillon et al., 2017). Time- and frequency-domain and non-linear variables were kept for analysis (Shaffer and Ginsberg, 2017), with particular attention being paid to vagally mediated variables [e.g., RMSSD, HR, HF, HF relative to HR (HF/HR), (LF+HF)/HR, and detrended fluctuation analysis alpha 1 (DFA1)].

2.3. Occipito-mastoid suture normalization

The OMSN technique (illustrated in Figure 1) is a passive and smooth osteopathic technique, regularly applied in general practice. The participant is in the dorsal decubitus position with the practitioner by his head. The investigator places his contralateral hand opposite the treated side transversally under the occiput with the pulp of the index, middle, and ring fingers under the occipital scale, medial to the occipito-mastoid structure. The homolateral hand is placed on the temporal bone with a five-finger grip: the thumb and index finger above and below the zygomatic process, respectively, the medius at the level of the external acoustic pore, the ring finger on the tip of the mastoid process, and the little finger on the mastoid portion. Functional treatment begins with feeling and then continues with tissue guidance in the direction of dysfunction across the three spatial planes where improved movement is sensed. The practitioner gradually facilitates these movements until a noticeable relaxation occurs, indicating normalization. The goal is to establish a state of balanced tension in the treated area, promoting alignment among mechanical, circulatory, and neurological mechanisms. Using a perceptive and light touch, no additional pressure other than simply accompanying the tissues in the direction of their ease is applied. In the present study, the technique was applied for 10 min, 5 min for each jugular foramen. For the SHAM group, the investigator just positioned the fingers as for OMSN, but with no intention of feeling nor treating.

2.4. Statistical analyses

The data are expressed as mean ± standard deviation (SD). Differences between groups in age, weight, height, and body mass index (BMI) were tested with unpaired *t*-tests. A two-way repeated measures ANOVA [time (pre- vs. post-) × group (OMSN vs. SHAM)] was performed to assess for an intervention effect. This analysis allowed the identification of differences between pre- and post-intervention (time effect) and within the intervention (group effect). All data passed Mauchly's sphericity test. When repeated measures ANOVA revealed a significant main effect (time or group) or interaction effect, multiple comparisons were performed to test the significance of the differences using Bonferroni adjustments. All statistical analyses were performed with IBM SPSS version 28

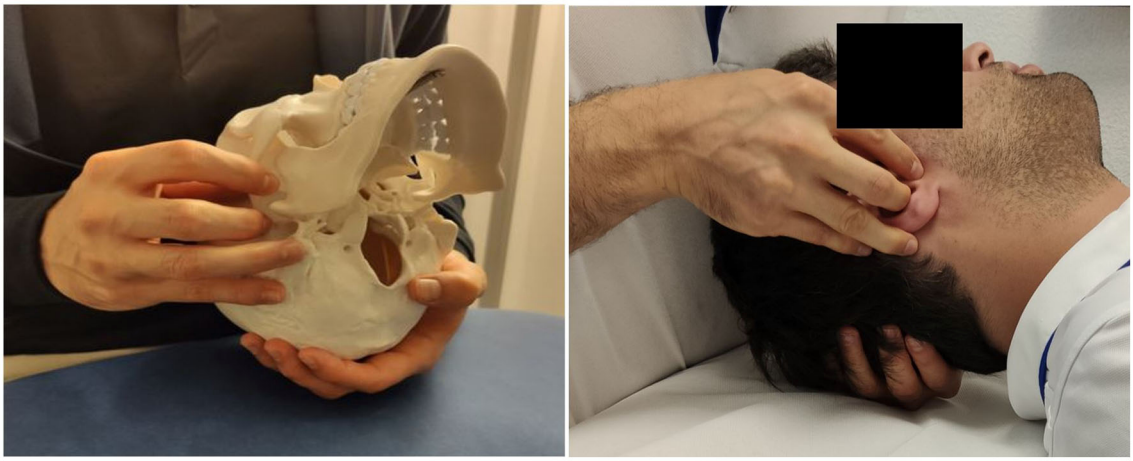

FIGURE 1
Manual grasp for the right OMSN on the skeleton (for illustration) and with a participant.

software (IBM Corp., Armonk, NY, USA). The level of significance was set to be at a $p \leq 0.05$.

3. Results

In total, 34 participants were randomly assigned to either the OMSN or SHAM groups. Once a group attained 17 participants, the last participants entering the study were attributed to the other group. The first two participants were excluded because the technique applied was incorrect. Two other participants were excluded from the analysis: one because of non-compliance with the protocol instructions (open eyes, repeated movements) and one who showed signs of arrhythmia and was referred for a cardiac check-up. Each excluded participant was replaced by a participant with the same intervention. A final number of 21 women and 9 men were included in the analysis. Groups were considered as homogenous as no difference in gender distribution, age, weight, or height was observed (see Table 1).

Table 2 presents pre- and post-intervention values and *p*-values for each variable and condition.

Independently from group intervention, a significant time effect was observed for SDNN, RMSSD, PNN50, LF, LF+HF, TP, (LF+HF)/HR, SD1, and SD2, which all increased, whereas HR decreased. No time effect was observed in HF. Group effect analysis showed no differences between interventions. When analyzing multiple comparisons for time and group interaction, RMSSD increased to a greater extent for the OMSN group ($p = 0.03$).

TABLE 1 Gender repartition, age, weight, and height of participants.

	OMSN	SHAM	*P*-value
M/F	4/11	5/10	
Age (year)	38 ± 16.5	37.1 ± 13.7	0.877
Weight (kg)	68.9 ± 12.3	69.5 ± 7.4	0.858
Height (cm)	168.3 ± 11.5	169.1 ± 7.5	0.822
BMI (kg/m^2)	24.3 ± 3.3	24.5 ± 3.4	0.884

Data are mean ± SD. OMSN: occipito-mastoidian suture normalization; M, male; F, female.

TABLE 2 Comparisons of time- and frequency-domain and non-linear HRV variables pre- and post-OMSN and SHAM.

	OMSN		SHAM		Two-way ANOVA *p*-value		
	PRE	POST	PRE	POST	Time effect	Group effect	Time* group interaction effect
SDNN (ms)	40.6 ± 21.1	53.5 ± 26.6	50.8 ± 30.6	57.2 ± 28.2	**0.002**	0.461	0.26
HR (bpm)	73.2 ± 10.7	68.6 ± 8.5	67 ± 10.7	64.6 ± 9.6	**<0.001**	0.164	0.108
RMSSD (ms)	**29.3 ± 21**	**37.4 ± 21.7***	42.6 ± 39.2	45.4 ± 35.6	**<0.001**	0.345	**0.03**
PNN50 (%)	8.8 ± 12.2	15.4 ± 16.4	19.7 ± 25.1	22.9 ± 25.1	**<0.001**	0.222	0.152
VLF (ms^2)	631.3 ± 551	1247.5 ± 1532.3	967.2 ± 996.4	1770.4 ± 2329	0.056	0.314	0.795
LF (ms^2)	758.7 ± 1220.2	1317 ± 1876.7	831.2 ± 1175.4	1020.3 ± 971.7	**0.041**	0.81	0.299
HF (ms^2)	540.9 ± 750.3	683.6 ± 987.3	1032.6 ± 1442.5	1075.3 ± 1359.9	0.15	0.305	0.432
LF/HF	2.6 ± 3.1	2.9 ± 3.5	2.4 ± 2.7	2.2 ± 2.1	0.646	0.653	0.351
LF+HF (ms^2)	1299.6 ± 1864.8	2000.6 ± 2781.8	1863.7 ± 2243.6	2095.6 ± 1932.8	**0.022**	0.681	0.234
TP (ms^2)	1930.9 ± 2251.3	3248.1 ± 4244.3	2830.9 ± 3164.2	3866 ± 3831.4	**0.02**	0.521	0.77
LF (nu)	60.8 ± 17.3	64.1 ± 18	55.6 ± 24	57 ± 22.5	0.455	0.379	0.761
HF (nu)	39.2 ± 17.3	35.9 ± 18	44.4 ± 24	43 ± 22.5	0.455	0.379	0.761
HF/HR	8.1 ± 11.9	10.7 ± 16.5	18.2 ± 27.2	19.3 ± 26.4	0.101	0.239	0.496
(LF+HF)/HR	19.5 ± 30.3	31.3 ± 47.2	32.8 ± 44.9	37 ± 40.3	**0.027**	0.523	0.523
Poincare plot, SD1 (ms)	20.8 ± 14.9	26.5 ± 15.4*	30.2 ± 27.8	32.2 ± 25.2	**<0.001**	0.345	**0.03**
Poincare plot, SD2 (ms)	53.1 ± 26.5	70.6 ± 34.7	64.4 ± 34.7	73 ± 34	**0.006**	0.544	0.32
Poincare plot, SD2/SD1	2.95 ± 0.95	2.92 ± 0.85	3.01 ± 1.46	2.82 ± 1.08	0.516	0.959	0.632
ApEn	1.06 ± 0.09	1.02 ± 0.09	0.99 ± 0.1	0.98 ± 0.09	0.198	0.086	0.375
SampEn	1.51 ± 0.24	1.47 ± 0.21	1.51 ± 0.36	1.53 ± 0.4	0.813	0.764	0.54
DFA, alpha 1	1.19 ± 0.24	1.23 ± 0.26	1.07 ± 0.3	1.08 ± 0.3	0.396	0.175	0.573
DFA, alpha 2	0.88 ± 0.25	0.82 ± 0.25	0.93 ± 0.2	0.86 ± 0.2	0.218	0.519	0.889
Correl dimension, D2	1.84 ± 1.51	2.4 ± 1.45	2.16 ± 1.6	2.12 ± 1.49	0.332	0.965	0.272

Data are mean ± SD.

OMSN, occipito-mastoidian suture normalization; SDNN, standard error of normal-to-normal interval; HR, heart rate; RMSSD, root mean square of successive difference; PNN50, percentage of successive R-R intervals that differ by >50 ms; VLF, very low frequencies; LF, low frequencies; HF, high frequencies; LF/HF, ratio LF in function of HF; TP, total power; nu, normalized units; ApEn, approximate entropy; SampEn, sample entropy; DFA, detrended fluctuation analysis; Corell, correlation.

*Variables statistically different with *post-hoc* analysis. Bold font indicates statistical significance.

4. Discussion

The objective of this study was to observe how HRV is modulated after a particular OMT. We showed that, after OMSN, RMSSD increased to a greater extent than a SHAM condition. HRV increased in both groups with several vagally mediated variables increasing independently from group intervention. This response was expected because constant adaptation to position occurs *via* the ANS and cardiovascular centers. Proprioceptors, chemoreceptors, and baroreceptors influence HR adjustment *via* the ANS, which is likely to decrease cardiac output (Shaffer et al., 2014). Given that manual contact happened also in SHAM, even without the intention of feeling and treating, an inherent effect on the patient's physiology may have occurred independently of a placebo effect, which itself may also have had an effect (Meissner, 2011; Benedetti, 2013; Cerritelli et al., 2016). No changes in vagally mediated HRV frequency-domain variable HF were found. The intention and application of the OMSN technique increased vagal tone (as evidenced by RMSSD increase), at least directly following a 10 min application.

OMTs allow a relaxation of myotendinous, aponeurotic, and even bony tissues for the skull according to Sutherland's clinical observations and, consequently, improved local vascular-nerve functioning (Sutherland, 2000; Sergueef, 2018). However, to date, those clinical observations remain unproven as do assumptions about cranial osteopathy. Some upper cervical OMT studies have shown influences on the PNS. In his thesis, Vaudron reported that among several cranial, facial, and osteoarticular techniques, the OMT technique applied to the occipito-mastoid suture had the greatest impact on the ANS, evaluated using a sitting HRV method (Vaudron, 2018). Furthermore, Rechberger et al., in their systematic review of 23 studies on the influence of osteopathy on the ANS, highlighted that despite a low number of participants, most selected studies showed an effect on the ANS (Rechberger et al., 2019), especially HVLAT and treatments of the suboccipital region. However, mechanisms underlying the increase in ANS activity remain unclear and are surprisingly not discussed in Rechberger's study. Importantly, they stated that no conclusion can be drawn as to whether OMT has a bigger impact on SNS or PNS activity. Our data suggest an increase in variables linked to both system activities (e.g., LF + HF and TP), with signs of an assumed parasympathetic increase, confirmed through the observed higher RMSSD following the OMSN technique. Carnevali et al. have proposed that the mechanisms of OMT influencing ANS are currently unclear (Carnevali et al., 2020), but they proposed two hypotheses: (1) musculoskeletal alterations may increase pro-inflammatory mediators, and thus sympathetic activity. Their corrections may then reduce sympathetic responses and improve HRV. Corrections around the vagus nerve may improve anti-inflammatory responses. However, in our study, it would seem difficult to imagine such a process happening in the minutes after the intervention. (2) Given that increased HRV after OMTs is also described in healthy individuals, other mechanisms should be involved. For example, there is evidence that the activation of low-threshold C mechanoreceptors and their connections to the insular cortex may positively influence the ANS (Carnevali et al., 2020). This may have likely been the case in our study.

Studies investigating OMT and HRV differed in the type of OMT performed, the population studied, and the HRV method used. For example, Henley et al. performed a cervical myofascial OMT, a touch-only sham OMT, and no-touch control on 17 healthy subjects while at a 50-degree head-up tilt (Henley et al., 2008). They showed an increase in HF when OMT was performed during the tilt, attesting to an acute effect on PNS activity during treatment. However, no significant effect was reported between pre- and post-treatment comparisons. They stated that head tilting induced a greater sympathetic tone, but it has also been shown that head-down neck flexion induces a parasympathetic withdrawal (Lee et al., 2001). The authors discuss this mechanism with the role of neck afferences and influences of neck flexion activating autonomic reflexes and vascular control *via* the stimulation of otolith organs.

Several studies have shown a positive influence of OMT on HF vs. a sham technique, supporting an increase in the parasympathetic tone of such an intervention. Giles et al. showed a significant increase in HF after a 15-min OMT including soft tissue manipulation in the cervical region and suboccipital decompression (Giles et al., 2013). Using an 8-min cranial OMT (augmentation + suppression) technique, Shi et al. evidenced a decreased sympathetic and an increased parasympathetic modulation post-treatment in 21 healthy participants (Shi et al., 2011). Both studies measured HRV in the supine position. In a randomized control trial (RCT) including 66 participants, Rufini et al. showed a positive effect on HRV vagally related variables of OMT (Ruffini et al., 2015); indeed, Cerritelli et al. arrived at similar conclusions in a cohort of 37 healthy participants. Ruffini et al. presented a non-linear analysis and showed that OMT significantly decreased DFA alpha 1 compared to a control group ($p < 0.001$) and with a trend compared to sham therapy ($p = 0.09$). However, in both studies, OMT intervention was based on the patient's request even if they were included as healthy (Cerritelli et al., 2020). In comparison to the above studies, we did not show any significant differences in vagally mediated HRV variables, except for RMSSD. Standard deviations in the frequency domain showed extreme inter-individual variations which make it difficult to conclude that there was an effect on HF. In our opinion, the best way to question parasympathetic tone *via* HRV is to analyze different vagally related HRV variables in parallel. Despite finding that only one significant variable increased after OMSN, our results are in line with different studies on OMT which seem to validate parasympathetic-related HRV increased after treatment (Shi et al., 2011; Giles et al., 2013; Ruffini et al., 2015; Cerritelli et al., 2020). Several studies show that OMT has an autonomic effect measured by HRV in healthy subjects, showing mainly an increase in vagal modulation and being independent of sex.

4.1. Limitations and recommendations

During our protocol, the application of the technique lasted only 10 min, which is relatively short if we consider the handling and feeling for each jugular foramen takes at least 1 min. However, given the short protocol duration, our results are promising as there is the possibility of an even greater effect of OMSN on

ANS, in the event of a longer application of the technique. We may also question the post-treatment duration effect. Indeed, it is difficult to know if the effect observed lasts for a significant period of time for the participant, and research on chronic effects should be conducted to investigate this. Moreover, as stated by Carnevali et al., the mechanisms behind increased vagal tone after OMT need to be clarified (Carnevali et al., 2020). Indeed, despite performing a maneuver aiming directly to mobilize the bone around the jugular foramen in our study, we could not exclude influences, even minor, of OMSN on mechanical, circulatory, and neurological mechanisms from other structures around the treated area on ANS modulation. For instance, nerve activity from the carotid canal (carotid sinus nerve or Hering's nerve), which is a small branch of the cranial nerve IX (Glossopharyngeal) that innervates the carotid sinus, and carotid body, may also influence ANS activity through short-term modification of blood pressure regulation. From a sports medicine perspective, as vagal tone is reduced post-moderately to high-intensity exercise, using OMSN may for instance help to improve recovery in athletes, but this needs to be confirmed through scientific evidence. Finally, considering our results on healthy subjects, investigations on patients (e.g., dysautonomia or hypertensive patients) should be considered.

Only one investigator performed the techniques on all the participants which allowed for standardized interventions. Thus, the conclusions of this study therefore concern only one practitioner. Although the technique used is not particularly complex to perform, an inter-practitioner application (involving different operators) would increase the external validity of this study. A larger sample size would also improve the generalizability of the technique and results.

The transposition of RCT methodology to the field of osteopathy cannot be complete due to the nature of the care tested. Indeed, the implementation of a double-blind design presupposes that an osteopath can perform a manual treatment without knowing if it is a real or a fake treatment, which is impossible. In this study, the operator learns the technique (OMSN or SHAM) to be applied as late as possible once the patient is settled with eyes closed and the cessation of non-essential communication is recorded. These measures were intended to minimize the single-blind bias inherent in manual therapy studies. These methodological difficulties, and even drawbacks, weaken the internal validity of this study. Moreover, as Cerritelli et al. pointed out in a systematic review of the methodology of osteopathic RCT-type studies, there are still no "guidelines" on the procedure for setting up sham treatment or placebo groups (Cerritelli et al., 2016). The methodology upon which we relied is therefore found in the majority of manual therapy studies. However, the heterogeneity of the protocols described in the literature weakens the reproducibility of the results, which makes it difficult to triangulate the conclusions between studies.

5. Conclusion

This study aimed to measure the impact of an OMSN on the ANS through the instrumental measurement of HRV. We were able to describe evidence of increased vagal tone post-intervention versus a control group. The various methodological biases, mainly related to the sample size and the limitations of the RCTs concerning manual care, put these results into perspective. However, the observations made are consistent with other studies concerning the location of application of the technique (suboccipital region) and the desired effect (increase in vagal tone). Positively influencing vagal tone with OMT has drastic practical implications (Carnevali et al., 2020). Other conditions such as dysautonomia, hypertensive patients, or stress management may benefit from this technique. Further studies may in future confirm the validity of these results.

Data availability statement

The raw data supporting the conclusions of this article will be made available by the authors, without undue reservation.

Ethics statement

The study involving humans were approved by the Commission cantonale d'éthique de la recherche sur l'être humain (CER-VD). The study were conducted in accordance with the local legislation and institutional requirements. The participants provided their written informed consent to participate in this study.

Author contributions

CBes: Conceptualization, Formal analysis, Software, Writing—original draft, Writing—review and editing. TM: Conceptualization, Data curation, Investigation, Writing—original draft, Writing—review and editing. CBen: Methodology, Software, Writing—review and editing. LS: Formal analysis, Writing—review and editing. VG: Supervision, Writing—review and editing.

Funding

The author(s) declare that no financial support was received for the research, authorship, and/or publication of this article.

Acknowledgments

All authors are grateful for the time allowed by each participant who participated in our study. A sincere thank you to Pr Paul Stapley for his proofreading of this manuscript.

Conflict of interest

The authors declare that the research was conducted in the absence of any commercial or financial relationships that could be construed as a potential conflict of interest.

The author(s) declared that they were an editorial board member of Frontiers, at the time of submission. This had no impact on the peer review process and the final decision.

Publisher's note

References

Benedetti, F. (2013). Placebo and the new physiology of the doctor-patient relationship. *Physiol. Rev.* 93, 1207–1246. doi: 10.1152/physrev.00043.2012

Bourdillon, N., Schmitt, L., Yazdani, S., Vesin, J. M., and Millet, G. P. (2017). Minimal window duration for accurate HRV recording in athletes. *Front. Neurosci.* 11, 456. doi: 10.3389/fnins.2017.00456

Carnevali, L., Lombardi, L., Fornari, M., and Sgoifo, A. (2020). Exploring the effects of osteopathic manipulative treatment on autonomic function through the lens of heart rate variability. *Front. Neurosci.* 14, 579365. doi: 10.3389/fnins.2020.579365

Cerritelli, F., Cardone, D., Pirino, A., Merla, A., and Scoppa, F. (2020). Does osteopathic manipulative treatment induce autonomic changes in healthy participants? A thermal imaging study. *Front. Neurosci.* 14, 887. doi: 10.3389/fnins.2020.00887

Cerritelli, F., Verzella, M., Cicchitti, L., D'alessandro, G., and Vanacore, N. (2016). The paradox of sham therapy and placebo effect in osteopathy: a systematic review. *Medicine* 95, e4728–e4728. doi: 10.1097/MD.0000000000004728

Gerritsen, R. J. S., and Band, G. P. H. (2018). Breath of life: the respiratory vagal stimulation model of contemplative activity. *Front. Hum. Neurosci.* 12, 397. doi: 10.3389/fnhum.2018.00397

Giles, P. D., Hensel, K. L., Pacchia, C. F., and Smith, M. L. (2013). Suboccipital decompression enhances heart rate variability indices of cardiac control in healthy subjects. *J. Altern. Complement. Med.* 19, 92–96. doi: 10.1089/acm.2011.0031

Grossman, P., and Taylor, E. W. (2007). Toward understanding respiratory sinus arrhythmia: Relations to cardiac vagal tone, evolution and biobehavioral functions. *Biol. Psychol.* 74, 263–285. doi: 10.1016/j.biopsycho.2005.11.014

Henley, C. E., Ivins, D., Mills, M., Wen, F. K., and Benjamin, B. A. (2008). Osteopathic manipulative treatment and its relationship to autonomic nervous system activity as demonstrated by heart rate variability: a repeated measures study. *Osteopath. Med. Prim. Care* 2, 7. doi: 10.1186/1750-4732-2-7

Laborde, S., Mosley, E., and Thayer, J. F. (2017). Heart rate variability and cardiac vagal tone in psychophysiological research—recommendations for experiment planning, data analysis, and data reporting. *Front. Psychol.* 8. doi: 10.3389/fpsyg.2017.00213

Lee, C. M., Wood, R. H., and Welsch, M. A. (2001). Influence of head-down and lateral decubitus neck flexion on heart rate variability. *J Appl Physiol.* 90, 127–132. doi: 10.1152/jappl.2001.90.1.127

Malik, M. (1996). Heart rate variability. Standards of measurement, physiological interpretation, and clinical use. Task force of the european society of cardiology and the north american society of pacing and electrophysiology. *Eur. Heart J.* 17, 354–381. doi: 10.1093/oxfordjournals.eurheartj.a014868

McCorry, L. K. (2007). Physiology of the autonomic nervous system. *Am. J. Pharm. Educ.* 71, 78–78. doi: 10.5688/aj710478

Meissner, K. (2011). The placebo effect and the autonomic nervous system: evidence for an intimate relationship. *Philos. Trans. R. Soc. Lond., B, Biol. Sci.* 366, 1808–1817. doi: 10.1098/rstb.2010.0403

Porges, S. W. (2009). The polyvagal theory: new insights into adaptive reactions of the autonomic nervous system. *Cleve. Clin. J. Med.* 76, S86–S90. doi: 10.3949/ccjm.76.s2.17

Purdy, W. R., Frank, J. J., and Oliver, B. (1996). Suboccipital dermatomyotomic stimulation and digital blood flow. *J. Am. Osteopath. Assoc.* 96, 285–289. doi: 10.7556/jaoa.1996.96.5.285

Quintana, D. S., and Heathers, J. A. J. (2014). Considerations in the assessment of heart rate variability in biobehavioral research. *Front. Psychol.* 5, 805. doi: 10.3389/fpsyg.2014.00805

Rechberger, V., Biberschick, M., and Porthun, J. (2019). Effectiveness of an osteopathic treatment on the autonomic nervous system: a systematic review of the literature. *Eur. J. Med. Res.* 24, 36. doi: 10.1186/s40001-019-0394-5

Rees, C. A. (2014). Lost among the trees? The autonomic nervous system and paediatrics. *Arch. Dis. Child.* 99, 552–562. doi: 10.1136/archdischild-2012-301863

Reichgott, M. (1990). "Clinical evidence of dysautonomia," in *Clinical Methods: The History, Physical, and Laboratory Examinations,* eds. Walker, H. K., Hall, W. D., Hurst, J. W. Boston: Butterworths.

Ruffini, N., D'alessandro, G., Mariani, N., Pollastrelli, A., Cardinali, L., and Cerritelli, F. (2015). Variations of high frequency parameter of heart rate variability following osteopathic manipulative treatment in healthy subjects compared to control group and sham therapy: randomized controlled trial. *Front. Neurosci.* 9, 272. doi: 10.3389/fnins.2015.00272

Sergueef, N. (2018). *Le B.A.BA de l'ostéopathie crânienne: Principes et applications*. New York, NY: Elsevier Health Sciences.

Shaffer, F., and Ginsberg, J. P. (2017). An overview of heart rate variability metrics and norms. *Front. Public Health* 5, 258. doi: 10.3389/fpubh.2017.00258

Shaffer, F., Mccraty, R., and Zerr, C. (2014). A healthy heart is not a metronome: An integrative review of the heart's anatomy and heart rate variability. *Front. Psychol.* 5, 01040. doi: 10.3389/fpsyg.2014.01040

Shi, X., Rehrer, S., Prajapati, P., Stoll, S. T., Gamber, R. G., and Downey, H. F. (2011). Effect of cranial osteopathic manipulative medicine on cerebral tissue oxygenation. *J. Am. Osteopath. Assoc.* 111, 660–666.

Steel, A., Blaich, R., Sundberg, T., and Adams, J. (2017). The role of osteopathy in clinical care: Broadening the evidence-base. *Int. J. Osteopathic Med.* 24, 32–36. doi: 10.1016/j.ijosm.2017.02.002

Sutherland, W. G. (2000). The cranial bowl 1944. *J. Am. Osteopath. Assoc.* 100, 568–573.

Tarvainen, M. P., Niskanen, J. P., Lipponen, J. A., Ranta-Aho, P. O., and Karjalainen, P. A. (2014). Kubios HRV–heart rate variability analysis software. *Comput. Methods Programs Biomed.* 113, 210–220. doi: 10.1016/j.cmpb.2013.07.024

Thayer, J. F., and Lane, R. D. (2009). Claude Bernard and the heart-brain connection: further elaboration of a model of neurovisceral integration. *Neurosci. Biobehav. Rev.* 33, 81–88. doi: 10.1016/j.neubiorev.2008.08.004

Vaudron, A. (2018). *Influence des techniques crâniennes et fasciales sur le système nerveux autonome*. Paris: Institut Dauphiné d'Ostéopathie.

Wehrwein, E. A., Orer, H. S., and Barman, S. M. (2016). Overview of the anatomy, physiology, and pharmacology of the autonomic nervous system. *Compr. Physiol.* 6, 1239–1278. doi: 10.1002/cphy.c150037

frontiers | Frontiers in Neuroscience

TYPE Original Research
PUBLISHED 14 November 2023
DOI 10.3389/fnins.2023.1280172

OPEN ACCESS

EDITED BY
Luiz Carlos Marques Vanderlei,
São Paulo State University, Brazil

REVIEWED BY
Yantao Xing,
Southeast University, China
Cheng Wang,
Central South University, China

*CORRESPONDENCE
Ying Liao
✉ liaoyingwww@163.com
Yaqian Huang
✉ yaqianhuang@126.com

RECEIVED 19 August 2023
ACCEPTED 18 October 2023
PUBLISHED 14 November 2023

CITATION
Yuan P, Lian Z, Wang Y, Zhang C, Jin H, Du J, Huang Y and Liao Y (2023) Poincaré plot can help predict the curative effect of metoprolol for pediatric postural orthostatic tachycardia syndrome.
Front. Neurosci. 17:1280172.
doi: 10.3389/fnins.2023.1280172

Poincaré plot can help predict the curative effect of metoprolol for pediatric postural orthostatic tachycardia syndrome

Piaoliu Yuan[1,2], Zhouhui Lian[3], Yuanyuan Wang[1], Chunyu Zhang[1], Hongfang Jin[1], Junbao Du[1,4], Yaqian Huang[1]* and Ying Liao[1]*

[1]Department of Pediatrics, Peking University First Hospital, Beijing, China, [2]Department of Pediatrics, The First Affiliated Hospital of Guangxi Medical University, Nanning, Guangxi, China, [3]Wang Xuan Institute of Computer Science, Peking University, Beijing, China, [4]State Key Laboratory of Vascular Homeostasis and Remodeling, Peking University, Beijing, China

Purpose: To study whether a Poincaré plot can help predict the curative effect of metoprolol for postural orthostatic tachycardia syndrome (POTS) in children.

Methods: Pediatric patients with POTS who were administered metoprolol were retrospectively included. The collected data included general data (sex, age, height, weight, and body mass index), the manifestations and treatment (baseline orthostatic intolerance symptom score and course of metoprolol treatment), vital signs (supine heart rate [HR], supine blood pressure, and increased HR during the standing test), HR variability indexes (standard deviation of normal-to-normal intervals [SDNN]; standard deviation of the averages of normal-to-normal intervals [SDANN]; mean standard deviation of the NN intervals for each 5-min segment [SDNNI]; root mean square of the successive differences [rMSSD]; percentage of adjacent NN intervals that differ by >50 ms [pNN50]; triangular index; ultra-low [ULF], very low [VLF], low [LF], and high frequency [HF]; total power [TP]; and LF/HF ratio), and graphical parameters of the Poincaré plot (longitudinal axis [L], transverse axis [T], and L/T). Receiver operator characteristic curves were used to calculate the predictive function of the indexes with significant differences between patients who responded and those who did not. The index combination with the highest predictive value was obtained through series–parallel analysis.

Results: Overall, 40 responders and 23 non-responders were included. The L and T in the Poincaré plots and rMSSD, pNN50, HF, and TP of the HR variability data were significantly lower in participants who responded to metoprolol than in participants who did not ($p < 0.001$). The L/T of participants who responded to metoprolol was greater than that of non-responders ($p < 0.001$). Moreover, we noted a strong correlation between every two indexes among L, T, rMSSD, pNN50, HF, TP, and L/T ($p < 0.05$). T < 573.9 ms combined with L/T > 2.9 had the best performance for predicting the effectiveness of metoprolol, with a sensitivity of 85.0%, specificity of 82.6%, and accuracy of 84.1%.

Conclusion: In the Poincaré plot, a T < 573.9 ms combined with an L/T > 2.9 helps predict good outcomes of using metoprolol to treat pediatric POTS.

KEYWORDS

Poincaré plot, metoprolol, therapeutic outcome, children, postural orthostatic tachycardia syndrome

Introduction

Pediatric orthostatic intolerance (OI), a clinical condition that can be relieved by lying down, typically after standing upright, can manifest as dizziness, cephalalgia, nausea, vomiting, chest distress, cardiopalmus, blurred vision, and even syncope (Stewart, 2002). OI most commonly occurs in school-aged children and adolescents and can affect their daily activities and attendance (Boris, 2018; Wang et al., 2018). Postural orthostatic tachycardia syndrome (POTS) is the primary cause of chronic OI in children (Stewart, 2013; Lin et al., 2016; Wang et al., 2018), for which metoprolol is most commonly prescribed (Chen et al., 2020; Wang et al., 2021). Metoprolol has been used indiscriminately in children diagnosed with POTS, resulting in distinct therapeutic effects. Only 57–63.6% of patients responded to metoprolol (Lai et al., 2009; Chen et al., 2011), possibly owing to the diversity and complexity of the pathogenesis of POTS (Boris, 2018; Wells et al., 2018; Chen et al., 2020). Currently, the pathogenesis of POTS includes central hypovolemia, hyperadrenergic state, decreased blood pumping function of skeletal muscles, abnormal local vasoconstriction function, and abnormal vasoactive factor release (Boris, 2018; Wells et al., 2018; Chen et al., 2020). Metoprolol acts as a blocker by antagonizing adrenergic receptor hyperactivation and has been speculated to work mainly in children with a hyperadrenergic state. Therefore, biomarkers are needed to identify children with a high adrenergic status in clinical practice to individualize the therapeutic regimen and improve the efficacy of pediatric POTS management. Previous studies have used plasma noradrenaline (Zhang et al., 2014), plasma copeptin (Zhao et al., 2014), C-type natriuretic peptide (CNP) (Zhao et al., 2014), and indexes of heart rate (HR) variability (Wang et al., 2019) to identify children with POTS for whom metoprolol could be effective. However, the plasma level of noradrenaline is easily affected by emotional factors, such as emotional stress and agitation, as well as pathological factors, such as the presence of an adrenal adenoma and pheochromocytoma. Additionally, the laboratory test for plasma copeptin and CNP requires blood to be drawn from children, and many clinical facilities cannot perform these tests, which may lead to popularization difficulties. Moreover, the predictive efficiency of the time domain index of HR variability needs to be improved. Therefore, we urgently need to find stable, easy-to-apply, and intuitive predictors to guide metoprolol administration.

Children with POTS usually have symptoms such as chest tightness or palpitations and require Holter electrocardiogram (ECG) monitoring to rule out potential arrhythmias. Poincaré plots are graphics derived from long-term (i.e., 24-h) ECG recordings (Carrasco et al., 2001; Naranjo Orellana et al., 2015) that have been widely used to diagnose arrhythmias, including identifying premature beats and diagnosing atrial fibrillation. In addition, Poincaré plots can intuitively reflect the comprehensive characteristics of the HR variability (Copie et al., 1996; Toichi et al., 1997), their shape can reflect the activity of the sympathetic and vagus nerves, and they are noninvasive, intuitive, and stable indicators of autonomic nervous function (Copie et al., 1996; Toichi et al., 1997). Based on this, we have previously reported in pediatric population that Poincaré plots can be used to distinguish vasovagal syncope (VVS) from POTS and predict the efficacy of metoprolol in the treatment of VVS (Yuan et al., 2022a,b). The mechanism of metoprolol treatment for POTS mainly involves addressing autonomic nervous function imbalance. In addition, Poincaré plots can be automatically generated by the Holter ECG monitoring equipment, which is noninvasive and intuitive and allows convenient access. Therefore, we speculated that Poincaré plots could be used to predict the clinical efficacy of metoprolol for POTS. Thus, we aimed to develop biomarkers derived from Poincaré plots to help predict the curative effect of metoprolol in pediatric POTS.

Materials and methods

Participants

Pediatric patients aged 6–18 years who were diagnosed with POTS between January 2012 and December 2020 at the Children's Syncope Center of Peking University First Hospital and received metoprolol for more than 1 month were included in the study.

The exclusion criteria were as follows: (1) the course of OI symptoms was <3 months before hospitalization; (2) diagnosis of other diseases that could affect autonomic functions or Poincaré plots, such as arrhythmia, infection, hypertension, diabetes, anemia, and thyroid dysfunction; (3) concurrent receipt of medications other than metoprolol that could affect autonomic functions or Poincaré plots; (4) not taking metoprolol as directed or having contraindications for metoprolol (i.e., sinus bradycardia, atrial-ventricular block, asthma, and allergy to metoprolol) (Wang et al., 2018); and (5) incomplete clinical data or poor Poincaré plot quality.

We collected data from each participant by searching the Medical Record System (Kaihua Medical Recording Management Digital System). The collected data included general data (sex, age, height, weight, and body mass index), the manifestations and treatment (baseline [i.e., the time of diagnosis] OI symptom score and course of metoprolol treatment), vital signs (supine HR, supine systolic blood pressure [BP], supine diastolic BP, increased HR during standing test [the maximum difference between upright HR and recumbent HR during standing test]), HR variability indexes (standard deviation of normal-to-normal intervals [SDNN]; standard deviation of the averages of normal-to-normal intervals [SDANN]; mean standard deviation of the NN intervals for each 5-min segment [SDNNI]; root mean square of the successive differences [rMSSD]; percentage of adjacent NN intervals that differ by >50 ms [pNN50]; triangular index; ultra-low [ULF], very low [VLF], low [LF], and high frequency [HF]; total power [TP]; and LF/HF ratio), and graphical parameters of the Poincaré plot (longitudinal axis [L], transverse axis [T], and L/T ratio).

This study complied with the Declaration of Helsinki and was approved by the Ethics Committee of Peking University First Hospital (2021 [150]). Informed consent was obtained from the legal guardians of the patients.

Diagnosis of POTS

POTS was diagnosed based on the following criteria: (1) triggers such as constant standing or rapid postural changes; (2) corresponding symptoms (e.g., dizziness, cephalalgia, lassitude, blurring of vision, chest distress, cardiopalmus, hand tremors, physical decline, and syncope); (3) a positive response that indicated POTS in the standing test or the initial 10 min of the head-up tilt test (HUTT); and (4) other diseases causing similar symptoms of OI were ruled out. The positive criteria for POTS in the associated tests included the following: (1) normal HR when lying on the back; (2) within the first 10 min after standing up in standing test or

tilted in HUTT an increase in HR (≥ 40 bpm) and/or a maximum HR ≥ 130 and ≥ 125 bpm for ages 6–12 and 13–18 years, respectively; (3) with out significant orthostatic hypotension (decline of BP < 20/10 mmHg) (Medow et al., 2017; Wang et al., 2018).

OI symptom score

The severity of POTS and the curative effect of metoprolol were evaluated using the OI symptom score, which was based on the following 10 major OI symptoms: syncope, dizziness, cephalalgia, chest distress, cardiopalmus, nausea, tremor, sweating, blurred vision, and lack of concentration (Li et al., 2016; Wang et al., 2019). To obtain the OI symptom score, the scores for each of the above symptoms were summed, based on the average frequency of OI symptoms before treatment and during follow-up: 0, no such symptoms; 1 point, no more than once/month; 2 points, more than once/month but no more than once/week; 3 points, more than once/week but no more than once/day; and 4 points, more than once/day (Li et al., 2016; Wang et al., 2019).

Standing test and HUTT

Standing test

Participants were required to lay on a bed for 10–30 min and then stand upright for 10 min. An ECG monitor (Dash 2000; General Electric, New York, USA) recorded the HR, BP, and ECG without interruption (Wang et al., 2018). All children received two to three standing tests during hospitalization and the highest increase of HR were recorded.

HUTT

Although the standing test is relatively simple and should be prioritized in clinical practice, the HUTT can also be used to help diagnose of POTS. Before starting, the children were informed of the need to abstain from food and water for 4 h and not to take medications affecting the autonomic tone and cardiovascular function. To begin the HUTT, participants were required to lay quietly on the examining bed (SHUT 100A Standley and Hut 821, Beijing Juchi Medical Technology Co., Ltd., Beijing, China) for approximately 10–30 min. The examination room was kept warm, quiet, and dimly lit. We used a multi-guide ECG (Dash 2000; General Electric, New York, USA) to record the HR, BP, and ECG. After tilting the bed to 60°, the patient stood passively on the tilted bed, and the above hemodynamic parameters were continuously monitored. If the child had a positive reaction, the test was terminated, and the examination bed was quickly returned to the horizontal position. Otherwise, the test was continued for 45 min (Wang et al., 2018).

Holter ECG monitoring and Poincaré plot parameters

Twenty-four-hour Holter examination: The day before and on the day of the examination, the children were asked to avoid food or drink (e.g., coffee, tea, and alcohol) and medications that could affect sympathetic and vagal nerve activity and avoid prolonged strenuous exercise and emotional agitation. The 24-h Holter ECG data were monitored and analyzed using the H3 + ™/H12 + ™ Mortara Holter ECG and H-Scribe 7.0, respectively (Mortara Instrument, Milwaukee, Wisconsin, USA). Poincaré plots were automatically constructed.

Figure 1A illustrates the construction of Poincaré plots. A point was obtained in the coordinate system by taking the duration of one heartbeat interval (ms) as the horizontal coordinate, and the duration of the next heartbeat interval (ms) as the vertical coordinate. Therefore, a point in the Poincaré plot was obtained for every three QRS (R) waves or two RR intervals. Scatter points with the same characteristics were clustered, forming the Poincaré plot of the Holter ECG data (Keeley et al., 1997). A Poincaré plot was constructed for each 24-h Holter ECG data set. The Poincaré plot is a statistical map of cardiac cycles. L denotes the length of the graph distributed along the 45° line, and T is the vertical distance between the two lines parallel to the 45° line and tangential to the dense part of the graph boundary (Brennan et al., 2002; Ueda et al., 2002; Chaidas et al., 2014; Figure 1B). Following the generation of all Poincaré plots, we used plotting software (Adobe Photoshop 2020, SAN Jose, California, USA) to measure the graphical parameters L and T (Figure 1B). L/T was calculated from L and T values. A specially assigned person measured the graphs using a method previously shown to have good stability and repeatability (Yuan et al., 2022a,b). The method and results of the stability and repeatability tests can be found in the Supplementary material.

Analysis of HR variability

The 12-lead 24-h Holter ECG monitor (H3 + ™/H12 + ™, Mortara Instrument, Milwaukee, Wisconsin, USA) used to obtain Poincaré plots was also used to examine the HR variability parameters. The sample frequency was 10,000 Hz, and the frequency response range was 0.05–60 Hz. The HR variability was assessed using an analyzer (H-Scribe 7.0; Mortara Instruments, Milwaukee, Wisconsin, USA). The first step in HR variability analysis is to identify the R-waves on the ECG waveform and thus determine the cardiac cycles. The Holter ECG analysis system (Mortara, H-Scribe 7.0 Holter analysis system) checks the signal quality on each beat to determine the best quality channels to be used. Beat detection channels may change dynamically as the analysis progresses. Intermittent periods of lead fail or artifact will cause analysis channel switching to ensure accurate beat labeling. Signal processing is performed to remove or lessen the types of noise and artifacts that occur during ambulatory recording. The computer-analyzed recordings were reviewed by two qualified clinicians to ensure a highly accurate final report. Each RR interval was examined to exclude ectopic HRs such as ventricular or supraventricular rhythms. Therefore, only normal-to-normal RR intervals were analyzed, and cases with an inadequate Holter ECG recording time (< 20 h) were excluded. Each segment analyzed in the time domain was composed of >50% of the normal RR interval, and each segment analyzed in the frequency domain was composed of >80% of the normal RR interval. The time-domain indexes of HR variability included SDNN, SDANN, SDNNI, rMSSD, pNN50, and the triangular index, while the frequency-domain indexes included ULF, VLF, LF, HF, TP, and LF/HF (Wang et al., 2019). The frequency-domain indexes were calculated by the spectrum analysis of the Fast Fourier Transform method. Records with frequencies >60 Hz were de-trended and low-pass filtered for removal. The power of frequency bands could

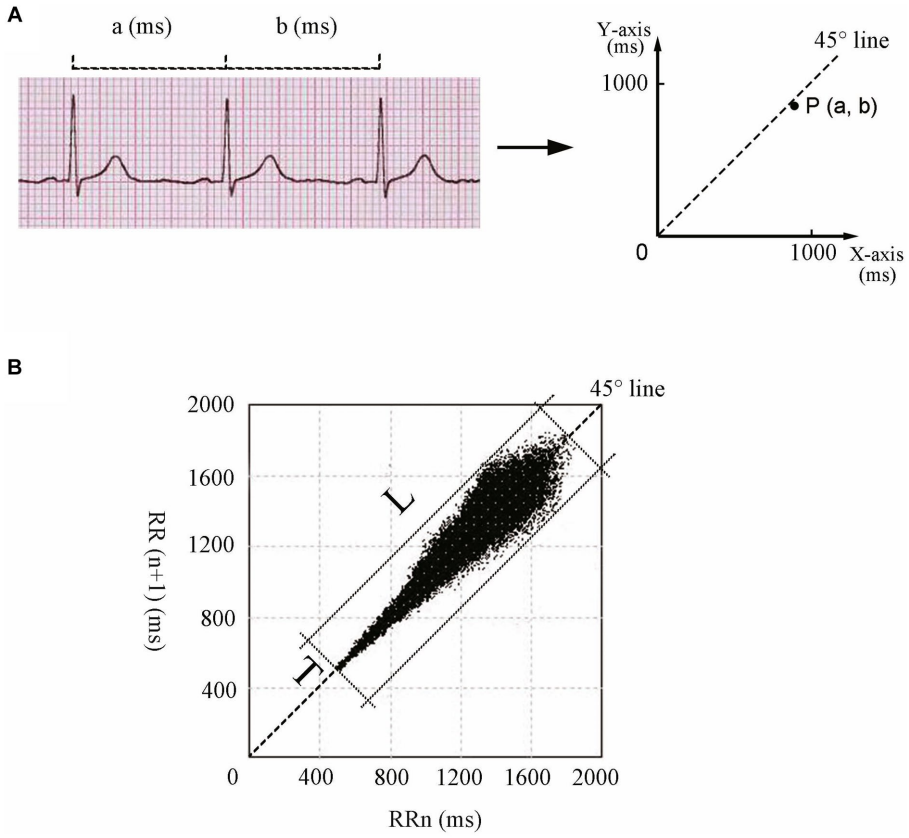

FIGURE 1
Construction and parameters of Poincaré plots. **(A)** Construction principle of Poincaré plots. Each dot in the Poincaré plot is determined by the duration of a heartbeat interval (a, ms) as the horizontal coordinate and the duration of the next heartbeat interval (b, ms) as the vertical coordinate. **(B)** L and T of the Poincaré plot for an 11-year-old girl. L of the Poincaré plot is the longest straight distance of the graph distributed along the 45° line, and T is the distance between the two straight lines parallel to the 45° line intersecting the dense part of the graph boundary. L, longitudinal axis; T, transverse axis.

be divided into four bands: ULF (0–0.003 Hz), VLF (0.003–0.04 Hz), LF (0.04–0.15 Hz), and HF (0.15–0.40 Hz). TP was the total power of NN interval change within 5 min (0–0.4 Hz), and LF/HF was the ratio of LF to HF.

Treatment with metoprolol and therapeutic effect evaluation

All enrolled participants received general treatment (i.e., health education, avoidance of triggers, increased water and salt intake, and physical compression maneuvers). The oral dose of metoprolol (AstraZeneca, London, United Kingdom) for all enrolled children with POTS was 0.5 mg/kg/day, with dosage increases as required but not exceeding 2 mg/kg (up to 50 mg) daily. Metoprolol was discontinued if the HR fell below 60 bpm at rest.

Baseline OI symptom scores were calculated before management with metoprolol, and follow-up started after the initial admission, during which POTS was first diagnosed. Participants were re-evaluated through rehospitalization, outpatient visits, or telephone interviews. Compliance with the therapy was recorded, and OI symptom scores were recalculated after 3 months of treatment with metoprolol. Participants were considered responders if the recalculated OI symptom scores decreased by at least two points compared with the baseline OI symptom scores. Otherwise, the participants were considered non-responders (Li et al., 2016; Wang et al., 2019).

Statistical analysis

SPSS 21.0 (IBM, New York, America) was used to conduct all statistical analyses. Normality was tested using the Shapiro–Wilk test. Normally distributed data are expressed as the mean ± standard deviation, and the independent sample *t* test was used to compare data between the two groups. Non-normally distributed data are expressed as the median (interquartile range [IQR], [P25, P75]), and the Mann–Whitney *U* nonparametric test was used to compare data between the two groups. Categorical data are expressed as *n* (%) and were compared between groups using the chi-square test. Spearman's linear correlation analysis was used to analyze the correlations. A receiver operating characteristic (ROC) curve was applied to evaluate whether the indexes helped predict the therapeutic outcome of metoprolol. The statistics were the area under the curve, 95% confidence interval, and *p*-value. Differences with *p*-values <0.05 were considered significant.

Results

Clinical data of responders and non-responders for metoprolol therapy

A total of 63 children with POTS (36 boys and 27 girls; median age: 12.0 years; range: 7.0–16.0 years), including 40 responders (21 boys and 19 girls; median age: 12.0 years; range: 7.0–16.0 years) and 23 non-responders (15 boys and 8 girls; median age: 13.0 years; range: 8.0–16.0 years), were analyzed. The results of the standing test performed by all 63 children were positive for POTS. Of the 51 children who underwent the HUTT, only 26 had positive POTS results. Figure 2 shows a flowchart of the selection of patients for this study. The L, T, rMSSD, pNN50, HF, and TP of the responders were significantly lower than those of the non-responders ($p < 0.05$), and the L/T and LF/HF of the responders were significantly higher than those of the non-responders ($p < 0.05$) (Table 1).

Predictive value of the Poincaré plot and HR variability in response to metoprolol

Spearman's linear correlation analysis was performed on the indexes (L, T, rMSSD, pNN50, HF, TP, L/T, and LF/HF) that were significantly different between patients who did and did not respond to metoprolol. A strong correlation was found between every two indexes, including L, T, rMSSD, pNN50, HF, TP, L/T, and LF/HF ($p < 0.05$). The ROC analysis found the above parameters of the Poincaré plot (Table 2; Figure 3) and the HR variability indexes (Table 2; Figure 4) significantly predicted the treatment outcome of using metoprolol ($p < 0.05$).

Performance of combined indexes for predicting the therapeutic outcome of metoprolol

Because of the high correlation between the above parameters, the above indexes (L, T, L/T, rMSSD, pNN50, HF, TP, and LF/HF) were analyzed in series and parallel to obtain the optimal prediction efficiency (Table 3). The results showed that a T < 573.9 ms combined with an L/T > 2.9 had the highest value in predicting the treatment outcome of using metoprolol (sensitivity: 85.0%; specificity: 82.6%; accuracy: 84.1%).

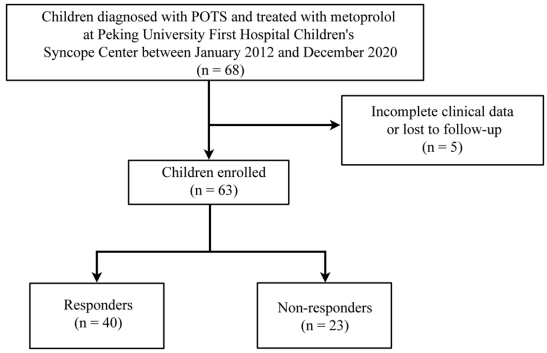

FIGURE 2
Flowchart of inclusion and exclusion of participants. POTS, postural orthostatic tachycardia syndrome.

Discussion

We innovatively proved that the L and T from the Poincaré plots, as well as rMSSD, pNN50, HF, and TP values for children who responded to metoprolol, were significantly smaller than those of children who did not respond to metoprolol for pediatric POTS. In contrast, the L/T and LF/HF of the children who responded to metoprolol were observably larger than those of children who did not. A series–parallel analysis revealed a high efficiency (sensitivity: 85.0%; specificity: 82.6%; accuracy: 84.1%), indicating a curative outcome for metoprolol treatment for pediatric POTS with a combination of T < 573.9 ms and L/T > 2.9. We demonstrated for the first time that Poincaré plots can be used as a conveniently accessed, noninvasive, and intuitive method to predict the efficacy of using metoprolol for POTS.

POTS has the highest incidence in pediatric patients with chronic OI (Spahic et al., 2019). Metoprolol, a selective β1 adrenergic receptor-blocker, has been reported to be effective in pediatric POTS (Bryarly et al., 2019). However, when β-blockers are used indiscriminately, the effectivity rate is only approximately 57–63.6% (Lai et al., 2009; Chen et al., 2011). Additionally, metoprolol has potential side effects when misused, such as hypotension, bradycardia, atrioventricular block, fatigue, and reduced exercise endurance (Zamir et al., 2022). Therefore, it is crucial to identify markers according to the pathogenesis of POTS to predict which children with POTS will respond to metoprolol and guide the application of metoprolol. The reported pathogenesis of POTS includes autonomic dysfunction (Shannon et al., 2000), abnormal blood vessel dilation (Liao et al., 2013), and hypovolemia (Zhang et al., 2012). Moreover, metoprolol is more effective in treating children with high-adrenergic status (Thieben et al., 2007). Zhang et al. (2014) found that orthostatic plasma noradrenaline could be used to predict the efficacy of using metoprolol to treat POTS. When noradrenaline levels were > 3.59 pg./mL, metoprolol was predicted to be effective, with a sensitivity of 76.9% and a specificity of 91.7% (Zhang et al., 2014). However, as previously mentioned, various physiological and pathological factors affect the plasma noradrenaline level. To identify patients suitable to receive metoprolol at the time of the initial diagnosis, Zhao et al. (2014) found that copeptin levels <10.225 pmol/L (sensitivity: 90.5%; specificity:78.6%) were useful, and Lin et al. (2015) found that CNP > 32.55 pg/mL (sensitivity: 95.8%; specificity: 70%) were applicable. However, assessing copeptin and CNP levels requires blood collection procedures. Wang et al. (2019) demonstrated that the HR variability (TR index <33.7 and SDNN index <79.0 ms) could be used as a predictor in this field, but these indexes are not intuitive. Skin sympathetic activity can be measured directly by microneurography, which can reflect the dynamic changes of sympathetic activity. However, microneurography, which records sympathetic activity by inserting thin tungsten needle electrodes into the nerve, is invasive and technically difficult; therefore, it is not the most feasible and convenient method for daily monitoring (Kusayama et al., 2020; Xing et al., 2022). A new method for real-time assessment of the autonomic nervous system, called neuECG, has recently been reported, which noninvasively records both skin

TABLE 1 Clinical data of patients who did and did not respond to metoprolol treatment for POTS.

Variables	Responders ($n = 40$)	Non-responders ($n = 23$)	t/Z/χ^2	P
Sex, male/female	21/19	15/8	0.964	0.326
Age, years	12.4 ± 2.1	12.3 ± 1.8	−0.135	0.893
Height, cm	159.7 ± 13.9	162.4 ± 8.4	0.964	0.339
Weight, kg	53.5 (39.1–60.0)	52.5 (42.8–60.5)	−0.029	0.977
BMI, kg/m^2	18.9 (17.1–23.1)	19.5 (18.2–22.8)	−0.671	0.502
Baseline OI symptom score, points	6.0 (4.0–8.8)	8.0 (5.0–12.0)	−1.559	0.119
Metoprolol treatment, months	2.0 (1.0–3.0)	2.0 (1.0–3.0)	−0.300	0.764
HR, bpm	75.5 (70.5–84.5)	45.0 (43.0–50.0)	0.215	0.830
Systolic pressure, mmHg	109.0 (102.0–119.8)	113.0 (110.0–117.0)	−1.307	0.191
Diastolic pressure, mmHg	60.5 (55.3–68.8)	66.0 (59.0–70.0)	−1.708	0.088
Maximum heart rate during standing test, bpm	124.0 (118.0–133.0)	123.0 (117.0–133.0)	−0.222	0.825
Increased heart rate during standing test[a], bpm	45.5 (42.0–52.0)	76.0 (69.0–83.0)	−0.215	0.830
SDNN, ms	136.5 ± 34.8	153.6 ± 34.9	1.872	0.066
Triangular index	28.0 (23.3–32.5)	34.0 (27.0–38.0)	−1.873	0.061
SDNNI	69.1 ± 25.0	77.8 ± 20.5	1.424	0.160
rMSSD, ms	44.3 ± 14.9	59.8 ± 24.1	2.793	0.009
pNN50, %	18.2 ± 10.0	25.1 ± 12.7	2.383	0.020
SDANN, ms	123.5 (100.3–154.5)	143.0 (111.0–152.0)	−1.506	0.132
ULF, ms^2	11,449.5 (8,767.9–18,367.3)	17,943.5 (9,622.5–22,780.7)	−1.613	0.107
VLF, ms^2	2,142.1 (1,677.6–3,016.3)	2,955.5 (1,922.3–4,296.0)	−1.799	0.072
LF, ms^2	881.4 (622.9–1,205.4)	1,139.3 (790.7–1,846.8)	−1.942	0.052
HF, ms^2	577.5 (382.7–937.0)	1,239.4 (289.0–1,864.3)	−2.470	0.014
TP, ms^2	3,017.6 (1,880.2–3,510.2)	4,410.0 (2,238.5–5,910.5)	−2.313	0.021
LF/HF	1.4 (1.2–1.8)	1.2 (0.8–1.7)	−2.063	0.039
L, ms	1,502.6 ± 225.2	1,733.7 ± 231.9	3.880	< 0.001
T, ms	432.7 ± 122.3	705.3 ± 201.2	5.901	< 0.001
L/T	3.6 (3.1–4.1)	2.4 (2.2–3.0)	−4.683	< 0.001

$p < 0.05$, statistically significant. POTS, postural orthostatic tachycardia syndrome; OI, orthostatic intolerance; HR, heart rate; bpm, beat per minute; SDNN, standard deviation of normal-to-normal intervals; SDNNI, standard deviation of the averages of NN intervals; rMSSD, root mean square of the successive differences; pNN50, percentage of adjacent NN intervals that differed by > 50 ms; SDANN, standard deviation of the averages of normal-to-normal intervals in all 5-min segments of the entire recording; ULF, ultralow frequency; VLF, very low frequency; LF, low frequency; HF, high frequency; TP, total power; L, longitudinal axis; T, transverse axis. [a]The maximum difference between upright and recumbent heart rates during the standing test.

sympathetic activity and ECG. neuECG has the advantages of being non-invasive, convenient, and accurate and having good signal recording performance. However, the electrical activity measured by neuECG on the skin surface comes from the heart, muscle, or nerve structure, and there is a lot of interference. In addition, neuECG is mainly used in healthy people and patients without cardiovascular disease, and its requirements for equipment are relatively high, which is not conducive to clinical application (Kusayama et al., 2020; Xing et al., 2022). Therefore, when managing children with POTS, it is essential to further explore stable, comfortable, and convenient predictors of the metoprolol treatment outcomes.

Poincaré plots are usually used in Holter ECG analysis, as they can display all the RR intervals of the 24-h Holter ECG data in one scatterplot and intuitively reflect autonomic activity using graphical characteristics. The T of the graph indicates the instant change in the cardiac cycle and is positively correlated with vagal nerve tension (Chaidas et al., 2014). Although the clinical value of L is not fully understood, some scholars consider it to indicate the sympathetic tone (Naranjo Orellana et al., 2015). The L/T reflects the interaction between sympathetic and vagal activities (Naranjo Orellana et al., 2015). Studies have shown that, with the augmentation of sympathetic function, the shape of the Poincaré plot becomes almost baseball bat-like, with the increase in L/T ratio (Toichi et al., 1997). Together, these factors form the theoretical basis for using a Poincaré plot to help predict the treatment outcomes of metoprolol.

In this study, we explored the application of Poincaré plots to identify children with POTS for whom metoprolol treatment is suitable. The results revealed that the L and T of pediatric patients who responded to metoprolol were visibly smaller than those who did not, and the L/T of children who responded was visibly greater than those who did not. The results indicated that the sympathetic activity of responders to metoprolol before treatment was greater than that of non-responders, suggesting that metoprolol may inhibit excessive sympathetic excitation by antagonizing β1-receptors thus improving the patients' symptoms. Moreover, the results showed that a T < 573.9 ms combined with an L/T > 2.9 had high sensitivity,

TABLE 2 Predictive value of the parameters on the efficacy of metoprolol treatment.

Variables	AUC	*P*	95% CI	Cut-off value	Sensitivity (%)	Specificity (%)
L	0.761	0.001	0.630–0.893	1,680.7 ms	77.5	73.9
T	0.866	< 0.001	0.764–0.969	573.9 ms	87.5	78.3
L/T	0.857	< 0.001	0.757–0.956	2.9	85.0	73.9
rMSSD	0.690	0.013	0.544–0.835	59.5 ms	85.0	52.2
pNN50	0.668	0.027	0.523–0.814	27.5 ms	85.0	47.8
HF	0.688	0.014	0.532–0.844	1,144.0 ms^2	90.0	56.5
TP	0.676	0.021	0.520–0.832	4,740.7 ms^2	95.0	47.8
LF/HF	0.657	0.039	0.509–0.806	1.1	92.5	43.5

$p < 0.05$, statistically significant. AUC, area under the curve; CI, confidence interval; L, longitudinal axis; T, transverse axis; rMSSD, root mean square of successive differences; pNN50, percentage of adjacent NN intervals that differed by > 50 ms; HF, high frequency; TP, total power; LF, low frequency.

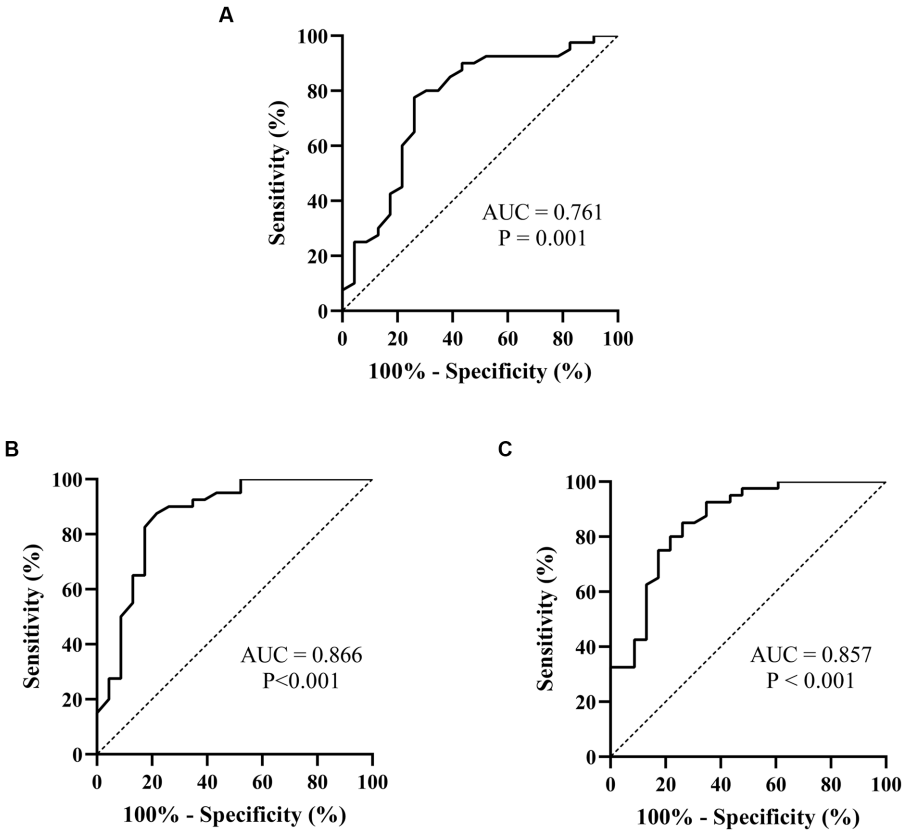

FIGURE 3
ROC curves of the Poincaré plot indexes for prejudging the outcome of metoprolol in treating pediatric POTS. **(A)** L; **(B)** T; **(C)** L/T. The ordinate represents the sensitivity to prejudge the treatment outcome of metoprolol, and the abscissa shows the false-positive rate (i.e., 100% – specificity). The sensitivity of the 45° line in the figure is equal to the false-positive rate, meaning no effect for prejudging. AUC, area under the curve; ROC, receiver operating characteristic; POTS, postural orthostatic tachycardia syndrome; L, longitudinal axis; T, transverse axis.

specificity, and accuracy in prejudging the treatment outcome of metoprolol for pediatric patients with POTS, reaching 85.0, 82.6, and 84.1%, respectively.

Wang et al. (2019) have shown that when the triangular index and SDNNI were ≤ 33.7 ms and ≤ 79.0 ms, respectively, a good outcome of metoprolol treatment for pediatric POTS can be prejudged (sensitivity: 85.3%; specificity: 81.8%; accuracy: 84.4%). HR variability indexes and Poincaré plots are tools for assessing autonomic function. We combined HR variability indexes and Poincaré plot indexes for prediction to further enhance efficiency. The results showed that the parameters from the Poincaré plot were better than the HR variability indexes, according to the series–parallel analysis in our study. We found that the HR variability indexes rMSSD, pNN50, HF, and TP of children who responded were distinctly lower than those who did not respond, similar to a previous finding (Wang et al., 2019). Time-domain indexes of HR variability (e.g., rMSSD and pNN50) can reflect changes in vagal tone, which is believed to be the result of vagal excitation (Wang et al., 2019). In our study, ROC analysis indicated

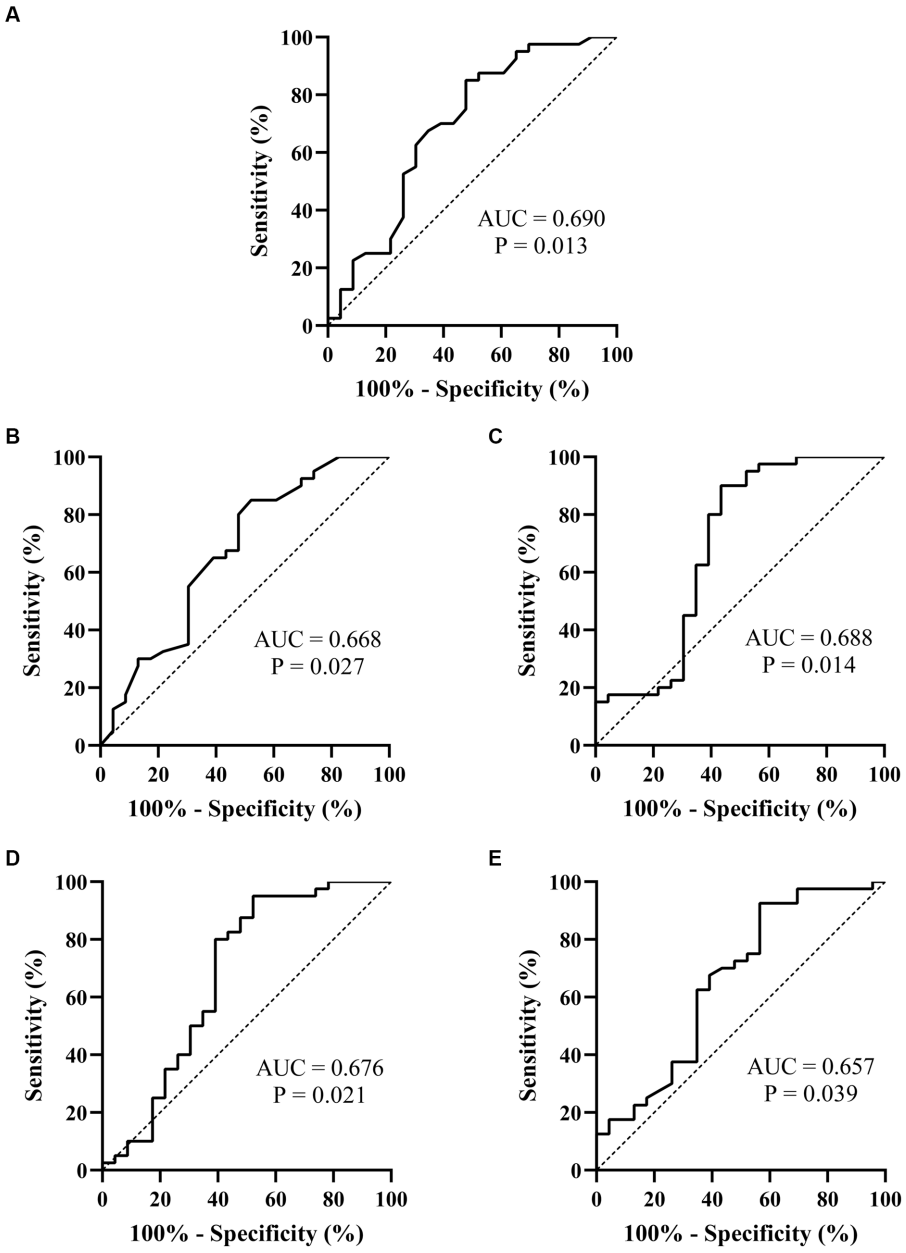

FIGURE 4
ROC curves of the heart rate variability indexes for prejudging the treatment outcome of metoprolol for pediatric POTS. **(A)** rMSSD; **(B)** pNN50; **(C)** HF; **(D)** TP; **(E)** LF/HF. The ordinate represents the sensitivity to prejudge the treatment outcome of metoprolol, and the abscissa shows the false positive rate (i.e., 100% – specificity). The sensitivity of the 45° line in the figure is equal to the false positive rate, meaning no effect for prejudging. POTS, postural orthostatic tachycardia syndrome; AUC, area under the curve; ROC, receiver operating characteristic; rMSSD, root mean square of the successive difference; pNN50, percentage of adjacent NN intervals that differ by >50 ms; HF, high frequency; TP, total power; LF, low frequency.

that the area under the curve of the parameters from the Poincaré plot was greater than the HR variability indexes when these parameters were measured in the same population. This indicates that the parameters of the Poincaré plot were better predictors than the HR variability indexes in predicting the treatment outcome of metoprolol. Finally, the Poincaré plot has the advantage of visualization, which is more intuitive than previous predictors. Graphically, the Poincaré plot of a "baseball bat shape" ($T < 573.9$ ms combined with $L/T > 2.9$) is more likely to indicate that the patient will respond well to the metoprolol treatment, while the Poincaré plot of a "tennis racket shape" ($T \geq 573.9$ ms and $L/T \leq 2.9$) is more likely to indicate a poor response. Therefore, our results showed that the Poincaré plot of children with POTS before treatment can be used as a noninvasive, stable, efficient, and intuitive indicator of the efficacy of metoprolol in children with POTS.

Our study had some limitations, including the single-center retrospective design, small number of samples, relatively basic graphic measurement methods, and lack of validation studies to verify the predictive efficiency of the indicators. In addition, some other methods can calculate HR variability, such as some nonlinear dynamic

10.3389/fnins.2023.1280172

TABLE 3 Series–parallel analysis to prejudge the outcome of metoprolol treatment for pediatric POTS.

Indexes of series–parallel analysis	Sensitivity (%)	Specificity (%)	Accuracy (%)
T < 573.9 ms combined with L/T > 2.9	85.0	82.6	84.1
T < 573.9 ms or L/T > 2.9	87.5	69.6	81.0
T < 573.9 ms combined with L < 1,680.7 ms	77.5	73.9	76.2
T < 573.9 ms or L < 1,680.7 ms	92.5	69.6	84.1
T < 573.9 ms combined with rMSSD <59.5 ms	80.0	78.3	79.4
T < 573.9 ms or rMSSD <59.5 ms	95.0	52.2	79.4
T < 573.9 ms combined with pNN50 < 27.5 ms	75.0	78.3	76.2
T < 573.9 ms or pNN50 < 27.5 ms	97.5	47.8	79.4
T < 573.9 ms combined with HF < 1,144.0 ms^2	87.5	78.3	84.1
T < 573.9 ms or HF < 1,144.0 ms^2	95.0	56.5	81.0
T < 573.9 ms combined with TP < 4,740.7 ms^2	82.5	78.3	81.0
T < 573.9 ms or TP < 4,740.7 ms^2	100	47.8	81.0
T < 573.9 ms combined with LF/HF > 1.1	80.0	78.3	79.4
T < 573.9 ms or LF/HF > 1.1	97.5	43.5	77.8
L < 1,680.7 ms combined with L/T > 2.9	70.0	87.0	76.2
L < 1,680.7 ms or L/T > 2.9	100.0	60.9	85.7
L < 1,680.7 ms combined with rMSSD <59.5 ms	72.5	69.6	71.4
L < 1,680.7 ms or rMSSD <59.5 ms	72.5	52.2	65.1
L < 1,680.7 ms combined with pNN50 < 27.5 ms	72.5	69.6	71.4
L < 1,680.7 ms or pNN50 < 27.5 ms	92.5	47.9	76.2
L < 1,680.7 ms combined with HF < 1,144.0 ms^2	82.5	73.9	79.4
L < 1,680.7 ms or HF < 1,144.0 ms^2	90.0	56.5	77.8
L < 1,680.7 ms combined with TP < 4,740.7 ms^2	77.5	73.9	76.2
L < 1,680.7 ms or TP < 4,740.7 ms^2	95.0	47.8	77.8
L < 1,680.7 ms combined with LF/HF > 1.1	75.0	73.9	74.6
L < 1,680.7 ms or LF/HF > 1.1	95.0	43.5	76.2
L/T > 2.9 combined with rMSSD <59.5 ms	75.0	73.9	74.6
L/T > 2.9 or rMSSD <59.5 ms	95.0	52.2	79.4
L/T > 2.9 combined with pNN50 < 27.5 ms	72.5	73.9	73.0
L/T > 2.9 or pNN50 < 27.5 ms	97.5	47.8	79.4
L/T > 2.9 combined with HF < 1,144.0 ms^2	82.5	73.9	79.4
L/T > 2.9 or HF < 1,144.0 ms^2	95.0	56.5	81.0
L/T > 2.9 combined with TP < 4,740.7 ms^2	80.0	78.3	79.4
L/T > 2.9 or TP < 4,740.7 ms^2	100.0	43.5	79.4
rMSSD <59.5 ms combined with pNN50 < 27.5 ms	82.5	52.2	71.4
rMSSD <59.5 ms or pNN50 < 27.5 ms	87.5	47.8	73.0
rMSSD <59.5 ms combined with HF < 1,144.0 ms^2	85.0	60.9	76.2
rMSSD <59.5 ms or HF < 1,144.0 ms^2	90.0	47.8	74.6
rMSSD <59.5 ms combined with TP < 4,740.7 ms^2	85.0	56.5	74.6
rMSSD <59.5 ms or TP < 4,740.7 ms^2	95.0	43.5	76.2
rMSSD <59.5 ms combined with LF/HF > 1.1	77.5	60.9	71.4
rMSSD <59.5 ms or LF/HF > 1.1	97.5	34.8	74.6
pNN50 < 27.5 ms combined with HF < 1,144.0 ms^2	77.5	65.2	73.0
pNN50 < 27.5 ms or HF < 1,144.0 ms^2	92.5	43.5	74.6

(Continued)

TABLE 3 (Continued)

Indexes of series–parallel analysis	Sensitivity (%)	Specificity (%)	Accuracy (%)
pNN50 < 27.5 ms combined with TP < 4,740.7 ms^2	85.0	56.5	74.6
pNN50 < 27.5 ms or TP < 4,740.7 ms^2	95.0	39.1	74.6
pNN50 < 27.5 ms combined with LF/HF > 1.1	77.5	60.9	71.4
pNN50 < 27.5 ms or LF/HF > 1.1	97.5	30.4	73.0
HF < 1,144.0 ms^2 combined with TP < 4,740.7 ms^2	90.0	60.9	79.4
HF < 1,144.0 ms^2 or TP < 4,740.7 ms^2	95.0	43.5	76.2
HF < 1,144.0 ms^2 combined with LF/HF > 1.1	82.5	56.5	73.0
HF < 1,144.0 ms^2 combined with TP < 4,740.7 ms^2	90.0	60.9	79.4
HF < 1,144.0 ms^2 or LF/HF > 1.1	97.5	43.5	77.8
TP < 4,740.7 ms^2 combined with LF/HF > 1.1	85.0	60.9	76.2
TP < 4,740.7 ms^2 or LF/HF > 1.1	100.0	30.4	74.6

L, longitudinal axis; T, transverse axis; rMSSD, root mean square of successive differences; pNN50, percentage of adjacent NN intervals that differed by > 50 ms; HF, high frequency; TP, total power; LF, low frequency.

indicators analyzed by entropy measures (Castiglioni et al., 2023). The role of other indicators for HR variability in predicting the efficacy of metoprolol should be discussed in the future. However, this study innovatively demonstrates that the noninvasive, stable, efficient, and intuitive parameters of the Poincaré plot can be used for children with POTS who may be suitable to undergo metoprolol treatment, which facilitates the individualized treatment of children with POTS. Further multicenter, prospective, large-sample, and external validation studies should be conducted to validate our results through more accurate graphic analysis techniques to promote better individualized treatments for children with POTS.

In conclusion, this study innovatively confirmed the predictive value of the Poincaré plot for treatment outcomes of using metoprolol for pediatric POTS. A T < 573.9 ms combined with an L/T > 2.9 (baseball bat shape) can help predict good outcomes for metoprolol treatment of pediatric POTS.

Data availability statement

The original contributions presented in the study are included in the article/Supplementary material, further inquiries can be directed to the corresponding authors.

Ethics statement

The studies involving humans were approved by Ethics Committee of Peking University First Hospital (2021 [150]). The studies were conducted in accordance with the local legislation and institutional requirements. Informed consent for participation in this study was provided by the participants' legal guardians/next of kin.

Author contributions

PY: Data curation, Investigation, Methodology, Software, Writing – original draft, Writing – review & editing. ZL: Data curation, Formal analysis, Investigation, Software, Writing – review & editing. YW: Data curation, Formal analysis, Investigation, Software, Writing – review & editing. CZ: Data curation, Formal analysis, Investigation, Software, Writing – review & editing. HJ: Funding acquisition, Project administration, Resources, Supervision, Writing – review & editing. JD: Funding acquisition, Project administration, Resources, Supervision, Writing – review & editing. YH: Conceptualization, Funding acquisition, Methodology, Project administration, Resources, Supervision, Writing – review & editing. YL: Conceptualization, Funding acquisition, Methodology, Project administration, Resources, Supervision, Writing – review & editing.

Funding

The author(s) declare financial support was received for the research, authorship, and/or publication of this article. This work was supported by the Fundamental Research Funds for the Central Universities, China. Clinical Medicine Plus X – Young Scholars Project (PKU2022LCXQ028), the Fundamental Research Funds for the Central Universities, China; and the National High-Level Hospital Clinical Research Funding (Multi-center Clinical Research Project of Peking University First Hospital) (2022CR59).

Acknowledgments

The authors would like to thank the enrolled patients and their guardians.

Conflict of interest

The authors declare that the research was conducted in the absence of any commercial or financial relationships that could be construed as a potential conflict of interest.

The author(s) declared that they were an editorial board member of Frontiers, at the time of submission. This had no impact on the peer review process and the final decision.

Publisher's note

All claims expressed in this article are solely those of the authors and do not necessarily represent those of their affiliated organizations, or those of the publisher, the editors and the reviewers. Any product that may be evaluated in this article, or claim that may be made by its manufacturer, is not guaranteed or endorsed by the publisher.

Supplementary material

The Supplementary material for this article can be found online at: https://www.frontiersin.org/articles/10.3389/fnins.2023.1280172/full#supplementary-material

References

Boris, J. R. (2018). Postural orthostatic tachycardia syndrome in children and adolescents. *Auton. Neurosci.* 215, 97–101. doi: 10.1016/j.autneu.2018.05.004

Brennan, M., Palaniswami, M., and Kamen, P. (2002). Poincaré plot interpretation using a physiological model of HRV based on a network of oscillators. *Am. J. Physiol. Heart Circ. Physiol.* 283, H1873–H1886. doi: 10.1152/ajpheart.00405.2000

Bryarly, M., Phillips, L. T., Fu, Q., Vernino, S., and Levine, B. D. (2019). Postural orthostatic tachycardia syndrome: JACC focus seminar. *J. Am. Coll. Cardiol.* 73, 1207–1228. doi: 10.1016/j.jacc.2018.11.059

Carrasco, S., Gaitán, M. J., González, R., and Yánez, O. (2001). Correlation among Poincaré plot indexes and time and frequency domain measures of heart rate variability. *J. Med. Eng. Technol.* 25, 240–248. doi: 10.1080/03091900110086651

Castiglioni, P., Merati, G., Parati, G., and Faini, A. (2023). Sample, fuzzy and distribution entropies of heart rate variability: what do they tell us on cardiovascular complexity? *Entropy (Basel, Switzerland)* 25:281. doi: 10.3390/e25020281

Chaidas, K., Tsaoussoglou, M., Theodorou, E., Lianou, L., Chrousos, G., and Kaditis, A. G. (2014). Poincaré plot width, morning urine norepinephrine levels, and autonomic imbalance in children with obstructive sleep apnea. *Pediatr. Neurol.* 51, 246–251. doi: 10.1016/j.pediatrneurol.2014.05.003

Chen, G., Du, J., Jin, H., and Huang, Y. (2020). Postural tachycardia syndrome in children and adolescents: pathophysiology and clinical management. *Front. Pediatr.* 8:474. doi: 10.3389/fped.2020.00474

Chen, L., Wang, L., Sun, J., Qin, J., Tang, C., Jin, H., et al. (2011). Midodrine hydrochloride is effective in the treatment of children with postural orthostatic tachycardia syndrome. *Circ. J.* 75, 927–931. doi: 10.1253/circj.CJ-10-0514

Copie, X., Pousset, F., Lechat, P., Jaillon, P., Guize, L., and Le Heuzey, J. Y. (1996). Effects of beta-blockade with bisoprolol on heart rate variability in advanced heart failure: analysis of scatterplots of R-R intervals at selected heart rates. *Am. Heart J.* 132, 369–375. doi: 10.1016/S0002-8703(96)90435-4

Keeley, E. C., Lange, R. A., Hillis, L. D., Joglar, J. A., and Page, R. L. (1997). Correlation between time-domain measures of heart rate variability and scatterplots in patients with healed myocardial infarcts and the influence of metoprolol. *Am. J. Cardiol.* 79, 412–414. doi: 10.1016/S0002-9149(96)00777-1

Kusayama, T., Wong, J., Liu, X., He, W., Doytchinova, A., Robinson, E. A., et al. (2020). Simultaneous noninvasive recording of electrocardiogram and skin sympathetic nerve activity (neuECG). *Nat. Protoc.* 15, 1853–1877. doi: 10.1038/s41596-020-0316-6

Lai, C. C., Fischer, P. R., Brands, C. K., Fisher, J. L., Porter, C. B., Driscoll, S. W., et al. (2009). Outcomes in adolescents with postural orthostatic tachycardia syndrome treated with midodrine and beta-blockers. *Pacing Clin. Electrophysiol.* 32, 234–238. doi: 10.1111/j.1540-8159.2008.02207.x

Li, H., Wang, Y., Liu, P., Chen, Y., Feng, X., Tang, C., et al. (2016). Body mass index (BMI) is associated with the therapeutic response to oral rehydration solution in children with postural tachycardia syndrome. *Pediatr. Cardiol.* 37, 1313–1318. doi: 10.1007/s00246-016-1436-1

Liao, Y., Yang, J., Zhang, F., Chen, S., Liu, X., Zhang, Q., et al. (2013). Flow-mediated vasodilation as a predictor of therapeutic response to midodrine hydrochloride in children with postural orthostatic tachycardia syndrome. *Am. J. Cardiol.* 112, 816–820. doi: 10.1016/j.amjcard.2013.05.008

Lin, J., Han, Z., Li, H., Chen, S. Y., Li, X., Liu, P., et al. (2015). Plasma C-type natriuretic peptide as a predictor for therapeutic response to metoprolol in children with postural tachycardia syndrome. *PLoS One* 10:e0121913. doi: 10.1371/journal.pone.0121913

Lin, J., Wang, Y., Zhang, Q., Liao, Y., Qi, J., Liu, P., et al. (2016). Underlying disease spectrum of syncope in children and adolescents in the past 30 years and health economic analysis: a single center report. *Chin. J. Prac. Pediatr.* 31, 350–355. doi: 10.7504/ek2016050609

Medow, M. S., Kothari, M. L., Goetz, A. M., O'Donnell-Smith, M. B., Terilli, C., and Stewart, J. M. (2017). Decreasing cerebral oxygen consumption during upright tilt in vasovagal syncope. *Physiol. Rep.* 5:13286. doi: 10.14814/phy2.13286

Naranjo Orellana, J., de la Cruz Torres, B., Sarabia Cachadiña, E., de Hoyo, M., and Domínguez Cobo, S. (2015). Two new indexes for the assessment of autonomic balance in elite soccer players. *Int. J. Sports Physiol. Perform.* 10, 452–457. doi: 10.1123/ijspp.2014-0235

Shannon, J. R., Flattem, N. L., Jordan, J., Jacob, G., Black, B. K., Biaggioni, I., et al. (2000). Orthostatic intolerance and tachycardia associated with norepinephrine-transporter deficiency. *N. Engl. J. Med.* 342, 541–549. doi: 10.1056/NEJM200002243420803

Spahic, J. M., Ricci, F., Aung, N., Axelsson, J., Melander, O., Sutton, R., et al. (2019). Proconvertase Furin is downregulated in postural orthostatic tachycardia syndrome. *Front. Neurosci.* 13:301. doi: 10.3389/fnins.2019.00301

Stewart, J. M. (2002). Orthostatic intolerance in pediatrics. *J. Pediatr.* 140, 404–411. doi: 10.1067/mpd.2002.122727

Stewart, J. M. (2013). Common syndromes of orthostatic intolerance. *Pediatrics* 131, 968–980. doi: 10.1542/peds.2012-2610

Thieben, M. J., Sandroni, P., Sletten, D. M., Benrud-Larson, L. M., Fealey, R. D., Vernino, S., et al. (2007). Postural orthostatic tachycardia syndrome: the mayo clinic experience. *Mayo Clin. Proc.* 82, 308–313. doi: 10.4065/82.3.308

Toichi, M., Sugiura, T., Murai, T., and Sengoku, A. (1997). A new method of assessing cardiac autonomic function and its comparison with spectral analysis and coefficient of variation of R-R interval. *J. Auton. Nerv. Syst.* 62, 79–84. doi: 10.1016/s0165-1838(96)00112-9

Ueda, T., Nakatsu, T., Yamane, S., Kurazono, S., Murakami, T., Mashima, K., et al. (2002). Correlation of Lorenz scatterplots with frequency domain heart rate variability. *Clin. Exp. Hypertens.* 24, 11–21. doi: 10.1081/CEH-100108711

Wang, C., Li, Y., Liao, Y., Tian, H., Huang, M., Dong, X., et al. (2018). 2018 Chinese pediatric cardiology society (CPCS) guideline for diagnosis and treatment of syncope in children and adolescents. *Sci. Bull.* 63, 1558–1564. doi: 10.1016/j.scib.2018.09.019

Wang, Y., Sun, Y., Zhang, Q., Zhang, C., Liu, P., Wang, Y., et al. (2021). Baseline corrected QT interval dispersion is useful to predict effectiveness of metoprolol on pediatric postural tachycardia syndrome. *Front. Cardiovasc. Med.* 8:808512. doi: 10.3389/fcvm.2021.808512

Wang, Y., Zhang, C., Chen, S., Liu, P., Wang, Y., Tang, C., et al. (2019). Heart rate variability predicts therapeutic response to metoprolol in children with postural tachycardia syndrome. *Front. Neurosci.* 13:1214. doi: 10.3389/fnins.2019.01214

Wells, R., Spurrier, A. J., Linz, D., Gallagher, C., Mahajan, R., Sanders, P., et al. (2018). Postural tachycardia syndrome: current perspectives. *Vasc. Health Risk Manag.* 14, 1–11. doi: 10.2147/VHRM.S127393

Xing, Y. T., Zhang, Y. K., Yang, C. X., Li, J. Q., Li, Y. W., Cui, C., et al. (2022). Design and evaluation of an autonomic nerve monitoring system based on skin sympathetic nerve activity. *Biomed. Signal Proc. Control* 76:103681. doi: 10.1016/j.bspc.2022.103681

Yuan, P., Li, X., Tao, C., Du, X., Zhang, C., Du, J., et al. (2022a). Poincaré plot can be a useful tool to select potential responders to metoprolol therapy in children with vasovagal syncope. *Int. J. Gen. Med.* 15, 2681–2693. doi: 10.2147/ijgm.s352928

Yuan, P., Lian, Z., Wang, Y., Wang, Y., Zhang, C., Du, J., et al. (2022b). Poincaré plot is useful for distinguishing vasovagal syncope from postural tachycardia syndrome in children. *Front. Pediatr.* 10:758100. doi: 10.3389/fped.2022.758100

Zamir, A., Hussain, I., Ur Rehman, A., Ashraf, W., Imran, I., Saeed, H., et al. (2022). Clinical pharmacokinetics of metoprolol: a systematic review. *Clin. Pharmacokinet.* 61, 1095–1114. doi: 10.1007/s40262-022-01145-y

Zhang, Q., Chen, X., Li, J., and Du, J. (2014). Orthostatic plasma norepinephrine level as a predictor for therapeutic response to metoprolol in children with postural tachycardia syndrome. *J. Transl. Med.* 12:249. doi: 10.1186/s12967-014-0249-3

Zhang, Q., Liao, Y., Tang, C., Du, J., and Jin, H. (2012). Twenty-four-hour urinary sodium excretion and postural orthostatic tachycardia syndrome. *J. Pediatr.* 161, 281–284. doi: 10.1016/j.jpeds.2012.01.054

Zhao, J., Du, S., Yang, J., Lin, J., Tang, C., Du, J., et al. (2014). Usefulness of plasma copeptin as a biomarker to predict the therapeutic effectiveness of metoprolol for postural tachycardia syndrome in children. *Am. J. Cardiol.* 114, 601–605. doi: 10.1016/j.amjcard.2014.05.039

frontiers | Frontiers in Physiology

TYPE Original Research
PUBLISHED 21 November 2023
DOI 10.3389/fphys.2023.1293946

OPEN ACCESS

EDITED BY
Vitor Engracia Valenti,
São Paulo State University, Brazil

REVIEWED BY
Övünç Polat,
Akdeniz University, Türkiye
José Javier Reyes-Lagos,
Universidad Autónoma del Estado de México, Mexico

*CORRESPONDENCE
Zahra Sharifi-Heris,
zahrasharifimdu@gmail.com

RECEIVED 13 September 2023
ACCEPTED 23 October 2023
PUBLISHED 21 November 2023

CITATION
Sharifi-Heris Z, Yang Z, Rahmani AM, Fortier MA, Sharifiheris H and Bender M (2023), Phenotyping the autonomic nervous system in pregnancy using remote sensors: potential for complication prediction.
Front. Physiol. 14:1293946.
doi: 10.3389/fphys.2023.1293946

Phenotyping the autonomic nervous system in pregnancy using remote sensors: potential for complication prediction

Zahra Sharifi-Heris[1]*, Zhongqi Yang[2], Amir M. Rahmani[1,2], Michelle A. Fortier[1,3], Hamid Sharifiheris[4] and Miriam Bender[1]

[1]Sue and Bill Gross School of Nursing, University of California, Irvine, Irvine, CA, United States, [2]Department of Computer Science, University of California, Irvine, Irvine, CA, United States, [3]Center on Stress and Health, University of California, Irvine, Irvine, CA, United States, [4]Department of Computer Science, Azad University of Ahar, Ahar, Iran

Objectives: The autonomic nervous system (ANS) plays a central role in dynamic adaptation during pregnancy in accordance with the pregnancy demands which otherwise can lead to various pregnancy complications. Despite the importance of understanding the ANS function during pregnancy, the literature lacks sufficiency in the ANS assessment. In this study, we aimed to identify the heart rate variability (HRV) function during the second and third trimesters of pregnancy and 1 week after childbirth and its relevant predictors in healthy pregnant Latina individuals in Orange County, CA.

Materials and methods: N = 16 participants were enrolled into the study from which N = 14 (N = 13 healthy and n = 1 complicated) participants proceeded to the analysis phase. For the analysis, we conducted supervised machine learning modeling including the hierarchical linear model to understand the association between time and HRV and random forest regression to investigate the factors that may affect HRV during pregnancy. A t-test was used for exploratory analysis to compare the complicated case with healthy pregnancies.

Results: The results of hierarchical linear model analysis showed a significant positive relationship between time (day) and average HRV (estimated effect = 0.06; $p < 0.0001$), regardless of being healthy or complicated, indicating that HRV increases during pregnancy significantly. Random forest regression results identified some lifestyle and sociodemographic factors such as activity, sleep, diet, and mental stress as important predictors for HRV changes in addition to time. The findings of the t-test indicated that the average weekly HRV of healthy and non-healthy subjects differed significantly ($p < 0.05$) during the 17 weeks of the study.

Conclusion: It is imperative to focus our attention on potential autonomic changes, particularly the possibility of increased parasympathetic activity as pregnancy advances. This observation may challenge the existing literature that often suggests a decline in parasympathetic activity toward the end of pregnancy. Moreover, our findings indicated the complexity of HRV prediction, involving various factors beyond the mere passage of time. To gain a more comprehensive

understanding of this dynamic state, future investigations should delve into the intricate relationship between autonomic activity, considering diverse parasympathetic and sympathetic metrics, and the progression of pregnancy.

KEYWORDS

autonomic nervous system, healthy pregnancy, pregnancy complications, smart wearable technology, physiology

Introduction

Various physiological changes occur during pregnancy contributing to the optimal growth and development of the fetus and help protect the mother from the pregnancy and delivery complications (Soma-Pillay et al., 2016). These changes are regulated through a non-linear complex relationship between various vital systems in the body and, to a great extent, by the autonomic nervous systems (ANS). The ANS role can be mainly explained by the adaptation of sympathetic (SNS) and parasympathetic (PNS) components and their responses to the pregnancy demands as stimuli (Waxenbaum, et al., 2019). SNS directs the body's rapid involuntary response to various demanding situations in or outside of the body (Bruno et al., 2012) and mediates the vigilance, arousal, and activation of the bodily responses to adapt to increased metabolic needs in response to internal and external stimuli including pregnancy (Braeken., 2014). PNS, on the other hand, is responsible for the stimulation of "rest-and-digest" or "feed-and-breed" activities that occur when the body is at rest (Johnson, 2019). Sympathetic and parasympathetic systems function as complementary components to maintain the hemostasis and hemodynamic adaptation in the body.

A failure in the ANS including SNS and PNS function has been described in various diseases, both those that directly afflict the nervous system and those afflicting other organs, where they indirectly trigger or enhance pathological symptoms in the body (Zygmunt and Stanczyk, 2010). Broadly speaking, every disorder or ailment is inherently linked to disturbances or dysfunctions in autonomic regulation or innervation (Ziemssen and Siepmann, 2019). Likewise, in pregnant individuals, ANS dysfunction has been considered to be one of the main contributors to the development of some maternal and/or neonatal disorders such as hypertensive disorders and preeclampsia (Yousif et al., 2019), gestational diabetes mellitus, and unexplained recurrent pregnancy loss (Kataoka et al., 2015). This may explain the ANS role in physiological regulation helping the individuals' body adjust to the pregnancy-related demands in order to prevent these disorders. On the other hand, for the aforementioned adverse pregnancy outcomes, evidence has identified several sociodemographic and medical history factors as potential risk factors, which are also associated with ANS dysfunction. These include age (Jandackova et al., 2016; Geovanini et al., 2020), prenatal alcohol consumption (Karpyak et al., 2014; Jurczyk et al., 2019), smoking (Harte et al., 2013; Bodin et al., 2017; Murgia et al., 2019), drug use (Nayak et al., 2020; Lu et al., 2022; Qiu et al., 2023), and body mass index (BMI) (Rodrigues and Quarto, 2018; Triggiani et al., 2019). Due to the associations between the aforementioned risk factors and pregnancy complications and ANS dysfunction, it seems that the ANS may explain the pathway between the risk factors and the pregnancy outcomes, which already indicated in ANS dysfunction (or maybe correctional but not optimal adaptation) in response to the risk factors resulting in pregnancy complications. However, the reliability of these results is questionable due to serious methodological limitations in the assessment of the ANS. Many studies have relied on short-duration (5–10 min) and non-continuous assessments (Sharifiheris et al., 2022), which is problematic considering that pregnancy is a dynamic and ever-changing condition that cannot be adequately captured through brief and episodic measurements. In order to comprehensively understand pathological and abnormal changes, it is essential to first establish a baseline of normal ANS function in healthy pregnancies. To initiate this inquiry, it is crucial to initially investigate whether a consistent pattern is present among individuals experiencing healthy pregnancies. This preliminary yet vital step will help us ascertain the feasibility of conducting a trial that compares healthy and unhealthy pregnancies, providing an opportunity to identify potential differences.

The most common tests for ANS assessment are those that evaluate the cardiovascular reflexes in response to provocative maneuvers. These tests include the orthostatic stress test, cold pressor test, deep breathing test, Valsalva maneuver, isometric hand grip test, head-up tilt test, and mental stress test (Zygmunt and Stanczyk, 2010; Ziemssen and Siepmann, 2019). Although the aforementioned ANS assessment maneuvers are widely applied in clinical settings for diagnostic purposes, the ability of these maneuvers to reflect ANS function in real life is questionable. This is due to the fact that the tests are often performed in a controlled situation in which individuals have to follow specific considerations in order to standardize the test situation for all people. For example, several hours before a test, caffeine, nicotine, alcohol, and certain medications are needed to be withheld. Additionally, tests are required to be performed in a specific environmental situation (e.g., temperature and humidity), and right before and during the test, people have to practice specific positions (standing up and lying down). These framed rules before and during the test and artificial setting for the test procedure cannot reflect one's ANS activity in the everyday life. Specifically, since the ANS follows a 24-h cycle of circadian rhythm, it cannot be represented in any duration less than 24 h. In addition, as discussed earlier, pregnancy is an ever-changing situation that episodic assessments are unable to reflect this dynamic situation. Thus, relying on the test results seems to be tricky to make a right decision regarding the ANS function.

In the current study, heart rate variability (HRV) has been applied to assess the ANS function. HRV is one of the well-known, non-invasive ANS biomarkers that is commonly applied in the recent literature to detect various physical and psychological

disorders resulted from ANS dysfunction (Duong et al., 2020). Variability of the heart rate indicates the flexibility to cope with the uncertain and changing environment through the cardiovascular system. HRV is a surrogate parameter of the ANS reflecting the complex interaction between organ systems and, specifically, the brain and the cardiovascular system to maintain hemostasis (Ernst, 2017). HRV applies the photoplethysmogram (PPG) technique and is equipped with a light source (red and infrared light-emitting diodes) and a detector to function. HRV can cover the existing literature gaps in ANS assessment. This is because PPG is embeddable in smart devices enabling continuous and long-term ANS assessment (Peng et al., 2015).

The overall purpose of this study is to determine the ANS function during normal (low risk) pregnancy across healthy pregnant populations when assessed by HRV using a tech-based wearable smart device. This investigation serves as a foundational step toward creating a screening tool that has potential to identify any abnormalities in the normal ANS patterns during pregnancy, enabling timely decision making. In this study, we will focus on the Latina population who are at more risk of developing pregnancy complications (Howell et al., 2017; Petersen et al., 2019).

Materials and methods

Study design

A prospective longitudinal observational study design was utilized in the current study. The study started at 22–24 gestational age (GA) and continued until 1 week after childbirth (16–19 weeks). A prospective study that is supposed to be carried out from the present time into the future is appropriate for this study because 1) our target population is required to meet specific criteria to be eligible for recruitment, 2) the dependent variable should be assessed in a specific time frame and consistently to be able to assess its pattern of changes and relationship with the independent variable, and 3) there is no existing data source that matches with the aim and requirements of the current study to carry out it in a retrospective design.

Sample and setting

Our target population comprises pregnant individuals who currently live in southern California. Following IRB approval, we recruited the study subjects from the Manchester Clinic using purposeful sampling. Specified criteria were considered to address the research questions of the study. The inclusion criteria were as follows: 1) identified healthy according to the American College of Obstetricians and Gynecologists (ACOG) (Appendix A), 2) GA between 20–24 weeks, 3) Latina, 4) proficient in English, and 5) have access to the internet and smart phone.

Sample size

This is a pilot study where there is no prior information to base the sample size on. In this situation, the recommendation from the literature suggests a sample size of 12 as being appropriate for the purposes of preliminary data collection and analysis (Julious, 2005). According to recent statistics, approximately 10% of the low-risk pregnancies still have a chance of progressing to complications (Rajbanshi et al., 2020). Considering additional 15% as the possible attrition rate, the final sample size was considered to be $n = 16$.

Measures

HRV

The Oura Ring was used to continuously capture HRV data in participants during the study. The Oura Ring is a water-proof smart ring made of highly scratch-resistant materials, including zirconia (Zr02), with a medical-grade, nickel-free, 100% non-allergenic, non-metallic inner molding. It is wireless (Bluetooth) and weighs approximately 3–4 g, depending on the size of the ring. A full battery charge would be enough to capture signals for 5–7 consecutive days (Kinnunen et al., 2020). The sensors embedded in the inner layer of the ring include a PPG, 3D accelerometer, gyroscope, and negative thermal coefficient (NTC) body temperature sensor. The ring has been used before in human subjects (de Zambotti et al., 2019; Maijala et al., 2019; Altini and Kinnunen, 2021). The Oura Ring also comes in different sizes, which can be selected based on personal comfort. See "data procedure section" for more details. The HRV metrics such as NN interval, RMSSD, SDANN, SDNN, pNN50, LF, HF, and LF/HF were supposed to be extracted from the interbeat interval (IBI) captured by sensors. The relevant machine learning coding was supposed to be applied in order to obtain the HRV metrics from IBI data.

Healthiness criteria assessment

To assure the healthy status of the subjects based on ACOG criteria, EPIC and REDCap were applied to constantly monitor for possible risk factors and confounding factors that have the potential to threaten the healthy situation of the participants.

EPIC is a platform that is considered to be the information backbone for a majority of the largest integrated health systems in the world. EPIC provided information regarding the obstetric, medical, and sociodemographic details of the participants that were required for eligibility assessment as well as weekly monitoring for the possible complications. Given that prenatal care visits become more frequent, with weekly visits toward the end of pregnancy, it indeed aligns perfectly with our choice of weekly monitoring for identifying potential complications updated in the EPIC system. This frequency ensures that we are in sync with the evolving needs of the participants and the timing of their prenatal care, making it a practical and well-aligned approach.

We also used REDCap to subjectively assess 1) the potential mental-related risk factors, identified by the ACOG, such as mental distress (stress, anxiety, and depression), and 2) lifestyle-related factors (activity, acute stress, sleep, and diet) as possible predictive factors for HRV.

For mental distress, we used the Patient Health Questionnaire-2 (PHQ-2), Perceived Stress Scale 4 (PSS-4), and Generalized Anxiety Disorder 2 (GAD-2) to assess depression, stress, and anxiety,

10.3389/fphys.2023.1293946

TABLE 1 Measurement frequency for the measures.

Assessment tool		Pregnancy (week)																		Postartum (week)	
		22–24	25	26	27	28	29	30	31	32	33	34	35	36	37	38	39	40	1
ANS (HRV) assessment	HRV	Continuous measurement via Oura/weekly capturing assessment																	
ACOG-identified risk factors	PSS-4	-+	--	--	--	-+	--	--	--	-+	--	--	--	-+	--	-+	--	-+	= +
	GAD-2	-+	--	-+	--	-+	--	+	--	-+	--	-+	--	-+	--	-+	--	-+	= +
	PHQ-2	-+	--	-+	--	-+	--	+	--	-+	--	-+	--	-+	--	-+	--	-+	= +
	EPIC-reported risk factors	-+	+	-+	+	+	+	+	+	-+	+	-+	+	-+	+	+	+	‡	= +
Descriptive characteristics	Sociodemographic characteristics	++	--	--	--	--	--	--	--	--	--	--	--	--	--	--	--	--	--
Potential predictors	Lifestyle-related factors in Oura	Continuous measurement via Oura/weekly capturing assessment																	
Potential predictors	Lifestyle-related factor assessment using daily surveys	Daily assessment																	

respectively. These measures for stress, anxiety, and depression have all been validated on pregnant individuals with an education level of at least junior high school in urban and rural settings (Essiben et al., 2018; Thomas et al., 2019; Whittle et al., 2019).

The short version of the Personal Health Questionnaire depression scale (PHQ-2) is a 4-point scale and includes two items to measure the "frequency of depressed mood" over the last 2 weeks. This scale includes four points ranging from 0 (not at all) to 3 (nearly every day). The possible highest and lowest total scores are 0 and 6, respectively. The cutoff point of the PHQ-2 is 3, and a score greater than 3 is considered to be major depression. The PHQ-2 has a good reliability (alpha Cronbach of 0.92), sensitivity (74%), and specificity (60%) in the United States (Gelaye et al., 2016) and was used for the US pregnant population (Bennett et al., 2008; Slavin et al., 2020).

The GAD-2 is a 4-point scale containing two items to assess "anxiety" and "worry" over the last 2 weeks. The possible responses vary ranging from 0 (not at all) to 3 (nearly every day). The total score ranges from 0 to 6; the higher the score, the severe the anxiety. The cutoff point of the GAD-2 is 3, and a score equal to and greater than 3 is considered to be major anxiety. The GAD-2 has 86% sensitivity and 83% specificity for the diagnosis of generalized anxiety disorder applying in the US population (Kroenke et al., 2007).

The PSS-4 is a 5-point scale and includes four items of "control," "confidence," "satisfaction," and "overcoming the difficulties" in the last month. The possible responses varied ranging from 0 (almost never) to 4 (very often). The possible highest and lowest total scores are 0 and 20, respectively, with the higher score showing higher stress. The cutoff point of the PSS-4 is 6, and a score equal to and greater than 6 is considered to be major stress. This 4-item scale has internal reliability with an alpha Cronbach of 0.69 among the US population (Warttig et al., 2013).

The frequency of mental distress assessment depends on the ability of the determined measurement scale to capture the potential mental distress. For example, the PSS-4 has been designed to assess stress over the last month; thus, monthly assessment is considered for stress assessment. For the PHQ-2 and GAD-2, biweekly assessment was considered. The measurement frequency is specified in Table 1.

For lifestyle-related elements, we applied a daily survey questionnaire to assess factors such as activity, sleep, stress, and diet reported by participants. The questions were distributed at the end of the day before they go to bed. The daily assessments offered several advantages. It allowed us to capture participants' perceptions of their lifestyle on a daily basis when the information was still fresh in their memory. This approach minimized the risk of forgetting details due to extended time intervals between assessments, which can often lead to less-accurate responses.

The lifestyle-related factors were also assessed objectively using the Oura Ring. These data included sleep metrics (e.g., total sleep time, sleep efficiency, time spent in different sleep stages (light, deep, and REM), sleep latency (time taken to fall asleep and the number of awakenings during the night), activity metrics (e.g., steps taken, active calories burned, and total active time), body temperature, heart rate (e.g., resting heart rate, average heart rate, and heart rate variability [HRV]), respiratory rate, O2 saturation, and readiness and recovery scores. The Oura-derived objective data were

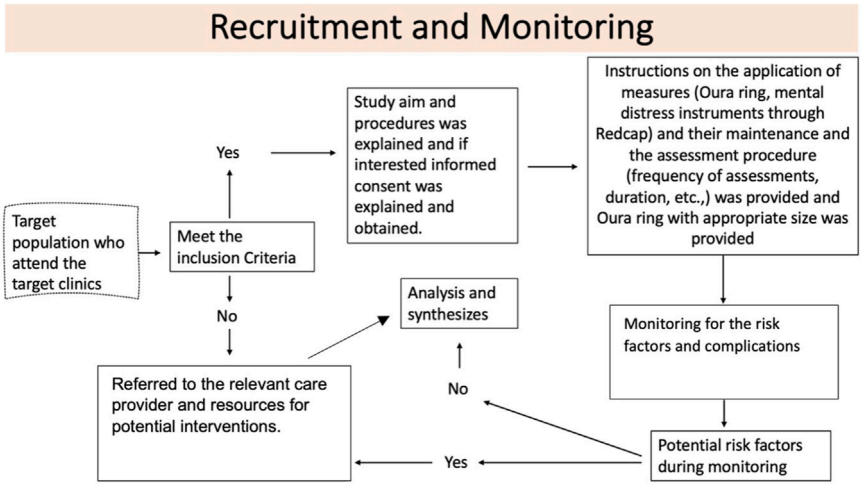

FIGURE 1
Recruitment procedure.

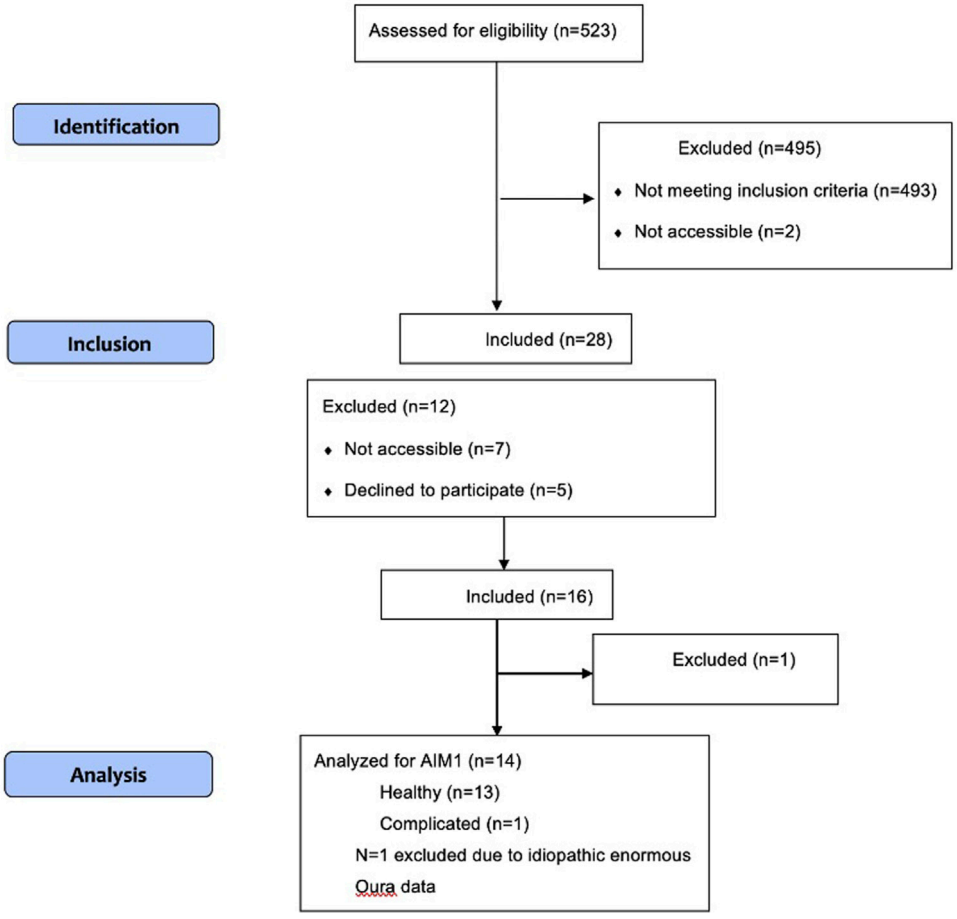

FIGURE 2
STROBE chart.

TABLE 2 Sociodemographic distribution.

Variable		Finding
Age (years) (mean [SD])		31.4 [3.85]
Height (cm) (mean [SD])		167 [6.53]
Weight (kg) (mean [SD])		68 [6.83]
BMI (mean [SD])		24.22 [2.06]
Education (years) (mean [SD])		17.73 [5.39]
Income level (number [%])	$18 - 34.999K	7 [50%]
	$35 – 99.999 K	5 [36%]
	$100 – 199.999 K	2 [14%]
Gravidity (number [%])	2	9 [64%]
	3	2 [14%]
	4	3 [22%]
Parity (number [%])	1	9 [64%]
	2	2 [14%]
	3	3 [22%]

monitored weekly to identify and address the possible technical issues in capturing data. If abnormal data (meaningless pattern) or shortage of data recorded (less than 30%) is observed, we contacted the participants for the possible technical issues or barriers that might be the potential reasons. The decision to adopt a weekly monitoring schedule was intentional for two primary reasons. First and foremost, it corresponds with the maximum syncing time interval recommended by Oura to maintain data within the app, ensuring that un-synced data are not treated as missing data. Second, the choice of a weekly assessment frequency strikes a balance, allowing for timely monitoring without imposing substantial burdens on both researchers and participants.

Descriptive information performed once at the beginning of the study to describe the population.

Study procedure

Following the IRB approval, a purposive sampling was conducted to screen the potential candidates in the selected clinic. The eligibility criteria were checked through the EPIC system. After establishing the eligibility criteria, prospective participants were identified and subsequently contacted in the clinic to confirm their eligibility and assess their interest in the study participation. If they met the inclusion criteria and consented to participate, they proceeded to the monitoring phase of the study. If no complications or risk factors were reported during monitoring, the participants were deemed healthy and proceeded to the analysis phase (Figure 1). However, if complications occurred, the participants were referred to the appropriate healthcare provider for potential interventions and still considered for comparison analysis as the exploratory aim.

Data cleaning

The data cleaning process involves three steps. First, data screening is performed to identify four types of abnormalities: missing data, inconsistencies and outliers, unusual patterns of distributions, and unexpected analysis results. The second step is the diagnostic phase, where each abnormal value is investigated to determine if it is erroneous, a true extreme, or has an unknown cause. For example, unrealistic age and BMI values were checked in the EPIC system to obtain the correct values. Additionally, extreme values for education were found to be due to participants having multiple degrees. Last, the treatment phase involves resolving the identified abnormal data by correcting, deleting, or leaving them unchanged. In this study, impossible values were replaced with the true values obtained from documents, and missing data were imputed using prediction techniques. However, for participant #13, who had unexplainable negative and out-of-range sleep and HRV data, the enormous values could not be treated, leading to their exclusion from the analysis.

Data analysis

We applied supervised techniques (e.g., the hierarchical linear regression/mixed effect model (HLM) and random forest regression (RFR)) to address the study aim in R and Python software. The HLM enabled us to understand the association between HRV and time across the participants. Even though it is not generalizable and statistically reliable due to lower sample size, we also came up with the exploratory result comparing a complicated case and healthy participants in a weekly basis using the *t*-test. Using other supervised techniques such as RFR, we tried to understand the potential predictors and predicting features' importance for HRV magnitude during pregnancy.

Results

Sampling

The recruitment started on August 21st and continued until November 16th in the Manchester Clinic affiliated to the UCI to enroll all required 16 participants into the study based on the inclusion criteria. We assessed 523 individuals for potential eligibility in the EPIC system. $N = 493$ did not meet the inclusion criteria, and $N = 2$ individuals were receiving prenatal service outside the facility where the study recruitment was taking place, thus excluded. $N = 28$ individuals were identified as eligible for the study. Out of this, $N = 7$ participants did not make their prenatal care appointment as they were scheduled. $N = 5$ declined to participate in the study ($n = 3$ needed their husband's permission; $n = 2$ brought no reason). Finally, $n = 16$ participants enrolled into the study (please see Figure 2 for the STROBE chart). One of the participants declined to continue in the middle of the study since she had broken her hand and was prohibited to wear any jewelry per her care provider's prescription. In addition, $N = 1$ participant experienced a complicated pregnancy (placental abruption) at 34 weeks. As a result, $N = 14$ healthy participants completed the study. However, instead of completely excluding the complicated pregnancy case, we included it in the analysis for

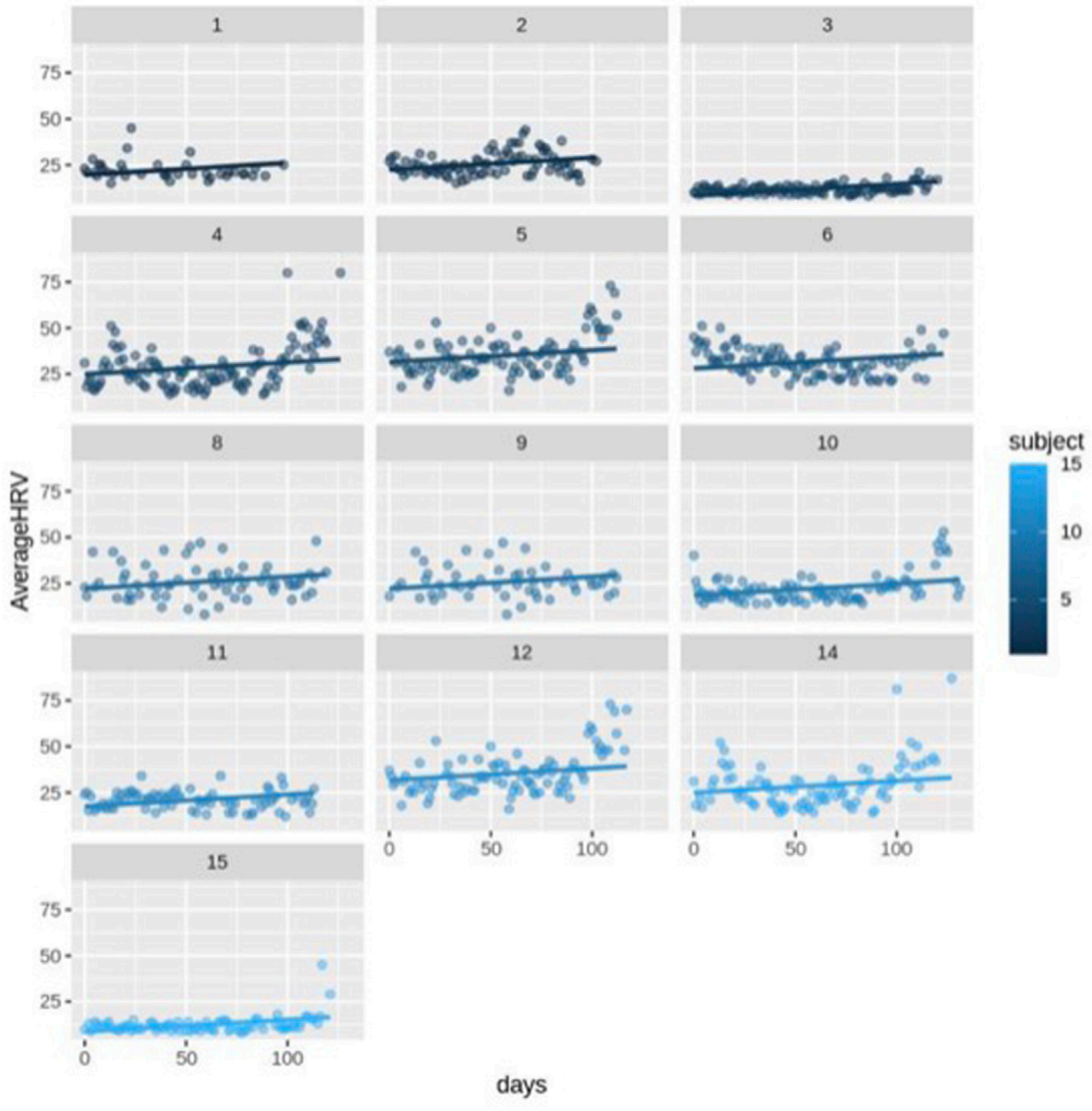

FIGURE 3
Scatter plot for HRV changes with different intercepts and the same slope over time (day) for healthy subjects (n = 13).

exploratory purposes. This allowed us to compare and gain insights into how it differed from the healthy participants in terms of HRV magnitude. In the data cleaning phase, N = 1 participant was excluded due to the idiopathic enormous Oura data. Thus, N = 13 accounting for healthy participants and N = 1 accounting for a complicated participant were considered for the final analysis.

Descriptive information

Sociodemographic characteristics of the study population (n = 14), upon enrollment, were assessed using a demographic questionnaire. As represented in Table 2, age, height, weight, and BMI are in the healthy category based on the ACOG criteria for healthy pregnancy. All the participants completed at least junior high school in terms of education. Approximately 50% of the participants (7/14) had income under $35 k, 64% (9/14) were in their second pregnancy, and all had given birth at least once before.

HRV analysis

Unfortunately, we were not able to obtain IBI data due to the policy change of the Oura company in providing such data. Several efforts were made to request for reconsideration, but no improvement was achieved. Thus, we used RMSSD, the existing HRV metric provided by the Oura company.

Hierarchical linear regression/mixed-effects model

We used the HLM to examine the relationship between time as the independent variable and RMSSD as the dependent variable to determine whether the time could impact and predict HRV magnitude.

First, we ran the model for all the participants (N = 14) including healthy (N = 13) and complicated cases (N = 1). The fixed-effects

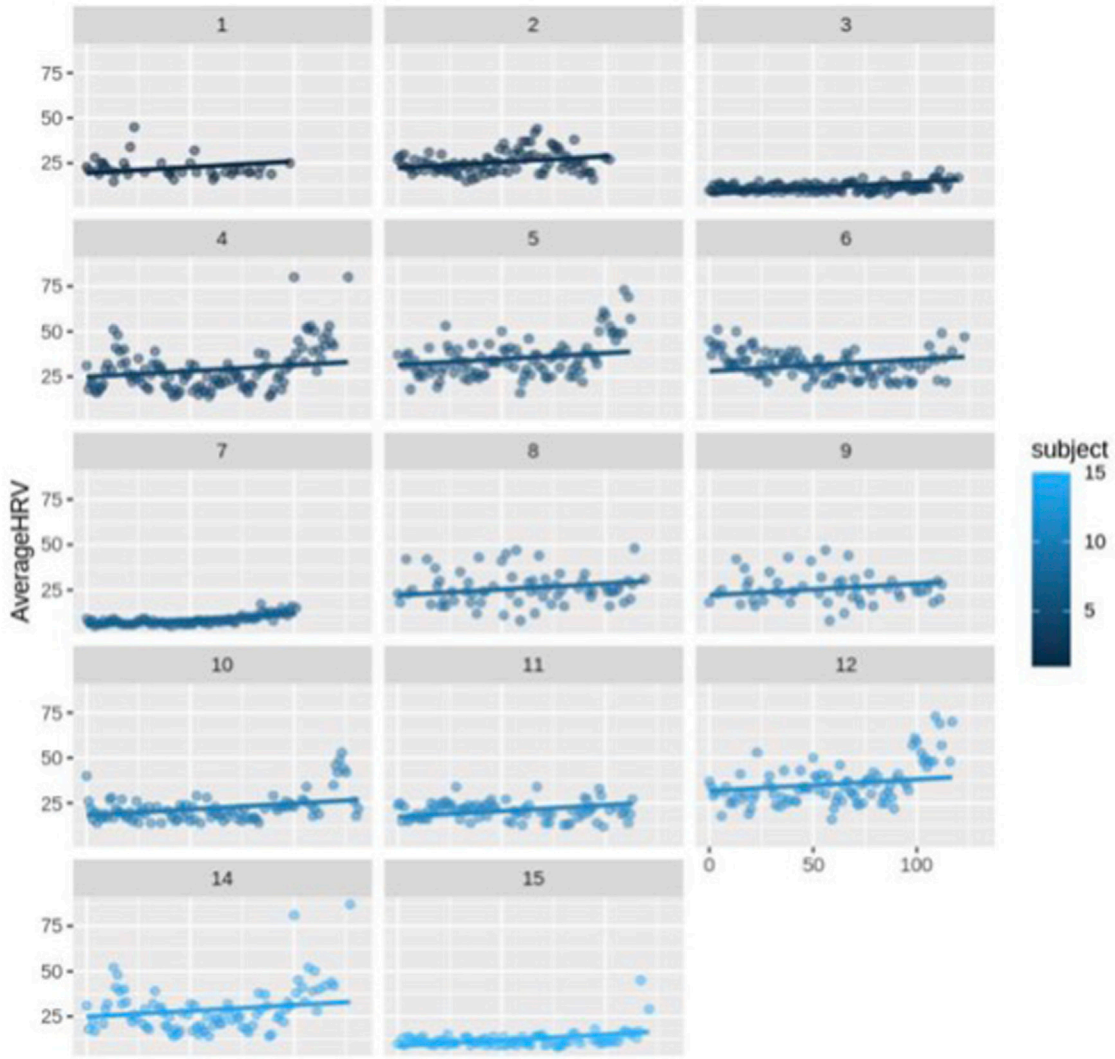

FIGURE 4
Scatter plot for HRV changes with different intercepts and the same slope over time (day) for each subject (n = 14).

estimates indicated that the intercept (average HRV) at day 0 is 2.037e-01 (20.37) and the slope (change in average HRV per day) is 0.06427, and both estimates are statistically significant ($p < 0.0001$). It means for each increase in day, HRV increases by 0.06427 across the participants (Figure 3; Figure 4).

The random error estimate indicated that there is a substantial variation in the intercepts across subjects with the standard deviation of 8.315. The residual standard deviation was 7.976. The correlation of fixed effects showed that there is a negative correlation between the intercept and the slope, which means that subjects with higher intercepts tend to have smaller slopes. Overall, this model suggested that there is a significant positive relationship between days and average HRV, and that there is substantial variation in average intercepts across all subjects.

Then, we excluded the $N = 1$ complicated case and ran the model for only healthy subjects. This model still indicated a significant positive connection between days and average HRV, as well as notable variability in average intercepts among the healthy subjects. The fixed-effects estimates indicated that the intercept at day 0 is 21.54 and the slope is 0.06442, and both estimates are statistically significant, p-value = 1.28e-07 and p-value < 2e-16, respectively ($p < 0.0001$). As it can be seen, excluding the complicated subject did not affect the significance of the HRV changes over time. It means for each increase in day, HRV still increases by approximately 0.06 in the healthy participants. The estimation of the random error reveals considerable variability in the intercepts among subjects, with a standard deviation of 7.35. The residual standard deviation is 8.28. The correlation of fixed effects demonstrates a negative association between the intercept and the slope, indicating that subjects with higher intercepts tend to have smaller slopes.

Random forest regression

In this study, we also used RFR to build regression models to predict HRV using multi-channel time series data. RFR is a type of ensemble learning method that combines multiple decision trees to make predictors. RFR works by randomly selecting subsets of the features and building decision trees on each subset and then

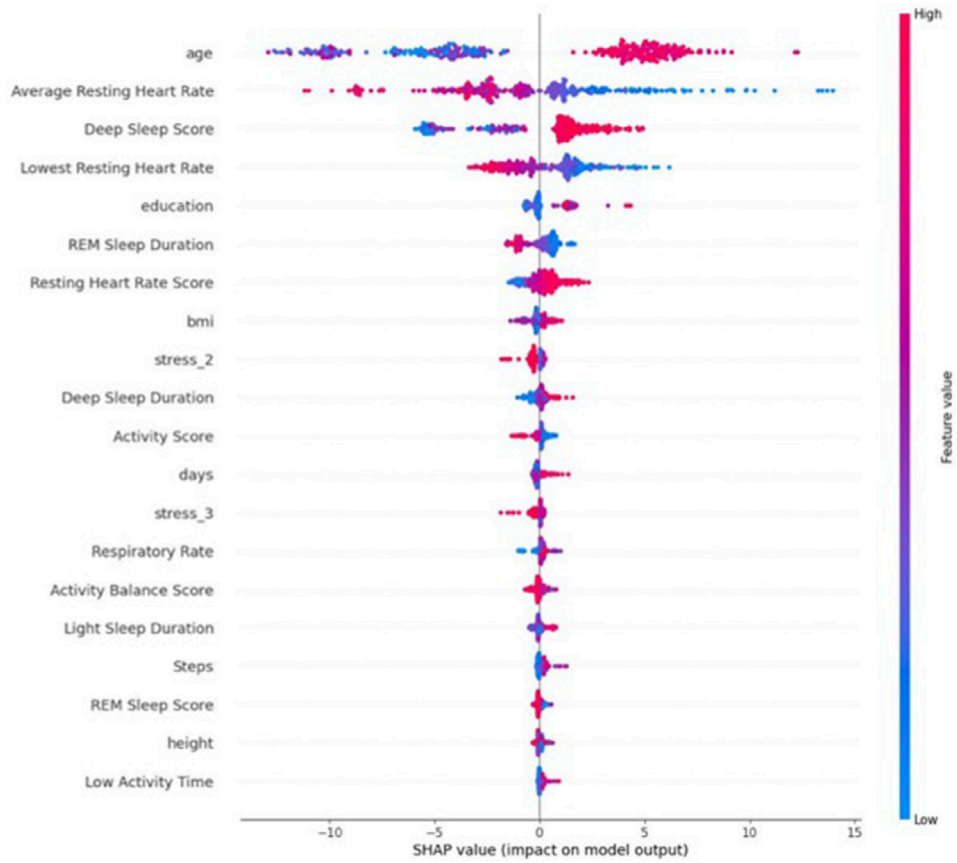

FIGURE 5
Shapley value for average HRV.

combining the results to make final predictors. All subjective (survey) and objective (Oura) data were applied in the RFR model to understand the importance of them in predicting the HRV magnitude in pregnancy.

As shown in Figure 5, the most important predictive features are age, average resting heart rate, deep sleep score, lowest resting heart rate, education, REM sleep duration, resting heart rate score, BMI, mental stress, deep sleep duration, activity score, time, respiratory rate, activity balance score, light sleep duration, steps, REM sleep score, and low-activity time. Some of these features have a positive correlation with HRV. For example, the higher the age, deep sleep score, education, resting heart rate score, and time (gestational age), the higher the HRV magnitude. Other features either had a negative (average resting heart rate, lowest resting heart rate, and REM sleep duration) or non-clear/multi-directional (step, activity score, BMI, respiratory rate, height, and steps) correlation with HRV. However, we should always be mindful that these correlations that come from the machine learning techniques such as RFR are inherently non-linear. This means that the relationship between the input variables (features) and the output variable (RMSSD, in this case) can be complex and not easily captured by simple linear equations. As a result, the associations between individual features and the outcome predicted by a machine learning model may not always be explicitly positive or negative. In other words, the impact of a particular feature on the predicted outcome may depend on its interactions with other features or on other factors that are not easily observable. This is where techniques like Shapley values can be useful. Shapley values are a way to measure the contribution of individual features to the predicted outcome of a machine learning model, taking into account their interactions with other features. They provide a more nuanced understanding of the relationships between features and outcomes, which can be helpful in identifying key factors that influence the predicted outcome. By generating Shapley value figures for the features in the RFR model, we can gain insights into the relative importance of different features and how they contribute to the overall prediction of HRV value. This can help us identify potential areas for further investigation or intervention and can also provide a more comprehensive understanding of the factors that influence HRV.

Figure 6 and Figure 7 indicate the important predictive features for the average HRV intercept and slope, respectively. As can be seen, features such as age, height, sleep, activity, and heart rate still are among important predictive features for average HRV intercept. Weight, restfulness, and total burn are features that seem to predict the average HRV intercept but not the average HRV value and average HRV slope. The average HRV slope shares common predictive features with average HRV and HRV intercept in the majority of the features. Food is the feature that appeared in the

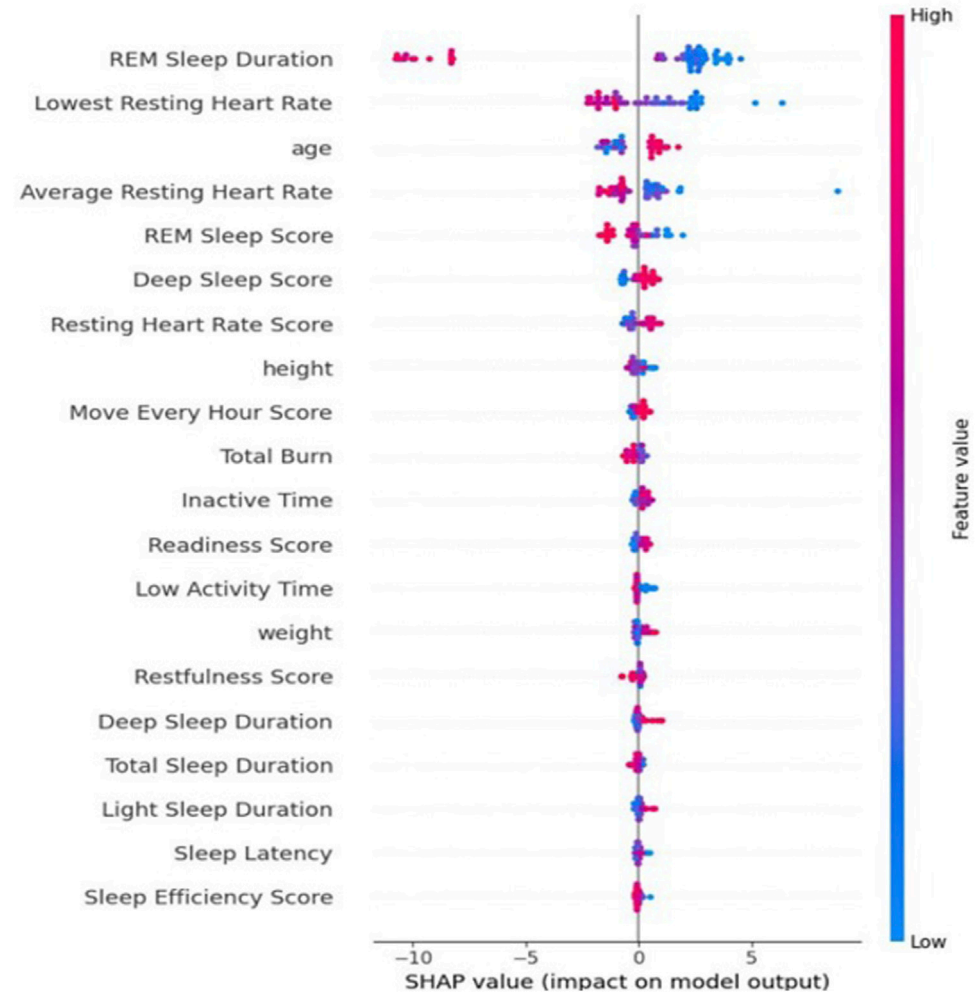

FIGURE 6
Shapley value for the average HRV intercept.

average HRV slope but not in the average HRV intercept and average HRV value.

The accuracy of the model was assessed using the root mean square error (RMSE) metric which is the difference between observed and predicted values in regression analysis. RMSE for the RFR model in the current study was 4.70 which is lower than the global baseline of RMSE (12.28), indicating that this model is more accurate than the global average prediction accuracy for healthy population.

Exploratory analysis

Although statistically unreliable due to small sample size, we compared the HRV magnitude between subjects who kept the healthy status by the end of the study and the complicated case. This may give an insight on the possible difference between healthy and complicated pregnant individuals.

t-test for weekly comparison of the participants

A *t*-test was used to compare the weekly HRV between the healthy (N = 13) and non-healthy (N = 1) participants. We calculated weekly average HRV across healthy participant to be able to compare it with complicated subject (subject #7). As shown in Figure 8, Figure 9, and Figure 10, an average HRV in healthy and non-healthy subjects is statistically significant ($p < 0.05$) during 17 weeks of the study length when assessed daily and weekly.

In addition to the weekly average HRV value, we considered the weekly average HRV slope and intercept to see how their changes occur in addition to the weekly average HRV. After week 7 of the study (31st gestational week), the weekly HRV slope difference between healthy and non-healthy subjects becomes significant ($p < 0.05$) (Figure 11). The average weekly intercept is statistically different ($p < 0.05$) between the healthy and non-healthy participants during the entire study (Figure 11).

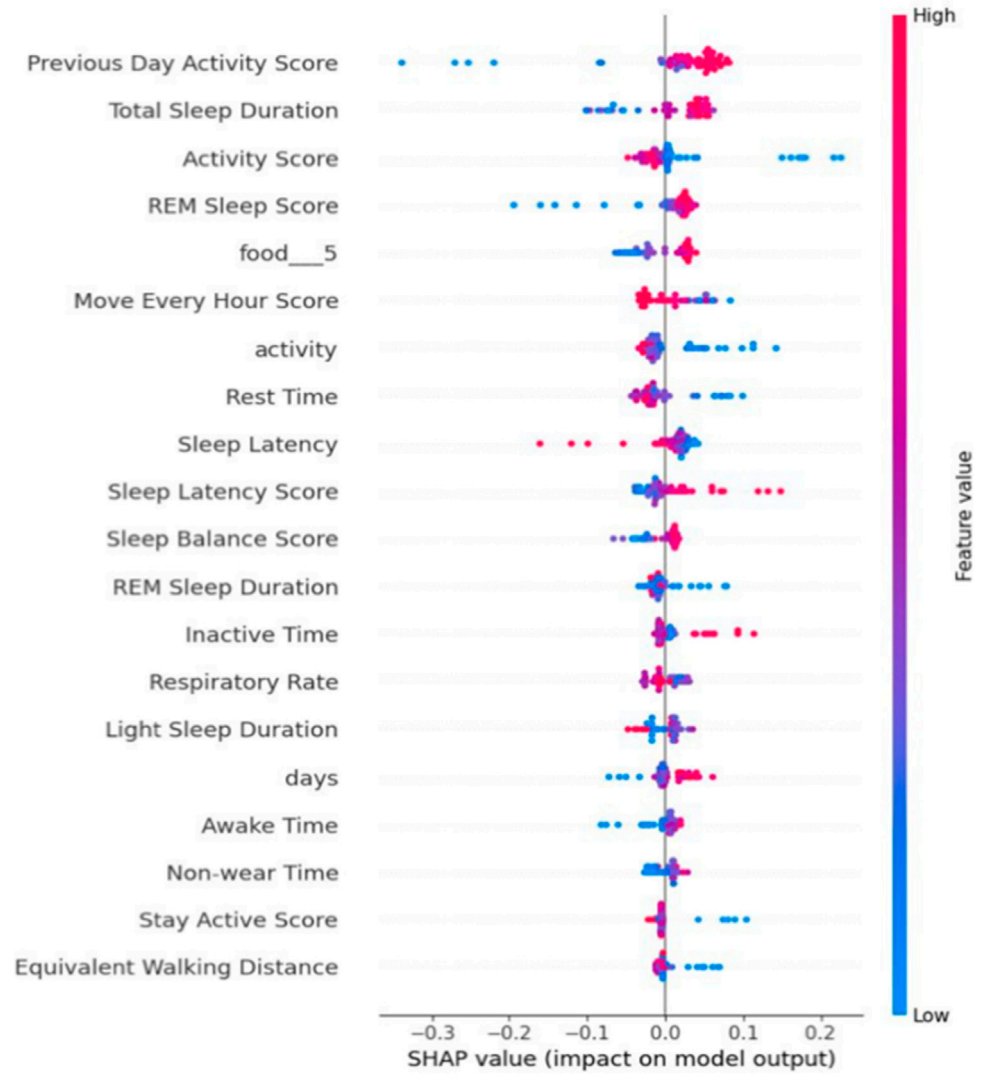

FIGURE 7
Shapley value for the average HRV slope.

Discussion

As discussed earlier, the ANS plays a crucial role in adapting to the unique demands of pregnancy and preventing complications. However, current methods for assessing the ANS function have limitations. To ensure a healthy pregnancy, it is important to accurately assess the ANS function. The aim of this study was to understand the pattern of different HRV metrics extracted from IBI data for healthy pregnant participants. However, we were not able to address the aim thoroughly due to the policy change of the Oura company in providing IBI data. Thus, we conducted planned analyses on the existing HRV (RMSSD) data provided by the Oura. We applied supervised machine learning techniques such as the HLM and RFR, as well as the *t*-test, to address the research question. The results of HLM analysis showed a significant positive relationship between time and average HRV regardless of being healthy or complicated, indicating that HRV increases over time significantly. The model also revealed substantial individual variation in intercepts and slopes between all subjects. The findings of comparison analysis using the *t*-test method indicated that the average HRV of healthy and unhealthy subjects differed significantly during the 17 weeks of the study. Overall, the results suggested that although the HRV is significantly different between the healthy and unhealthy participants, time could be a predictor of HRV magnitude in both groups. Additionally, the findings from the RFR analysis suggested that HRV could be influenced by factors beyond time alone, such as lifestyle, mental health, and sociodemographic factors. This indicates that HRV is not solely determined by time, but it also has the potential to be influenced and regulated. Therefore, if the existing literature's association between HRV and pregnancy complications is validated, it may be possible to predict and address these complications by making relevant lifestyle adjustments and accommodations. Among the effective factors, sleep, activity, BMI, diet, and mental stress were the most significant predictive features for HRV.

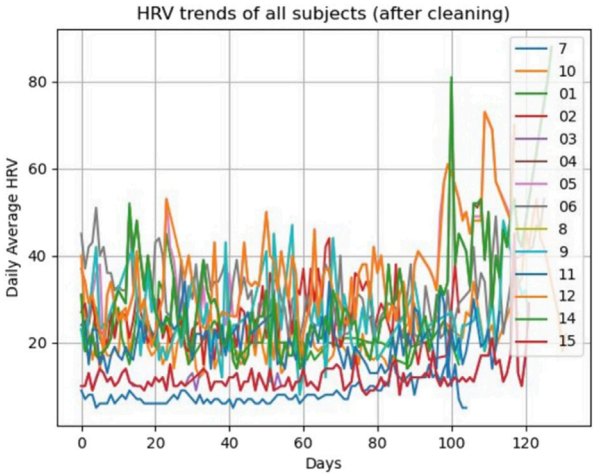

FIGURE 8
HRV pattern for all 14 subjects during the study.

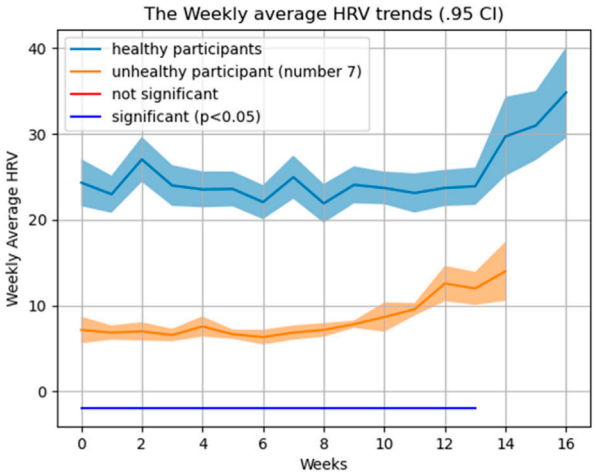

FIGURE 10
HRV pattern for healthy and unhealthy subjects during the study (weekly).

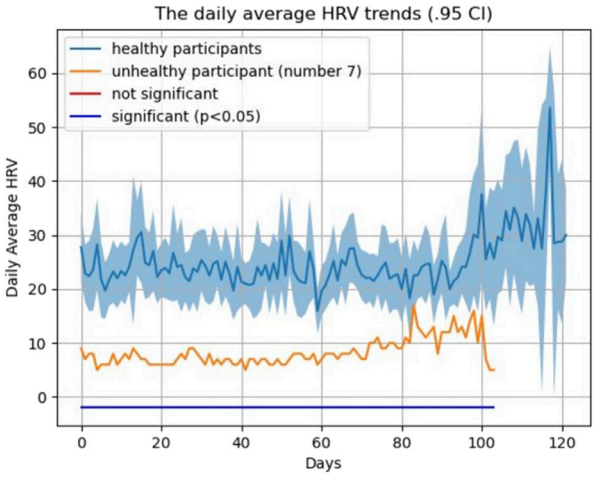

FIGURE 9
HRV pattern for healthy and unhealthy subjects during the study (daily).

To the best of our knowledge, there is only one study that assessed HRV changes longitudinally during pregnancy. Sarhaddi et al. (2022) conducted a study to assess trends in the heart rate and HRV parameters during pregnancy and the 3-month *postpartum* period. Their findings indicated that RMSSD is higher in the third trimester than that in the second trimester, which aligns with our results. However, these results conflict with the findings from the studies that assessed HRV non-continuously during pregnancy using short-term and episodic assessments (Sharifiheris et al., 2022).

In the systematic review conducted by Sharifiheris et al. (2022), HRV was operationalized in three main groups of the frequency domain, time domain, and non-linear domain. In the reviewed studies, RMSSD, which is characterized as time domain metrics, tends to decrease during pregnancy, as opposed to the findings of the current study. However, the studies with such a finding often suffered from serious limitations. For example, the assessment duration was 5–10 min in the majority of the studies. This short-term assessment duration threatens the reliability of the findings; as according to the literature, any duration less than 24 h is unable to represent ANS function.

We could not find any study that concerned with predictive factors of HRV, other than time, in pregnant women. However, the literature supports the finding of this study that HRV is not solely under impact of time. Due to its complex task, the ANS has various relationships with internal and external elements. For example, age (Jandackova et al., 2016; Geovanini et al., 2020), prenatal alcohol consumption (Karpyak et al., 2014; Jurczyk et al., 2019), smoking (Harte et al., 2013; Bodin et al., 2017; Murgia et al., 2019), drug use (Nayak et al., 2020; Lu et al., 2022; Qiu et al., 2023), and BMI (Rodrigues and Quarto, 2018; Triggiani et al., 2019) have been shown to have a correlation with HRV. Although demographic factors such as age cannot be controlled, other factors that are mainly lifestyle-related factors are adjustable by the individual. The current study's results align with these findings indicating that lifestyle-related factors such as sleep, activity, diet, and mental stress affect HRV changes over time.

Understanding HRV seems to be crucial since, 1) as discussed earlier, it has potential to be predicted and, thus, can be adjusted for better outcomes, 2) more importantly, it can predict common pregnancy complications. For instance, there are a few studies that showed HRV can predict maternal mental stress and emotional states during pregnancy with high accuracy (Cao et al., 2022; Li et al., 2022). In addition to these studies that were concerned with the emotional and mental outcome of HRV, there are studies that applied HRV classification for physical pregnancy-induced complications such as hypertensive disorders. For example, Tejera et al. (2011) conducted a study to understand the accuracy of HRV indexes in classifying normal, hypertensive, and preeclamptic pregnancies using the machine learning approach. The results showed that the applied artificial neural network (ANN) model was able to accurately classify the three pregnancy

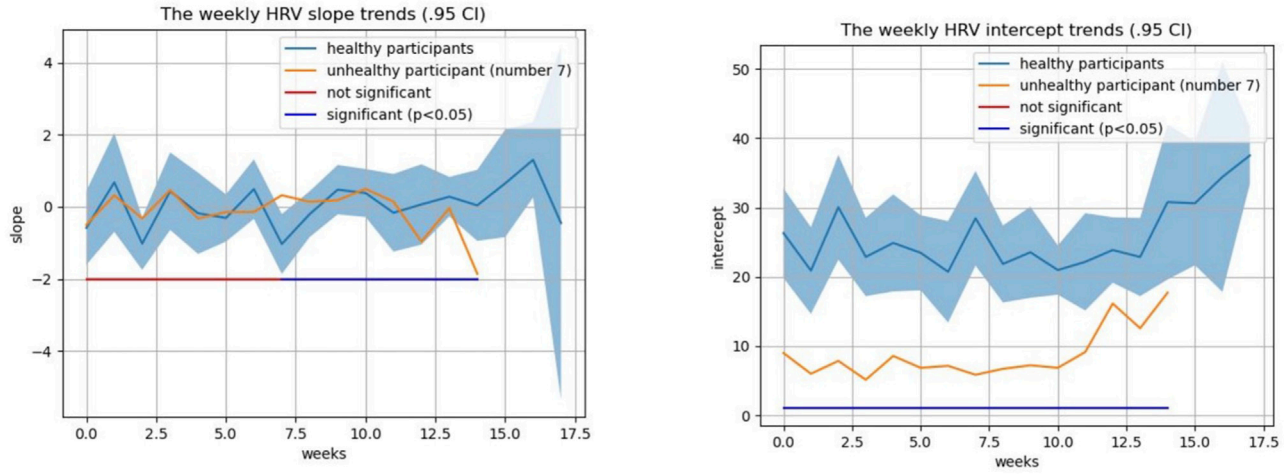

FIGURE 11
Average HRV intercept and slope comparison between healthy and complicated subjects.

groups including normotensive, hypertensive, and preeclamptic groups based on HRV measures.

The collective evidence presented in these studies demonstrates the potential of HRV within the context of pregnancy and predicting various pregnancy outcomes. These findings suggest that HRV data can provide valuable information about the physiological and psychological states of pregnant women and may have important implications for the diagnosis and management of various pregnancy-related conditions.

Furthermore, the studies' results highlight the importance of incorporating HRV data into routine prenatal care to provide a more comprehensive understanding of maternal health. HRV analysis has been shown to offer valuable insight into fetal growth, preeclampsia, gestational diabetes, and other pregnancy-related conditions. Various studies have shown that HRV analysis can provide early warning signs of complications, allowing for timely interventions to improve maternal and fetal health outcomes. In our study, low RMSSD in placental abruption as compared to healthy individuals showed HRV's potential for prediction application. Placental abruption is a significant contributing factor to preterm birth, a condition associated with sympathetic predominance of the ANS in the existing literature (Aye et al., 2018; Jasinski et al., 2022). Placental abruption involves the partial or complete separation of the placenta from the uterine wall before the onset of labor. Understanding the temporal relationship between placental abruption and ANS dysfunction is a complex endeavor, as ANS dysregulation can play multiple roles. It can act as a preceding factor explaining placental abruption or serve as a compensatory response following placental abruption to maintain homeostasis.

In the first scenario, placental abruption may arise as a consequence of hypertensive disorders, which have been consistently linked to an increased risk of placental abruption. This association is primarily attributed to the impact of hypertensive disorders on placental function through vasoconstriction. This vasoconstriction, the narrowing of blood vessels, ultimately reduces blood flow to the uterus and placenta, potentially leading to their separation from the uterine wall.

In the second scenario, placental abruption can result in maternal hypovolemia, characterized by a reduced blood volume due to bleeding following the abruption. This condition triggers physiological responses that impact the ANS, leading to an overactivation of the sympathetic branch. Indeed, in an effort to compensate for hypovolemia, the sympathetic nervous system may become dominant, potentially resulting in a reduction in parasympathetic activity.

Given its application in the literature, HRV should be given careful consideration in prenatal care. Additional research is necessary to confirm these findings and identify the most optimal approaches for integrating HRV analysis into standard prenatal care practices.

Limitations and strengths

This study prioritized a minoritized group, pregnant Latina women, who are at a greater risk of developing pregnancy complications, and thus, better understanding of potential mechanisms of action of complications is critical. The application of smart technology also enabled us to communicate with our participants easily and improve engagement. We also considered strict inclusion and exclusion criteria which increases the internal validity of the study. Since more than 80% of pregnancies are identified as low risk, this also increases the generalizability of our study and, thus, external validity.

Although we tried to minimize the limitations, our study still suffered from a few limitations. We were not able to address our first aim which was extracting and tracking the various HRV patterns using IBI data due to the policy change of Oura in providing such data. This taught us, for the future study(s), to identify the target company thoroughly and obtain a signed contract promising the data access. Lack of access to various metrics of HRV disabled us to represent the ANS comprehensively. We had to rely on the single HRV metric, RMSSD, which is not enough to reflect sympathetic–parasympathetic activity. In addition, this is a pilot

study for which the main aim is an investigation or small-scale trial to assess the feasibility and potential of a larger study. Thus, the statistical findings may not be reliable in this small trial, specifically the analysis that compares the healthy and complicated pregnancies as we only had one complicated case that statistically is not able to represent the complicated pregnancies. However, these analyses still give insights regarding the potential changes of HRV in healthy pregnant women during the second and third trimesters of pregnancy and its possible predictors.

Conclusion

In this study, we were able to capture HRV changes over time and investigate the patterns and trends that occur during pregnancy. This allowed us to demonstrate that HRV increases over time during pregnancy regardless of the health status of the pregnancy. We were also able to identify specific gestational weeks at which the HRV magnitude was significantly different between healthy and unhealthy subjects. Although statistically unreliable, we showed that there is a difference between complicated and healthy pregnancy in terms of the average HRV value.

RFR analysis also allowed us to identify potential predictors of HRV during pregnancy in addition to time. These predictors included, but not limited to, age, BMI, weight, height, activity, sleep, food, and mental stress.

Data availability statement

The raw data supporting the conclusion of this article will be made available by the authors, without undue reservation.

Ethics statement

The studies involving humans were approved by the IRB #777 University of California Irvine. The studies were conducted in accordance with the local legislation and institutional requirements. The participants provided their written informed consent to participate in this study.

Author contributions

ZS-H: conceptualization, investigation, methodology, project administration, resources, software, supervision, visualization, and writing–original draft. ZY: data curation, formal analysis, software, and writing–review and editing. AR: methodology, resources, and writing–review and editing. MF: methodology and writing–review and editing. HS: formal analysis, software, and writing–review and editing. MB: project administration, resources, supervision, and writing–review and editing.

Funding

The authors declare that no financial support was received for the research, authorship, and/or publication of this article.

Conflict of interest

The authors declare that the research was conducted in the absence of any commercial or financial relationships that could be construed as a potential conflict of interest.

Publisher's note

References

Altini, M., and Kinnunen, H. (2021). The promise of sleep: a multi-sensor approach for accurate sleep stage detection using the Oura ring. *Sensors* 21 (13), 4302. doi:10.3390/s21134302

Aye, C. Y., Lewandowski, A. J., Oster, J., Upton, R., Davis, E., Kenworthy, Y., et al. (2018). Neonatal autonomic function after pregnancy complications and early cardiovascular development. *Pediatr. Res.* 84 (1), 85–91. doi:10.1038/s41390-018-0021-0

Bennett, I. M., Coco, A., Coyne, J. C., Mitchell, A. J., Nicholson, J., Johnson, E., et al. (2008). Efficiency of a two-item pre-screen to reduce the burden of depression screening in pregnancy and postpartum: an IMPLICIT network study. *J. Am. Board Fam. Med.* 21 (4), 317–325. doi:10.3122/jabfm.2008.04.080048

Bodin, F., McIntyre, K. M., Schwartz, J. E., McKinley, P. S., Cardetti, C., Shapiro, P. A., et al. (2017). The association of cigarette smoking with high frequency heart rate variability: an ecological momentary assessment study. *Psychosom. Med.* 79 (9), 1045–1050. doi:10.1097/PSY.0000000000000507

Braeken, M. A. R. I. J. K. E. (2014). Psychological functioning and the autonomic nervous system during pregnancy. Doctoral dissertation, PhD thesis. Tilburg, the Netherlands: Tilburg University. Impact on mother and child.

Bruno, R. M., Ghiadoni, L., Seravalle, G., Dell'Oro, R., Taddei, S., and Grassi, G. (2012). Sympathetic regulation of vascular function in health and disease. *Front. physiology* 3, 284. doi:10.3389/fphys.2012.00284

Cao, R., Rahmani, A. M., and Lindsay, K. L. (2022). Prenatal stress assessment using heart rate variability and salivary cortisol: a machine learning-based approach. *Plos one* 17 (9), e0274298. doi:10.1371/journal.pone.0274298

de Zambotti, M., Rosas, L., Colrain, I. M., and Baker, F. C. (2019). The sleep of the ring: comparison of the OURA sleep tracker against polysomnography. *Behav. Sleep. Med.* 17 (2), 124–136. doi:10.1080/15402002.2017.1300587

Duong, H. T. H., Tadesse, G. A., Nhat, P. T. H., Van Hao, N., Prince, J., Duong, T. D., et al. (2020). Heart rate variability as an indicator of autonomic nervous system disturbance in tetanus. *Am. J. Trop. Med. Hyg.* 102 (2), 403–407. doi:10.4269/ajtmh.19-0720

Ernst, G. (2017). Heart-rate variability—more than heart beats? *Front. public health* 5, 240. doi:10.3389/fpubh.2017.00240

Essiben, F., Um, E. M. N., Ojong, S., Gimnwi, F., Olen, K., and Nana, P. N. (2018). GAD-7 and PHQ-9 measurement of perinatal anxiety and depression in women with hypertensive disorders of pregnancy in Yaounde, Cameroon. *Int. J. Reproduction, Contracept. Obstetrics Gynecol.* 7 (6), 2069. doi:10.18203/2320-1770.ijrcog20182312

Gelaye, B., Wilson, I., Berhane, H. Y., Deyessa, N., Bahretibeb, Y., Wondimagegn, D., et al. (2016). Diagnostic validity of the patient health questionnaire-2 (PHQ-2) among Ethiopian adults. *Compr. psychiatry* 70, 216–221. doi:10.1016/j.comppsych.2016.07.011

Geovanini, G. R., Vasques, E. R., de Oliveira Alvim, R., Mill, J. G., Andreão, R. V., Vasques, B. K., et al. (2020). Age and sex differences in heart rate variability and vagal specific patterns–Baependi heart study. *Glob. Heart* 15 (1), 71. doi:10.5334/gh.873

Harte, C. B., Liverant, G. I., Sloan, D. M., Kamholz, B. W., Rosebrock, L. E., Fava, M., et al. (2013). Association between smoking and heart rate variability among individuals with depression. *Ann. Behav. Med.* 46 (1), 73–80. doi:10.1007/s12160-013-9476-8

Howell, E. A., Egorova, N. N., Janevic, T., Balbierz, M. A., Zeitlin, J., and Hebert, P. L. (2017). Severe maternal morbidity among Hispanic women in New York City: investigation of health disparities. *Obstetrics Gynecol.* 129 (2), 285–294. doi:10.1097/AOG.0000000000001864

Jandackova, V. K., Scholes, S., Britton, A., and Steptoe, A. (2016). Are changes in heart rate variability in middle-aged and older people normative or caused by pathological conditions? Findings from a large population-based longitudinal cohort study. *J. Am. Heart Assoc.* 5 (2), e002365. doi:10.1161/JAHA.115.002365

Jasinski, S. R., Rowan, S., Presby, D. M., Claydon, E., and Capodilupo, E. R. (2022). *Wearable-derived maternal heart rate variability as A novel digital biomarker of preterm birth*. medRxiv, 2022–2111.

Johnson, J. O. (2019). "Autonomic nervous system: physiology," in *Pharmacology and physiology for anesthesia* (Elsevier), 270–281.

Julious, S. A. (2005). Sample size of 12 per group rule of thumb for a pilot study. *Pharm. Statistics J. Appl. Statistics Pharm. Industry* 4 (4), 287–291. doi:10.1002/pst.185

Jurczyk, M., Dyląg, K. A., Skowron, K., and Gil, K. (2019). Prenatal alcohol exposure and autonomic nervous system dysfunction: a review article. *Folia Medica Cracoviensia* 59 (3), 15–21. doi:10.24425/fmc.2019.131132

Karpyak, V. M., Romanowicz, M., Schmidt, J. E., Lewis, K. A., and Bostwick, J. M. (2014). Characteristics of heart rate variability in alcohol-dependent subjects and nondependent chronic alcohol users. *Alcohol. Clin. Exp. Res.* 38 (1), 9–26. doi:10.1111/acer.12270

Kataoka, K., Tomiya, Y., Sakamoto, A., Kamada, Y., Hiramatsu, Y., and Nakatsuka, M. (2015). Altered autonomic nervous system activity in women with unexplained recurrent pregnancy loss. *J. Obstetrics Gynaecol. Res.* 41 (6), 912–918. doi:10.1111/jog.12653

Kinnunen, H., Rantanen, A., Kenttä, T., and Koskimäki, H. (2020). Feasible assessment of recovery and cardiovascular health: accuracy of nocturnal HR and HRV assessed via ring PPG in comparison to medical grade ECG. *Physiol. Meas.* 41 (4), 04NT01. doi:10.1088/1361-6579/ab840a

Kroenke, K., Spitzer, R. L., Williams, J. B., Monahan, P. O., and Löwe, B. (2007). Anxiety disorders in primary care: prevalence, impairment, comorbidity, and detection. *Ann. Intern. Med.* 146 (5), 317–325. doi:10.7326/0003-4819-146-5-200703060-00004

Li, X., Ono, C., Warita, N., Shoji, T., Nakagawa, T., Usukura, H., et al. (2022). Heart rate information-based machine learning prediction of emotions among pregnant women. *Front. Psychiatry* 12, 799029. doi:10.3389/fpsyt.2021.799029

Lu, M. K., Chou, L. W., Chang, K. M., Lee, H. Y., and Kang, H. J. (2022). Substance misuse decreases heart rate variability. *J. Sensors* 2022, 1–7. doi:10.1155/2022/3222839

Maijala, A., Kinnunen, H., Koskimäki, H., Jämsä, T., and Kangas, M. (2019). Nocturnal finger skin temperature in menstrual cycle tracking: ambulatory pilot study using a wearable Oura ring. *BMC Women's Health* 19 (1), 150–210. doi:10.1186/s12905-019-0844-9

Murgia, F., Melotti, R., Foco, L., Gögele, M., Meraviglia, V., Motta, B., et al. (2019). Effects of smoking status, history and intensity on heart rate variability in the general population: the CHRIS study. *PLoS One* 14 (4), e0215053. doi:10.1371/journal.pone.0215053

Nayak, S. K., Pradhan, B. K., Banerjee, I., and Pal, K. (2020). Analysis of heart rate variability to understand the effect of cannabis consumption on Indian male paddy-field workers. *Biomed. Signal Process. Control* 62, 102072. doi:10.1016/j.bspc.2020.102072

Peng, R. C., Zhou, X. L., Lin, W. H., and Zhang, Y. T. (2015). Extraction of heart rate variability from smartphone photoplethysmograms. *Comput. Math. methods Med.* 2015, 516826. doi:10.1155/2015/516826

Petersen, E. E., Davis, N. L., Goodman, D., Cox, S., Syverson, C., Seed, K., et al. (2019). Racial/ethnic disparities in pregnancy-related deaths—United States, 2007–2016. *Morb. Mortal. Wkly. Rep.* 68 (35), 762–765. doi:10.15585/mmwr.mm6835a3

Qiu, H., Zhang, H., Han, D. D., Derakhshandeh, R., Wang, X., Goyal, N., et al. (2023). Increased vulnerability to atrial and ventricular arrhythmias caused by different types of inhaled tobacco or marijuana products. *Heart rhythm.* 20 (1), 76–86. doi:10.1016/j.hrthm.2022.09.021

Rajbanshi, S., Norhayati, M. N., and Nik Hazlina, N. H. (2020). High-risk pregnancies and their association with severe maternal morbidity in Nepal: a prospective cohort study. *PloS one* 15 (12), e0244072. doi:10.1371/journal.pone.0244072

Rodrigues, T. S., and Quarto, L. J. G. (2018). Body mass index may influence heart rate variability. *Arq. Bras. Cardiol.* 111, 640–642. doi:10.5935/abc.20180201

Sarhaddi, F., Azimi, I., Axelin, A., Niela-Vilen, H., Liljeberg, P., and Rahmani, A. M. (2022). Trends in heart rate and heart rate variability during pregnancy and the 3-month postpartum period: continuous monitoring in a free-living context. *JMIR mHealth uHealth* 10 (6), e33458. doi:10.2196/33458

Sharifiheris, Z., Rahmani, A., Onwuka, J., and Bender, M. (2022). The utilization of heart rate variability for autonomic nervous system assessment in healthy pregnant women: systematic review. *JMIR Bioinforma. Biotechnol.* 3 (1), e36791. doi:10.2196/36791

Slavin, V., Creedy, D. K., and Gamble, J. (2020). Comparison of screening accuracy of the Patient Health Questionnaire-2 using two case-identification methods during pregnancy and postpartum. *BMC Pregnancy Childbirth* 20, 211–215. doi:10.1186/s12884-020-02891-2

Soma-Pillay, P., Nelson-Piercy, C., Tolppanen, H., and Mebazaa, A. (2016). Physiological changes in pregnancy: review articles. *Cardiovasc. J. Afr.* 27 (2), 89–94. doi:10.5830/CVJA-2016-021

Tejera, E., Jose areias, M., Rodrigues, A., Ramoa, A., Manuel nieto-villar, J., and Rebelo, I. (2011). Artificial neural network for normal, hypertensive, and preeclamptic pregnancy classification using maternal heart rate variability indexes. *J. Maternal-Fetal Neonatal Med.* 24 (9), 1147–1151. doi:10.3109/14767058.2010.545916

Thomas, J. L., Lewis, J. B., Martinez, I., Cunningham, S. D., Siddique, M., Tobin, J. N., et al. (2019). Associations between intimate partner violence profiles and mental health among low-income, urban pregnant adolescents. *BMC pregnancy childbirth* 19 (1), 120. doi:10.1186/s12884-019-2256-0

Triggiani, A. I., Valenzano, A., Trimigno, V., Di Palma, A., Moscatelli, F., Cibelli, G., et al. (2019). Heart rate variability reduction is related to a high amount of visceral adiposity in healthy young women. *PloS one* 14 (9), e0223058. doi:10.1371/journal.pone.0223058

Warttig, S. L., Forshaw, M. J., South, J., and White, A. K. (2013). New, normative, English-sample data for the short form perceived stress scale (PSS-4). *J. health Psychol.* 18 (12), 1617–1628. doi:10.1177/1359105313508346

Waxenbaum, J. A., Reddy, V., and Varacallo, M. (2019). *Anatomy, autonomic nervous system*.

Whittle, H. J., Sheira, L. A., Wolfe, W. R., Frongillo, E. A., Palar, K., Merenstein, D., et al. (2019). Food insecurity is associated with anxiety, stress, and symptoms of posttraumatic stress disorder in a cohort of women with or at risk of HIV in the United States. *J. Nutr.* 149 (8), 1393–1403. doi:10.1093/jn/nxz093

Yousif, D., Bellos, I., Penzlin, A. I., Hijazi, M. M., Illigens, B. M. W., Pinter, A., et al. (2019). Autonomic dysfunction in preeclampsia: a systematic review. *Front. Neurology* 10, 816. doi:10.3389/fneur.2019.00816

Ziemssen, T., and Siepmann, T. (2019). The investigation of the cardiovascular and sudomotor autonomic nervous system—a review. *Front. neurology* 10, 53. doi:10.3389/fneur.2019.00053

Zygmunt, A., and Stanczyk, J. (2010). Methods of evaluation of autonomic nervous system function. *Archives Med. Sci.* 6 (1), 11–18. doi:10.5114/aoms.2010.13500

10.3389/fphys.2023.1293946

Appendix A

TABLE A1 Criteria for healthy pregnancy in the American College of Obstetricians and Gynecologists.

I. Social/personal	II. Obstetric history	III. Medical and family history	IV. Present pregnancy
Maternal age (<17, >35 years)	Gravida (1 or >5)	Diabetes	Pre-pregnancy BMI ≤25
Education (<6 years)	Para (0 or >5)	Hypertension	Height <145 cm
Marital status (unmarried)	Abortions (>2)	Renal diseases	Pregnancy-induced hypertension
Economic status (poor)	Miscarriages (1+)	Cardiovascular diseases (e.g., phlebitis)	Bleeding
Smoking, alcohol consumer, or drug user	Fetal deaths (≥1)		Pre-eclampsia
Domestic violence	Bleeding in T3	Blood diseases	Multiple pregnancy
	Stillbirths (≥1)	Endocrine diseases	Abnormal fetal presentation
	Previous cesarean (≥1)	No medication use except for perinatal vitamins and folate	Gestational diabetes mellitus
	Preterm deliveries (≥1)	STDs	Placenta previa
	Birth weights (<2500 gr)	Respiratory diseases	Cervix insufficiency
	Infant deaths (≥1)	Central nervous diseases	An Rh-negative woman with an Rh-positive husband who is not willing to take RhoGAM
	Toxemia (≥1)	Abdominal visceral disorders	
	Birth defects (≥1)	Genetic or congenital disorder	
		Autoimmune disease	
		Infectious diseases	
		Mental illness (mental distress such as stress, anxiety, and depression)*	

*PHQ-2, PSS-4, and GAD-2 were used to assess depression, stress, and anxiety, respectively.

frontiers | Frontiers in Neuroscience

TYPE Case Report
PUBLISHED 19 January 2024
DOI 10.3389/fnins.2024.1333188

OPEN ACCESS

EDITED BY
Vitor Engracia Valenti,
São Paulo State University, Brazil

REVIEWED BY
Félix Javier Jiménez-Jiménez,
Hospital Universitario del Sureste, Spain
Shangru Lyu,
Moderna Inc., United States

*CORRESPONDENCE
Weiwei Zhang
✉ sxbqeyyzww@163.com

RECEIVED 04 November 2023
ACCEPTED 03 January 2024
PUBLISHED 19 January 2024

CITATION
Li Y, Zhang W, Wang H and Zhang W (2024) Case report: A new treatment for restless leg syndrome: three cases.
Front. Neurosci. 18:1333188.
doi: 10.3389/fnins.2024.1333188

Case report: A new treatment for restless leg syndrome: three cases

Ying Li, Wenjing Zhang, Hui Wang and Weiwei Zhang*

Third Hospital of Shanxi Medical University, Shanxi Bethune Hospital, Shanxi Academy of Medical Sciences, Tongji Shanxi Hospital, Taiyuan, China

Restless legs syndrome is a movement disorder that seriously affects the quality of life of patients. It is characterized by marked discomfort mainly occurring in the deep tissues of the lower extremities, including deep muscle or bone chafing, as well as crawling sensations or pulling sensations. These sensations often cause patients to awaken after falling asleep and to feel the urge to walk around, which seriously affects their sleep quality. Patients with restless leg syndrome exhibit significantly enhanced sympathetic nerve activity and immune disorders, while stellate ganglion blockage can block sympathetic nerves and regulate immune cells and cytokines to maintain immune system homeostasis. We report three patients with restless legs syndrome complicated with severe nephrotic syndrome. After treatment with stellate ganglion block, the symptoms in the restless legs were relieved within 1 month, and the quality of sleep was significantly improved. Our findings suggest that stellate ganglion block has broad promise in the management of restless legs syndrome patients with severe comorbidities.

KEYWORDS

stellate ganglion block, restless leg syndrome, kidney failure, sympathetic nerve, sleep monitoring report

1 Introduction

Restless legs syndrome (RLS) is a sensorimotor disease of the nervous system, with an overall prevalence of up to 10% (Ferini-Strambi and Manconi, 2009), and it especially has a high incidence in end-stage renal disease populations. It is characterized by a spontaneous, unbearable painful sensation or abnormal sensations such as ant-crawling and burning sensations, which are more common in the lower limbs and can appear or become aggravated at rest and at night (Trenkwalder et al., 2005). The main goals of treatment for RLS are to relieve symptoms and improve sleep quality. Clinically, dopamine receptor agonists are often used as representative drug treatments; however, when they are used at low doses in the short term, they can quickly relieve symptoms but usually lead to worsening of disease severity (Anguelova et al., 2018). Alternative treatments, such as exercise training, light therapy, and acupuncture, have been shown to be effective at relieving RLS symptoms, but these treatments are long, causing the symptoms to respond slowly (Xu et al., 2018). Therefore, it is necessary to find suitable alternative treatments.

The pathogenesis of RLS is complex and involves various factors, such as brain iron deficiency, altered dopaminergic neuron transmission, peripheral neuropathy, chronic inflammation, and immune deficiency (Weinstock et al., 2012; Allen, 2015; Didato et al., 2020). In recent years, studies have shown that the development of RLS is associated with excessive activation of sympathetic nerves (Stevens, 2015; Bergmann et al., 2021), and

inflammation and immune changes are common in RLS patients (Weinstock et al., 2012). Stellate ganglion block (SGB) is a safe and effective minimally invasive treatment. With the innovation of ultrasound monitoring and guidance technology, the safety of SGB can be guaranteed (Narouze, 2014). SGB is mainly used to treat pain, stress, and sleep disorders by blocking sympathetic nerves (Liao et al., 2016; Gu et al., 2022). Moreover, SGB can play a role in regulating immune responses by blocking the sympathetic innervation of immune organs (Lipov et al., 2020). Therefore, we hypothesized that SGB might be effective at relieving RLS symptoms. Relevant research evidence from domestic and foreign studies is insufficient, and there is no experimental evidence supporting the possible therapeutic effect of SGB on RLS.

We report three cases of RLS with severe nephrotic syndrome diagnosed by the updated International Restless Legs Syndrome Study Group (IRLSSG) consensus criterion (Allen et al., 2014). The patients experienced remission after treatment via SGB and experienced few recurrences during follow-up. These observations suggest that the use of stellate ganglion blockade in RLS may be of great clinical value.

2 Case report

2.1 Case 1

A 47-year-old male, was admitted to the Nephrology Department of our hospital in August 2021 due to dysfunction of the left forearm due to an arteriovenous fistula. He had a history of chronic kidney disease for more than 20 years and had been diagnosed with focal segmental glomerulosclerosis in 2004. He was treated with hormones and immunosuppressants for more than 10 years, during which his creatinine increased progressively. In 2019, he progressed to the uremia stage of chronic renal failure, and his condition was stable after regular hemodialysis. After being admitted to the hospital this time, the doctor observed that his mental state was not good. By careful questioning, during the past 2 years, he had frequently experienced spontaneous shaking of his legs after falling asleep, causing him to awaken. The symptoms were slightly relieved by his arising and engaging in physical activity. The average frequency of the attacks was approximately 5–7 times per hour. The attacks also occurred during the day, but the symptoms were milder than those at night. These symptoms seriously affected the patient's work efficiency during the day and quality of sleep at night. The effect of dopamine drugs was not good, so the drug was stopped by the patient on his own volition. After a comprehensive evaluation by nephrologists and anesthesiologists, the patient was diagnosed with RLS with an International Registry Sleep Scale (IRLS) score of 34, and he was given SGB therapy once every other day for a total of 6 treatments. The above symptoms basically disappeared 1 month after the treatment, and the IRLS score decreased to 8. To date, only occasional spontaneous shaking of the legs has been observed during exertion, with an IRLS score of 10. In addition, a polysomnography evaluation revealed that the patient's sleep quality improved significantly after treatment; his episodes of snoring, airflow limitation, and paradoxical breathing were reduced; and the longest sleep pause time was also significantly reduced.

2.2 Case 2

A 57-year-old male, was admitted to our hospital in July 2021 due to the need for hemodialysis. The patient was diagnosed with nephrotic syndrome in 2020. After onset, he was treated with hormones and cyclosporine combined with symptomatic treatments such as acid suppression, calcium supplementation, and immune regulation. However, the disease still progressed, but the symptoms were relieved after regular hemodialysis. The patient had been experiencing frequent twitching symptoms in both calves since January 2020, mostly before he fell asleep, which could be immediately relieved by standing. The frequency of falls was as high as 8–10 times per hour, which affected his ability to fall asleep. However, there were no symptoms after the patient had fallen asleep. The symptoms were slightly relieved after hemodialysis. After a comprehensive evaluation by the nephrology department and anesthesiologist, the patient was diagnosed with RLS, with an IRLS score of 29. After the evaluation, the patient was treated 4 times with SGB, after which his symptoms were relieved. After 2 weeks, the symptoms worsened. After 2 supplementary treatments, the symptoms were relieved, and there were occasional seizures. The average sleep time was approximately 3 h earlier. One month later, the IRLS score decreased to 18. Half a year later, the patient felt that the frequency of leg twitching had increased slightly, but the symptoms could be relieved after hemofiltration. At this evaluation, the IRLS score was 11. He now felt that this condition had little impact on his normal life and did not seek further treatment. Thus far, compared with that before treatment, the patient's sleep quality has significantly improved, and polysomnography has shown that the longest sleep pause time has been reduced.

2.3 Case 3

A 24-year-old female, was admitted to our hospital in August 2021 due to renal hypertension. In addition, she had a history of stage 5 chronic kidney disease, renal bone disease, and type 1 diabetes. An examination revealed that an arteriovenous fistula in the left forearm was dysfunctional, and it was treated surgically. Anticoagulation, dialysis and other symptomatic treatments were performed after the operation, and the patient's condition was stable. Since 2020, the patient had had difficulty falling asleep at night, manifested as spontaneous twitching of the waist and legs before bed, with a frequency of approximately 5–8 times per hour, which could be relieved after stretching. Occasionally, the patient needed to walk around to get relief; and the number of awakenings at night was more than 10. After a comprehensive evaluation by the nephrology department and anesthesiologists, she was diagnosed with RLS, with an IRLS score of 31. After a full assessment of the patient, an SGB was administered 6 times, the symptoms were slightly relieved at first, and the International Respiratory Scale (IRLS) score decreased to 22 1 month later. It has been more than half a year now, and occasionally, the patient's leg twitches; she wakes up approximately 1–2 times a month; and the IRLS score has dropped to 10. The polysomnography results showed that the patient's sleep disorder index was significantly lower, and the proportion of time the patient spent snoring was also lower (Tables 1–3).

TABLE 1 Clinical characteristics of the patients.

Case	Case 1	Case 2	Case 3
Age (years)	47	57	24
Gender	Male	Male	Female
Smoking history	No	No	No
Drinking history	More than 20 years	No	No
History of diabetes	No	No	Type I Diabetes, 2 years
History of hypertension	17 years, Blood pressure as high as 200/110 mmHg	More than 10 years, Blood pressure as high as 180/100 mmHg	2 years, Blood pressure as high as 210/100 mmHg
Renal diseases history	More than 3 years	More than 4 years	More than 2 years
History of other diseases	No	No	No
Family history of disease	His father suffers from hypertension	No	No

TABLE 2 Patient information on stellate ganglion block treatment.

Case		Case 1	Case 2	Case 3
The start date of RLS treatment		2021.08	2021.07	2021.08
Therapy method		0.5% Ropivacaine 5 mL, alternate left and right, every other day		
Operating steps		The patient was placed in a supine position with his head was tilted to one side. Under ultrasound guidance, puncture was performed to the vicinity of the 6th cervical vertebrae and the anterior tuberosity of the transverse process to a depth of 3.0–3.5 cm. After the retrieval revealed that there was no blood, cerebrospinal fluid, or gas, 5 mL of 0.5% ropivacaine was slowly injected. After the operation, the patient was asked if there was any discomfort. The patient was asked to change to a sitting position, and he was observed as to whether there was Horner syndrome.		
Adverse reactions		No	No	No
Number of SGB treatments		6	4 + 2	6
IRLS score	Initial	34	29	31
	Followed up for 1 month	8	18	22
	Finish (2022.12)	10	11	10

TABLE 3 Patient sleep monitoring reports.

			Initial	One month	Now
Case1	Sleep percentage	Snoring	35.5%	8.1%	7.9%
		Airflow restriction	17.1%	11.0%	11.2%
		Paradoxical breathing	13.7%	0%	0%
	Disorder index		18.4/h	14.3/h	13.8/h
	Longest sleep apnea period		81.9 s	30.1 sç	35.4 s
Case2	Sleep percentage	Snoring	0.7%	5.9%	3.4%
		Airflow restriction	11.3%	15.6%	13.2%
		Paradoxical breathing	4.8%	11.0%	7.9%
	Disorder index		19.5/h	17.7/h	16.6/h
	Longest sleep apnea period		73.1 sç	53.2 s	40.8 s
Case3	Sleep percentage	Snoring	27.8%	15.7%	15.4%
		Airflow restriction	12.4%	11.9%	12.3%
		Paradoxical breathing	0%	0%	0%
	Disorder index		18.9/h	14.2/h	13.9/h
	Longest sleep apnea period		34.2 s	28.9 s	23.5 s

3 Discussion

RLS is a common neglected disease that requires careful observation and history-taking to make a definite diagnosis and to take further diagnostic and therapeutic measures (Kambampati et al., 2020). Similarly, the patient in our report was diagnosed with nephrotic syndrome when he was hospitalized in the nephrology department of our hospital, and the doctor invited the anesthesiologist for consultation after the patient was asked about the details of the case. Therefore, it is very important to increase the reporting of RLS, which may help us identify additional patients who meet the diagnostic criteria for this disease and take timely treatment measures.

The mechanism of action of SGB mainly involves the sympathetic nervous system, affecting both the central nervous system and the peripheral nervous system. On the one hand, it restores the body's autonomic nervous system, endocrine system, immune system, etc. (Lipov et al., 2020). On the other hand, blocking preganglionic and postganglionic nerve fibers inhibits gland secretion and pain transmission in organs and systems dominated by sympathetic nerves in the distribution area (Noma et al., 2013). SGB has been widely used to treat pain syndrome, stress and sleep disorders (Makharita et al., 2012).

There is a correlation between the sympathetic nervous system and the development of RLS. One study showed that hypofunction of the A11 diencephalospinal pathway (a brain dopaminergic pathway that innervates preganglionic sympathetic neurons and the dorsal horn of the spinal cord) leads to increased RLS-related sensory input coupled with increased peripheral sympathetic outflow, ultimately leading to RLS symptoms (Walters and Rye, 2009). Additionally, the sympathetic nervous system plays an important role in the regulation of the immune system (Kenney and Ganta, 2014). Recent studies have shown that several RLS-related diseases are related to systemic inflammation and/or immune disorders (Tanaka and Okusa, 2020; Zhu et al., 2022). Inflammation-mediated elevation of IL-6 can lead to an increase in hepcidin, a hormone that regulates iron levels, which in turn reduces serum iron levels and induces RLS symptoms (Alaçam Köksal et al., 2023). SGB can modulate a variety of immune cells and cytokines (Lipov et al., 2020). Studies by Yang et al. have shown that SGB leads to a decrease in the concentration of proinflammatory cytokines such as IL-6 (Yang et al., 2015). Therefore, SGB may be effective at controlling symptoms of RLS and improving sleep quality.

We reported 3 patients with nephrotic syndrome requiring hemodialysis. After several SGBs, the patients' restless leg symptoms and sleep quality improved significantly. This finding suggested that SGB is effective in patients with severe comorbidities and can provide a good long-term prognosis. Moreover, this opens up additional possibilities for RLS patients with nephrotic syndrome. For patients with nephrotic syndrome, SGBs act locally, and there is no problem with unstable blood drug concentrations during dialysis. Moreover, it can eliminate patients' anxiety about the long-term use of drugs that will increase the burden on the kidneys and lead to aggravation of the disease.

Judging from the treatment effect, the patients' symptoms were relieved or gradually relieved in the short term after treatment. Generally, the long-term prognosis is good, and patients are highly satisfied with the treatment effect. Although longer-term follow-up data are lacking, there may be cases of relapse over time. However, our available data still suggest that SGB holds promise as an alternative therapy in RLS patients with nephrotic syndrome.

In conclusion, SGB has broad application prospects in the treatment of patients with RLS. In the future, we will conduct randomized controlled trials to evaluate the safety and efficacy of SGB and provide experimental evidence for whether this therapy can be applied clinically.

Data availability statement

The original contributions presented in the study are included in the article/supplementary material, further inquiries can be directed to the corresponding author.

Ethics statement

The studies involving humans were approved by Medical Ethics Committee, Shanxi Academy of Medical Sciences, Shanxi Bethune Hospital. The studies were conducted in accordance with the local legislation and institutional requirements. The participants provided their written informed consent to participate in this study. Written informed consent was obtained from the individual(s) for the publication of any potentially identifiable images or data included in this article.

Author contributions

YL: Writing – original draft. WenZ: Writing – review & editing. HW: Writing – review & editing. WeiZ: Writing – review & editing.

Funding

The author(s) declare financial support was received for the research, authorship, and/or publication of this article. This work was supported by the scientific research project of Shanxi Provincial Health Commission 253 (#2022068), the basic research general project of Shanxi Provincial Department of Science and Technology (#202203021221245), and China Zhongguancun Precision Medicine Science and Technology Foundation (#Z-2021-002).

Conflict of interest

The authors declare that the research was conducted in the absence of any commercial or financial relationships that could be construed as a potential conflict of interest.

Publisher's note

References

Alaçam Köksal, S., Boncuk Ulaş, S., Acar, B. A., Acar, T., Güzey Aras, Y., and Köroğlu, M. (2023). Evaluation of the relationship between idiopathic restless legs syndrome and serum hepcidin levels. *Brain Behav.* 13:e3259. doi: 10.1002/brb3.3259

Allen, R. P. (2015). Restless leg syndrome/Willis-Ekbom disease pathophysiology. *Sleep Med. Clin.* 10, 207–214, xi. doi: 10.1016/j.jsmc.2015.05.022

Allen, R. P., Picchietti, D. L., Garcia-Borreguero, D., Ondo, W. G., Walters, A. S., Winkelman, J. W., et al. (2014). Restless legs syndrome/Willis-Ekbom disease diagnostic criteria: updated international restless legs syndrome study group (IRLSSG) consensus criteria--history, rationale, description, and significance. *Sleep Med.* 15, 860–873. doi: 10.1016/j.sleep.2014.03.025

Anguelova, G. V., Vlak, M. H. M., Kurvers, A. G. Y., and Rijsman, R. M. (2018). Pharmacologic and nonpharmacologic treatment of restless legs syndrome. *Sleep Med. Clin.* 13, 219–230. doi: 10.1016/j.jsmc.2018.02.005

Bergmann, M., Heidbreder, A., Stefani, A., Raccagni, C., Brandauer, E., Rudzki, D., et al. (2021). Signs of sympathetic and endothelial cell activation in the skin of patients with restless legs syndrome. *Sleep Med.* 84, 227–236. doi: 10.1016/j.sleep.2021.05.044

Didato, G., Di Giacomo, R., Rosa, G. J., Dominese, A., de Curtis, M., and Lanteri, P. (2020). Restless legs syndrome across the lifespan: symptoms, pathophysiology, management and daily life impact of the different patterns of disease presentation. *Int. J. Environ. Res. Public Health* 17:3658. doi: 10.3390/ijerph17103658

Ferini-Strambi, L., and Manconi, M. (2009). Treatment of restless legs syndrome. *Parkinsonism Relat. Disord.* 15, S65–S70. doi: 10.1016/S1353-8020(09)70838-7

Gu, C., Zhai, M., Lü, A., Liu, L., Hu, H., Liu, X., et al. (2022). Ultrasound-guided stellate ganglion block improves sleep quality in elderly patients early after thoracoscopic surgery for lung cancer: a randomized controlled study. *Nan Fang Yi Ke Da Xue Xue Bao* 42, 1807–1814. doi: 10.12122/j.issn.1673-4254.2022.12.08

Kambampati, S., Wasim, S., Kukkar, V., Awad, V. M., and Malik, B. H. (2020). Restless leg syndrome in the setting of patients with end-stage renal disease on hemodialysis: a literature review. *Cureus* 12:e9965. doi: 10.7759/cureus.9965

Kenney, M. J., and Ganta, C. K. (2014). Autonomic nervous system and immune system interactions. *Compr. Physiol.* 4, 1177–1200. doi: 10.1002/cphy.c130051

Liao, C. D., Tsauo, J. Y., Liou, T. H., Chen, H. C., and Rau, C. L. (2016). Efficacy of noninvasive stellate ganglion blockade performed using physical agent modalities in patients with sympathetic hyperactivity-associated disorders: a systematic review and Meta-analysis. *PLoS One* 11:e0167476. doi: 10.1371/journal.pone.0167476

Lipov, E., Gluncic, V., Lukić, I. K., and Candido, K. (2020). How does stellate ganglion block alleviate immunologically-linked disorders? *Med. Hypotheses* 144:110000. doi: 10.1016/j.mehy.2020.110000

Makharita, M. Y., Amr, Y. M., and El-Bayoumy, Y. (2012). Effect of early stellate ganglion blockade for facial pain from acute herpes zoster and incidence of postherpetic neuralgia. *Pain Physician* 15, 467–474. doi: 10.36076/ppj.2012/15/467

Narouze, S. (2014). Ultrasound-guided stellate ganglion block: safety and efficacy. *Curr. Pain Headache Rep.* 18:424. doi: 10.1007/s11916-014-0424-5

Noma, N., Kamo, H., Nakaya, Y., Dezawa, K., Young, A., Khan, J., et al. (2013). Stellate ganglion block as an early intervention in sympathetically maintained headache and orofacial pain caused by temporal arteritis. *Pain Med.* 14, 392–397. doi: 10.1111/pme.12040

Stevens, M. S. (2015). Restless legs syndrome/Willis-Ekbom disease morbidity: burden, quality of life, cardiovascular aspects, and sleep. *Sleep Med. Clin.* 10, 369–373. doi: 10.1016/j.jsmc.2015.05.017

Tanaka, S., and Okusa, M. D. (2020). Crosstalk between the nervous system and the kidney. *Kidney Int.* 97, 466–476. doi: 10.1016/j.kint.2019.10.032

Trenkwalder, C., Paulus, W., and Walters, A. S. (2005). The restless legs syndrome. *Lancet* 4, 465–475. doi: 10.1016/S1474-4422(05)70139-3

Walters, A. S., and Rye, D. B. (2009). Review of the relationship of restless legs syndrome and periodic limb movements in sleep to hypertension, heart disease, and stroke. *Sleep* 32, 589–597. doi: 10.1093/sleep/32.5.589

Weinstock, L. B., Walters, A. S., and Paueksakon, P. (2012). Restless legs syndrome--theoretical roles of inflammatory and immune mechanisms. *Sleep Med. Rev.* 16, 341–354. doi: 10.1016/j.smrv.2011.09.003

Xu, X. M., Liu, Y., Jia, S. Y., Dong, M. X., Cao, D., and Wei, Y. D. (2018). Complementary and alternative therapies for restless legs syndrome: an evidence-based systematic review. *Sleep Med. Rev.* 38, 158–167. doi: 10.1016/j.smrv.2017.06.003

Yang, X., Shi, Z., Li, X., and Li, J. (2015). Impacts of stellate ganglion block on plasma NF-κB and inflammatory factors of TBI patients. *Int. J. Clin. Exp. Med.* 8, 15630–15638.

Zhu, B., Yin, D., Zhao, H., and Zhang, L. (2022). The immunology of Parkinson's disease. *Semin. Immunopathol.* 44, 659–672. doi: 10.1007/s00281-022-00947-3

frontiers | Frontiers in Physiology

TYPE Original Research
PUBLISHED 19 February 2024
DOI 10.3389/fphys.2024.1340061

OPEN ACCESS

EDITED BY
Luiz Carlos Marques Vanderlei,
São Paulo State University, Brazil

REVIEWED BY
Alan José Barbosa Magalhães,
São Paulo State University, Brazil
Gang Li,
Zhejiang Normal University, China

*CORRESPONDENCE
Wendong Hu,
doatea@fmmu.edu.cn
Lin Cong,
hzbconglin@fmmu.edu.cn

†These authors have contributed equally to this work and share first authorship

RECEIVED 17 November 2023
ACCEPTED 31 January 2024
PUBLISHED 19 February 2024

CITATION
Cheng S, Li W, Hui D, Ma J, Zhang T, Teng C, Dang W, Xiong K, Hu W and Cong L (2024), Acute combined effects of concurrent physical activities on autonomic nervous activation during cognitive tasks.
Front. Physiol. 15:1340061.
doi: 10.3389/fphys.2024.1340061

Acute combined effects of concurrent physical activities on autonomic nervous activation during cognitive tasks

Shan Cheng[1†], Wenbin Li[2†], Duoduo Hui[1], Jin Ma[1], Taihui Zhang[1], Chaolin Teng[1], Weitao Dang[1], Kaiwen Xiong[1], Wendong Hu[1*] and Lin Cong[1*]

[1]Department of Aerospace Medical Equipment, School of Aerospace Medicine, Air Force Medical University, Xi'an, Shaanxi, China, [2]Department of Aerospace Hygiene, School of Aerospace Medicine, Air Force Medical University, Xi'an, Shaanxi, China

Backgrounds: The validity of heart rate variability (HRV) has been substantiated in mental workload assessments. However, cognitive tasks often coincide with physical exertion in practical mental work, but their synergic effects on HRV remains insufficiently established. The study aims were to investigate the combined effects of cognitive and physical load on autonomic nerve functions.

Methods: Thirty-five healthy male subjects (aged 23.5 ± 3.3 years) were eligible and enrolled in the study. The subjects engaged in n-back cognitive tasks (1-back, 2-back, and 3-back) under three distinct physical conditions, involving isotonic contraction of the left upper limb with loads of 0 kg, 3 kg, and 5 kg. Electrocardiogram signals and cognitive task performance were recorded throughout the tasks, and post-task assessment of subjective experiences were conducted using the NASA-TLX scale.

Results: The execution of n-back tasks resulted in enhanced perceptions of task-load feelings and increased reaction times among subjects, accompanied by a decline in the accuracy rate ($p < 0.05$). These effects were synchronously intensified by the imposition of physical load. Comparative analysis with a no-physical-load scenario revealed significant alterations in the HRV of the subjects during the cognitive task under moderate and high physical conditions. The main features were a decreased power of the high frequency component ($p < 0.05$) and an increased low frequency component ($p < 0.05$), signifying an elevation in sympathetic activity. This physiological response manifested similarly at both moderate and high physical levels. In addition, a discernible linear correlation was observed between HRV and task-load feelings, as well as task performance under the influence of physical load ($p < 0.05$).

Conclusion: HRV can serve as a viable indicator for assessing mental workload in the context of physical activities, making it suitable for real-world mental work scenarios.

KEYWORDS

heart rate variability, cognitive task, physical load, combined effects, mental work scenarios, electrocardiogram (ECG)

1 Introduction

In specific occupations such as airplane pilots and automobile drivers, mental workload constitutes a crucial risk factor that imperils personnel safety and demands careful consideration. Elevated mental load during tasks can precipitate mental fatigue, which eventually leads to an escalation in human errors and safety accidents (Jacquet et al., 2020; Ramírez-Moreno et al., 2021). Statistics indicate a direct correlation between driver fatigue and 20% of traffic accidents (Wilson et al., 2020). Conversely, insufficient mental workload may compromise alertness levels, hindering the timely mobilization of brain resources and potentially resulting in an accident. Real-time monitoring of the mental load level of operators during tasks holds practical significance, enabling the prompt and accurate identification of mental status and effectively minimizing the risk of accidents.

Current mental workload assessment methods, encompassing subjective and objective approaches, have distinct advantages and drawbacks. Subjective methods, such as the NASA task load index (NASA-TLX) (Wilson et al., 2021) and fatigue assessment scale (Ramírez-Moreno et al., 2021), use rating scales to evaluate mental workload at specific moments but face challenges in real-time monitoring due to questionnaire interruptions. Maintaining the natural working environment and operators' activities is crucial, but subjective methods may compromise task execution (Albuquerque et al., 2020). In contrast, objective measurement methods, including electroencephalogram (EEG) (Zhang et al., 2021; Chitti et al., 2021; Wriessnegger et al., 2021), eye movement features (represented by blink, pupil diameter and saccade) (Bafna and Hansen, 2021), heart rate variability (HRV) (Burlacu et al., 2021) and postural stability indicators (Cheng et al., 2018; Sun et al., 2019), rely on biological signals and offer promising avenues for effective and objective mental workload assessment without disrupting tasks. These approaches pave the way for more precise and real-time monitoring, ensuring a comprehensive understanding of mental workload dynamics during various activities.

Recent progress in wearable technology has revolutionized the acquisition of biological signals in real work scenarios. Advanced features such as wireless transmission, miniaturized amplifiers (Wascher et al., 2023), and dry electrodes (Ramírez-Moreno et al., 2021) have enhanced the application of highly portable EEG head-mounted devices, proving crucial for research in real mobile environments. Technologies like the ballistocardiogram (BCG), using a fiber sensor cushion (Xu et al., 2021) or photoplethysmogram (PPG) integrated into a helmet (Wilson et al., 2020) have enabled the simultaneous collection of biological signals alongside the primary task, offering the capability to capture changes in the operators' functional status before an alteration in task performance occurs. With superior temporal resolution compared to subjective methods, these approaches serve as pivotal tools for real-time mental workload assessment during tasks.

Comparing ECG to portable EEG acquisition technology, the former exhibits significantly enhanced anti-interference capabilities (Wang et al., 2016; Dai et al., 2021; Klug and Gramann, 2021; Teng et al., 2021), showing efficacy in evaluating mental fatigue within laboratory settings. Studies have demonstrated a correlation between ECG signals and psychomotor vigilance task (PVT) performance, as well as the effectiveness of HRV indices in assessing cognitive task-related errors. Leveraging sensitive features extracted from ECG, algorithms like learning vector quantization and random forest tree classifiers achieve impressive accuracy in identifying fatigue states, underscoring HRV as a potential indicator for evaluating worker fatigue (Chua et al., 2012; Zhao et al., 2012; Pan et al., 2021; Xu et al., 2021; Takada et al., 2022).

However, the authentic mental work environment, dominated by a cognitive load (CL), is frequently accompanied by physical activities, stress, pressure and other non-cognitive factors, all of which can alter the characteristics of biological signals. Currently, researchers have initiated investigations into the impact of increased physical load (PL), stress and other factors during cognitive tasks on physiological and psychological functions. For instance, significant changes in EEG-related indexes were observed when subjects engaged in a cognitive task while cycling (Xu et al., 2018). In the study by Zink and others, subjects were tasked with performing a three-level Oddball auditory task while cycling. EEG analysis showed a decrease in the P300 component of event-related potentials during physical activities in unrestrained conditions (Zink et al., 2016). Blons research group found that vagus nerve activities and entropy indexes increased in the cognitive task alone, while the entropy index of HRV decreased with the addition of stress factors (Blons et al., 2019). Confounding factors in a real work scenario may disrupt the balance of sympathetic and parasympathetic nerve activity, resulting in substantial variations in sensitivity (47.1%–95%) and specificity (74.6%–98%) in driving fatigue recognition parameters based on HRV indicators across different studies (Burlacu et al., 2021).

While mental workload in most existing research protocols is induced by sleep deprivation (Cheng et al., 2021), continuous cognitive tasks such as an n-back task (Karthikeyan et al., 2021; Wriessnegger et al., 2021) and a Stroop task (Nikooharf Salehi et al., 2022), these protocols often overlook the role of non-cognitive variables, particularly physical factors. The real-time evaluation of mental workload based on ECG signals is undoubtedly influenced by dynamics. Because the working process of mental workers is not static, then PL becomes an important non-cognitive factors. Therefore, the aims of this study were to explore the changes in ECG signals during different PL and CL under a background of dynamic tasks.

2 Materials and methods

2.1 Subjects

Thirty-five male subjects, aged between 20 and 32 years (mean 23.5 ± 3.3 years), were enrolled in the study. Inclusion criteria were: being right-handed; absence of diseases and injury affecting physical activities in the past 3 months; and no recent use of alcohol and specific medications. Based on self-reporting, subjects had a minimum of ≥6 h of sleep per day during the week preceding the study experiments. Additionally, subjects willingly provided written informed consent and agreed not to withdraw from the ongoing study for subjective reasons or concerns.

2.2 Experimental tasks

2.2.1 Design of cognitive load

In the current study, the n-back working memory task program introduced by Wriessnegger et al. (2021), was applied to induce mental workload and fatigue states in the study subjects. At the initiation of the n-back task, subjects received instructions, followed by a sequence of letters. Their task was determined whether the current presented letter matched the one shown n letters prior, essentially identifying the target letter in the sequence. The criteria for the target letter were established such that if the current letter matched the one presented n letter before, it was considered the target letter. Three variation of n-back tasks (1-back, 2-back, and 3-back) with differing difficulty levels were employed. Each trial consisted of 20 letters, including 5 target letters. Prior to the trial, a 2-s instruction informed subjects about the type of n-back task to be performed. Subsequently, each trial lasted 40 s, with each letter displayed for 0.5 s and an interval of 1.5 s. Subjects were required to press the symbol "↑" symbol on the keyboard upon recognizing the target letter. Following the completion of a trial, subjects had a 6-s break. Thus, one trial encompassed 50 s. To complete each run of a specific n-back task type, a total of 6 consecutive trials were conducted, taking approximately 5 min.

2.2.2 Design of physical load

In these experiments, isotonic contraction of the left upper limb was used to simulate the PL encountered during mental work, ensuring no interfere with n-back tasks performed using the right hand. Contractile resistance was introduced by holding a dumbbell, categorized into three levels of PL: no PL (none, 0 kg); moderate PL (medium, 3 kg); and a high PL (high, 5 kg). When applying PL to the subject, the preparation posture involved a 90-degrees flexion of the left arm. During lifting, the forearm was maintained an angle <45° from the upper arm, indicating effective contraction. The lift frequency during the cognitive task was once every 2 s, aligning with the letter presentation frequency of n-back tasks.

2.3 Assessment of task load

2.3.1 Subjective scale assessment

The NASA-TLX was used to evaluate the experiences of subjects across six dimensions: mental demand, physical demand, time demand, self-performance, effort level and the frustration level. Subjects self-evaluated their feelings on a 21-point scale for each dimension. The six dimensions were combined into 15 pairs, and subjects were tasked with selecting the more significant factor within each pair. Subsequently, weights ranging from 1/21 to 6/21 were assigned based on the frequency of selections, ordered from the lowest to the highest. The total score was then calculated.

2.3.2 HRV based on ECG data

In this study, the Dutch Spirit multi-channel biofeedback system was used to record ECG data at a sampling frequency of 256 Hz during the task. Initially, municipal electricity interference, myoelectric interference and baseline drift noise in ECG signal were mitigated using median filtering and moving average methods. Subsequently, the difference threshold method was used to extract the peak value of QRS, yielding the RR interval. To ensure the accuracy of RR interval calculation, outlier values were identified and screened using the fill outliers' function in Matlab software, followed by linear interpolation between adjacent non-outlier values. This processed resulted in the acquisition of a preprocessed RR interval sequence from the raw ECG signal. The HRV characteristics of each stage were extracted based on the RR interval.

The time domain characteristic indices were computed through time series analysis of the RR interval, including: (1) mean heart rate (meanHR); (2) standard deviation of normal-to-normal beats (SDNN), representing the overall profile of HRV by calculating the standard deviation of all RR intervals within a specific time; (3) the number and percentage of difference between adjacent RR intervals exceeding 50 ms (NN50, pNN50), sensitive indicators of vagus nerve activity, with higher values signifying increased vagus nerve excitability; and (4) root mean square difference (RMSSD); the root mean square value of the differences between adjacent RR intervals, reflecting the high-frequency component of HRV, where higher values indicate greater vagal tone.

Autoregressive models were used in this study to analyze the frequency domain characteristics of HRV. The power spectrum of the RR interval sequence was categorized into three primary frequency bands: high frequency band (HF: 0.150–0.400 Hz), low frequency band (LF: 0.040–0.150 Hz), and very low frequency band (VLF: 0.003–0.040 Hz). Key frequency-domain parameters included: (1) VLF, LF and HF, representing the absolute power density in VLF, LF, and HF bands, respectively. LF indicates the level of sympathetic nerves activity, while HF reflects the regulatory strength of the vagus nerve. Total power density (Total) is the sum of VLF, LF and HF, providing a measure of overall HRV; (2) the LF/HF ratio, signifies the balance between sympathetic and vagal nerve activity; (3) the normalized low-frequency power (nLF) is the value of LF relative to the sum of LF and HF, indicating the relative levels of sympathetic nerves activity; and (4) normalized HF power (nHF), reflecting the degree of vagal regulation.

2.3.3 Cognitive performance

The outcomes derived from the n-back task employed in this study primarily fall into two categories: (1) Reaction time (RT) for identifying the target letter, encompassing mean RT (MRT), standard deviation of RT (SDRT), maximum RT (maxRT), and minimum RT (minRT); (2) Performance indicators consisted of the ratio of correct reactions (CNR), the ratio of missing reactions (MNR) and ratio of incorrect reactions (WNR).

2.4 Experimental procedure

In this study, two independent variables (CL and PL) were established and implemented through a repeated measurement design with cross-control within the group (Figure 1). Specifically, CL featured three levels (1-back, 2-back, 3-back), while PL also had three levels (None, Medium, High). The experimental protocol unfolded across three stages, each with distinct PL levels, and there was a 1-week interval between stages. First, the ECG signals were collected from subjects in a resting state before each stage, serving as the baseline data. The three

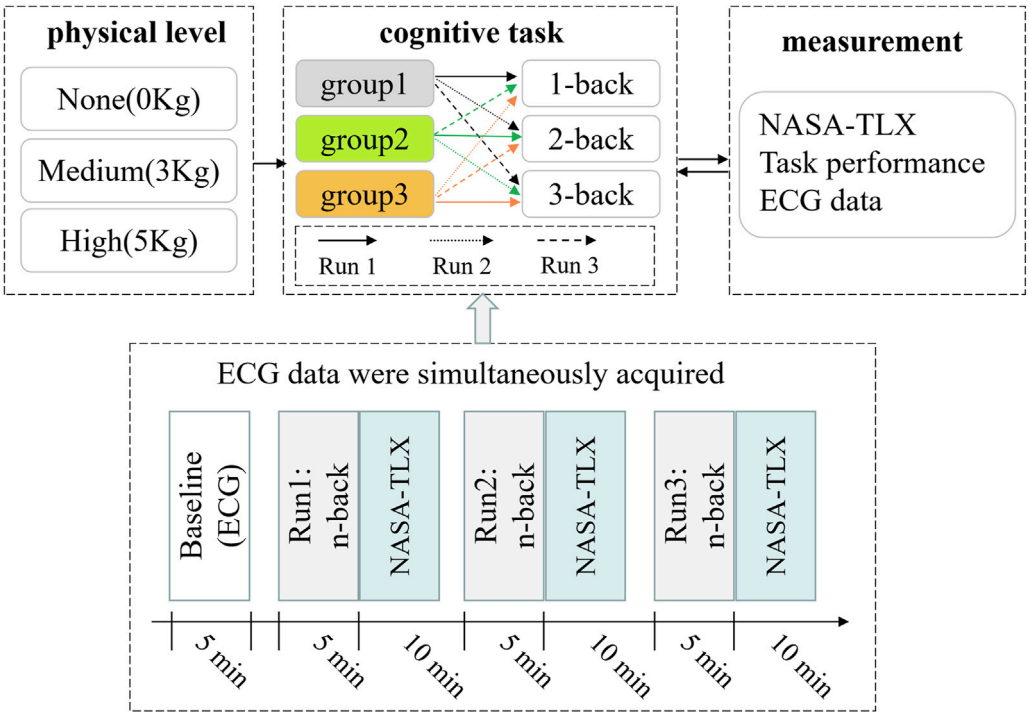

FIGURE 1
Experimental design and flow chart. Run1, Run2, and Run3 represent n-back tasks with three difficulty levels running in a preset order, respectively.

electrodes of the ECG were placed, respectively beneath the midpoint of the left clavicle, beneath the midpoint of the right clavicle, and slightly to the left of the xiphoid process.

Subsequently, subjects sequentially performed n-back cognitive tasks of varying difficulty levels, with concurrent recording of ECG signals. Following each run of n-back tasks, the NASA-TLX index was used to evaluate the subjective task load.

When conducting the n-back tasks across three difficulty levels (1-back, 2-back, 3-back), a crossover design within the group was implemented to avoid the effect of task orders (Figure 1). For example, under the no-physical level condition (none), all subjects were equitably and randomly allocated into three sub-groups (group 1, group 2, and group 3) to execute the n-back task following a pre-designed sequence. Group 1 underwent tasks in the order of 1-back, 2-back and 3-back; group 2 performed cognitive tasks in the sequence of 2-back, 3-back and 1-back; group 3 executed tasks in the order of 3-back, 1-back, and 2-back. A 10-min interval was allowed between successive n-back tasks. A similar task order protocol was applied to subjects in the medium and high physical level conditions, as in the no-physical condition.

2.5 Statistical analysis

All statistical analyses were performing using SPSS ver. 23.0. In cases where the collected data exhibited a normal distribution and homogeneity of variance, repeated measures analysis of variance (rmANOVA) and a paired *t*-test were used for multiple comparisons. If there were assumptions that were not met, the Friedman test and Wilcoxon signed rank test were employed. First, the analysis focused on examining differences of subjective feelings and task performance across n-back cognitive tasks to assess mental load levels. Subsequently, the impact of PL on HRV features were analyzed. Finally, Spearman's rank correlation was used to evaluate the correlation between HRV and subjective feelings, as well as task performance. A significance of $p < 0.05$ was considered to indicative of a statistically significant finding.

3 Results

3.1 Mental load level induced by n-back tasks under PL

The main effects of CL and PL on NASA-TLX score and task performance were determined through rmANOVA. As the difficulty of the n-back task increased, the subjective task load demonstrated a significant rise (mental demand: $F = 44.800$, $p < 0.001$; effort: $F = 12.412$, $p < 0.001$; frustration level: $F = 24.350$, $p < 0.001$). Additionally, an increase in PL resulted in a significant elevation of the task load level, particularly in time demand ($F = 5.026$, $p = 0.007$) and effort ($F = 11.078$, $p < 0.001$). Similarly, the cognitive tasks had a significant impact on subjects' reaction time, leading to a significant prolongation (MRT: $F = 58.045$, $p < 0.001$; SDRT: $F = 90.316$, $p < 0.001$), along with a remarkable decrease in the rate of correct responses (CNR: $F = 73.439$, $p < 0.001$). PL also influenced subjects' reaction times, resulting in a significant prolongation (MRT: $F = 3.924$, $p = 0.021$; SDRT: $F = 4.770$, $p = 0.009$) and a decrease in CNR ($F = 3.984$, $p = 0.020$) (See Supplementary Material).

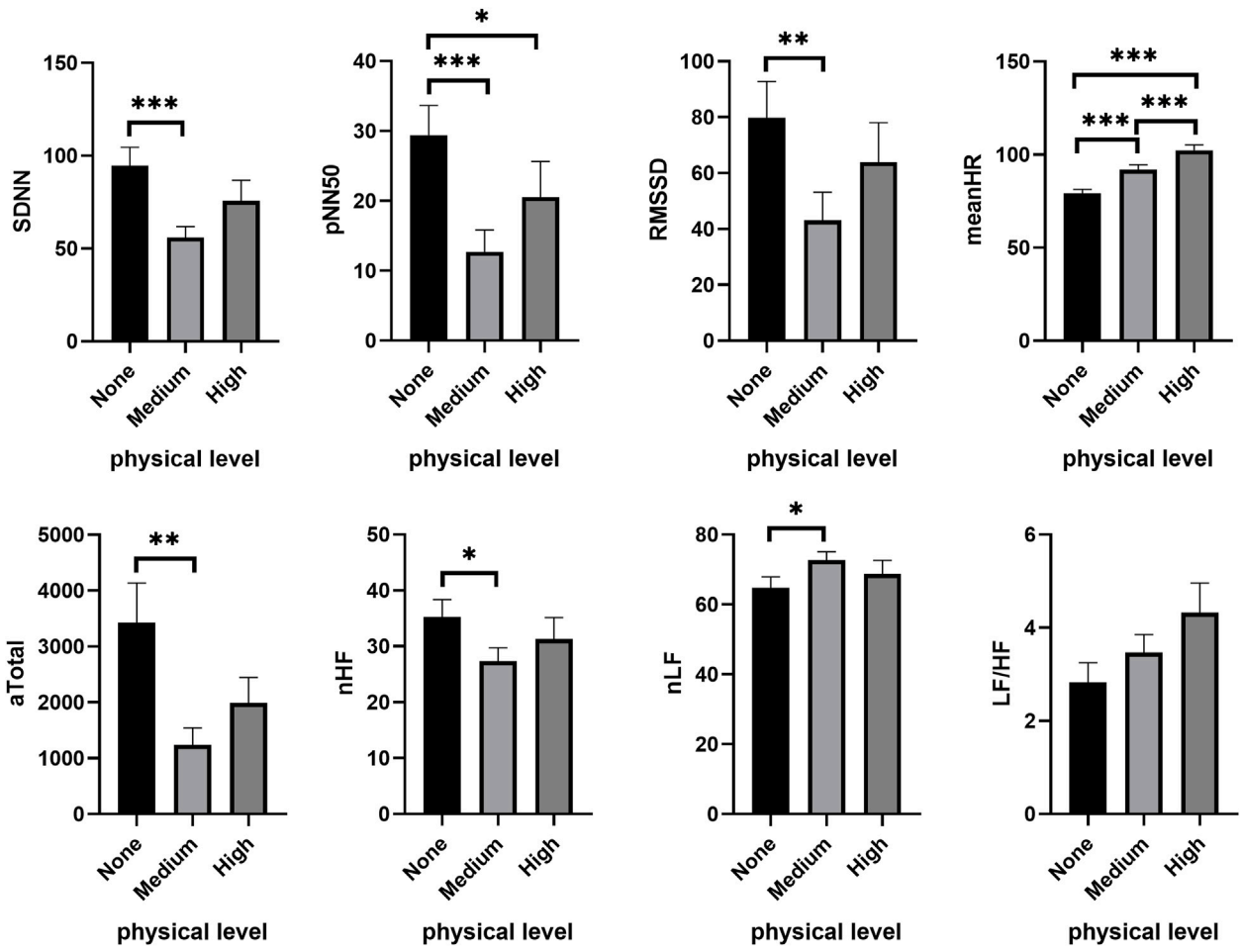

FIGURE 2
Changes of HRV features under different PL in the low CL condition. "None," "Medium" and "High" respectively show the physical level during tasks. *$p < 0.05$, **$p < 0.01$, ***$p < 0.001$. Data are plotted the mean ± SEM. aTotal, Absolute value of total power density; CL, cognitive load; LF/HF, ratio of low-frequency and high frequency power; meanHR, mean heart rate; nHF, normalized high frequency power; nLF, normalized low-frequency power; PL, physical load; pNN50, percentage of the difference between adjacent RR intervals >50 ms; RMSSD, root mean square difference; SDNN, standard deviation of normal to normal beats.

3.2 Combined effects of PL with CL on autonomic nervous activity

The autonomic nervous system exhibited similar activity across different PL groups (See Supplementary Material). Under a low CL condition (1-back), PL significantly reduced SDNN ($\chi^2 = 21.063$, $p < 0.001$), NN50 ($\chi^2 = 12.110$, $p = 0.002$), pNN50 ($\chi^2 = 17.055$, $p < 0.001$) and RMSSD ($\chi^2 = 12.000$, $p = 0.002$), while meanHR obviously increased ($\chi^2 = 40.268$, $p < 0.001$). In comparison to no PL (none), subjects' SDNN (Wilcoxon signed ranks test, $Z = -4.282$, $p < 0.001$), NN50 ($Z = -3.413$, $p = 0.001$), pNN50 ($Z = -3.805$, $p < 0.001$), RMSSD ($Z = -3.272$, $p = 0.001$) and meanHR ($Z = -3.572$, $p < 0.001$) were all significantly increased at medium PL (Figure 2). At high PL, the subjects' pNN50 ($Z = -2.281$, $p = 0.023$) was significantly decreased, while meanHR ($Z = -4.544$, $p < 0.001$) significantly increased. Compared with medium PL, meanHR ($Z = -3.331$, $p < 0.001$) significantly increased. In addition, PL significantly reduced the power density value of HRV, including VLF ($\chi^2 = 21.438$, $p < 0.001$), LF ($\chi^2 = 10.938$, $p = 0.004$), HF ($\chi^2 = 9.750$, $p = 0.008$) and Total ($\chi^2 = 10.563$, $p = 0.005$), all of which decreased significantly. Compared to no PL, VLF ($Z = -3.160$, $p = 0.002$), LF ($Z = -3.160$, $p = 0.002$), HF ($Z = -3.141$, $p = 0.002$), Total ($Z = -3.403$, $p = 0.001$), nHF ($Z = -2.151$, $p = 0.032$) decreased significantly at medium PL, while nLF ($Z = -2.151$, $p = 0.032$) increased significantly. At high PL, VLF ($Z = -4.245$, $p < 0.001$) was further reduced.

The effects of PL on HRV under higher CL (2-back and 3-back) mirrored that observed under low CL (1-back). In the moderate CL condition (2-back), PL significantly decreased SDNN ($\chi^2 = 6.750$, $p = 0.034$), NN50 ($\chi^2 = 14.736$, $p = 0.001$), pNN50 ($\chi^2 = 16.528$, $p < 0.001$) and RMSSD ($\chi^2 = 11.313$, $p = 0.003$), while the meanHR increased ($\chi^2 = 43.938$, $p < 0.001$). Furthermore, PL also significantly reduced the absolute values of HF ($\chi^2 = 12.000$, $p = 0.002$) and Total ($\chi^2 = 7.000$, $p = 0.030$) during cognitive tasks. As shown in Figure 3, compared to no PL (none), time-domain and frequency-domain features of HRV underwent significant changes under the medium PL condition, including SDNN ($Z = -2.122$, $p = 0.034$), NN50 ($Z = -3.245$, $p = 0.001$), pNN50 ($Z = -3.282$, $p = 0.001$), RMSSD

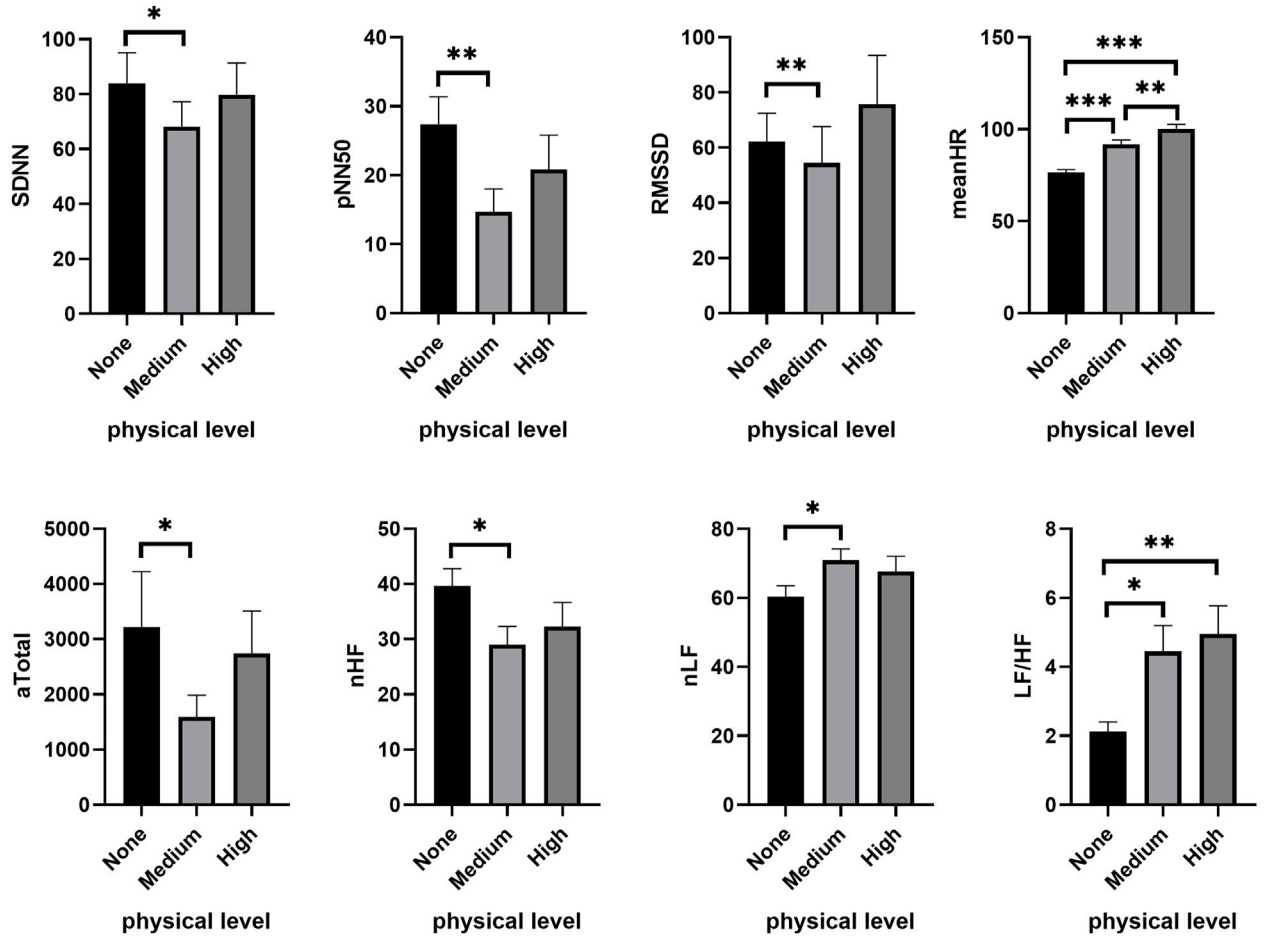

FIGURE 3
Changes of HRV features under different PL in the moderate CL condition. *$p < 0.05$, **$p < 0.01$, ***$p < 0.001$. Data are plotted as the mean ± SEM. CL, cognitive load; PL, physical load.

($Z = -2.655$, $p = 0.008$), LF/HF ($Z = -2.580$, $p = 0.010$), and the proportion of low frequencies (nLF) ($Z = -2.188$, $p = 0.029$). These latter changes in HRV were not obvious under the high PL condition.

In the high CL condition (3-back), subjects exhibited a significant decrease in SDNN ($\chi^2 = 6.063$, $p = 0.048$), NN50 ($\chi^2 = 8.368$, $p = 0.015$), pNN50 ($\chi^2 = 9.424$, $p = 0.009$) and RMSSD ($\chi^2 = 7.313$, $p = 0.026$) with increasing PL, along with a significant rise in meanHR ($\chi^2 = 26.313$, $p < 0.001$). The reduction in subjects' HF ($\chi^2 = 7.938$, $p = 0.019$), Total ($\chi^2 = 6.750$, $p = 0.034$), nHF ($\chi^2 = 6.813$, $p = 0.033$), and the increase in the ratio of LF/HF ($\chi^2 = 9.250$, $p = 0.010$) and nLF ($\chi^2 = 6.813$, $p = 0.033$) were induced by increasing PL during the cognitive task. Figure 4 shows that certain HRV parameters changed noticeably at medium PL, including a decrease in NN50 ($Z = -2.469$, $p = 0.014$), pNN50 ($Z = -2.739$, $p = 0.006$) and the proportion of HF (nHF: $Z = -2.394$, $p = 0.017$), coupled with an increase in the LF/HF ratio ($Z = -3.216$, $p = 0.001$) and nLF ($Z = -2.394$, $p = 0.017$) (Figure 4). No significant difference was found between medium and high PL.

Regardless of the CL, these results suggested that subjects' HR increased with an elevation in PL, while the absolute energy in different frequency bands decreased. The relative proportion of the frequency value increased, while the proportion of HF decreased.

3.3 Correlation of HRV with CL under the effects of PL

Spearman's correlation analysis revealed a significant relationship between HRV indexes under different CL conditions and subjective feelings in the absence of PL (none). In Table 1, the NASA-TLX total score exhibited a significant positive correlation with the LF/HF ratio ($r = 0.204$, $p = 0.049$) and nLF ($r = 0.226$, $p = 0.003$), and a negative correlation with aTotal ($r = -0.272$, $p = 0.008$), nHF ($r = -0.226$, $p = 0.003$), SDNN ($r = -0.324$, $p = 0.002$), pNN50 ($r = -0.260$, $p = 0.012$) and RMSSD ($r = -0.297$, $p = 0.004$). Under the medium PL condition, the meanHR showed a positive correlation with the NASA-TLX score ($r = 0.210$, $p = 0.044$). Furthermore, the RT for a cognitive task exhibited a positive correlation with the LF/HF ratio ($r = 0.223$, $p = 0.032$) and nLF ($r = 0.205$, $p = 0.049$), while showing a negative correlation with nHF ($r = -0.205$, $p = 0.049$). In the presence of high PL, significant correlations were found between HRV with subjective workload. For

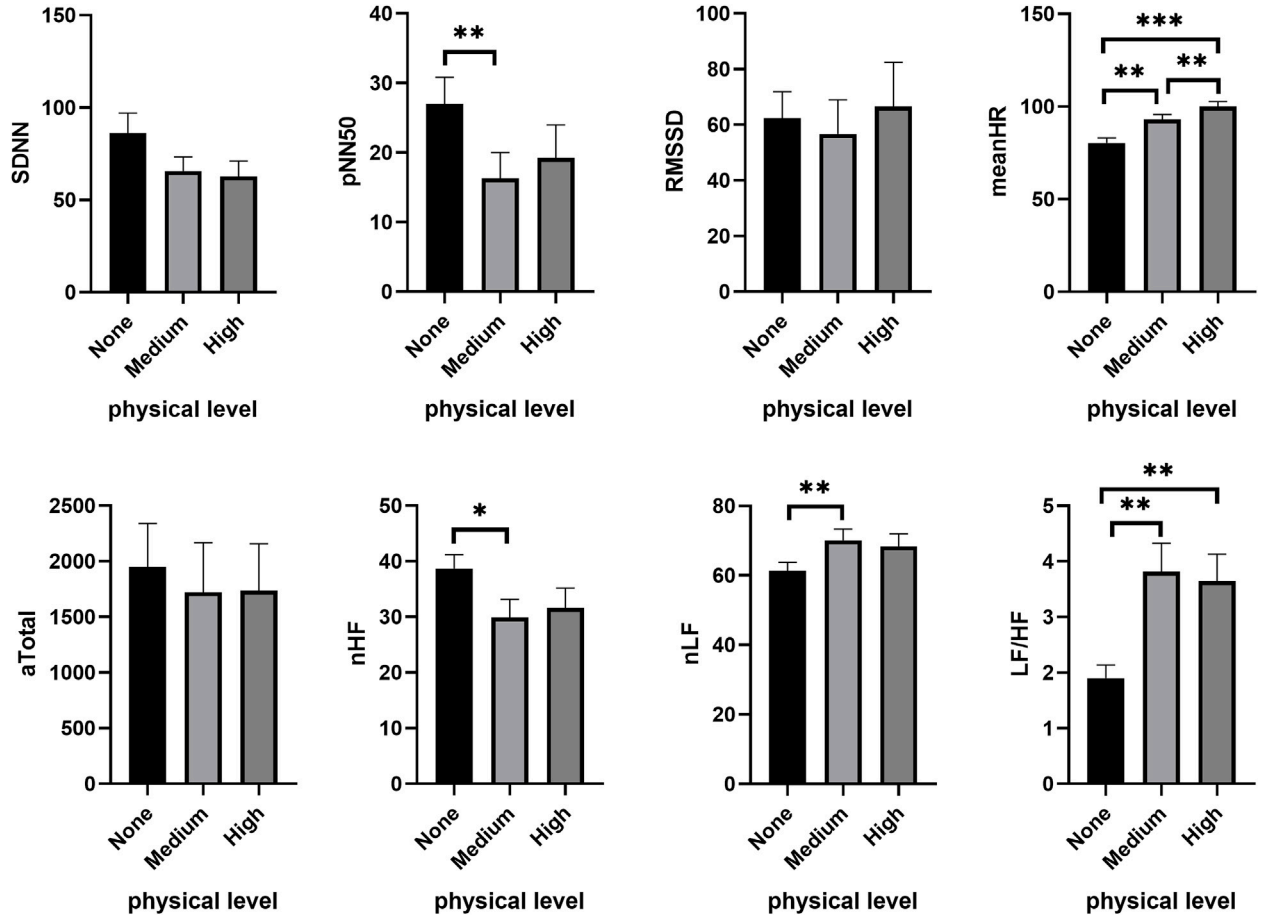

FIGURE 4
Changes of HRV features under different PL in high CL condition. *$p < 0.05$, **$p < 0.01$, ***$p < 0.001$. Data are presented as the mean ± SEM.

example, the NASA-TLX total score revealed a significant correlation between LF/HF ($r = 0.271$, $p = 0.009$), nLF ($r = 0.270$, $p = 0.009$) and nHF ($r = -0.270$, $p = 0.009$).

4 Discussion

In the present study, the HRV of subjects were investigated during cognitive tasks under moderate and high physical conditions, and the results showed significant alterations compared to scenarios without physical load. Additionally, a clear linear correlation was found between HRV and task-load perceptions, as well as task performance under the influence of physical load ($p < 0.05$).

Researchers could approach the real-time monitoring of mental workload during dynamic tasks by considering the interaction between various physiological loads and cognitive tasks. Previous experimental paradigms employed to induce mental workload often overlooked the impact of non-cognitive factors (PL, stress, etc.) within an authentic dynamic work scenario. Cheng et al. investigated postural control changes in a mentally fatigue state induced by 36 h of sleep deprivation (Cheng et al., 2018). Karthikeyan et al. employed a 1-h visuo-spatial 2-back task to study the effects of anodal transcranial direct current stimulation on working memory under fatigue (Karthikeyan et al., 2021). Additionally, a 60 min Stoop color-word task (Nikooharf Salehi et al., 2022) and a flight simulator task (Pan et al., 2021) were used to induce a mental state of fatigue. While these models may be suitable for scenarios involving static operators, they might not be applicable to actual dynamic settings, such as those encountered by pilots, firefighters and first responders. Therefore, in the present study, isotonic contraction of the upper limbs of subjects at various resistances were used to simulate the PL that dynamic operators encounter during mental work.

Regardless of the impact of PL, the n-back tasks of varying difficulties in this study elicited distinct levels of mental load. Evaluation through the NASA-TLX scale showed significant increases in psychological needs, time demand, effort and frustration levels, coupled with a significant decrease in self-performance. The n-back task performance exhibited adverse effects, including the extension of the MRT and maxRT, an increase in wrong responding rates, and a decrease in correct rates. These outcomes are in good agreement with the findings of previous study (Wriessnegger et al., 2021). To induce diverse levels of mental workload, Wriessnegger et al. instructed subjects to engage in three types of n-back tasks (1-back, 2-back, and 3-back) for three trials (20 min each, 60 min in total) (Wriessnegger et al., 2021). Moreover, this study also found that PL could further enhance the subjective perceptions on task loads when subjects undertook

TABLE 1 Correlation coefficients between HRV and cognitive task load under the influence of PL.

HRV	None physical level		Medium physical level		High physical level	
	Subjective feelings	Mean reaction time	Subjective feelings	Mean reaction time	Subjective feelings	Mean reaction time
aVLF	−.275**	−0.198	−0.042	0.028	−0.035	−0.042
aLF	−.240*	−0.071	−0.076	0.136	−0.069	−0.127
aHF	−.329**	−0.016	−0.082	0.035	−0.182	−0.116
aTotal	−.272**	−0.105	−0.053	0.08	−0.122	−0.095
LF/HF	.204*	−0.100	−0.013	.223*	.271**	0.028
nHF	−.226*	0.092	0.004	−.205*	−.270**	−0.027
nLF	.226*	−0.092	−0.004	.205*	.270**	0.027
SDNN	−.324**	−0.15	−0.023	0.095	−0.142	−0.146
NN50	−.228*	−0.031	0.004	0.100	−0.171	−0.086
pNN50	−.260*	−0.001	−0.034	0.08	−0.162	−0.087
RMSSD	−.297**	−0.045	−0.038	0.062	−0.156	−0.107
MeanHR	0.103	0.138	.210*	−0.049	−0.121	0.022

Note: Spearman's rho was used to determine the correlation between HRV, and task load. *$p < 0.05$, **$p < 0.01$.
aHF, absolute value of power density in high frequency band; aLF, absolute value of power density in low frequency band; aTotal, absolute value of total power density; aVLF, absolute value of power density in very low frequency band; LF/HF, ratio of low-frequency and high frequency power; meanHR, mean heart rate; nHF, normalized high frequency power; nLF, normalized low-frequency power; NN50, number and percentage of the difference between adjacent RR, intervals >50 ms; pNN50, percentage of the difference between adjacent RR, intervals >50 ms; RMSSD, root mean square difference; SDNN, standard deviation of normal to normal beats.

n-back cognitive tasks. This result is consistent with previous outcomes, as demonstrated in the study by Albuquerque et al., where the mental demand scores of NASA-TLX further increased when subjects performed multi-cognitive tasks under the effect of PLs (Albuquerque et al., 2020).

Although our findings, indicating that PL can significantly increase the RT of cognitive tasks and reduce task performance, may appear somewhat inconsistent with previous studies, it is noteworthy that beneficial effects of physical activities have been reported. Most previous studies have demonstrated significantly faster response times during cognitive tasks (Zhu et al., 2021; Engeroff et al., 2022) and improved accuracy rates (Gao et al., 2021; Zheng et al., 2022) following physical activities or exercise interventions, such as cycling. Upon analyzing the experimental conditions, it became evident that the positive effects on works' cognitive ability typically manifest after acute physical exercises, a condition distinct from our study.

The concurrent presence of PL has been associated with a reduction in EEG activity (Xu et al., 2018) and ERP component amplitudes (P_{300} wave) (Zink et al., 2016) during the performance of cognitive tasks. Studies utilizing functional near infrared spectroscopy have also suggested that while acute aerobic exercise improves working memory performance, activities in the bilateral frontal pole area, dorsolateral prefrontal cortex (dlPFC) and other regions may decrease (Zheng et al., 2022). However, after acute exercise, the degree of activation of dlPFC (Fujihara et al., 2021) and its correlation with behavioral performance were enhanced (Zhang et al., 2021). Taken together, these results suggest that improvement of behavioral performance after physical activity may stem from the compensatory activation of relevant brain areas after exercise.

In the absence of influence of PL, subjects' HRV features underwent significant changes as the cognitive task load increased. The autonomic nervous system, consisting of the sympathetic and parasympathetic nervous systems, regulates the arousal level of workers and is closely related to fluctuation in HR (Maiorana et al., 2022; Garis et al., 2023). The substantial reduction in the high-frequency value of HRV and the low-frequency value may be indicative of increased activity in the sympathetic nervous system, and *vice versa*. Studies have reported that an increase in mental workload or the onset of mental fatigue leads to activation of the sympathetic nervous system (Wehrens et al., 2012; Chen et al., 2013). However, it is essential to acknowledge that physical activity has a significant influence on the autonomic nervous system. Alfonso et al. conducted a study involving 123 HRV recordings in the morning and 66 recordings of training intensity over a 6-week period with 5 recreational road cyclists. The results indicated that the higher training intensity on a given day correlated with a lower normalized HF and higher LF/HF values the next morning (Alfonso and Capdevila, 2022). It is plausible that under the influence of PL, sympathetic nervous system activity increases and vagal activity decreases.

Under the combined condition of a cognitive task and physical factors in our study, HRV also exhibited significant changes with an increase in PL, wherein the HF component of HRV decreased, and the LF component increased. These results suggest a decrease in vagal activity and an increase in sympathetic nervous system activity, aligning with observations made by previous researchers. Dallaway et al. studied the effects of mental fatigue on grip strength training by using a Stroop color classification task (with response inhibition) and n-back memory update task (without response

inhibition). They found that the Stroop and 2-back tasks elicited higher HRs, lower HRV and greater fatigue compared to the control task (Dallaway et al., 2022). During isometric contraction of the quadriceps femoris while performing cognitive tasks, subjects' sympathetic nervous system activity increased along with the sense of muscle exertion (Chatain et al., 2019). However, in the presence of PL, HRV did not exhibit statistically significant changes when subjects performed cognitive tasks at different levels. Another study that explored the cognitive task induced by smartphone use during resistance exercise found no significant effect on HRV (Fortes et al., 2022). These findings suggest that physical factors may play a dominant role in the combined effect, thereby attenuating the influence of CL on HRV.

Moreover, correlation analysis showed a liner relationship between HRV indexes, subjective feelings, and cognitive performance under the influence of PL during cognitive tasks. The degree of correlation varied in our study with different levels of PL. These results suggest that HRV remains a potential effective indicator of task load in actual dynamic mental work scenarios when combined with physical factors. Previous research also noted an increase in the high-frequency component of HRV and enhanced vagal activity when fatigue reached a critical level (Vaara et al., 2009; Konishi et al., 2013). Thus, as the degree of mental fatigue intensifies, the effects of CL and PL may be opposing, potentially compromising the evaluation validity of mental workload and fatigue states based on HRV.

One limitation of the present study was the use of a repeated-measures design to examine the primary effects of PL during cognitive tasks. A within-subjects experimental paradigm was applied when performing the n-back task under different PL conditions to cancel the influence of individual differences. To eliminate practicing effects, a 1-week interval between conditioning sessions was implemented; however, the PL condition was introduced later, potentially inducing an adaptation phenomenon. This study did not explore the validity of mental workload assessment based on ECG signals under the combined effects of PL and CL. Receiver operating curve analysis has indicated a good validity for fatigue assessment models, even when considering the influence of PL. Assessment models constructed by a random forest classifier showed average area under the curve values exceeding 0.995 for the two-classification mental workload method, based on features such as EEG, skin temperature, galvanic skin response and blood volume pulse features (Albuquerque et al., 2020). Further studies are needed to investigate the effect of physical factors on ECG-based evaluation models and their validity in assessing mental workload.

5 Conclusion

This study adopted the combined experimental paradigm involving CL and PL to simulate the characteristics of real dynamic mental work scenarios. The observed increase in subjects' task-load perceptions and reaction times indicated an increased level of mental workload. Concurrent PL during cognitive tasks enhanced the reaction. Regarding the combined effects of PL and CL on autonomic nervous system activity, PL emerged as the dominant factor, marked by an elevation in the LF component and a reduction in the HF component of HRV features, with sympathetic nervous system excitation contributing to this phenomenon. The combined effect adds complexity to the real-time assessment and evaluation of mental work based on the ECG. Additionally, the findings highlighted that HRV can effectively reflect changes in subjective feelings and task performance during mental work under the effects of PL. It should be noted that the validity of HRV under more demanding mental working conditions requires further exploration. Our study offers preliminary evidence of the evolving features of HRV under a mental workload, laying a theoretical understanding for the accurate and real-time assessment of the task-load level for mental workers in authentic dynamic scenarios.

Data availability statement

The original contributions presented in the study are included in the article/Supplementary Material, further inquiries can be directed to the corresponding authors.

Ethics statement

The studies involving humans were approved by the Ethics Committee of the Air Force Medical University. The studies were conducted in accordance with the local legislation and institutional requirements. Written informed consent for participation in this study was provided by the participants. Written informed consent was obtained from the individual(s) for the publication of any potentially identifiable images or data included in this article.

Author contributions

SC: Conceptualization, Data curation, Formal Analysis, Funding acquisition, Investigation, Methodology, Project administration, Software, Writing–original draft, Writing–review and editing. WL: Conceptualization, Data curation, Formal Analysis, Funding acquisition, Methodology, Project administration, Writing–original draft, Writing–review and editing. DH: Data curation, Methodology, Project administration, Software, Supervision, Validation, Writing–original draft. JM: Data curation, Methodology, Software, Supervision, Validation, Visualization, Writing–original draft. TZ: Data curation, Methodology, Validation, Visualization, Writing–original draft. CT: Methodology, Software, Validation, Visualization, Writing–review and editing. WD: Funding acquisition, Methodology, Software, Visualization, Writing–review and editing. KX: Methodology, Project administration, Validation, Visualization, Writing–review and editing. WH: Conceptualization, Funding acquisition, Methodology, Project administration, Resources, Supervision, Visualization, Writing–review and editing. LC: Conceptualization, Funding acquisition, Methodology, Project administration, Resources, Supervision, Validation, Visualization, Writing–review and editing.

Funding

The author(s) declare financial support was received for the research, authorship, and/or publication of this article. This study was supported by National Natural Science Foundation of China (grant numbers: U1933201 and 72201271) and the Key R&D Program of Shaanxi Province (grant numbers: 2022SF-114, 2022SF-428, 2023-YBSF-018 and 2022SF-052).

Conflict of interest

The authors declare that the research was conducted in the absence of any commercial or financial relationships that could be construed as a potential conflict of interest.

Publisher's note

Supplementary material

The Supplementary Material for this article can be found online at: https://www.frontiersin.org/articles/10.3389/fphys.2024.1340061/full#supplementary-material

References

Albuquerque, I., Tiwari, A., Parent, M., Cassani, R., Gagnon, J. F., Lafond, D., et al. (2020). WAUC: a multi-modal database for mental workload assessment under physical activity. *Front. Neurosci.* 14, 549524. doi:10.3389/fnins.2020.549524

Alfonso, C., and Capdevila, L. (2022). Heart rate variability, mood and performance: a pilot study on the interrelation of these variables in amateur road cyclists. *PeerJ* 10, e13094. doi:10.7717/peerj.13094

Bafna, T., and Hansen, J. P. (2021). Mental fatigue measurement using eye metrics: a systematic literature review. *Psychophysiology* 58 (6), e13828. doi:10.1111/psyp.13828

Blons, E., Arsac, L. M., Gilfriche, P., McLeod, H., Lespinet-Najib, V., Grivel, E., et al. (2019). Alterations in heart-brain interactions under mild stress during a cognitive task are reflected in entropy of heart rate dynamics. *Sci. Rep.* 9 (1), 18190. doi:10.1038/s41598-019-54547-7

Burlacu, A., Brinza, C., Brezulianu, A., and Covic, A. (2021). Accurate and early detection of sleepiness, fatigue and stress levels in drivers through Heart Rate Variability parameters: a systematic review. *Rev. Cardiovasc Med.* 22 (3), 845–852. doi:10.31083/j.rcm2203090

Chatain, C., Radel, R., Vercruyssen, F., Rabahi, T., Vallier, J. M., Bernard, T., et al. (2019). Influence of cognitive load on the dynamics of neurophysiological adjustments during fatiguing exercise. *Psychophysiology* 56 (6), e13343. doi:10.1111/psyp.13343

Chen, W. R., Shi, X. M., Yang, T. S., Zhao, L. C., and Gao, L. G. (2013). Protective effect of metoprolol on arrhythmia and heart rate variability in healthy people with 24 hours of sleep deprivation. *J. Interv. Card. Electrophysiol.* 36 (3), 267–272. discussion 272. doi:10.1007/s10840-012-9728-8

Cheng, S., Ma, J., Sun, J., Wang, J., Xiao, X., Wang, Y., et al. (2018). Differences in sensory reweighting due to loss of visual and proprioceptive cues in postural stability support among sleep-deprived cadet pilots. *Gait Posture* 63, 97–103. doi:10.1016/j.gaitpost.2018.04.037

Cheng, S., Yang, J., Su, M., Sun, J., Xiong, K., Ma, J., et al. (2021). Postural stability change under sleep deprivation and mental fatigue status. *Aerosp. Med. Hum. Perform.* 92 (8), 627–632. doi:10.3357/amhp.5755.2021

Chitti, S., Kumar, J. T., and Kumar, V. S. (2021). EEG signal feature selection algorithm and support vector machine model in patient's fatigue recognition. *Arab. J. Sci. Eng.* 48, 11135–11141. doi:10.1007/s13369-021-06206-1

Chua, E. C., Tan, W. Q., Yeo, S. C., Lau, P., Lee, I., Mien, I. H., et al. (2012). Heart rate variability can be used to estimate sleepiness-related decrements in psychomotor vigilance during total sleep deprivation. *Sleep* 35 (3), 325–334. doi:10.5665/sleep.1688

Dai, Y., Duan, F., Feng, F., Sun, Z., Zhang, Y., Caiafa, C. F., et al. (2021). A fast approach to removing muscle artifacts for EEG with signal serialization based ensemble empirical mode decomposition. *Entropy (Basel)* 23 (9), 1170. doi:10.3390/e23091170

Dallaway, N., Lucas, S. J. E., and Ring, C. (2022). Cognitive tasks elicit mental fatigue and impair subsequent physical task endurance: effects of task duration and type. *Psychophysiology* 59 (12), e14126. doi:10.1111/psyp.14126

Engeroff, T., Banzer, W., and Niederer, D. (2022). The impact of regular activity and exercise intensity on the acute effects of resistance exercise on cognitive function. *Scand. J. Med. Sci. Sports* 32 (1), 94–105. doi:10.1111/sms.14050

Fortes, L. S., Lima Júnior, D., Costa, Y. P., Albuquerque, M. R., Nakamura, F. Y., and Fonseca, F. S. (2022). Effects of social media on smartphone use before and during velocity-based resistance exercise on cognitive interference control and physiological measures in trained adults. *Appl. Neuropsychol. Adult* 29 (5), 1188–1197. doi:10.1080/23279095.2020.1863796

Fujihara, H., Megumi, A., and Yasumura, A. (2021). The acute effect of moderate-intensity exercise on inhibitory control and activation of prefrontal cortex in younger and older adults. *Exp. Brain Res.* 239 (6), 1765–1778. doi:10.1007/s00221-021-06086-9

Gao, L., Zhu, L., Hu, L., Hu, H., Wang, S., Bezerianos, A., et al. (2021). Mid-task physical exercise keeps your mind vigilant: evidences from behavioral performance and EEG functional connectivity. *IEEE Trans. Neural Syst. Rehabil. Eng.* 29, 31–40. doi:10.1109/tnsre.2020.3030106

Garis, G., Haupts, M., Duning, T., and Hildebrandt, H. (2023). Heart rate variability and fatigue in MS: two parallel pathways representing disseminated inflammatory processes? *Neurol. Sci.* 44 (1), 83–98. doi:10.1007/s10072-022-06385-1

Jacquet, T., Poulin-Charronnat, B., Bard, P., and Lepers, R. (2020). Persistence of mental fatigue on motor control. *Front. Psychol.* 11, 588253. doi:10.3389/fpsyg.2020.588253

Karthikeyan, R., Smoot, M. R., and Mehta, R. K. (2021). Anodal tDCS augments and preserves working memory beyond time-on-task deficits. *Sci. Rep.* 11 (1), 19134. doi:10.1038/s41598-021-98636-y

Klug, M., and Gramann, K. (2021). Identifying key factors for improving ICA-based decomposition of EEG data in mobile and stationary experiments. *Eur. J. Neurosci.* 54 (12), 8406–8420. doi:10.1111/ejn.14992

Konishi, M., Takahashi, M., Endo, N., Numao, S., Takagi, S., Miyashita, M., et al. (2013). Effects of sleep deprivation on autonomic and endocrine functions throughout the day and on exercise tolerance in the evening. *J. Sports Sci.* 31 (3), 248–255. doi:10.1080/02640414.2012.733824

Maiorana, N., Brugnera, A., Galiano, V., Ferrara, R., Poletti, B., Marconi, A. M., et al. (2022). Emotional and autonomic response to visual erotic stimulation in patients with functional hypothalamic amenorrhea. *Front. Endocrinol. (Lausanne)* 13, 982845. doi:10.3389/fendo.2022.982845

Nikooharf Salehi, E., Jaydari Fard, S., Jaberzadeh, S., and Zoghi, M. (2022). Transcranial direct current stimulation reduces the negative impact of mental fatigue on swimming performance. *J. Mot. Behav.* 54 (3), 327–336. doi:10.1080/00222895.2021.1962238

Pan, T., Wang, H., Si, H., Li, Y., and Shang, L. (2021). Identification of pilots' fatigue status based on electrocardiogram signals. *Sensors (Basel)* 21 (9), 3003. doi:10.3390/s21093003

Ramírez-Moreno, M. A., Carrillo-Tijerina, P., Candela-Leal, M. O., Alanis-Espinosa, M., Tudón-Martínez, J. C., Roman-Flores, A., et al. (2021). Evaluation of a fast test based on biometric signals to assess mental fatigue at the workplace-A pilot study. *Int. J. Environ. Res. Public Health* 18 (22), 11891. doi:10.3390/ijerph182211891

Sun, J., Cheng, S., Ma, J., Xiong, K., Su, M., and Hu, W. (2019). Assessment of the static upright balance index and brain blood oxygen levels as parameters to evaluate pilot workload. *PLoS One* 14 (3), e0214277. doi:10.1371/journal.pone.0214277

Takada, N., Laohakangvalvit, T., and Sugaya, M. (2022). Human error prediction using heart rate variability and electroencephalography. *Sensors (Basel)* 22 (23), 9194. doi:10.3390/s22239194

Teng, C. L., Zhang, Y. Y., Wang, W., Luo, Y. Y., Wang, G., and Xu, J. (2021). A novel method based on combination of independent component analysis and ensemble empirical mode decomposition for removing electrooculogram artifacts from multichannel electroencephalogram signals. *Front. Neurosci.* 15, 729403. doi:10.3389/fnins.2021.729403

Vaara, J., Kyröläinen, H., Koivu, M., Tulppo, M., and Finni, T. (2009). The effect of 60-h sleep deprivation on cardiovascular regulation and body temperature. *Eur. J. Appl. Physiol.* 105 (3), 439–444. doi:10.1007/s00421-008-0921-5

Wang, G., Teng, C., Li, K., Zhang, Z., and Yan, X. (2016). The removal of EOG artifacts from EEG signals using independent component analysis and multivariate empirical mode decomposition. *IEEE J. Biomed. Health Inf.* 20 (5), 1301–1308. doi:10.1109/jbhi.2015.2450196

Wascher, E., Reiser, J., Rinkenauer, G., Larrá, M., Dreger, F. A., Schneider, D., et al. (2023). Neuroergonomics on the go: an evaluation of the potential of mobile EEG for workplace assessment and design. *Hum. Factors* 65 (1), 86–106. doi:10.1177/00187208211007707

Wehrens, S. M., Hampton, S. M., and Skene, D. J. (2012). Heart rate variability and endothelial function after sleep deprivation and recovery sleep among male shift and non-shift workers. *Scand. J. Work Environ. Health* 38 (2), 171–181. doi:10.5271/sjweh.3197

Wilson, M. K., Ballard, T., Strickland, L., Amy Boeing, A., Cham, B., Griffin, M. A., et al. (2021). Understanding fatigue in a naval submarine: applying biomathematical models and workload measurement in an intensive longitudinal design. *Appl. Ergon.* 94, 103412. doi:10.1016/j.apergo.2021.103412

Wilson, N., Guragain, B., Verma, A., Archer, L., and Tavakolian, K. (2020). Blending human and machine: feasibility of measuring fatigue through the aviation headset. *Hum. Factors* 62 (4), 553–564. doi:10.1177/0018720819849783

Wriessnegger, S. C., Raggam, P., Kostoglou, K., and Müller-Putz, G. R. (2021). Mental state detection using riemannian geometry on electroencephalogram brain signals. *Front. Hum. Neurosci.* 15, 746081. doi:10.3389/fnhum.2021.746081

Xu, R., Zhang, C., He, F., Zhao, X., Qi, H., Zhou, P., et al. (2018). How physical activities affect mental fatigue based on EEG energy, connectivity, and complexity. *Front. Neurol.* 9, 915. doi:10.3389/fneur.2018.00915

Xu, Y., Yang, Z., Li, G., Tian, J., and Jiang, Y. (2021). A practical application for quantitative brain fatigue evaluation based on machine learning and ballistocardiogram. *Healthc. (Basel)* 9 (11), 1453. doi:10.3390/healthcare9111453

Zhang, H., Wang, J., Geng, X., Li, C., and Wang, S. (2021a). Objective assessments of mental fatigue during a continuous long-term stress condition. *Front. Hum. Neurosci.* 15, 733426. doi:10.3389/fnhum.2021.733426

Zhang, Y., Shi, W., Wang, H., Liu, M., and Tang, D. (2021b). The impact of acute exercise on implicit cognitive reappraisal in association with left dorsolateral prefronta activation: a fNIRS study. *Behav. Brain Res.* 406, 113233. doi:10.1016/j.bbr.2021.113233

Zhao, C., Zhao, M., Liu, J., and Zheng, C. (2012). Electroencephalogram and electrocardiograph assessment of mental fatigue in a driving simulator. *Accid. Anal. Prev.* 45, 83–90. doi:10.1016/j.aap.2011.11.019

Zheng, K., Deng, Z., Qian, J., Chen, Y., Li, S., and Huang, T. (2022). Changes in working memory performance and cortical activity during acute aerobic exercise in young adults. *Front. Behav. Neurosci.* 16, 884490. doi:10.3389/fnbeh.2022.884490

Zhu, Y., Sun, F., Chiu, M. M., and Siu, A. Y. (2021). Effects of high-intensity interval exercise and moderate-intensity continuous exercise on executive function of healthy young males. *Physiol. Behav.* 239, 113505. doi:10.1016/j.physbeh.2021.113505

Zink, R., Hunyadi, B., Huffel, S. V., and Vos, M. D. (2016). Mobile EEG on the bike: disentangling attentional and physical contributions to auditory attention tasks. *J. Neural Eng.* 13 (4), 046017. doi:10.1088/1741-2560/13/4/046017

frontiers | Frontiers in Neuroscience

TYPE Original Research
PUBLISHED 07 March 2024
DOI 10.3389/fnins.2024.1287809

OPEN ACCESS

EDITED BY
Vitor Engracia Valenti,
São Paulo State University, Brazil

REVIEWED BY
Jesus Antonio Sanchez-Perez,
Georgia Institute of Technology, United States
Stefan Kampusch,
AURIMOD GmbH, Austria
Asim H. Gazi,
Harvard University, United States

*CORRESPONDENCE
Jie Liu
✉ feixilj@163.com
Yue Yu
✉ yuyuemd@163.com

†These authors have contributed equally to this work

RECEIVED 02 September 2023
ACCEPTED 28 February 2024
PUBLISHED 07 March 2024

CITATION
Huang Y, Liu J, Lv C, Sun C, Meng M, Lowe S and Yu Y (2024) Integrative effects of transcutaneous auricular vagus nerve stimulation on esophageal motility and pharyngeal symptoms via vagal mechanisms in patients with laryngopharyngeal reflux disease.
Front. Neurosci. 18:1287809.
doi: 10.3389/fnins.2024.1287809

Integrative effects of transcutaneous auricular vagus nerve stimulation on esophageal motility and pharyngeal symptoms via vagal mechanisms in patients with laryngopharyngeal reflux disease

Yizhou Huang[1†], Jie Liu[2*†], Chaolan Lv[2], Chenyu Sun[3], Muzi Meng[4], Scott Lowe[5] and Yue Yu[2*]

[1]Department of Gastroenterology, The PLA Navy Anqing Hospital, Anqing, Anhui, China, [2]Department of Gastroenterology, Division of Life Sciences and Medicine, The First Affiliated Hospital of USTC, University of Science and Technology of China, Hefei, Anhui, China, [3]Department of General Surgery, The Second Affiliated Hospital of Anhui Medical University, Hefei, Anhui, China, [4]Bronxcare Health System, New York, NY, United States, [5]College of Osteopathic Medicine, Kansas City University, Kansas City, MO, United States

Background and aim: Laryngopharyngeal reflux disease (LPRD) is primarily characterized by discomfort in the pharynx and has limited treatment options. This research aimed to assess the efficacy of transcutaneous auricular vagus nerve stimulation (tVNS) in patients with LPRD and delve into the potential underlying mechanisms.

Methods: A total of 44 participants, diagnosed with LPRD were divided into two groups randomly. Twice-daily stimulation was delivered for 2 weeks for patients in experimental group, with stimulation ranging from 1.0 mA to 1.5 mA ($n = 22$), while the control group underwent sham tVNS ($n = 22$) with the same stimulation parameters and different anatomical location. The severity of symptoms and levels of anxiety and depression were monitored using questionnaires. High-resolution esophageal manometry data were collected, and the patients' autonomic function was assessed through heart rate variability analysis.

Results: There was a positive correlation between reflux symptom index (RSI) scores and low frequency/high frequency (LF/HF) ratio ($r = 0.619$; $p < 0.001$), Hamilton anxiety scale (HAMA) scores ($r = 0.623$; $p < 0.001$), and Hamilton depression scale (HAMD) scores ($r = 0.593$; $p < 0.001$). Compared to the pre-tVNS phase, RSI ($p < 0.001$), HAMA ($p < 0.001$), and HAMD ($p < 0.001$) scores were significantly reduced after 2 weeks of treatment. Additionally, the resting pressure of the upper esophageal sphincter (UESP; $p < 0.05$) and lower esophageal sphincter (LESP; $p < 0.05$) showed significant enhancement. Notably, tVNS led to an increase in root mean square of successive differences (RMSSD; $p < 0.05$) and high frequency (HF; $p < 0.05$) within heart rate variability compared to the pre-treatment baseline. Compared to the control group, RSI ($p < 0.001$), HAMA ($p < 0.001$), and HAMD ($p < 0.001$) scores in tVNS group were significantly lower at the end of treatment. Similarly, the resting pressure of UESP ($p < 0.05$) and LESP ($p < 0.05$) in tVNS group were significantly higher than that of control group.

Notably, RMSSD ($p < 0.05$) and HF ($p < 0.05$) in tVNS group were significantly higher than that of control group.

Conclusion: This study demonstrated that tVNS as a therapeutic approach is effective in alleviating LPRD symptoms. Furthermore, it suggests that improvements in esophageal motility could be associated with vagus nerve-dependent mechanisms.

KEYWORDS

vagus nerve stimulation, neuromodulation, autonomic function, heart rate variability, laryngopharyngeal reflux disease

1 Introduction

Laryngopharyngeal reflux disease (LPRD) is characterized by the regurgitation of stomach contents into the larynx and pharynx, leading to an inflammatory response in the mucous membranes of the throat. This inflammatory process manifests as a range of symptoms, including hoarseness, persistent cough, difficulty swallowing (dysphagia), and the sensation of a lump (globus) in the throat (Mishra et al., 2020). The condition significantly diminishes the quality of life for affected individuals and increases their susceptibility to various laryngeal disorders, such as reflux laryngitis, subglottic stenosis, laryngeal cancer, granulomas, contact ulcers, and vocal cord nodules (Falk and Vivian, 2016). It is recognized that 24-h pH-metry is the gold standard test for diagnosing LPR (Mishra et al., 2020). But it is an expensive and time consuming investigation. Thus there are some simplified approaches for monitoring and quantifying the symptoms, such as Reflux Symptom Index (RSI), Reflux Finding Score, CarlssonDent, ReQuest, GerdQ, etc. (Zhang et al., 2023).

The upper esophageal sphincter (UES), a crucial barrier against reflux, maintains a close relationship with the vagus nerve, while disturbances in autonomic function have been associated with the development of LPRD (Benjamin et al., 2017; Wang et al., 2019). Although proton pump inhibitors (PPIs) have gained recognition as a therapeutic approach for LPRD, only around half of patients respond to PPI treatment, and some experience minimal relief in symptoms when compared to a placebo (Steward et al., 2004). Therefore, there is a need for exploring complementary and alternative medicine (CAM) as a treatment for LPRD. A recent study found that transcutaneous electrical acupoint stimulation (TEAS) combined with PPI showed a significantly greater improvement in LPRD symptoms (Shen et al., 2023).

Transcutaneous auricular vagus nerve stimulation (tVNS), an alternative to invasive vagus nerve stimulation (IVNS), has found utility in addressing functional gastrointestinal disorders (FGID), inflammatory bowel disease (IBS), and other conditions (Ventureyra, 2000; Carreno and Frazer, 2016; Keute et al., 2018; Hong et al., 2019). The auricular branch of the vagus nerve extends to the cymba concha in the outer ear. By non-invasively stimulating this region, inflammation can be suppressed, and vagal activity enhanced (Steward et al., 2004). The present study endeavors to assess the impact of tVNS on alleviating LPRD symptoms and improving esophageal function. Furthermore, the investigation seeks to elucidate the potential autonomic mechanisms underlying these effects in individuals afflicted by LPRD.

2 Patients and methods

2.1 Study participants

This preliminary investigation employed a randomized, single-blind, and sham-controlled approach to assess the effects of transcutaneous auricular vagus nerve stimulation (tVNS) in individuals diagnosed with laryngopharyngeal reflux disease (LPRD). Notably, the participants did not participate directly in shaping the study's design, recruitment, or implementation. Inclusion criteria consisted of individuals aged 18 to 65 years, possessing a reflux symptom index (RSI) score exceeding >13, having been diagnosed with LPRD for a duration surpassing 3 months, and demonstrating a willingness to adhere to the stipulated treatment regimen.

Exclusion criteria encompassed conditions such as diabetes, malignancies, respiratory disorders, endocrine abnormalities, cardiac ailments, upper gastrointestinal afflictions, or other significant systemic maladies. Additionally, those who had recently used medications with the potential to impact autonomic function or acid suppression, individuals engaged in prolonged smoking or excessive alcohol consumption, women experiencing menstruation, pregnancy, or lactation, and subjects exhibiting allergies to the electrodes were excluded from participation. Within the confines of these criteria, a total of 44 LPRD patients were recruited to partake in the investigation, each providing informed consent prior to their involvement.

Ethical considerations were rigorously upheld, and the study was granted approval by the Ethics Committee of The First Affiliated Hospital of USTC (2016 L36).

2.2 Study protocol

Forty-four participants were allocated into two groups through a randomized allocation, maintaining an equitable 1:1 ratio. The random assignment was executed using a random digital table within the Statistical Package for the Social Sciences (SPSS) software. Prior to undergoing their designated interventions, individuals within each group were instructed to complete a battery of three distinct questionnaires, namely the 14-item Hamilton Anxiety Scale (HAMA), the 17-item Hamilton Depression Scale (HAMD), and the Reflux Symptom Index (RSI). Furthermore, comprehensive evaluations were conducted, encompassing a high-resolution esophageal manometry (HREM) examination and continuous electrocardiogram (ECG) monitoring.

Following the initial assessments, participants were subjected to either tVNS or sham tVNS sessions, with a frequency of twice daily for a duration of 2 weeks within clinic. To ensure impartiality and mitigate potential subjective biases, the post-treatment evaluations of all subjects were carried out by an investigator who had no prior involvement during the stimulation phase. The content of the follow-up assessment remained consistent with the baseline evaluation, while meticulous attention was directed toward assessing the safety and tolerability of the interventions. The procedural outline of this study is elucidated in Figure 1.

2.3 tVNS and sham-tVNS treatment

The bilateral auricular concha regions exhibit a rich distribution of the vagus nerve. Prior research has documented that stimulating the concha regions of both ears can yield enhancements in esophageal motility and elevation of vagal activity. Consequently, in this study, tVNS was conducted on the bilateral auricular concha areas, a method supported by previous findings (Zhu et al., 2021; Long et al., 2022; see Figure 2). The stimulation point for tVNS was at cavity concha, while sham point was at the earlobe. The cavity concha was found to be solely innervate by the vagus nerve and great auricular nerve in earlier studies (Peuker and Filler, 2002).

Preceding the stimulation procedure, the auricular skin was meticulously disinfected using alcohol. Subsequently, a pair of surface electrode pads were precisely positioned on the bilateral concha areas. Stimulation was administered employing a watch-sized stimulator (SNM-FDCM01, Ningbo Maida Medical Device, Inc., Ningbo, China). In parallel, the sham tVNS intervention was conducted at a distinct anatomical location (Zhang et al., 2018). tVNS sessions lasting 30 min. Noteworthy is the uniformity of stimulus parameters across both interventions: pulse trains alternating between 2 s of stimulation and 3 s of rest, a pulse width measuring 0.5 ms, a pulse frequency set at 25 Hz, and a pulse amplitude ranging from 1.0 mA to 1.5 mA, determined based on patient tolerability and preference. To eliminate any potential bias, all participants remained unaware of the specific treatment modality being administered (Zhu et al., 2021). A stimulation of 2/3 s ON/OFF cycle was selected owing to its effectiveness in enhancing GI motility in a previous study (Shi et al., 2021).

2.4 Measurements

2.4.1 Assessment of RSI, HAMA, and HAMD

The RSI was employed as both a diagnostic and evaluative tool for patients with LPRD (Belafsky et al., 2002). Succinctly, RSI gauges the severity of symptoms experienced by individuals over the preceding month, utilizing a scoring system that assigns values ranging from 0 (indicating no issue) to 5 (representing a severe problem) for each of its nine constituent items. Higher cumulative scores correspond to more pronounced symptomatology, with the maximum potential overall score reaching 45. In this study, RSI was modified to only account for the previous 2 weeks.

Meanwhile, the HAMA and HAMD have established themselves as widely utilized instruments for assessing the manifestation of anxiety and depression within clinical contexts (Hamilton, 1959; Hamilton, 1960). HAMA encompasses 14 distinct items, each rated on a scale spanning from 0 (absent) to 4 (severe), culminating in a cumulative score range of 0 to 56. In contrast, the HAMD comprises 17 items, contributing to a maximum total score of 62. These aforementioned questionnaires have consistently demonstrated commendable reliability and validity in effectively appraising psychological states (Pappa et al., 2020; Yang et al., 2022).

2.4.2 High-resolution esophageal manometry

Esophageal motility analysis was conducted using a water-perfused esophageal manometric catheter furnished with 24 pressure sensors distributed at 1 cm intervals (MedKinetic, Ningbo, China). The procedural protocol encompassed a sequence of key steps, commencing with two initial baseline recordings conducted in the absence of swallowing. Subsequent to this, the examination progressed with the administration of 10 swallows of 5 mL of water, followed by the execution of two consecutive swallows involving 2 mL of water, each completed within a span of 5 s. For the analysis of HREM parameters, a dedicated suite of analytical software (Medview 360) was deployed for comprehensive assessment (Yu et al., 2019).

During the process of swallowing, discrete aspects of esophageal manometry data were gathered from each patient, incorporating variables such as upper esophageal sphincter pressure (UESP), upper esophageal sphincter length (UESL), lower esophageal sphincter pressure (LESP), lower esophageal sphincter length (LESL), contraction front velocity (CFV), distal latency (DL), distal contraction integral (DCI), and integrated relaxation pressure (IRP). The median DCI is recognized as a marker of esophageal

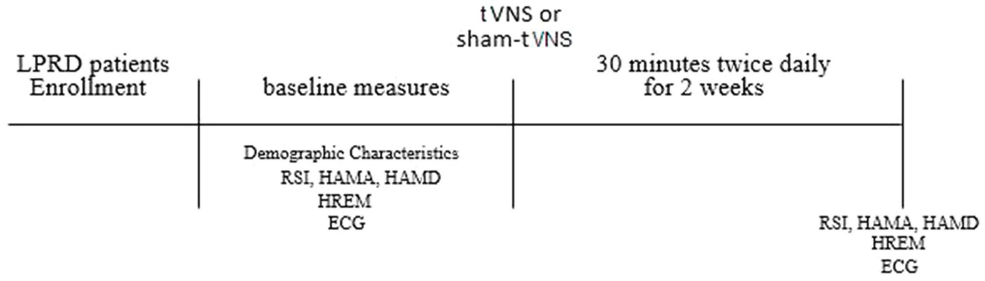

FIGURE 1
Study protocol. LPRD, Laryngopharyngeal reflux disease; tVNS, transcutaneous auricular vagus nerve stimulation; RSI, reflux symptom index; HAMA, 14-item Hamilton Anxiety Scale; HAMD, 17-item Hamilton Depression Scale; HREM, high-resolution esophageal manometry; ECG, electrocardiogram.

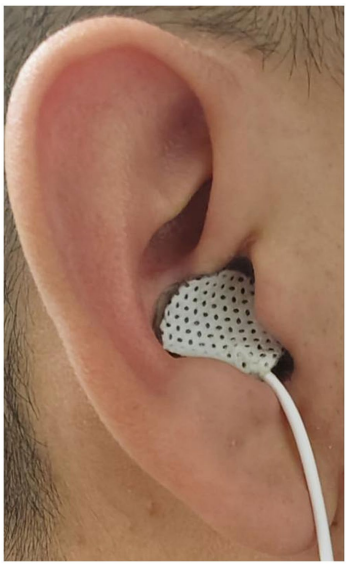

FIGURE 2
Overview of stimulation methodology and location.

TABLE 1 Baseline characteristics of patients treated with tVNS or sham-tVNS.

	tVNS (n = 22)	sham-tVNS (n = 22)	t/x^2	p-value
Male, n (%)	10 (45.45%)	10 (45.45%)		1
Age (yr)	45.50 ± 10.84	48.27 ± 10.02	−0.881	0.383
BMI (kg/m^2)	22.19 ± 1.46	21.71 ± 1.00	1.263	0.214
Duration (months)	20.82 ± 3.71	19.19 ± 4.32	1.344	0.186

tVNS, transcutaneous auricular vagus nerve stimulation; BMI, body mass index.

contractile vigor. IRP represents mean esophagogastric junction (EGJ) pressure measured with an electronic equivalent of a sleeve sensor for four continuous or non-continuous seconds of relaxation in the 10-s window following deglutitive UES relaxation. DL is the interval between UES relaxation and the contractile deceleration point. CFV refers to the slope of the tangent approximating the 30 mmHg isobaric contour between the proximal pressure trough and the CDP.

2.4.3 Assessment of autonomic functions

The ECG recordings (CT-082, Hangzhou Baihui Electrocardiograms, China) with 12 leads and 10 electrodes yielded short-term (5-min) heart rate variability (HRV) data, which underwent thorough processing using the HRV analysis software (Cardiotrak Holtersystem version: 1.2.0.0, Hangzhou Baihui Electrocardiograms, China). Our attention is directed toward two pivotal time-domain HRV measurements: the Standard Deviation of the normal-to-normal intervals (SDNN) and the Root Mean Square of Successive Differences (RMSSD). In addition, an exploration of frequency-domain HRV parameters was undertaken, encompassing total power (TP) in the frequency range of 0.00 to 0.40 Hz, low-frequency (LF) power spanning 0.04 to 0.15 Hz, high-frequency (HF) power within the 0.15 to 0.40 Hz spectrum, the ratio of high-frequency power to total power (HF% or HF/Tot), and the ratio of low-to-high frequency power (LF/HF).

Of note, RMSSD, HF, and HF% primarily serve as indices of vagal activity, while SDNN and TP predominantly reflect the composite autonomic nervous system activity involving both sympathetic and vagal components. The LF parameter is modulated by both sympathetic and vagal influences, with sympathetic predominance. On the other hand, LF/HF offers insights into the equilibrium between sympathetic and vagal innervation (Baldissarelli et al., 2017; Wang et al., 2018).

2.5 Statistical analyses

For all statistical analyses, SPSS version 22.0 software was employed. Descriptive statistics for quantitative variables were presented as mean values accompanied by their corresponding standard deviations (SD). Changes in the data pre- and post-treatment were evaluated utilizing a paired t-test, while the difference between the two groups were tested by using independent t-test. Normality test was conducted using Shapiro–Wilk test. The t-tests and Pearson correlation tested were appropriate for analyzing data. Categorical variables were expressed as rates and subjected to analysis using the χ-2 test. The threshold for statistical significance was set at a p-value less than 0.05. Furthermore, to explore relationships between variables, correlation analysis was executed employing Pearson's correlation test.

3 Results

3.1 Patient characteristics

The stimulation procedure did not give rise to any adverse events, including but not limited to occurrences such as headache, lightheadedness, tinnitus, tachycardia, or rash. A total of 45 LPRD patients were recruited, while a single participant dropped out due to contracting an upper respiratory virus infection during the course of treatment. This individual exhibited improvement subsequent to receiving antiviral medication. The comprehensive demographic and clinical data of the 44 subjects who successfully completed the course of tVNS or sham-tVNS intervention are meticulously presented in Table 1. Examination of variables encompassing sex, age, body mass index (BMI), and duration of the disease revealed notable similarity between the tVNS and sham-tVNS groups.

3.2 Effects of tVNS and sham-tVNS on RSI, anxiety and depression

The tVNS group's ΔRSI scores were significantly less than that for the sham-tVNS group (11.18 ± 1.26 vs. 0.23 ± 1.69, $p < 0.001$; Figure 3). Similarly, tVNS effectively improved patients' anxiety and depression status [ΔHAMA scores (12.19 ± 1.62 vs. 0.41 ± 0.38, $p < 0.001$; ΔHAMD 10.14 ± 1.59 vs. 0.36 ± 1.29, $p < 0.001$)] compared to sham group. Furthermore, the HAMA and HAMD scores were significantly lower in the tVNS group compared to the sham-tVNS group at the end of treatment (4.86 ± 1.08 vs. 16.00 ± 1.86, $p < 0.001$; 4.82 ± 1.30 vs. 14.41 ± 2.03, $p < 0.001$; Figures 4A,B). Interestingly, the

RSI score of the patients before treatment were positively correlated with HAMA (r = 0.623; $p < 0.001$) and HAMD (r = 0.593; $p < 0.001$; Figures 5A,B). The difference of RSI, anxiety and depression in the two groups were shown in Table 2.

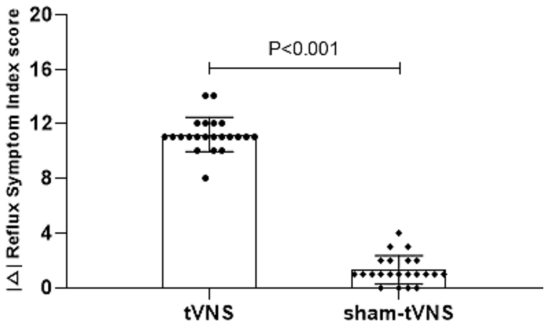

FIGURE 3
The effect of tVNS ($n = 22$) compared with sham-tVNS ($n = 22$) on delta RSI score. *$p < 0.05$ vs. before treatment.

3.3 Effects of tVNS and sham-tVNS on high-resolution esophageal manometry

The Δ UESP of the tVNS group was significantly higher than that of the sham group (29.32 ± 10.25 vs. 2.48 ± 6.56 mmHg, $p < 0.001$). Similarly, the Δ LESP of the tVNS group was significantly higher than that of the sham group (4.31 ± 4.93 vs. −0.25 ± 2.28 mmHg, $p = 0.01$). There was no change of the UESL (5.14 ± 0.81 vs. 5.05 ± 1.01, $p = 0.744$) and LESL (2.99 ± 0.42 vs. 2.97 ± 0.37, $p = 0.879$) in tVNS group compared to sham group after the two groups received different interventions. CFV (4.52 ± 1.14 vs. 3.50 ± 0.85, delta = 1.02 ± 0.88, $p < 0.05$) and DL (7.96 ± 1.09 vs. 7.02 ± 0.91, delta = 0.94 ± 0.81, $p < 0.05$) had a significant decrease, while DCI (2047.13 ± 477.61 vs. 2453.90 ± 509.11, $p < 0.05$) and IRP (4.97 ± 1.67 vs. 8.02 ± 2.04, $p < 0.05$) had a significant increase after tVNS compared to baseline. In contrast, there was no change of the CFV (4.51 ± 0.80 vs. 4.49 ± 0.75, $p = 0.938$), DL (8.10 ± 0.92 vs. 7.90 ± 0.99, $p = 0.501$), DCI (1941.50 ± 601.33 vs. 2052.62 ± 479.63, $p = 0.502$) and IRP (4.94 ± 1.84 vs. 5.02 ± 1.56, $p = 0.875$) after sham-tVNS compared to baseline (Tables 3, 4).

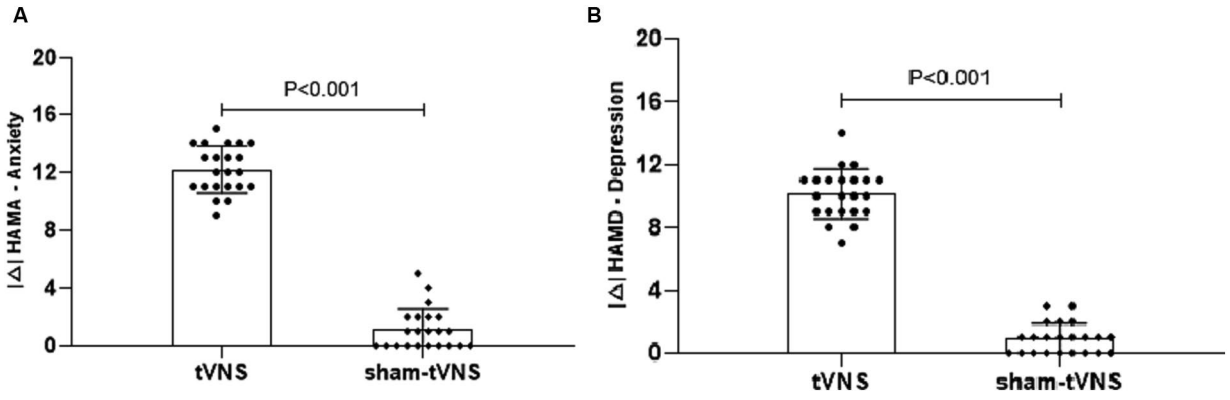

FIGURE 4
(A) The effect of tVNS ($n = 22$) compared with sham-tVNS ($n = 22$) on delta HAMA score. *$p < 0.05$ vs. before treatment. **(B)** Effect of tVNS ($n = 22$) and sham-tVNS ($n = 22$) on delta HAMD score. *$p < 0.05$ vs. before treatment.

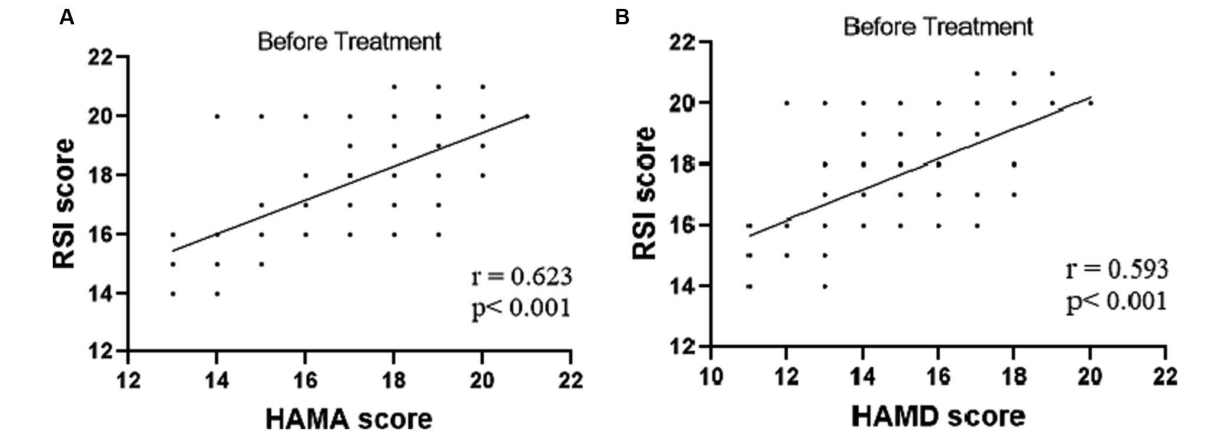

FIGURE 5
(A) Correlation of HAMA score with RSI score ($n = 44$). **(B)** Correlation of HAMD score with RSI score ($n = 44$).

10.3389/fnins.2024.1287809

TABLE 2 Effects of tVNS and sham-tVNS on throat symptom and mental health.

	RSI score			HAMA			HAMD		
	Before treatment	After treatment	Difference	Before treatment	After treatment	Difference	Before treatment	After treatment	Difference
tVNS ($n = 22$)	17.55 ± 1.85	6.36 ± 1.59	11.18 ± 1.26	17.05 ± 2.30	4.86 ± 1.08	12.19 ± 1.62	14.95 ± 2.36	4.82 ± 1.30	10.14 ± 1.59
sham-tVNS ($n = 22$)	17.86 ± 2.21	17.64 ± 1.36	0.23 ± 1.69	16.41 ± 2.02	16.00 ± 1.86	0.41 ± 0.38	14.77 ± 2.45	14.41 ± 2.03	0.36 ± 1.29
t	0.52	25.24	24.40	0.34	23.67	22.85	0.25	16.86	22.43
P	0.61	**<0.001**	**<0.001**	0.74	**<0.001**	**<0.001**	0.803	**<0.001**	**<0.001**

tVNS, transcutaneous auricular vagus nerve stimulation. *$P < 0.05$ vs. before treatment. RSI, reflux symptom index; HAMA, 14-item Hamilton Anxiety Scale; HAMD, 17-item Hamilton Depression Scale.

3.4 Effects of tVNS and sham-tVNS on autonomic functions

Combined RSI and HRV spectral analysis prior to receiving tVNS and sham-tVNS showed that RSI was positively correlated with LF/HF ($r = 0.619$; $p < 0.001$) and negatively correlated with HF% ($r = -0.521$; $p < 0.001$; Figures 6A,B). The Δ RMSSD of the tVNS group was significantly higher than that of the sham group (6.16 ± 3.37 vs. 3.56 ± 2.13 ms, $p < 0.050$). Similarly, the Δ HF of the tVNS group was significantly higher than that of the sham group (259.98 ± 40.26 vs. 8.82 ± 3.40 ms^2, $p < 0.05$; Figures 7A,B). The difference of autonomic functions in the two groups were shown in Table 5.

4 Discussion

Some methods employing vagus nerve stimulation (VNS) has garnered approval as an intervention for various conditions, including epilepsy, depression, and migraine (Ryvlin et al., 2014; Beh and Friedman, 2019; Bottomley et al., 2020; Farmer et al., 2021). Recently, the impact of VNS on patients with functional dyspepsia was investigated, employing the SNM-FDC01 device to transcutaneously stimulate the vagus nerve at the bilateral auricular cymba concha regions. Through a comprehensive assessment encompassing acute and chronic trials, tVNS exhibited the capacity to enhance vagal nerve activity, thereby ameliorating gastric accommodation and motility. These effects resulted in marked improvements in the significant dyspeptic symptoms experienced by patients (Zhu et al., 2021). Farmer et al. (2021) proposed a set of minimal reporting items to guide future tVNS studies. The suggested items address specific technical aspects of the device and stimulation parameters. It is necessary to study and define standardized protocols for treatment, since still studies are often using inhomogeneous study designs and stimulation parameters.

The current study underscores the efficacy of noninvasive tVNS treatment targeting the auricular branch of the vagus nerve. This was administered externally through electrodes, conducted twice daily over a 2-week duration, and yielded noteworthy enhancements in both pharyngeal discomfort and mental well-being among patients grappling with LPRD. Notably, this endeavor was undertaken as a randomized, single-blind, sham-controlled pilot trial, ensuring the subjects remained uninformed about the specific treatment allocation. Moreover, objective measurements, encompassing UES pressure and autonomic functions, revealed substantial improvements in individuals who received active tVNS in comparison to those subjected to sham-tVNS. Previous study demonstrated that plasma melatonin concentration could be increased by tVNS, thus relieving peripheral neuropathic pain (Wang et al., 2022). Meanwhile, multiple tVNS sessions are antidiabetic in diabetes through triggering of tidal secretion of melatonin (Li et al., 2014; Wang et al., 2015).

While acid suppression therapy stands as the favored therapeutic approach for LPRD, its efficacy may be compromised in certain patients due to intricate factors including dietary and sleep patterns (Cui et al., 2019; Lechien et al., 2021). In this context, the current investigation highlights that significant amelioration of LPRD symptoms, as ascertained by the RSI score, transpired over a span of 2 weeks following tVNS intervention. Notably, Belafsky et al. suggest

TABLE 3 Effects of tVNS and sham-tVNS on high-resolution esophageal manometry.

	tVNS (n = 22)		sham-tVNS (n = 22)	
	Before treatment	After treatment	Before treatment	After treatment
UESP (mmHg)	51.80 ± 9.34	81.12 ± 12.18*	53.40 ± 8.84	55.88 ± 8.45
UESL (cm)	5.14 ± 0.81	5.05 ± 1.01	4.99 ± 1.08	5.07 ± 0.78
LESP (mmHg)	20.78 ± 5.47	25.09 ± 5.05*	20.13 ± 6.14	19.88 ± 4.77
LESL (cm)	2.99 ± 0.42	2.97 ± 0.37	2.99 ± 0.43	2.95 ± 0.34
CFV (cm/s)	4.52 ± 1.14	3.50 ± 0.85*	4.51 ± 0.80	4.49 ± 0.75
DL (s)	7.96 ± 1.09	7.02 ± 0.91*	8.10 ± 0.92	7.90 ± 0.99
DCI (mmHg•cm•s)	2047.13 ± 477.61	2453.90 ± 509.11*	1941.50 ± 601.33	2052.62 ± 479.63
IRP (mmHg)	4.97 ± 1.67	8.02 ± 2.04*	4.94 ± 1.84	5.02 ± 1.56

tVNS, transcutaneous auricular vagus nerve stimulation; UESP, upper esophageal sphincter pressure; UESL, upper esophageal sphincter length; LESP, lower esophageal sphincter pressure; LESL, lower esophageal sphincter length; CFV, contraction front velocity; DL, distal latency; DCI, distal contraction integral; IRP, integrated relaxation pressure. *$p < 0.05$ vs. before treatment.

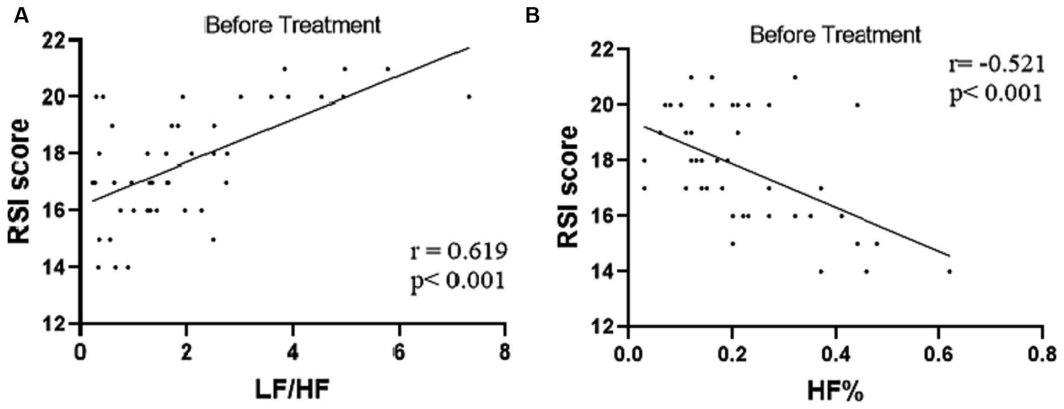

FIGURE 6
(A) Correlation of LF/HF with RSI score (n = 44). **(B)** Correlation of HF% with RSI score (n = 44).

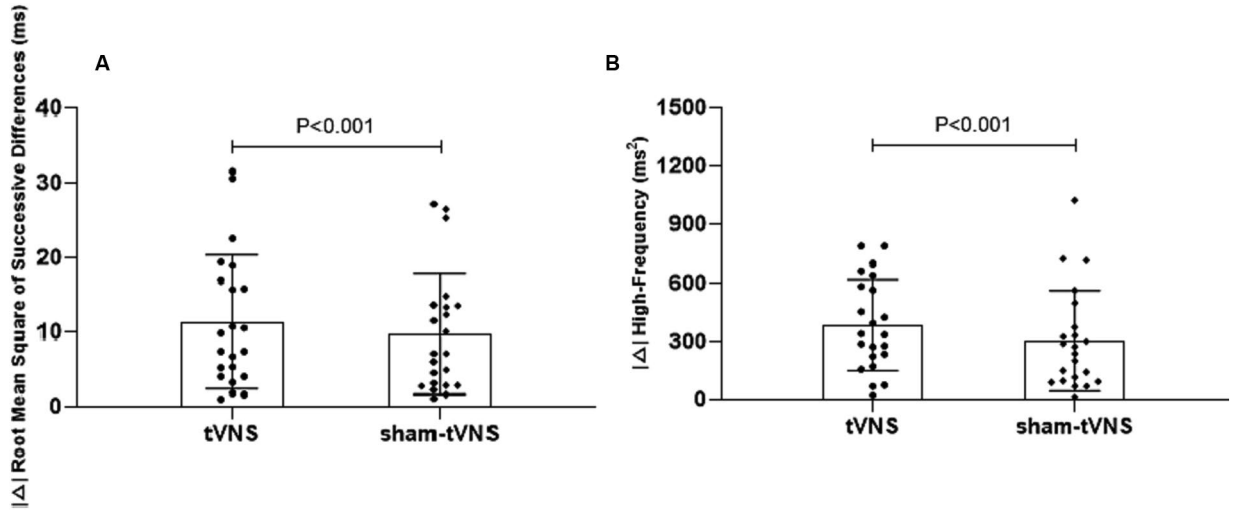

FIGURE 7
(A) The effect of tVNS (n = 22) compared with sham-tVNS (n = 22) on delta RMSSD. *$p < 0.05$ vs. before treatment. **(B)** Effect of tVNS (n = 22) and sham-tVNS (n = 22) on delta HF. *$p < 0.05$ vs. before treatment.

TABLE 4 Effects of tVNS and sham-tVNS on high-resolution esophageal manometry.

	UESP (mmHg)			UESL (cm)			LESP (mmHg)			LESL (cm)		
	Before treatment	After treatment	Difference	Before treatment	After treatment	Difference	Before treatment	After treatment	Difference	Before treatment	After treatment	Difference
tVNS (n = 22)	51.80 ± 9.34	81.12 ± 12.18	29.32 ± 10.25	5.14 ± 0.81	5.05 ± 1.01	0.09 ± 0.48	20.78 ± 5.47	25.09 ± 5.05	4.31 ± 4.93	2.99 ± 0.42	2.97 ± 0.37	0.02 ± 0.34
sham-tVNS (n = 22)	53.40 ± 8.84	55.88 ± 8.45	2.48 ± 6.56	4.99 ± 1.08	5.07 ± 0.78	0.08 ± 0.46	20.13 ± 6.14	19.88 ± 4.77	−0.25 ± 2.28	2.99 ± 0.43	2.95 ± 0.34	0.04 ± 0.32
t	0.76	12.12	15.28	0.58	0.43	0.39	0.17	4.56	5.29	0.08	0.19	0.22
P	0.53	**<0.001**	**<0.001**	0.73	0.78	0.81	0.88	**0.03**	**0.01**	0.93	0.85	0.81
	CFV (cm/s)			DL (s)			DCI (mmHg•cm•s)			IRP (mmHg)		
tVNS (n = 22)	4.52 ± 1.14	3.50 ± 0.85	1.02 ± 0.88	7.96 ± 1.09	7.02 ± 0.91	0.94 ± 0.81	2047.13 ± 477.61	2453.90 ± 509.11	406.77 ± 327.21	4.97 ± 1.67	8.02 ± 2.04	3.05 ± 1.26
sham-tVNS (n = 22)	4.51 ± 0.80	4.49 ± 0.75	−0.02 ± 0.66	8.10 ± 0.92	7.90 ± 0.99	0.14 ± 0.62	1941.50 ± 601.33	2052.62 ± 479.63	111.12 ± 408.89	4.94 ± 1.84	5.02 ± 1.56	0.08 ± 1.19
t	0.08	4.93	5.02	0.19	3.98	4.02	0.58	11.28	15.59	0.53	9.98	10.26
P	0.93	**0.02**	**0.02**	0.86	**0.04**	**0.04**	0.73	**<0.001**	**<0.001**	0.77	**<0.001**	**<0.001**

tVNS, transcutaneous auricular vagus nerve stimulation; UESP, upper esophageal sphincter pressure; UESL, upper esophageal sphincter length; LESP, lower esophageal sphincter pressure; LESL, lower esophageal sphincter length; CFV, contraction front velocity; DL, distal latency; DCI, distal contraction integral; IRP, integrated relaxation pressure. *P < 0.05 vs. before treatment.

RSI scores surpassing 13 indicate the likelihood of LPRD, and the subsequent reduction below this threshold post-tVNS suggests resolution of the condition (Morice et al., 2022). Insight from prior studies also suggests a close interplay between depression, anxiety, and the occurrence of LPRD (Liu et al., 2022). Indeed, Caparroz et al. (2019) propose that LPRD patients often grapple with anxiety and/or depression attributed to compromised autonomic regulatory function. In congruence with these observations, the present study unveils a positive correlation between reflux symptoms and both anxiety and depressive symptoms, manifesting as significant associations between RSI scores and scores from the HAMA or the HAMD. This empirical discovery aligns with research by Huang et al. (2022). Remarkably, the application of tVNS led to a pronounced reduction in anxiety and depression scores among LPRD patients. These effects are likely attributed to the central impacts of tVNS, which have been noted in previous studies involving patients with neurological disorders (Redgrave et al., 2018; Sun et al., 2022).

The UES and LES constitute vital elements of the esophageal-pharyngeal mechanical barrier. The LES, functioning as the primary defense against reflux, inhibits the retrograde flow of gastroduodenal contents into the esophagus. Simultaneously, the UES safeguards the upper pharyngeal region against the ingress of these contents. In the context of diminished LES function, a compensatory elevation in UES resting pressure can mitigate potential reflux incidents, an anatomical foundation paramount in LPRD (Hunt et al., 1970). Factors such as age-related changes and esophageal pathologies may precipitate UES relaxation, facilitating reflux into the pharyngeal area, thereby perpetuating a cycle whereby symptomatology impacts UES contractile function, creating a self-perpetuating loop (Vardouniotis et al., 2009). Subsequent to short-term or sustained exposure to esophageal acid, diastolic reflex in the esophagus intensifies, while contractile reflex weakens, contributing to UES relaxation (Lang et al., 2019). Altered vagal modulation can disrupt LES and UES function, a phenomenon evident in cases of vagal hypoplasia (Wang et al., 2019). Studies by Szczesniak et al. (2011) and Ranjbar et al. (2022) revealed substantial pressure irregularities in the LES and UES of LPRD patients, underlining the prevalence of comorbid esophageal dyskinesia in these individuals (Szczesniak et al. 2011; Ranjbar et al. 2022). Our previous study reported that transcutaneous electrical acustimulation improved the reflux symptoms in GERD patients by increasing LESP, which may be mediated via the autonomic and enteric mechanisms (Yu et al., 2019).

In a similar vein, HRV spectral analysis proved instrumental in quantifying parasympathetic and sympathetic activity (Pachon-M et al., 2020). This approach, applied to LPRD patients, unveiled a positive correlation between sympathetic activity and the Reflux Symptom Index (RSI), coupled with a negative correlation between parasympathetic activity and RSI. Such findings align with prior research by Wang et al. (2019). While acknowledging this, it's important to underscore that our study centered exclusively on LPRD patients, precluding direct comparison with healthy volunteers, thus preventing definitive confirmation of autonomic nervous function impairment in LPRD patients. Reduced parasympathetic activity and sympathetic imbalance are implicated in conditions like refractory gastroesophageal reflux disease (rGERD) and functional outlet obstructive constipation (FOOC; Liu et al., 2020). Strategies aimed at enhancing parasympathetic activity might offer efficacy in addressing these disorders (Liu et al., 2020; Yang et al., 2022). Meanwhile, our latest basic study reported that tVNS significantly improved the constipation-predominant irritable

TABLE 5 Effects of tVNS and sham-tVNS on autonomic functions.

	RMSSD			HF		
	Before treatment	After treatment	Difference	Before treatment	After treatment	Difference
tVNS ($n = 22$)	40.54 ± 12.30	46.70 ± 11.87	6.16 ± 3.37	596.46 ± 59.86	856.44 ± 39.40	259.98 ± 40.26
sham-tVNS ($n = 22$)	36.86 ± 11.85	40.42 ± 12.23	3.56 ± 2.13	598.44 ± 59.63	607.26 ± 57.25	8.82 ± 3.40
t	2.17	12.48	10.28	0.18	23.56	20.18
P	0.38	**<0.001**	**<0.001**	0.59	**<0.001**	**<0.001**

tVNS, transcutaneous auricular vagus nerve stimulation. *$P < 0.05$ vs. before treatment. RMSSD, root mean square of successive differences; HF, high frequency.

bowel syndrome symptoms (Liu et al., 2024). Interestingly, the current study demonstrated tVNS-induced elevation of parasympathetic activity among LPRD patients compared to baseline. Prior research utilizing functional magnetic resonance imaging (fMRI) analysis highlighted increased blood-oxygen-level-dependent (BOLD) signals in brain regions such as the postcentral gyrus, bilateral insula, frontal cortex, operculum, and cerebellum in response to tVNS. These responses may be attributed to the stimulation of afferent fibers of the auricular branch of the vagus nerve and in turn a possible modulation of efferent parasympathetic fibers via the brain. This mechanistic cascade culminates in amplified proximal esophageal constriction (Badran et al., 2018; Tsou et al., 2021).

5 Limitations

Notwithstanding, this pilot clinical inquiry entails several limitations. It functions as a single-blind study conducted within a single center, involving a relatively small sample size. The absence of long-term follow-up observations necessitates cautious interpretation of the study's results, as they may not entirely encapsulate the prolonged effects of tVNS treatment in the entirety of LPRD patients. As a means to rectify these limitations, the prospect of executing a large-scale, multicenter, double-blind pilot study emerges to yield a more comprehensive comprehension of the response of LPRD patients to tVNS treatment. Notably, the cavity concha was found to not only be innervate by the vagus nerve in earlier studies (Peuker and Filler, 2002), which may have a certain impact on the results. Finally, we acknowledge that false positives were not controlled for via statistical corrections, though the study's exploratory nature entailed numerous, related statistical comparisons.

6 Conclusion

In summation, the present short-term tVNS intervention yielded improvements in pharyngeal discomfort and mental well-being, concomitant with heightened UES pressure and augmented parasympathetic activity. These enhancements are likely underpinned by intricate autonomic and esophageal mechanisms. Offering a needleless, self-administered approach, tVNS emerges as a potentially accessible and cost-effective adjunctive therapy for individuals with LPRD. However, further exploration is requisite to uncover the cellular and molecular pathways through which tVNS mitigates LPRD and its enduring effects on patients.

Data availability statement

The original contributions presented in the study are included in the article/supplementary material, further inquiries can be directed to the corresponding author.

Ethics statement

The studies involving humans were approved by Ethics Committee of the First Affiliated Hospital of USTC (Registration No: 2016-L36). The studies were conducted in accordance with the local legislation and institutional requirements. The participants provided their written informed consent to participate in this study.

Author contributions

YH: Writing – original draft, Writing – review & editing. JL: Writing – original draft, Writing – review & editing. CL: Writing – original draft, Writing – review & editing. CS: Writing – review & editing. MM: Writing – review & editing. SL: Writing – review & editing. YY: Writing – original draft, Writing – review & editing.

Funding

The author(s) declare that financial support was received for the research, authorship, and/or publication of this article. This study was supported by the External Science and Technology Cooperation Planning Projects of Anhui Province of China (no. 1604b0602021).

Acknowledgments

The authors thank all participants in this research.

Conflict of interest

The authors declare that the research was conducted in the absence of any commercial or financial relationships that could be construed as a potential conflict of interest.

Publisher's note

References

Badran, B. W., Dowdle, L. T., Mithoefer, O. J., LaBate, N. T., Coatsworth, J., Brown, J. C., et al. (2018). Neurophysiologic effects of transcutaneous auricular vagus nerve stimulation (taVNS) via electrical stimulation of the tragus: A concurrent taVNS/fMRI study and review. *Brain Stimul.* 11, 492–500. doi: 10.1016/j.brs.2017.12.009

Baldissarelli, J., Santi, A., Schmatz, R., Abdalla, F. H., Cardoso, A. M., Martins, C. C., et al. (2017). Hypothyroidism enhanced Ectonucleotidases and acetylcholinesterase activities in rat Synaptosomes can be prevented by the naturally occurring polyphenol quercetin. *Cell. Mol. Neurobiol.* 37, 53–63. doi: 10.1007/s10571-016-0342-7

Beh, S. C., and Friedman, D. I. (2019). Acute vestibular migraine treatment with noninvasive vagus nerve stimulation. *Neurology* 93, E1715–E1719. doi: 10.1212/WNL.0000000000008388

Belafsky, P. C., Postma, G. N., and Koufman, J. A. (2002). Validity and reliability of the reflux symptom index (RSI). *J. Voice* 16, 274–277. doi: 10.1016/S0892-1997(02)00097-8

Benjamin, T., Zackria, S., Lopez, R., Richter, J., and Thota, P. N. (2017). Upper esophageal sphincter abnormalities and high-resolution esophageal manometry findings in patients with laryngopharyngeal reflux. *Scand. J. Gastroenterol.* 52, 816–821. doi: 10.1080/00365521.2017.1322139

Bottomley, J. M., LeReun, C., Diamantopoulos, A., Mitchell, S., and Gaynes, B. N. (2020). Vagus nerve stimulation (VNS) therapy in patients with treatment resistant depression: A systematic review and meta-analysis. *Compr. Psychiatry* 98:152156. doi: 10.1016/j.comppsych.2019.152156

Caparroz, F. A., Torres Campanholo, M. A., Regina, C. G., Park, S. W., Haddad, L., Gregório, L. C., et al. (2019). Clinical and polysomnographic predictors of laryngopharyngeal reflux in obstructive sleep apnea syndrome. *Braz. J. Otorhinolaryngol.* 85, 408–415. doi: 10.1016/j.bjorl.2018.03.007

Carreno, F. R., and Frazer, A. (2016). The allure of transcutaneous Vagus nerve stimulation as a novel therapeutic modality. *Biol. Psychiatry* 79, 260–261. doi: 10.1016/j.biopsych.2015.11.016

Cui, X. H., Zhang, Y. P., Yan, X. Y., Liu, J. W., Li, L. N., Jiang, X. W., et al. (2019). Relationship between sleep status and laryngopharyngeal reflux disease in adult patients in otolaryngology clinic. *Zhonghua Er Bi Yan Hou Tou Jing Wai Ke Za Zhi* 54, 754–759. doi: 10.3760/cma.j.issn.1673-0860.2019.10.009

Falk, G. L., and Vivian, S. J. (2016). Laryngopharyngeal reflux: diagnosis, treatment and latest research. *Eur Surg Acta Chirurg Austr.* 48, 74–91. doi: 10.1007/s10353-016-0385-5

Farmer, A. D., Strzelczyk, A., Finisguerra, A., Gourine, A. V., Gharabaghi, A., Hasan, A., et al. (2021). International consensus based review and recommendations for minimum reporting standards in research on transcutaneous Vagus nerve stimulation (version 2020). *Front. Hum. Neurosci.* 14:568051. doi: 10.3389/fnhum.2020.568051

Hamilton, M. (1959). The assessment of anxiety states by rating. *Br. J. Med. Psychol.* 32, 50–55. doi: 10.1111/j.2044-8341.1959.tb00467.x

Hamilton, M. (1960). A RATING SCALE FOR DEPRESSION. *J. Neurol. Neurosurg. Psychiatry* 23, 56–62. doi: 10.1136/jnnp.23.1.56

Hong, G.-S., Pintea, B., Lingohr, P., Coch, C., Randau, T., Schaefer, N., et al. (2019). Effect of transcutaneous vagus nerve stimulation on muscle activity in the gastrointestinal tract (transVaGa): a prospective clinical trial. *Int. J. Colorectal Dis.* 34, 417–422. doi: 10.1007/s00384-018-3204-6

Huang, F., Liao, Q., Gan, X., and Wen, W. (2022). Correlation between refractory laryngopharyngeal reflux disease and symptoms of anxiety and depression. *Neuropsychiatr. Dis. Treat.* 18, 925–932. doi: 10.2147/NDT.S349933

Hunt, P. S., Connell, A. M., and Smiley, T. B. (1970). The cricopharyngeal sphincter in gastric reflux. *Gut* 11, 303–306. doi: 10.1136/gut.11.4.303

Keute, M., Ruhnau, P., Heinze, H.-J., and Zaehle, T. (2018). Behavioral and electrophysiological evidence for GABAergic modulation through transcutaneous vagus nerve stimulation. *Clin. Neurophysiol.* 129, 1789–1795. doi: 10.1016/j.clinph.2018.05.026

Lang, I. M., Medda, B. K., and Shaker, R. (2019). Effects of esophageal acidification on esophageal reflexes controlling the upper esophageal sphincter. *Am. J. Physiol. Gastrointest. Liver Physiol.* 316, G45–G54. doi: 10.1152/ajpgi.00292.2018

Lechien, J. R., Bobin, F., Muls, V., Saussez, S., and Hans, S. (2021). Laryngopharyngeal reflux disease is More severe in obese patients: A prospective multicenter study. *Laryngoscope* 131, E2742–E2748. doi: 10.1002/lary.29676

Li, S., Zhai, X., Rong, P., McCabe, M. F., Wang, X., Zhao, J., et al. (2014). Therapeutic effect of vagus nerve stimulation on depressive-like behavior, hyperglycemia and insulin receptor expression in Zucker fatty rats. *PLoS One* 9:e112066. doi: 10.1371/journal.pone.0112066

Liu, J., Chen, H., Wu, D., Wei, R., Lv, C., Dong, J., et al. (2020). Ameliorating effects of transcutaneous electrical Acustimulation at Neiguan (PC6) and Zusanli (ST36) Acupoints combined with adaptive biofeedback training on functional outlet obstruction constipation. *Evid. Based Complement. Alternat. Med.* 2020, 1–10. doi: 10.1155/2020/8798974

Liu, J., Dai, Q., Qu, T., Ma, J., Lv, C., Wang, H., et al. (2024). Ameliorating effects of transcutaneous auricular vagus nerve stimulation on a mouse model of constipation-predominant irritable bowel syndrome. *Neurobiol. Dis.* 193:106440. doi: 10.1016/j.nbd.2024.106440

Liu, Y., Wu, J., Xiao, F., Gu, X., and Ji, L. (2022). Correlation and influencing factors between laryngopharyngeal reflux disease and sleep status in patients. *Front. Surg.* 9:845653. doi: 10.3389/fsurg.2022.845653

Long, L., Zang, Q., Jia, G., Fan, M., Zhang, L., Qi, Y., et al. (2022). Transcutaneous auricular Vagus nerve stimulation promotes white matter repair and improves dysphagia symptoms in cerebral ischemia model rats. *Front. Behav. Neurosci.* 16:419. doi: 10.3389/fnbeh.2022.811419

Mishra, P., Agrawal, D., and Artham, P. (2020). Screening test for LPRD: history versus video laryngoscopy. *Indian J. Otolaryngol. Head Neck Surg.* 72, 422–427. doi: 10.1007/s12070-020-01828-7

Morice, D. R. L., Elhassan, H. A., Myint-Wilks, L., Barnett, R. E., Rasheed, A., Collins, H., et al. (2022). Laryngopharyngeal reflux: is laparoscopic fundoplication an effective treatment? *Ann. R. Coll. Surg. Engl.* 104, 79–87. doi: 10.1308/rcsann.2021.0046

Pachon-M, J. C., Pachon-M, E. I., Pachon, C. T. C., Santillana-P, T. G., Lobo, T. J., Pachon-M, J. C., et al. (2020). Long-term evaluation of the vagal denervation by Cardioneuroablation using Holter and heart rate variability. *Circ. Arrhythm. Electrophysiol.* 13:e008703. doi: 10.1161/CIRCEP.120.008703

Pappa, S., Ntella, V., Giannakas, T., Giannakoulis, V. G., Papoutsi, E., and Katsaounou, P. (2020). Prevalence of depression, anxiety, and insomnia among healthcare workers during the COVID-19 pandemic: A systematic review and meta-analysis. *Brain Behav. Immun.* 88, 901–907. doi: 10.1016/j.bbi.2020.05.026

Peuker, E. T., and Filler, T. J. (2002). The nerve supply of the human auricle. *Clin. Anat.* 15, 35–37. doi: 10.1002/ca.1089

Ranjbar, P. A., Alnouri, G., Vance, D., Park, J., Suresh, A., Acharya, P., et al. (2022). The prevalence of esophageal disorders among voice patients with laryngopharyngeal reflux-a retrospective study. *J. Voice* 36, 410–412. doi: 10.1016/j.jvoice.2020.07.005

Redgrave, J., Day, D., Leung, H., Laud, P. J., Ali, A., Lindert, R., et al. (2018). Safety and tolerability of transcutaneous Vagus nerve stimulation in humans; a systematic review. *Brain Stimul.* 11, 1225–1238. doi: 10.1016/j.brs.2018.08.010

Ryvlin, P., Gilliam, F. G., Nguyen, D. K., Colicchio, G., Iudice, A., Tinuper, P., et al. (2014). The long-term effect of vagus nerve stimulation on quality of life in patients with pharmacoresistant focal epilepsy: the PuLsE (open prospective randomized Long-term effectiveness) trial. *Epilepsia* 55, 893–900. doi: 10.1111/epi.12611

Shen, H., Han, Y., Yao, C., Tao, Y., Wu, J., Gao, C., et al. (2023). Transcutaneous electrical acupoint stimulation for suspected laryngopharyngeal reflux disease. *Eur. Arch. Otorhinolaryngol.* 280, 1815–1825. doi: 10.1007/s00405-022-07698-9

Shi, X., Hu, Y., Zhang, B., Li, W., Chen, J. D., and Liu, F. (2021). Ameliorating effects and mechanisms of transcutaneous auricular vagal nerve stimulation on abdominal pain and constipation. *JCI Insight* 6:e150052. doi: 10.1172/jci.insight.150052

Steward, D. L., Wilson, K. M., Kelly, D. H., Patil, M. S., Schwartzbauer, H. R., Long, J. D., et al. (2004). Proton pump inhibitor therapy for chronic laryngo-pharyngitis: A randomized placebo-control trial. *Otolaryngol. Head Neck Surg.* 131, 342–350. doi: 10.1016/j.otohns.2004.03.037

Sun, J., Ma, Y., Du, Z., Wang, Z., Guo, C., Luo, Y., et al. (2022). Immediate modulation of transcutaneous auricular Vagus nerve stimulation in patients with treatment-resistant depression: A resting-state functional magnetic resonance imaging study. *Front. Psych.* 13:783. doi: 10.3389/fpsyt.2022.923783

Szczesniak, M. M., Williams, R. B., and Cook, I. J. (2011). Mechanisms of esophago-pharyngeal acid regurgitation in human subjects. *PLoS One* 6:e22630. doi: 10.1371/journal.pone.0022630

Tsou, Y.-A., Chen, S.-H., Wu, W.-C., Tsai, M. H., Bassa, D., Shih, L. C., et al. (2021). Esophageal pressure and clinical assessments in the gastroesophageal reflux disease patients with laryngopharyngeal reflux disease. *J. Clin. Med.* 10:5262. doi: 10.3390/jcm10225262

Vardouniotis, A. S., Karatzanis, A. D., Tzortzaki, E., Athanasakis, E., Samara, K. D., Chalkiadakis, G., et al. (2009). Molecular pathways and genetic factors in the

pathogenesis of laryngopharyngeal reflux. *Eur. Arch. Otorhinolaryngol.* 266, 795–801. doi: 10.1007/s00405-009-0966-z

Ventureyra, E. C. G. (2000). Transcutaneous vagus nerve stimulation for partial onset seizure therapy—A new concept. *Childs Nerv. Syst.* 16, 101–102. doi: 10.1007/s003810050021

Wang, X., Chu, L., Liu, C., Wei, R., Xue, X., Xu, Y., et al. (2018). Therapeutic effects of Saussurea involucrata injection against severe acute pancreatitis-induced brain injury in rats. *Biomed. Pharmacother.* 100, 564–574. doi: 10.1016/j.biopha.2018.02.044

Wang, S., Li, S., Zhai, X., Rong, P., He, J., Liu, L., et al. (2022). Transcutaneous auricular vagal nerve stimulation releases extrapineal melatonin and reduces thermal hypersensitivity in Zucker diabetic fatty rats. *Front. Neurosci.* 16:916822. doi: 10.3389/fnins.2022.916822

Wang, A. M., Wang, G., Huang, N., Zheng, Y. Y., Yang, F., Qiu, X., et al. (2019). Association between laryngopharyngeal reflux disease and autonomic nerve dysfunction. *Eur. Arch. Otorhinolaryngol.* 276, 2283–2287. doi: 10.1007/s00405-019-05482-w

Wang, S., Zhai, X., Li, S., McCabe, M. F., Wang, X., and Rong, P. (2015). Transcutaneous vagus nerve stimulation induces tidal melatonin secretion and has an antidiabetic effect in Zucker fatty rats. *PLoS One* 10:e0124195. doi: 10.1371/journal.pone.0124195

Yang, R., Du, X., Li, Z., Zhao, X., Lyu, X., Ye, G., et al. (2022). Association of Subclinical Hypothyroidism with Anxiety Symptom in young first-episode and drug-naive patients with major depressive disorder. *Front. Psych.* 13:920723. doi: 10.3389/fpsyt.2022.920723

Yu, Y., Wei, R., Liu, Z., Xu, J., Xu, C., and Chen, J. D. Z. (2019). Ameliorating effects of transcutaneous electrical Acustimulation combined with deep breathing training on refractory gastroesophageal reflux disease mediated via the autonomic pathway. *Neuromodulation* 22, 751–757. doi: 10.1111/ner.13021

Zhang, C., Liu, Z., Liu, L., Li, J., Wang, X., Ju, J., et al. (2023). A study of the diagnostic value of the sign and symptom questionnaires for laryngopharyngeal reflux disease. *Otolaryngol. Head Neck Surg.* 170:474. doi: 10.1002/ohn.564

Zhang, B., Xu, F., Hu, P., Zhang, M., Tong, K., Ma, G., et al. (2018). Needleless transcutaneous electrical Acustimulation: A pilot study evaluating improvement in post-operative recovery. *Am. J. Gastroenterol.* 113, 1026–1035. doi: 10.1038/s41395-018-0156-y

Zhu, Y., Xu, F., Lu, D., Rong, P., Cheng, J., Li, M., et al. (2021). Transcutaneous auricular vagal nerve stimulation improves functional dyspepsia by enhancing vagal efferent activity. *Am. J. Physiol. Gastrointest. Liver Physiol.* 320, G700–G711. doi: 10.1152/ajpgi.00426.2020

frontiers | Frontiers in Neuroscience

TYPE Original Research
PUBLISHED 08 March 2024
DOI 10.3389/fnins.2024.1346634

OPEN ACCESS

EDITED BY
Vitor Engracia Valenti,
São Paulo State University, Brazil

REVIEWED BY
Jack Jiaqi Zhang,
Hong Kong Polytechnic University,
Hong Kong SAR, China
Jitka Veldema,
Bielefeld University, Germany

*CORRESPONDENCE
Zhong-Li Jiang
✉ jiangzhongli@njmu.edu.cn

†These authors have contributed equally to this work and share first authorship

RECEIVED 29 November 2023
ACCEPTED 27 February 2024
PUBLISHED 08 March 2024

CITATION
Wang M-H, Wang Y-X, Xie M, Chen L-Y, He M-F, Lin F and Jiang Z-L (2024) Transcutaneous auricular vagus nerve stimulation with task-oriented training improves upper extremity function in patients with subacute stroke: a randomized clinical trial.
Front. Neurosci. 18:1346634.
doi: 10.3389/fnins.2024.1346634

Transcutaneous auricular vagus nerve stimulation with task-oriented training improves upper extremity function in patients with subacute stroke: a randomized clinical trial

Meng-Huan Wang[1,2†], Yi-Xiu Wang[1,2†], Min Xie[3], Li-Yan Chen[1,2], Meng-Fei He[1,2], Feng Lin[2,3] and Zhong-Li Jiang[2,3*]

[1]School of Rehabilitation Medicine, Nanjing Medical University, Nanjing, Jiangsu, China, [2]Department of Rehabilitation Medicine, The First Affiliated Hospital of Nanjing Medical University, Nanjing, Jiangsu, China, [3]Department of Rehabilitation Medicine, Sir Run Run Hospital, Nanjing Medical University, Nanjing, Jiangsu, China

Background: Transcutaneous auricular vagus nerve stimulation (taVNS) has emerged as a promising brain stimulation modality in poststroke upper extremity rehabilitation. Although several studies have examined the safety and reliability of taVNS, the mechanisms underlying motor recovery in stroke patients remain unclear.

Objectives: This study aimed to investigate the effects of taVNS paired with task-oriented training (TOT) on upper extremity function in patients with subacute stroke and explore the potential underlying mechanisms.

Methods: In this double-blinded, randomized, controlled pilot trial, 40 patients with subacute stroke were randomly assigned to two groups: the VNS group (VG), receiving taVNS during TOT, and the Sham group (SG), receiving sham taVNS during TOT. The intervention was delivered 5 days per week for 4 weeks. Upper extremity function was measured using the Fugl-Meyer Assessment-Upper Extremity (FMA-UE), the Action Research Arm Test (ARAT). Activities of daily living were measured by the modified Barthel Index (MBI). Motor-evoked potentials (MEPs) were measured to evaluate cortical excitability. Assessments were administered at baseline and post-intervention. Additionally, the immediate effect of taVNS was detected using functional near-infrared spectroscopy (fNIRS) and heart rate variability (HRV) before intervention.

Results: The VG showed significant improvements in upper extremity function (FMA-UE, ARAT) and activities of daily living (MBI) compared to the SG at post-intervention. Furthermore, the VG demonstrated a higher rate of elicited ipsilesional MEPs and a shorter latency of MEPs in the contralesional M1. In the VG, improvements in FMA-UE were significantly associated with reduced latency of contralesional MEPs. Additionally, fNIRS revealed increased activation in the contralesional prefrontal cortex and ipsilesional sensorimotor cortex in the VG in contrast to the SG. However, no significant between-group differences were found in HRV.

Conclusion: The combination of taVNS with TOT effectively improves upper extremity function in patients with subacute stroke, potentially through

modulating the bilateral cortex excitability to facilitate task-specific functional recovery.

KEYWORDS

transcutaneous auricular vagus nerve stimulation, task-oriented training, motor evoked potentials, functional near-infrared spectroscopy, stroke, upper extremity rehabilitation

1 Introduction

A cerebrovascular accident (CVA), often referred to as a stroke, arises from an interruption of blood flow or bleeding in a region of the brain, resulting in impaired brain function. According to the Global Burden of Disease (GBD) study, stroke is the primary cause of mortality among Chinese adults and the second leading cause of death worldwide (Zhou et al., 2019; GBD 2019 Stroke Collaborators, 2021). Reports indicate that 55–75% of stroke patients continue to experience upper extremity motor dysfunction within 3–6 months of onset (Kwakkel et al., 2003). Upper extremity motor dysfunction markedly influences the prognosis of patients, impacting their mobility, daily activities, and overall quality of life (Lai et al., 2002; Nichols-Larsen et al., 2005). For poststroke upper extremity rehabilitation, the task-oriented training (TOT) involves structured movement training based on daily activities to engage patients actively, thereby promoting motor function during the targeted task practice (Yoo and Park, 2015). Motor priming, a type of implicit learning wherein external stimulation prompts changes in the motor cortex and behavior, has been reported in motor skill learning recently (Jin et al., 2019). Previous research demonstrated that stimulation-based priming combined with TOT could facilitate brain reorganization and enhance upper extremity dexterity (Higgins et al., 2013; Alsubiheen et al., 2022). The most commonly used non-invasive brain stimulation techniques include transcranial magnetic stimulation (TMS) and transcranial direct current stimulation (tDCS) (Chhatbar et al., 2017; Bai et al., 2022; Zhang et al., 2022). However, the application of TMS and tDCS is limited by the need for high precision requirements and complex operations.

Vagus nerve stimulation (VNS) acts as a promising brain stimulation-based priming technique involving various forms of stimulation applied to the vagus nerve network. By regulating the balance of the autonomic nervous system and targeting neuroprotective and neuroplasticity pathways, VNS holds potential as a therapeutic tool in various neurological and psychiatric conditions (Ma et al., 2019). A multicenter, randomized, double-blind trial (VNS-REHAB) conducted by Dawson et al. (2021) confirmed the effectiveness of implanted VNS (iVNS) paired with upper extremity training in patients with ischemic stroke. However, the application process of iVNS may carry a high rate of potential complications due to its invasiveness (Ma et al., 2019). Recently, transcutaneous auricular VNS (taVNS), as a safe and easy-to-use neuromodulation technique, has been proposed, which utilizes transcutaneous stimulation of the cymba conchae and tragus innervated by fibers of the auricular branch of the vagus nerve (ABVN). Neuroimaging studies have demonstrated that taVNS can elicit brain activation effects similar to iVNS (Badran et al., 2018). Several studies (Capone et al., 2017; Redgrave et al., 2018; Wu et al., 2020; Chang et al., 2021; Li et al., 2022) have combined taVNS with regular rehabilitation training or robot-assisted arm training to improve upper extremity function in hemiplegic patients. To ensure consistency in taVNS research, an international consensus has been established for minimum reporting standards, which reported that a signal with a pulse width between 200 and 300 μs at 25 Hz, and a duty cycle of 30 s on, 30 s off has often been adopted in studies (Farmer et al., 2021). Nonetheless, the mechanism by which taVNS achieves task-specific benefits in upper extremity function remains unclear. In this study, we hypothesized that combining taVNS with TOT simultaneously would present a novel approach to enhance upper extremity function recovery in stroke patients. To assess the immediate and long-term effects of taVNS on hemodynamics and cortical excitability, we employed functional near-infrared spectroscopy (fNIRS) and single-pulse transcranial magnetic stimulation (TMS), respectively. The primary objective of this study was to investigate the effects and potential mechanisms of taVNS paired with TOT in facilitating the recovery of upper extremity function in patients with subacute stroke.

2 Materials and methods

2.1 Participants

The stroke patients with upper extremity motor dysfunction were recruited from the Department of Rehabilitation Medicine at Sir Run Run Hospital of Nanjing Medical University between February 2020 and December 2022. The inclusion criteria were as follows: (1) first-time occurrence of a unilateral supratentorial stroke confirmed by computed tomography (CT) or magnetic resonance imaging (MRI) within 6 months of onset; (2) presence of unilateral hemiplegia of the upper extremity; (3) upper extremity impairment ≥ third level in the Functional Test for the Hemiparetic Upper Extremity (FTHUE), and FMA-UE scores ranged from 20 ~ 50; and (4) normal cognitive function with the ability to follow instructions and complete the study. The exclusion criteria were as follows: (1) presence of implanted electronic devices, intracerebral vascular clips, or other electrically activated or sensitive support systems; (2) presence of abnormal skin conditions that may interfere with the stimulation or the stimulation device, such as scar tissue, broken skin; (3) presence of severe cardiovascular, pulmonary, or advanced diseases affecting other systems; (4) previous impairment of the vagus nerve; (5) upper extremity dysfunction caused by reasons other than stroke; (6) use of neuropsychotropic drugs such as antidepressants or benzodiazepines; (7) Botox injection within the past 3 months; (8) resting heart rate below 60 beats per minute; and (9) presence of asthma, tumors, or

severe dysphagia. The trial was performed in accordance with the principles of the Declaration of Helsinki and received approval from the Ethics Committee of Sir Run Run Hospital, Nanjing Medical University (No. 2020-SR-001). All participants signed informed consent. Further details regarding the subjects can be found in Table 1.

TABLE 1 Demographics and baseline clinical characteristic.

Characteristics	Groups		
	VNS group (n = 20)	Sham group (n = 20)	p-value
Age (years)	55 (11)	57 (11)	0.515[a]
Gender			
male	18 (90)	15 (75)	0.407[b]
female	2 (10)	5 (25)	
Stroke onset (months)	3.20 (2.04)	4.15 (1.60)	0.074[a]
Hemiparetic side			
left	9 (45)	8 (40)	0.749[c]
right	11 (55)	12 (60)	
Stroke type			
ischemic	13 (65)	14 (70)	0.736[c]
hemorrhagic	7 (35)	6 (30)	
FMA-UE	31 (9)	30 (9)	0.665[d]
ARAT	16 (11)	15 (11)	0.968[d]
FTHUE	5.85 (2.06)	6.05 (2.76)	0.945[a]
MBI	72 (17)	69 (15)	0.543[a]
HR	83 (11)	79 (12)	0.271[a]

[a]Welch two sample t-test; [b]Fisher's exact test; 'Pearson's Chi-squared test; [d]Wilcoxon rank sum test. FMA-UE,Fugl-Meyer assessment-upper extremity; ARAT, Action Research Arm Test; FTHUE, Functional Test for the Hemiparetic Upper Extremity; MBI, Modified Barthel Index; HR, average heart rate.

2.2 Study design

This pilot study was designed as a randomized, double-blind, sham-controlled clinical trial, which followed the CONSORT checklist (Supplementary material S1). The patients were randomly assigned (1:1) to either the VNS group (VG) or the Sham group (SG) using a random number table. The patients in the VG received real taVNS during 1 h of task-oriented training, while the patients in the SG received sham taVNS during task-oriented training. The treatment was delivered 5 ays per week for 4 weeks. To minimize subjective bias, different individuals performed the roles of the TOT therapist, taVNS operator, and outcome assessor. To explore the immediate effect of taVNS, an fNIRS examination with HRV assessment was conducted before the first treatment session. The study flow is shown in Figure 1.

2.3 Intervention

2.3.1 Transcutaneous auricular vagus nerve stimulation (taVNS)

The taVNS treatment was delivered simultaneously with TOT for 1 h in accordance with Zhang et al. (2023), using the Auricular Vagus Nerve Stimulator (tVNS501, RISHENA Co., Ltd., Changzhou, China). A specialized earphone with two dot-like electrodes delivered electric stimulation to the left auricular cymba concha of patients in the VG. Conversely, patients in the SG wore the same earphones without electrodes. Although they could observe the current reading on the stimulator, no actual current was delivered, resulting in ineffective stimulation. Before stimulation, the left auricular concha of each patient was cleaned using alcohol wipes. According to the international consensus for minimum reporting standards (Farmer et al., 2021), the stimulation parameters were configured as follows: 500 μs square pulses at 25 Hz for 30 s, with a duty cycle of 1:1. The current intensity was individually adjusted to a tolerable level for each patient, ensuring that it did not exceed 10 mA (with an average of 6.55 ± 1.57 mA in the VG) (Capone et al., 2017; Redgrave et al., 2018; Wu et al., 2020; Li et al., 2022).

2.3.2 Task-oriented training (TOT)

Both groups of patients underwent TOT practice, which was supervised or assisted by a well-trained occupational therapist. The TOT practice involved eight exercises, requiring patients to perform as many trials as possible in each session. Each session of task-oriented training lasted for 1 h. The occupational therapist was allowed to adjust the intensity of each exercise based on the patient's training objectives and functional performance. The detailed steps of the TOT were as follows (Kim et al., 2013; Tang et al., 2014): (1) instruct patients to place their hand on a table with adjustable height; (2) instruct patients to touch the tip of their nose; (3) instruct patients to rotate their forearm and alternate the palm upwards and downwards; (4) instruct patients to bend the elbow to a 90-degree angle, position the forearm neutrally, and extend the wrist joint to touch a designated object on the table as far as possible; (5) while maintaining the same position as in step (4), instruct patients to grip and release a water bottle placed on the table; (6) instruct patients to pick up a cup from the table, simulating a drinking motion, then return it to its original position; (7) instruct patients to pour peanuts from a cup onto a plate on the table without using compensatory trunk movements; (8) instruct patients to manipulate objects with the assistant of a hand-function robot (Gloreha Professional 2, Idrogenet, Italy).

2.4 Outcome measurements

The long-term outcomes were assessed using clinical scales and motor-evoked potentials (MEPs) elicited by single-pulse TMS. The Fugl-Meyer Assessment-Upper Extremity (FMA-UE) and the Action Research Arm Test (ARAT) were employed to evaluate the function of the hemiplegic upper extremity, and the modified Barthel Index (MBI) was used to evaluate the activity of daily living (Chen et al., 2021). The MEPs were applied to evaluate the cortico-spinal excitability. The primary outcome measure was the change score of the Upper Extremity Fugl-Meyer Assessment (UE-FMA). All outcomes were evaluated before the first treatment and after the final treatment. Additionally, in order to explore the feasibility of the current study and assess the immediate effect of taVNS during grasp tasks with the hemiplegic hand, an fNIRS examination was conducted before the first treatment session. HRV data were collected before and after the

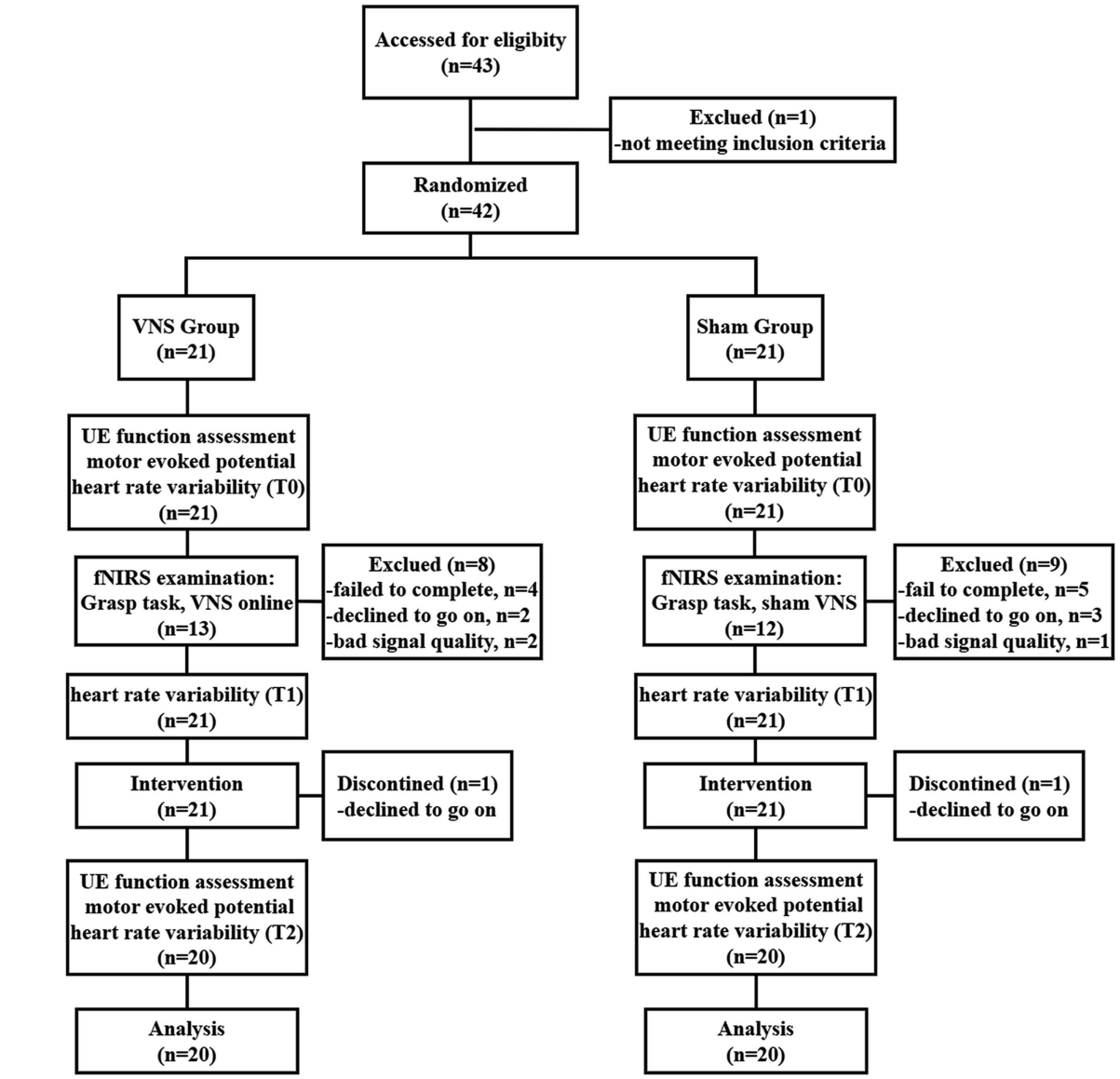

FIGURE 1
Study flow diagram. VNS: vagus nerve stimulation; UE, Upper extremity; fNIRS, Functional near-infrared spectroscopy.

fNIRS examination (T0, T1) and after the last treatment (T2) to assess the effectiveness of taVNS on the vagus nerve network.

2.4.1 Upper extremity function assessment

The Fugl-Meyer Assessment-Upper Extremity (FMA-UE) is a widely used tool for evaluating upper extremity impairment and coordination/speed in stroke patients. The FMA-UE comprises 33 items, each scored on a scale ranging from 0 to 2, culminating in a total score of 66 points (Gladstone et al., 2002; Rech et al., 2020).

The Action Research Arm Test (ARAT) is a standardized observational scale extensively used to assess the functional abilities of the upper extremity in stroke survivors, closely reflecting their daily activities. The ARAT consists of 19 items categorized into four subtests: grasping, gripping, pinching, and gross movement. Each item is scored on a scale from 0 to 3, with a maximum possible score of 57 (Hsieh et al., 1998; Zhao et al., 2019a, b).

The Modified Barthel Index (MBI) is a frequently used outcome measure to evaluate performance in activities of daily living (ADL) among stroke patients. The MBI comprises 10 items, with a total score of 100 (Shah et al., 1989).

2.4.2 Motor-evoked potentials examination

Motor-evoked potentials (MEPs) refer to the action potentials elicited by single-pulse TMS of the primary motor cortex (M1), providing insight into cortico-spinal excitability. MEP latency refers to the time taken for the motor response to occur after the stimulation of the motor cortex. It is calculated by measuring the time interval between the onset of stimulation and the onset of the MEP waveform (Rossi et al., 2021; Vucic et al., 2023). In certain research, the MEPs have been considered as indicators of motor cortical excitability in stroke patients (Mäkelä et al., 2015; Jo et al., 2016). Therefore, we utilized MEPs to evaluate the long-term effects of the intervention

on motor cortical excitability. The examination procedure in this study adhered to established practice guidelines (Fried et al., 2021). A figure-eight coil (Xiangyu Medical Co., Ltd., Henan, China) was placed over the M1 to elicit the MEPs, while surface electromyography (sEMG) was recorded from the first dorsal interosseous (FDI) muscle. The initial intensity was set at 30% of the maximum stimulator output (MSO). Then the intensity was increased by 5% until the minimum stimulus produced minimal motor-evoked responses (≥50 μV in at least 5 out of 10 trials) in the FDI. The average latency and amplitude of the bilateral MEPs were recorded. The detailed information can be found in Supplementary material S2. If MEPs could not be elicited even at 100% MSO, it was recorded as "NA." The examination was well tolerated by the patient without any adverse events.

2.4.3 Heart rate variability examination

HRV refers to the fluctuation in the time intervals between adjacent heartbeats. The link between vagus nerve activity and HRV has been established, as the heart is innervated by the vagus motor fibers (Shaffer and Ginsberg, 2017; Capilupi et al., 2020). In our study, we conducted HRV examination to determine whether taVNS effectively targeted the vagus nerve. The average heart rate (HR), the standard deviation of the normal-to-normal (NN) intervals (SDNN), and the square root of the mean squared differences of successive NN intervals (RMSSD) were recorded as time-domain measures of HRV. Additionally, the ratio of low-frequency to high-frequency power (LF/HF ratio) was recorded as a frequency-domain measure of HRV. The detailed processing pipelines for HRV can be found in Supplementary material S2. An increase in parasympathetic activity induced by taVNS correlates with increases in SDNN and RMSSD, and decreases in HR and LF/HF ratio (Marek, 1996). We compared the data collected at T0 with that at T1 and T2 to examine the immediate and long-term effectiveness of taVNS. All the patients completed the examination.

2.4.4 Functional near-infrared spectroscopy (fNIRS) examination

fNIRS is a non-invasive brain imaging technique that detects variations in oxyhemoglobin (HbO2) and deoxyhemoglobin (HbR) within the regional cortex. Increased cortical neural activity leads to escalated metabolic demand, resulting in augmented blood flow in the surrounding vasculature, consequently elevating HbO2 concentrations and reducing HbR concentrations (Huppert et al., 2006; Buxton, 2009). Applying specific near-infrared light, fNIRS can measure brain metabolic alterations associated with neuronal activity (Buxton, 2013; Pinti et al., 2020). Studies have shown strong consistency between fNIRS and functional magnetic resonance imaging (fMRI) (Sasai et al., 2012).

This study used a continuous-wave near-infrared imaging device (NIRSmart II-3000A, Huichuang Medical Co., Ltd., China) consisting of 14 light sources (λ1|2 = 730|850 nm) with an average power of <1 mW and 14 avalanche photodiode detectors operating at 11 Hz sampling rate. The sources and detectors were distributed over the bilateral prefrontal cortex (PFC) and sensorimotor cortex (SMC) according to the 10–20 international standard electrode placement system, constituting 35 channels. The montage of the probes and channels is detailed in Figure 2A. The Patriot localization system was employed to determine the Montreal Neurological Institute (MNI) spatial coordinates for each channel and to annotate the corresponding Brodmann areas. The corresponding brain areas for each fNIRS channel are shown in Figure 2B, Supplementary material S3.

The fNIRS examination was conducted in a quiet room with subdued lighting. To investigate the immediate effect on task-related cortical responses in the patients during the treatment, we simulated a scenario in which patients received taVNS while performing TOT. Initially, a 10-min resting state was recorded, during which patients were instructed to keep their eyes closed, maintain restfulness, and minimize head movements. Subsequently, patients were instructed to perform the grasp task using their hemiplegic hands during the examination, which was practicable and related to the procedure of TOT. The task adopted a block design comprising 20 blocks, each consisting of 15 s of repetitive grasp trials followed by 20 s of rest. Computer-generated auditory cues were provided to guide the patients during the task performance. Patients in the VG received concurrent taVNS, whereas patients in the SG received sham taVNS (Figure 2C).

2.5 Data analysis

2.5.1 fNIRS signal processing

The fNIRS signal was processed using MATLAB R2013b (MathWorks, USA), and the Homer2 package was employed for preprocessing the raw data. The following steps were performed: (1) conversion of light intensity to optical density; (2) detection and correction of motion artifacts; (3) application of a bandpass filter (0.01–0.08 Hz) to the signal; (4) conversion of optical density to concentrations of (de)oxygenated hemoglobin based on the modified Beer–Lambert law. Subsequently, the mean concentration of HbO2 during the resting state was calculated to conduct inter-group baseline comparisons. Additionally, the MATLAB-based NIRS-SPM toolkit was utilized to detect brain area activation. To align the data, patients' hemispheres were flipped, considering the left hemisphere as the ipsilesional hemisphere. Beta values (β) for each channel were calculated using the general linear model (GLM) analysis. Group-level comparison was conducted using an independent t test with a false discovery rate (FDR) correction. Detailed procedures for data processing were shown in Supplementary material S2. BrainNet Viewer (Xia et al., 2013) was employed for 3D visualization of brain activation, and space registration was performed using the NFRI method to convert the channel space into Montreal Neurological Institute (MNI) space.

2.5.2 Clinical data analysis

The statistical analysis was conducted using the open-source statistical software Jamovi (Version 2.4.8) (JAMOVI, 2023). The Shapiro-Wilks test was performed to assess the normality of the data. For baseline demographic and clinical characteristics, the Chi-square test or Fisher's exact test was used for categorical variables. The two-sample t-test and the Mann–Whitney test were used for continuous variables. A 2 × 2 analysis of covariance (ANCOVA) was used to determine the effects of the treatment on the FMA-UE, ARAT, MBI, and contralesional MEPs parameters, considering time (baseline, post-treatment) as the within-subject factor, group (VNS, Sham) as the between-subjects factor, and baseline data as a covariate. Due to the impairment of cortico-spinal tract integrity after stroke (Yarossi et al., 2019), the statistical analysis for ipsilesional MEP was

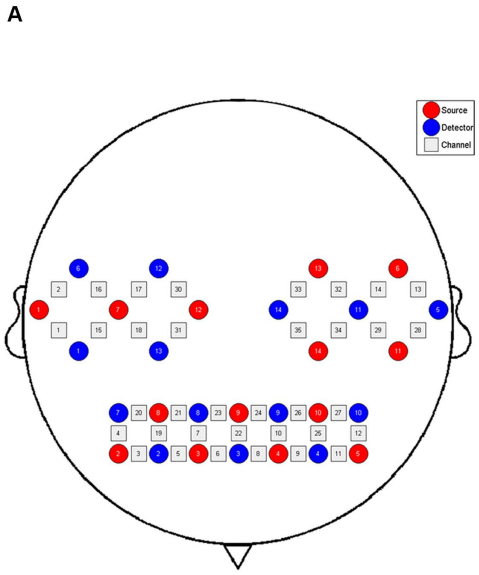

B

ROI	Region	Channels		
		contralesional hemisphere	ipsilesional hemisphere	middle
Sensorimotor cortex	1, 2, 3 - Primary somatosensory cortex	2, 16	13, 14	
	4 - Primary motor cortex	17, 30	32, 33	
	6 - Pre-motor & supplementary motor cortex	1, 15, 18, 31	28, 29, 34, 35	
Prefrontal cortex	45 - Pars triangularis Broca's area	4, 20	12, 27	
	9, 46 - Dorsolateral prefrontal cortex	19, 21	25, 26	
	47 – Inferior prefrontal gyrus	3	11	
	10, 11 - Frontopolar & orbitofrontal area	5, 6, 7, 23	8, 9, 10, 24	22

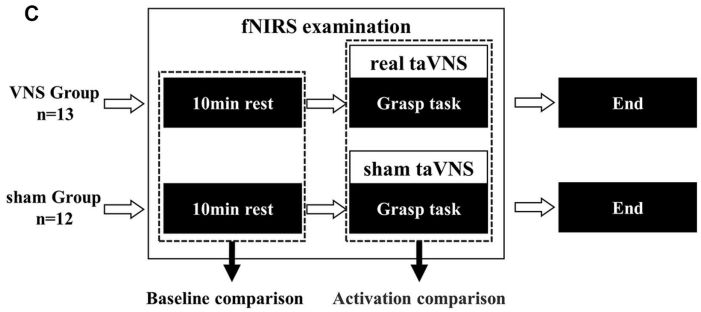

FIGURE 2
Procedure of the fNIRS examination. **(A)** Channel arrangements with numbers marked on a 2D brain template. **(B)** The regions of interest based on the Brodmann area of each channel. **(C)** Pipeline of the fNIRS examination.

determined based on the number of MEPs collected. A 3 × 2 repeated measures analysis of variance (RMANOVA) was conducted to determine the effects on the HRV, considering time (T0, T1, T2) as the between-subjects factor and group (VNS, Sham) as the between-subjects factor. A linear regression analysis was used to analyze the correlation between the recovery of upper extremity function and changes in MEPs. A significance level of $p < 0.05$ was considered statistically significant for all tests.

3 Results

Forty-three patients were recruited, with 21 allocated to the VG and 21 to the SG. The flow chart can be found in Figure 1. Two participants (one from the VG and another from the SG) dropped out of the study due to unwillingness. In addition, eight participants in the VG and nine participants in the SG were excluded from the fNIRS data analysis. Detailed reasons for participants' exclusion are shown in Figure 1.

3.1 Demographics and clinical characteristics

Table 1 presents a summary of the demographics and clinical characteristics of the patients. There were no statistically significant differences in any of the variables between the two groups. Furthermore, no adverse events were reported throughout the entire duration of the study.

3.2 Outcomes for upper extremity function

The ANCOVA revealed that patients in both groups showed significant improvements in FMA-UE, ARAT, MBI compared to baseline. Regarding the inter-group comparison, there were statistically greater improvements in FMA-UE, ARAT, and MBI in the VG (Figure 3, Table 2).

3.3 Outcomes for MEPs

In our study, only 4 patients were able to elicit ipsilesional MEPs at baseline (VG, $n = 3$; SG, $n = 1$). After 20 sessions of treatment, the number of patients who could elicit ipsilesional MEPs increased to 12 cases (VG, $n = 9$; SG, $n = 3$). To determine the effects on the elicitation rate of ipsilesional MEPs, we employed the Chi-square test or Fisher's exact test for between-group comparison and the McNemar test for within-group comparison. The Fisher's exact test indicated that the baseline elicited ipsilesional MEPs were comparable across groups. After treatment, the VG showed significantly higher elicitation rates of ipsilesional MEPs than baseline and SG (Figure 3, Table 3).

The contralesional MEPs were collected from all included patients. The ANCOVA found that the contralesional latency of MEPs in the VG significantly shortened compared with baseline. While no significant change in the SG was detected. There was a statistically significant reduction in contralesional latency of MEPs in the VG (Figure 3, Table 4). However, no significant difference was found in contralesional amplitude of MEPs within or between groups (Figure 3, Table 4). Additionally, the univariable regression revealed that there

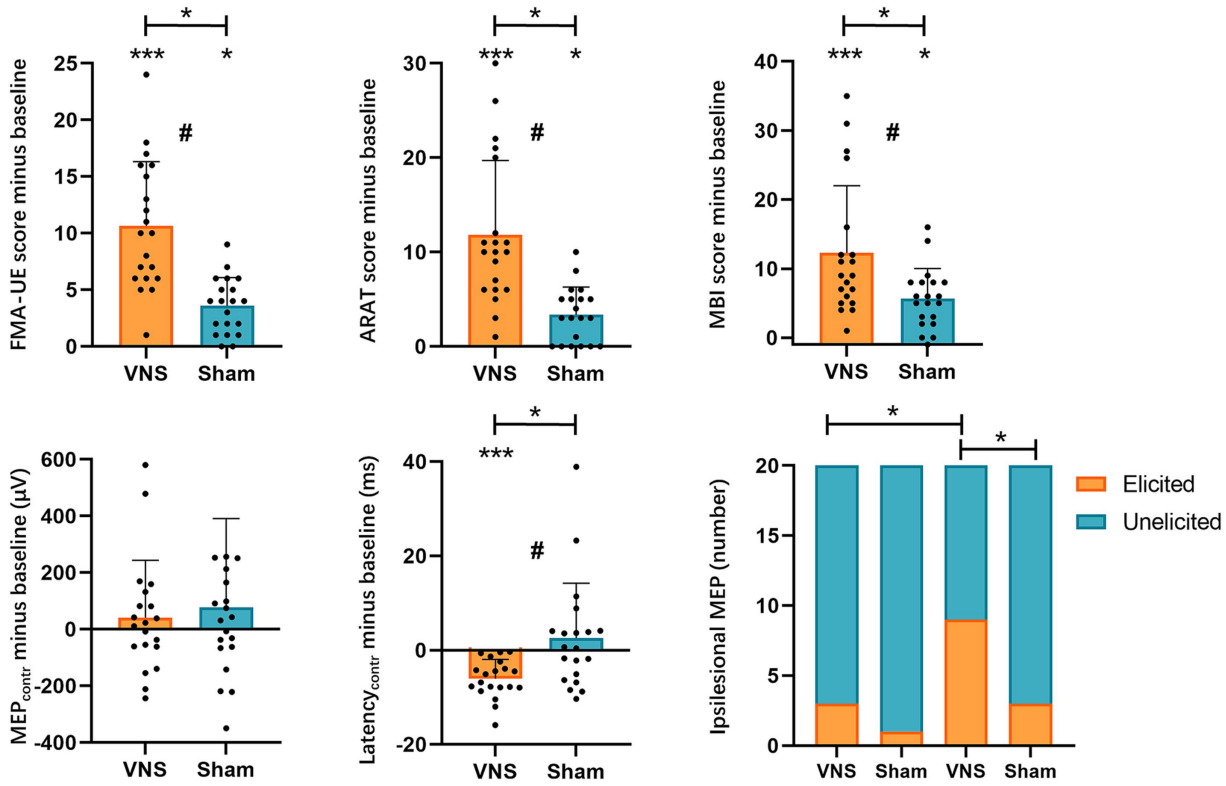

FIGURE 3
Effects of taVNS on upper extremity function and MEPs. FMA-UE, Fugl-Meyer Assessment-Upper Extremity; ARAT, Action Research Arm Test; MBI, modified Barthel Index; MEPs, motor-evoked potentials; VNS, taVNS group; Sham: Sham group; *, $p < 0.05$; **, $p < 0.01$; ***, $p < 0.001$; #, a significant time × intervention interaction in ANCOVA.

TABLE 2 Within-group and between-group comparisons for clinical scales.

Variable	Groups				Within-group differences				Between-group differences	
	Pre-treatment		Post-treatment		Mean (SD)		LS Mean (95% CI)		Difference in LS Mean (95% CI)	*p* value
	VNS	Sham	VNS	Sham	VNS	Sham	VNS	Sham		
FMA-UE[#]	30.5 (8.9)	29.6 (8.7)	41.1 (12)	33.2 (8.3)	10.7 (5.7)	3.6 (2.5)	10.61 (8.63, 12.6)	3.64 (1.65, 5.62)	6.98 (4.26, 9.70)	<0.001
ARAT[#]	15.7 (11)	15.4 (11)	27.5 (15)	18.8 (11)	11.8 (7.9)	3.4 (2.9)	11.84 (9.16, 14.5)	3.36 (0.69, 6.04)	8.47 (4.82, 12.1)	<0.001
MBI[#]	72.2 (17)	69.1 (15)	84.4 (11)	74.8 (14)	12.3 (9.7)	5.7 (4.4)	12.77 (10.2, 15.3)	5.18 (2.61, 7.75)	7.59 (4.07, 11.1)	<0.001

Based on an ANCOVA model after adjusting baseline value. ANCOVA, Analysis of Covariance; CI, Confidence Interval; LS, Least Squares; SD, Standard Deviation. FMA-UE, Fugl-Meyer assessment-upper extremity; ARAT, Action Research Arm Test; MBI, Modified Barthel Index; [#]significant time × intervention interaction.

were significant correlations between the improvements in FMA-UE and the changes in the contralesional latency of MEPs (Figure 4).

3.4 Outcomes for fNIRS

The resting state fNIRS data showed there were no significant differences in baseline. As for task fNIRS data, group-level comparison revealed that the channels in the ipsilesional postcentral gyrus ($PoCG_{ipsi}$, CH14), precentral gyrus ($PreCG_{ipsi}$, CH32), supplementary motor area (SMA_{ipsi}, CH34), middle frontal gyrus orbital part ($ORBmid_{ipsi}$, CH9), contralesional orbital middle frontal gyrus ($ORBmid_{contr}$, CH5, CH7, CH23), and dorsolateral superior frontal gyrus ($SFGdor_{contr}$, CH21) showed significantly larger activation in the VG compared to the SG ($p_{FDR} < 0.05$). The specific coordination of activated channels is shown in Figure 5.

3.5 Outcomes for HRV

The 3 × 2 RMANOVA revealed significant group*time interactions for HR, SDNN, and LF/HF, but not for RMSSD. We also found significant group main effects in HR and LF/HF. For the interaction effect, Bonferroni *post hoc* tests showed that patients in the VG

TABLE 3 Outcomes for ipsilesional motor-evoked potentials.

Ipsilesional MEPs	Pre-treatment		*p* value	Post-treatment		*p* value
	VNS n (%)	Sham n (%)		VNS n (%)	Sham n (%)	
Elicited	3 (15)	1 (5)	0.605[a]	9 (45)[b]*	3 (15)	0.038[c]*
Unelicited	17 (85)	19 (95)		11 (55)	17 (85)	

MEP, motor evoked potential; [a]Fisher's exact test; [b]McNemar test; [c]Chi square test; *$p < 0.05$.

TABLE 4 Outcomes for contralesional motor-evoked potentials.

Variable	Groups				Within-group differences				Between-group differences	
	Pre-treatment		Post-treatment		Mean (SD)		LS Mean (95% CI)		Difference in LS Mean (95% CI)	*p* value
	VNS	sham	VNS	sham	VNS	sham	VNS	sham		
MEP (μV)	247.5 (143.5)	202.3 (125)	288.8 (180.5)	279.7 (277)	41.4 (202.6)	77.3 (313.9)	62.1 (−45.9, 170.1)	56.6 (−51.4, 164.6)	5.5 (−143.3, 154.3,)	0.943
Latency (ms) [#]	19.1 (6.7)	17.3 (4.8)	13.1 (6.3)	19.9 (11.3)	−6.0 (4.1)	2.6 (11.7)	−5.7 (−9.6, −1.8)	2.2 (−1.7, 6.1)	−7.9 (−13.3, −2.5)	0.007

Based on an ANCOVA model after adjusting baseline value. ANCOVA, Analysis of Covariance, CI, Confidence Interval, LS, Least Squares, SD, Standard Deviation; MEP, motor-evoked potential amplitude; [#]significant time × intervention interaction.

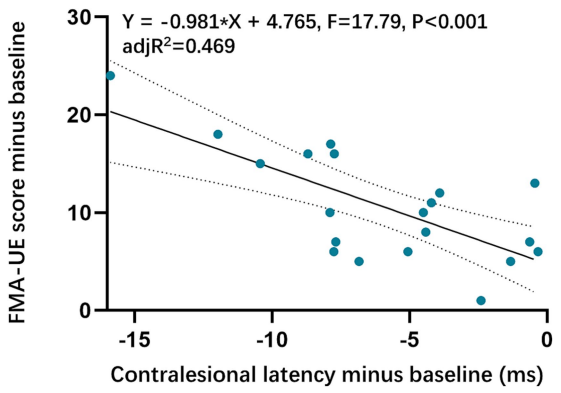

FIGURE 4
Correlations between Upper extremity function and contralesional MEPs latency. FMA-UE, the Fugl-Meyer Assessment-Upper Extremity.

presented significantly decreased HR at T1, T2 compared with T0, increased SDNN at T2 compared with T0, and decreased LF/HF at T1, T2 compared with T0. However, no between-group difference was found after Bonferroni correction (Figure 6, Table 5).

4 Discussion

In recent years, non-invasive VNS has garnered increasing attention due to its potential to improve upper extremity motor function in stroke patients, although its underlying neural mechanisms are not fully understood. In order to explore the feasibility of the current study, we conducted HRV and fNIRS examinations prior to the initiation of the treatment. The effectiveness of taVNS was assessed using HRV examination. Our current results demonstrated significant decreases in HR, LF/HF ratio, and a marked increase in SDNN in the VG, whereas no changes were observed in the SG. These results indicated that taVNS indeed modulated the vagus nerve network. Subsequently, using fNIRS, we observed greater hemodynamic responses in the bilateral PFC and the ipsilesional SMC during the grasp task with taVNS, suggesting an enhancement of cortical activation. In the fNIRS study conducted by Kunii et al. (2021), the effects of iVNS on cerebral blood flow (CBF) during a resting state and a verbal fluency task were investigated. They found that no changes in CBF were observed during the resting state, while the verbal fluency task led to a significant increase in CBF. Wang et al. (2023) found that a single session of taVNS could significantly bolster the activation within damaged cerebral territories in stroke patients without destabilizing cerebral lateralization. These findings provide evidence that taVNS can effectively activate the task-specific cortex during motor task performance, supporting the immediate effect of taVNS.

The TOT approach aims to teach stroke patients specific task strategies and improve their ability to adapt to the environment through functional tasks related to daily life. Previous fMRI studies (Jang et al., 2003; McCombe Waller et al., 2014) have reported that TOT could improve upper extremity function in post-stroke patients. These studies found that activity in the related motor cortex increased with the recovery of upper extremity motor function. In our study, we observed improvements in the motor capacity of the upper extremity (FMA-UE), arm-hand capacity (ARAT), and activities of daily living (MBI) in both groups. However, patients in the taVNS group demonstrated greater improvements in upper extremity function, which is consistent with previous research (Hoonhorst et al., 2015; Capone et al., 2017; Redgrave et al., 2018; Chang et al., 2021; Li et al., 2022). Notably, the improvement observed in the VG was clinically significant, surpassing the minimal clinically important difference (MCID) of 9–10 points for the FMA-UE in individuals with subacute stroke (Singer and Garcia-Vega, 2017). Khodaparast et al. (2016) observed that the rate of forelimb strength recovery (86%) in ischemic stroke rats was significantly higher after receiving VNS with rehabilitation training compared to the simple rehabilitation group (47%) and the delayed VNS group (42%). Morrison et al. (2019, 2020) reported that intracortical microstimulation with VNS can improve

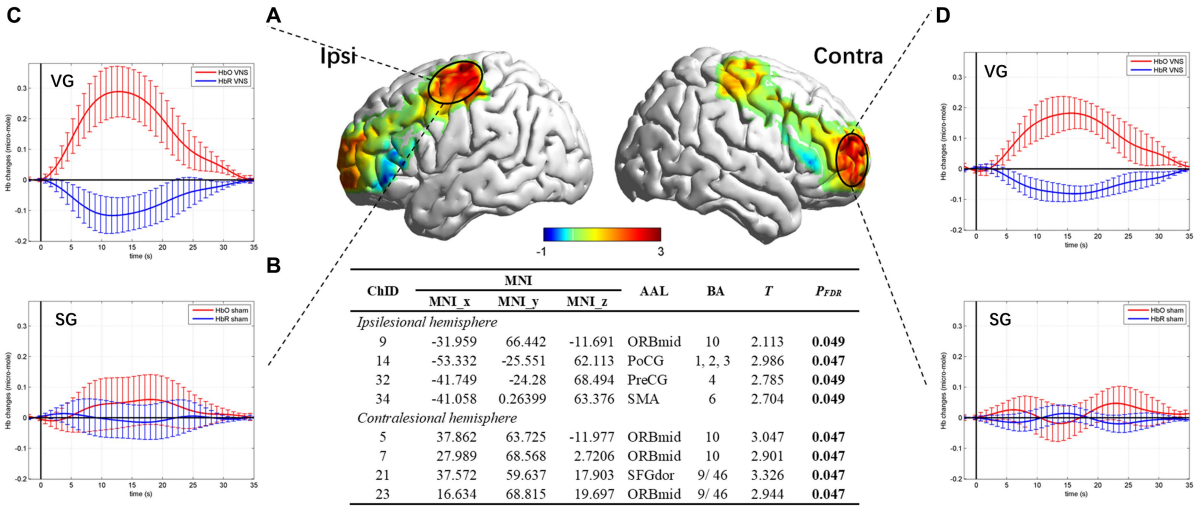

ChID	MNI			AAL	BA	*T*	P_{FDR}
	MNI_x	MNI_y	MNI_z				
Ipsilesional hemisphere							
9	-31.959	66.442	-11.691	ORBmid	10	2.113	**0.049**
14	-53.332	-25.551	62.113	PoCG	1, 2, 3	2.986	**0.047**
32	-41.749	-24.28	68.494	PreCG	4	2.785	**0.049**
34	-41.058	0.26399	63.376	SMA	6	2.704	**0.049**
Contralesional hemisphere							
5	37.862	63.725	-11.977	ORBmid	10	3.047	**0.047**
7	27.989	68.568	2.7206	ORBmid	10	2.901	**0.047**
21	37.572	59.637	17.903	SFGdor	9/ 46	3.326	**0.047**
23	16.634	68.815	19.697	ORBmid	9/ 46	2.944	**0.047**

FIGURE 5
Brain activation map and hemodynamics response for task state. **(A)** Cortical activation map marked on a three-dimensional template (Colin 27 version 2019, using the interpolated mapping algorithm) in ipsilesional and contralesional vision. **(B)** Results from the independent *t*-test of beta values between the VG and the SG. Channels with a significant difference were listed. **(C)** Hemodynamic curve in $PoCG_{ipsi}$. **(D)** Hemodynamic curve in MFG_{contr}.

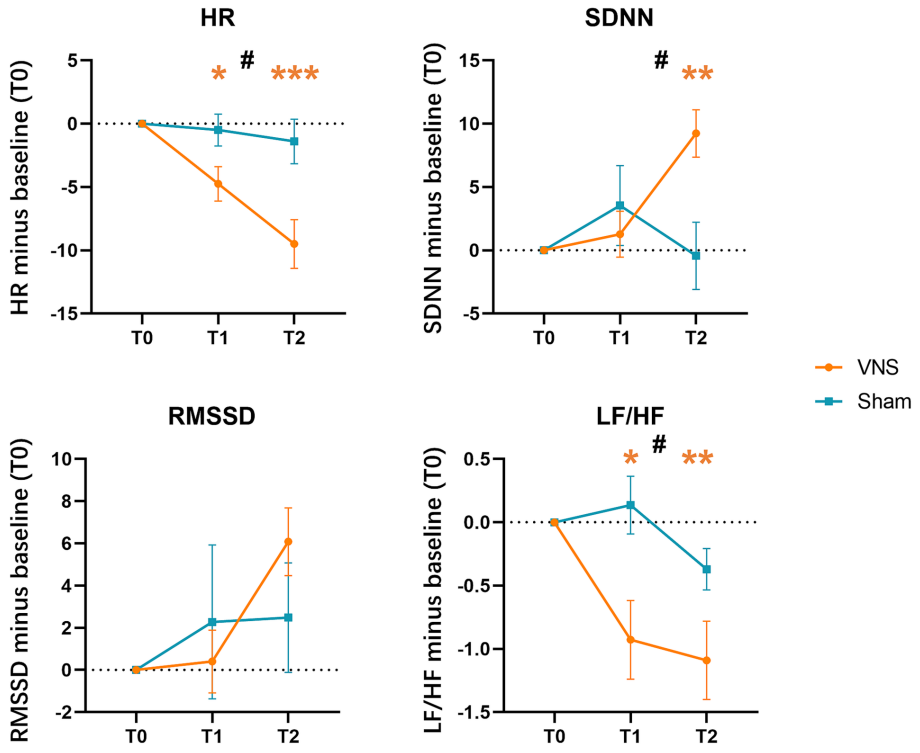

FIGURE 6
Effects of taVNS on heart rate variability. HR, averaged heart rate; SDNN, the standard deviation of the normal-to-normal intervals; RMSSD, the square root of the mean squared differences of successive normal-to-normal intervals; LF/HF, the ratio of low-frequency to high-frequency power; * in orange color: $p < 0.05$ compared with T0 in VNS group; ** in orange color: $p < 0.01$ compared with T0 in VNS group; *** in orange color: $p < 0.001$ compared with T0 in VNS group; #: a significant time × intervention interaction in repeated-measures ANOVA.

motor cortical plasticity in mice. In this study, significant improvements were observed in upper extremity motor function, indicating that taVNS paired with task-specific activities may promote neuroplastic changes.

Neuroanatomy research has provided insights into the mechanisms underlying the activation of the locus ceruleus-noradrenaline (LC-NE) release system by taVNS. Norepinephrine (NE) is an excitatory neurotransmitter, while the locus coeruleus (LC)

TABLE 5 Repeated-measures ANOVA for HRV outcomes.

Variable	Group	Descriptive analysis			Within-group differences		Repeated-measures ANOVA			
		T0	T1	T2	T1-T0 in LS Mean (95% CI)	T2-T0 in LS Mean (95% CI)	Effect	F	p	η^2P
HR[a]	VNS	82.5 (11)	77.8 (9.96)	73 (9.56)	−6.47 (−9.8, −3.2)	−10.77 (−15.6, −6.0)	Time	0.866	0.402	0.024
	Sham	78.5 (11.6)	78 (11.4)	77.2 (12.1)	−1.57 (−4.5, 1.4)	−2.16 (−6.5, 2.1)	Time*Group	7.795	0.002	0.178
							Group	10.043	0.003	0.218
SDNN	VNS	29.9 (12.8)	31.2 (11.3)	39.2 (10.8)	4.28 (−1.9, 10.5)	10.84 (5.0, 16.7)	Time	2.190	0.119	0.057
	Sham	28.3 (13)	31.8 (12.7)	27.8 (10.5)	4.90 (−0.7, 10.5)	0.97 (−4.3, 6.2)	Time*Group	6.180	0.003	0.147
							Group	2.370	0.132	0.062
RMSSD	VNS	23.3 (9.92)	23.7 (8.99)	29.3 (9.85)	4.44 (−2.4, 11.3)	7.94 (2.4, 13.5)	Time	0.660	0.520	0.018
	Sham	24.3 (11.7)	26.6 (13.6)	26.8 (7.74)	4.51 (−1.6, 10.6)	3.78 (−1.2, 8.8)	Time*Group	0.865	0.425	0.023
							Group	0.498	0.485	0.014
LF/HF	VNS	2.32 (1.42)	1.39 (0.908)	1.23 (0.849)	−0.60 (−1.3, 0.1)	−0.74 (−1.4, −0.1)	Time	0.328	0.721	0.009
	Sham	1.82 (1.02)	1.96 (1.28)	1.45 (1.02)	0.33 (−0.3, 0.9)	−0.14 (−0.7, 0.4)	Time*Group	3.270	0.044	0.083
							Group	5.732	0.022	0.137

SD, Standard Deviation; LS, Least Squares; CI, Confidence Interval; HR, average heart rate; SDNN, standard deviation of the NN intervals; RMSSD, square root of the mean squared differences of successive NN intervals; LF/HF, low-to-high frequency power ratio; [a]The Greenhouse–Geisser correction was used for not obeying the sphericity assumption.

is the primary source of the norepinephrine-producing neurons in the brain. Studies indicated that both short-term and long-term VNS can increase neuronal firing rates of the LC, leading to increased NE concentrations in the amygdala, hippocampus, and prefrontal cortex. The VNS-induced NE could maintain long-term activity (Groves et al., 2005; Hulsey et al., 2017). NE can enhance cortical excitability and plasticity, which are associated with daytime vigilance, attention, and motor learning (Duffau, 2006; Ciampa et al., 2022). The fMRI studies by Kraus et al. (2007) and Dietrich et al. (2008) have detected blood oxygenation level-dependent (BOLD) signal activations in the bilateral sensorimotor cortex and prefrontal cortex during taVNS. Furthermore, Frangos and Komisaruk (2017) observed sustained activation of the bilateral precentral gyrus for nearly 10 min (9 min, in fact) following taVNS. Combining these findings with the results of fNIRS in our trial, it is plausible to speculate that taVNS can induce bilateral hemisphere activation during the treatment, which may be attributable to the related neurotransmitter release.

In this study, we utilized single-pulse TMS to assess long-term changes in motor cortex excitability by measuring MEPs in both hemispheres. The study found a relatively low elicitation rate of ipsilesional MEPs in patients at baseline. However, the elicitation rate of ipsilesional MEPs increased significantly from 15% before treatment to 45% after treatment in the VG, which is consistent with previous studies (Escudero et al., 1998; Powell et al., 2019; Yarossi et al., 2019). Moreover, the average latency of ipsilesional MEPs in the VG decreased from 63.53 ms to 55.36 ms, while the amplitude increased from 87.60 μV to 140.18 μV, suggesting a trend toward increased cortical excitability in the ipsilesional M1. Cakar et al. (2016) reported a positive correlation between shorter MEP latency, increased amplitude, and improved motor function in stroke patients. Additionally, we observed a reduction in the latency of contralesional MEPs, indicating the modulation of the contralesional M1. Increased intracortical excitability of contralesional M1 has been observed in subacute and chronic stroke patients (Bütefisch, 2003; Bütefisch et al., 2008), with suggestions that the increased excitability is associated with better recovery of upper extremity function (Bütefisch, 2015). Bi-hemispheric transcranial direct current stimulation (tDCS) studies using fMRI have supported this notion, proposing a cooperative role of contralesional M1 rather than competition (Waters et al., 2017). Furthermore, a randomized controlled trial conducted by Hsu et al. (2023) demonstrated that improvements in FMA-UE scores in subacute stroke patients correlated with changes in functional connectivity within the bilateral intra-hemisphere networks. In our study, we found a significant correlation between the decrease in latency of contralesional MEPs and improvements in FMA-UE scores, which is consistent with previous literature (Wang et al., 2020). Based on these findings, the long-term combined intervention may modulate bilateral motor cortical excitability and facilitate training-specific motor performance.

5 Limitations

This study has several limitations that need to be addressed in future research. First, the small sample size and the high dropout rate of the fNIRS examination in this study might result in insufficient statistical power, potentially increasing the chance of a type I error. A larger sample size is needed to confirm these findings and achieve more reliable results. Second, it is worth noting that, due to the limited number of positive events (elicited ipsilesional MEPs), the significance and generalizability of this result should be carefully considered. Finally, follow-up assessments were not conducted to investigate the sustained effects of taVNS in this study, which should be considered in future studies.

6 Conclusion

In conclusion, our study provides evidence that the combined intervention of taVNS with TOT is effective in enhancing upper extremity motor function in patients with post-stroke hemiplegia. This improvement can be attributed to the modulation of cortical excitability in both hemispheres, which facilitates the remodeling of motor function.

Data availability statement

The raw data supporting the conclusions of this article will be made available by the authors, without undue reservation.

Ethics statement

The studies involving humans were approved by the Ethics Committee of Sir Run Run Hospital, Nanjing Medical University (No. 2020-SR-001). The studies were conducted in accordance with the local legislation and institutional requirements. The participants provided their written informed consent to participate in this study.

Author contributions

M-HW: Conceptualization, Data curation, Formal analysis, Software, Visualization, Writing – original draft. Y-XW Conceptualization, Writing – review & editing. MX: Investigation, Methodology, Validation, Writing – review & editing. L-YC: Investigation, Methodology, Writing – review & editing. M-FH: Investigation, Methodology, Writing – review & editing. FL: Conceptualization, Project administration, Supervision, Writing – review & editing. Z-LJ: Conceptualization, Funding acquisition, Project administration, Resources, Supervision, Writing – review & editing.

Funding

The author(s) declare that financial support was received for the research, authorship, and/or publication of this article. This work was supported by the National Key R&D Program of China (grant numbers No.2020YFC2008505).

Acknowledgments

The authors thank all the individuals who participated in this study.

Conflict of interest

The authors declare that the research was conducted in the absence of any commercial or financial relationships that could be construed as a potential conflict of interest.

Publisher's note

All claims expressed in this article are solely those of the authors and do not necessarily represent those of their affiliated organizations, or those of the publisher, the editors and the reviewers. Any product that may be evaluated in this article, or claim that may be made by its manufacturer, is not guaranteed or endorsed by the publisher.

Supplementary material

The Supplementary material for this article can be found online at: https://www.frontiersin.org/articles/10.3389/fnins.2024.1346634/full#supplementary-material

References

Alsubiheen, A. M., Choi, W., Yu, W., and Lee, H. (2022). The effect of task-oriented activities training on upper-limb function, daily activities, and quality of life in chronic stroke patients: a randomized controlled trial. *Int. J. Environ. Res. Public Health* 19:14125. doi: 10.3390/ijerph192114125

Badran, B. W., Dowdle, L. T., Mithoefer, O. J., LaBate, N. T., Coatsworth, J., Brown, J. C., et al. (2018). Neurophysiologic effects of transcutaneous auricular vagus nerve stimulation (taVNS) via electrical stimulation of the tragus: a concurrent taVNS/fMRI study and review. *Brain Stimul.* 11, 492–500. doi: 10.1016/j.brs.2017.12.009

Bai, Z., Zhang, J., and Fong, K. N. K. (2022). Effects of transcranial magnetic stimulation in modulating cortical excitability in patients with stroke: a systematic review and meta-analysis. *J. Neuroeng. Rehabil.* 19:24. doi: 10.1186/s12984-022-00999-4

Bütefisch, C. M. (2003). Remote changes in cortical excitability after stroke. *Brain* 126, 470–481. doi: 10.1093/brain/awg044

Bütefisch, C. M. (2015). Role of the Contralesional hemisphere in post-stroke recovery of upper extremity motor function. *Front. Neurol.* 6:214. doi: 10.3389/fneur.2015.00214

Bütefisch, C. M., Wessling, M., Netz, J., Seitz, R. J., and Hömberg, V. (2008). Relationship between interhemispheric inhibition and motor cortex excitability in subacute stroke patients. *Neurorehabil. Neural Repair* 22, 4–21. doi: 10.1177/1545968307301769

Buxton, R. B.. *Introduction to functional magnetic resonance imaging: principles and techniques*. Cambridge; New York: Cambridge University Press (2009).

Buxton, R. B. (2013). The physics of functional magnetic resonance imaging (fMRI). *Rep. Prog. Phys.* 76:096601. doi: 10.1088/0034-4885/76/9/096601

Cakar, E., Akyuz, G., Durmus, O., Bayman, L., Yagci, I., Karadag-Saygi, E., et al. (2016). The relationships of motor-evoked potentials to hand dexterity, motor function, and spasticity in chronic stroke patients: a transcranial magnetic stimulation study. *Acta Neurol. Belg.* 116, 481–487. doi: 10.1007/s13760-016-0633-2

Capilupi, M. J., Kerath, S. M., and Becker, L. B. (2020). Vagus nerve stimulation and the cardiovascular system. *Cold Spring Harb. Perspect. Med.* 10:a034173. doi: 10.1101/cshperspect.a034173

Capone, F., Miccinilli, S., Pellegrino, G., Zollo, L., Simonetti, D., Bressi, F., et al. (2017). Transcutaneous Vagus nerve stimulation combined with robotic rehabilitation improves upper limb function after stroke. *Neural Plast.* 2017, 1–6. doi: 10.1155/2017/7876507

Chang, J. L., Coggins, A. N., Saul, M., Paget-Blanc, A., Straka, M., Wright, J., et al. (2021). Transcutaneous auricular Vagus nerve stimulation (tAVNS) delivered during upper limb interactive robotic training demonstrates novel antagonist control for reaching movements following stroke. *Front. Neurosci.* 15:767302. doi: 10.3389/fnins.2021.767302

Chen, Z. J., He, C., Gu, M. H., Xu, J., and Huang, X. L. (2021). Kinematic evaluation via inertial measurement unit associated with upper extremity motor function in subacute stroke: a cross-sectional study. *J. Healthc. Eng.* 2021, 1–7. doi: 10.1155/2021/4071645

Chhatbar, P. Y., Chen, R., Deardorff, R., Dellenbach, B., Kautz, S. A., George, M. S., et al. (2017). Safety and tolerability of transcranial direct current stimulation to stroke patients -a phase I current escalation study. *Brain Stimul.* 10, 553–559. doi: 10.1016/j.brs.2017.02.007

Ciampa, C. J., Parent, J. H., Harrison, T. M., Fain, R. M., Betts, M. J., Maass, A., et al. (2022). Associations among locus coeruleus catecholamines, tau pathology, and memory in aging. *Neuropsychopharmacology* 47, 1106–1113. doi: 10.1038/s41386-022-01269-6

Dawson, J., Liu, C. Y., Francisco, G. E., Cramer, S. C., Wolf, S. L., Dixit, A., et al. (2021). Vagus nerve stimulation paired with rehabilitation for upper limb motor function after ischaemic stroke (VNS-REHAB): a randomised, blinded, pivotal, device trial. *Lancet* 397, 1545–1553. doi: 10.1016/S0140-6736(21)00475-X

Dietrich, S., Smith, J., Scherzinger, C., Hofmann-Preiß, K., Freitag, T., Eisenkolb, A., et al. (2008). A novel transcutaneous vagus nerve stimulation leads to brainstem and cerebral activations measured by functional MRI. *Biomed. Tech.* 53, 104–111. doi: 10.1515/BMT.2008.022

Duffau, H. (2006). Brain plasticity: from pathophysiological mechanisms to therapeutic applications. *J. Clin. Neurosci.* 13, 885–897. doi: 10.1016/j.jocn.2005.11.045

Escudero, J. V., Sancho, J., Bautista, D., Escudero, M., and López-Trigo, J. (1998). Prognostic value of motor evoked potential obtained by transcranial magnetic brain stimulation in motor function recovery in patients with acute ischemic stroke. *Stroke* 29, 1854–1859. doi: 10.1161/01.STR.29.9.1854

Farmer, A. D., Strzelczyk, A., Finisguerra, A., Gourine, A. V., Gharabaghi, A., Hasan, A., et al. (2021). International consensus based review and recommendations for minimum reporting standards in research on transcutaneous Vagus nerve stimulation (version 2020). *Front. Hum. Neurosci.* 14:568051. doi: 10.3389/fnhum.2020.568051

Frangos, E., and Komisaruk, B. R. (2017). Access to vagal projections via cutaneous electrical stimulation of the neck: fMRI evidence in healthy humans. *Brain Stimul.* 10, 19–27. doi: 10.1016/j.brs.2016.10.008

Fried, P. J., Santarnecchi, E., Antal, A., Bartres-Faz, D., Bestmann, S., Carpenter, L. L., et al. (2021). Training in the practice of noninvasive brain stimulation: recommendations from an IFCN committee. *Clin. Neurophysiol.* 132, 819–837. doi: 10.1016/j.clinph.2020.11.018

GBD 2019 Stroke Collaborators (2021). Global, regional, and national burden of stroke and its risk factors, 1990-2019: a systematic analysis for the global burden of disease study 2019. *Lancet Neurol.* 20, 795–820. doi: 10.1016/S1474-4422(21)00252-0

Gladstone, D. J., Danells, C. J., and Black, S. E. (2002). The fugl-meyer assessment of motor recovery after stroke: a critical review of its measurement properties. *Neurorehabil. Neural Repair* 16, 232–240. doi: 10.1177/154596802401105171

Groves, D. A., Bowman, E. M., and Brown, V. J. (2005). Recordings from the rat locus coeruleus during acute vagal nerve stimulation in the anaesthetised rat. *Neurosci. Lett.* 379, 174–179. doi: 10.1016/j.neulet.2004.12.055

Higgins, J., Koski, L., and Xie, H. (2013). Combining rTMS and task-oriented training in the rehabilitation of the arm after stroke: a pilot randomized controlled trial. *Stroke Res. Treat.* 2013:539146, 1–8. doi: 10.1155/2013/539146

Hoonhorst, M. H., Nijland, R. H., van den Berg, J. S., Emmelot, C. H., Kollen, B. J., and Kwakkel, G. (2015). How do Fugl-Meyer arm motor scores relate to dexterity according to the action research arm test at 6 months Poststroke? *Arch. Phys. Med. Rehabil.* 96, 1845–1849. doi: 10.1016/j.apmr.2015.06.009

Hsieh, C. L., Hsueh, I. P., Chiang, F. M., and Lin, P. H. (1998). Inter-rater reliability and validity of the action research arm test in stroke patients. *Age Ageing* 27, 107–113. doi: 10.1093/ageing/27.2.107

Hsu, S.-P., Lu, C.-F., Lin, B.-F., Tang, C.-W., Kuo, I.-J., Tsai, Y.-A., et al. (2023). Effects of bihemispheric transcranial direct current stimulation on motor recovery in subacute stroke patients: a double-blind, randomized sham-controlled trial. *J. Neuroeng. Rehabil.* 20:27. doi: 10.1186/s12984-023-01153-4

Hulsey, D. R., Riley, J. R., Loerwald, K. W., Rennaker, R. L., Kilgard, M. P., and Hays, S. A. (2017). Parametric characterization of neural activity in the locus coeruleus in response to vagus nerve stimulation. *Exp. Neurol.* 289, 21–30. doi: 10.1016/j.expneurol.2016.12.005

Huppert, T. J., Hoge, R. D., Diamond, S. G., Franceschini, M. A., and Boas, D. A. (2006). A temporal comparison of BOLD, ASL, and NIRS hemodynamic responses to motor stimuli in adult humans. *NeuroImage* 29, 368–382. doi: 10.1016/j.neuroimage.2005.08.065

JAMOVI. Open statistical software for the desktop and cloud. (2023) Available at:https://www.jamovi.org/.

Jang, S. H., Kim, Y.-H., Cho, S.-H., Lee, J.-H., Park, J.-W., and Kwon, Y.-H. (2003). Cortical reorganization induced by task-oriented training in chronic hemiplegic stroke patients. *Neuroreport* 14, 137–141. doi: 10.1097/00001756-200301200-00025

Jin, M., Zhang, Z., Bai, Z., and Fong, K. N. K. (2019). Timing-dependent interaction effects of tDCS with mirror therapy on upper extremity motor recovery in patients with chronic stroke: a randomized controlled pilot study. *J. Neurol. Sci.* 405:116436. doi: 10.1016/j.jns.2019.116436

Jo, J. Y., Lee, A., Kim, M. S., Park, E., Chang, W. H., Shin, Y. I., et al. (2016). Prediction of motor recovery using quantitative parameters of motor evoked potential in patients with stroke. *Ann. Rehabil. Med.* 40, 806–815. doi: 10.5535/arm.2016.40.5.806

Khodaparast, N., Kilgard, M. P., Casavant, R., Ruiz, A., Qureshi, I., Ganzer, P. D., et al. (2016). Vagus nerve stimulation during rehabilitative training improves forelimb recovery after chronic ischemic stroke in rats. *Neurorehabil. Neural Repair* 30, 676–684. doi: 10.1177/1545968315616494

Kim, T. H., In, T. S., and Cho, H. (2013). Task-related training combined with transcutaneous electrical nerve stimulation promotes upper limb functions in patients with chronic stroke. *Tohoku J. Exp. Med.* 231, 93–100. doi: 10.1620/tjem.231.93

Kraus, T., Hösl, K., Kiess, O., Schanze, A., Kornhuber, J., and Forster, C. (2007). BOLD fMRI deactivation of limbic and temporal brain structures and mood enhancing effect by transcutaneous vagus nerve stimulation. *J. Neural Transm. (Vienna)* 114, 1485–1493. doi: 10.1007/s00702-007-0755-z

Kunii, N., Koizumi, T., Kawai, K., Shimada, S., and Saito, N. (2021). Vagus nerve stimulation amplifies task-induced cerebral blood flow increase. *Front. Hum. Neurosci.* 15:726087. doi: 10.3389/fnhum.2021.726087

Kwakkel, G., Kollen, B. J., van der Grond, J., and Prevo, A. J. H. (2003). Probability of regaining dexterity in the flaccid upper limb: impact of severity of paresis and time since onset in acute stroke. *Stroke* 34, 2181–2186. doi: 10.1161/01.STR.0000087172.16305.CD

Lai, S.-M., Studenski, S., Duncan, P. W., and Perera, S. (2002). Persisting consequences of stroke measured by the stroke impact scale. *Stroke* 33, 1840–1844. doi: 10.1161/01.str.0000019289.15440.f2

Li, J.-N., Xie, C.-C., Li, C.-Q., Zhang, G.-F., Tang, H., Jin, C.-N., et al. (2022). Efficacy and safety of transcutaneous auricular vagus nerve stimulation combined with conventional rehabilitation training in acute stroke patients: a randomized controlled trial conducted for 1 year involving 60 patients. *Neural Regen. Res.* 17, 1809–1813. doi: 10.4103/1673-5374.332155

Ma, J., Qiao, P., Li, Q., Wang, Y., Zhang, L., Yan, L.-J., et al. (2019). Vagus nerve stimulation as a promising adjunctive treatment for ischemic stroke. *Neurochem. Int.* 131:104539. doi: 10.1016/j.neuint.2019.104539

Mäkelä, J. P., Lioumis, P., Laaksonen, K., Forss, N., Tatlisumak, T., Kaste, M., et al. (2015). Cortical excitability measured with nTMS and MEG during stroke recovery. *Neural Plast.* 2015, 1–8. doi: 10.1155/2015/309546

Marek, M. (1996). Heart rate variability: standards of measurement, physiological interpretation, and clinical use. Task force of the European Society of Cardiology and the north American Society of Pacing and Electrophysiology. *Circulation* 17, 354–381.

McCombe Waller, S., Whitall, J., Jenkins, T., Magder, L. S., Hanley, D. F., Goldberg, A., et al. (2014). Sequencing bilateral and unilateral task-oriented training versus task oriented training alone to improve arm function in individuals with chronic stroke. *BMC Neurol.* 14:236. doi: 10.1186/s12883-014-0236-6

Morrison, R. A., Danaphongse, T. T., Pruitt, D. T., Adcock, K. S., Mathew, J. K., Abe, S. T., et al. (2020). A limited range of vagus nerve stimulation intensities produce motor cortex reorganization when delivered during training. *Behav. Brain Res.* 391:112705. doi: 10.1016/j.bbr.2020.112705

Morrison, R. A., Hulsey, D. R., Adcock, K. S., Rennaker, R. L., Kilgard, M. P., and Hays, S. A. (2019). Vagus nerve stimulation intensity influences motor cortex plasticity. *Brain Stimul.* 12, 256–262. doi: 10.1016/j.brs.2018.10.017

Nichols-Larsen, D. S., Clark, P. C., Zeringue, A., Greenspan, A., and Blanton, S. (2005). Factors influencing stroke survivors' quality of life during subacute recovery. *Stroke* 36, 1480–1484. doi: 10.1161/01.STR.0000170706.13595.4f

Pinti, P., Tachtsidis, I., Hamilton, A., Hirsch, J., Aichelburg, C., Gilbert, S., et al. (2020). The present and future use of functional near-infrared spectroscopy (fNIRS) for cognitive neuroscience. *Ann. N. Y. Acad. Sci.* 1464, 5–29. doi: 10.1111/nyas.13948

Powell, E. S., Westgate, P. M., Goldstein, L. B., and Sawaki, L. (2019). Absence of motor-evoked potentials does not predict poor recovery in patients with severe-moderate stroke: an exploratory analysis. *Arch. Rehabil. Res. Clin. Transl.* 1:100023. doi: 10.1016/j.arrct.2019.100023

Rech, K. D., Salazar, A. P., Marchese, R. R., Schifino, G., Cimolin, V., and Pagnussat, A. S. (2020). Fugl-Meyer assessment scores are related with kinematic measures in people with chronic hemiparesis after stroke. *J. Stroke Cerebrovasc. Dis.* 29:104463. doi: 10.1016/j.jstrokecerebrovasdis.2019.104463

Redgrave, J. N., Moore, L., Oyekunle, T., Ebrahim, M., Falidas, K., Snowdon, N., et al. (2018). Transcutaneous auricular Vagus nerve stimulation with concurrent upper limb repetitive task practice for Poststroke motor recovery: a pilot study. *J. Stroke Cerebrovasc. Dis.* 27, 1998–2005. doi: 10.1016/j.jstrokecerebrovasdis.2018.02.056

Rossi, S., Antal, A., Bestmann, S., Bikson, M., Brewer, C., Brockmöller, J., et al. (2021). Safety and recommendations for TMS use in healthy subjects and patient populations, with updates on training, ethical and regulatory issues: expert guidelines. *Clin. Neurophysiol.* 132, 269–306. doi: 10.1016/j.clinph.2020.10.003

Sasai, S., Homae, F., Watanabe, H., Sasaki, A. T., Tanabe, H. C., Sadato, N., et al. (2012). A NIRS-fMRI study of resting state network. *NeuroImage* 63, 179–193. doi: 10.1016/j.neuroimage.2012.06.011

Shaffer, F., and Ginsberg, J. P. (2017). An overview of heart rate variability metrics and norms. *Front. Public Health* 5:258. doi: 10.3389/fpubh.2017.00258

Shah, S., Vanclay, F., and Cooper, B. (1989). Improving the sensitivity of the Barthel index for stroke rehabilitation. *J. Clin. Epidemiol.* 42, 703–709. doi: 10.1016/0895-4356(89)90065-6

Singer, B., and Garcia-Vega, J. (2017). The Fugl-Meyer upper extremity scale. *J. Physiother.* 63:53. doi: 10.1016/j.jphys.2016.08.010

Tang, C., Ding, Z., Li, C., Chen, C., Ding, L., Zhang, X., et al. (2014). Effects of motor imagery combined with task-oriented training on the recovery of upper extremity

function after stroke: a randomized controlled trial. *Chin. J. Phys. Med. Rehabil.* 36, 832–837. doi: 10.3760/cma.j.issn.0254-1424.2014.011.004

Vucic, S., Stanley Chen, K.-H., Kiernan, M. C., Hallett, M., Benninger, D. H., Di Lazzaro, V., et al. (2023). Clinical diagnostic utility of transcranial magnetic stimulation in neurological disorders. Updated report of an IFCN committee. *Clin. Neurophysiol.* 150, 131–175. doi: 10.1016/j.clinph.2023.03.010

Wang, L., Gao, F., Dai, Y., Wang, Z., Liang, F., Wu, J., et al. (2023). Transcutaneous auricular vagus nerve stimulation on upper limb motor function with stroke: a functional near-infrared spectroscopy pilot study. *Front. Neurosci.* 17:1297887. doi: 10.3389/fnins.2023.1297887

Wang, Q., Zhang, D., Zhao, Y.-Y., Hai, H., and Ma, Y.-W. (2020). Effects of high-frequency repetitive transcranial magnetic stimulation over the contralesional motor cortex on motor recovery in severe hemiplegic stroke: a randomized clinical trial. *Brain Stimul.* 13, 979–986. doi: 10.1016/j.brs.2020.03.020

Waters, S., Wiestler, T., and Diedrichsen, J. (2017). Cooperation not competition: Bihemispheric tDCS and fMRI show role for ipsilateral hemisphere in motor learning. *J. Neurosci.* 37, 7500–7512. doi: 10.1523/JNEUROSCI.3414-16.2017

Wu, D., Ma, J., Zhang, L., Wang, S., Tan, B., and Jia, G. (2020). Effect and safety of transcutaneous auricular Vagus nerve stimulation on recovery of upper limb motor function in subacute ischemic stroke patients: a randomized pilot study. *Neural Plast.* 2020, 1–9. doi: 10.1155/2020/8841752

Xia, M., Wang, J., and He, Y. (2013). BrainNet viewer: a network visualization tool for human brain connectomics. *PLoS One* 8:e68910. doi: 10.1371/journal.pone.0068910

Yarossi, M., Patel, J., Qiu, Q., Massood, S., Fluet, G., Merians, A., et al. (2019). The association between reorganization of bilateral M1 topography and function in response to early intensive hand focused upper limb rehabilitation following stroke is dependent on Ipsilesional corticospinal tract integrity. *Front. Neurol.* 10:258. doi: 10.3389/fneur.2019.00258

Yoo, C., and Park, J. (2015). Impact of task-oriented training on hand function and activities of daily living after stroke. *J. Phys. Ther. Sci.* 27, 2529–2531. doi: 10.1589/jpts.27.2529

Zhang, J. J., Bai, Z., and Fong, K. N. K. (2022). Priming intermittent Theta burst stimulation for Hemiparetic upper limb after stroke: a randomized controlled trial. *Stroke* 53, 2171–2181. doi: 10.1161/STROKEAHA.121.037870

Zhang, H., Cao, X., Wang, L., Tong, Q., Sun, H., Gan, C., et al. (2023). Transcutaneous auricular vagus nerve stimulation improves gait and cortical activity in Parkinson's disease: a pilot randomized study. *CNS Neurosci. Ther.* 29, 3889–3900. doi: 10.1111/cns.14309

Zhao, J.-L., Chen, P.-M., Li, W.-F., Bian, R.-H., Ding, M.-H., Li, H., et al. (2019a). Translation and initial validation of the Chinese version of the action research arm test in people with stroke. *Biomed. Res. Int.* 2019, 5416560–5416569. doi: 10.1155/2019/5416560

Zhao, J.-L., Chen, P.-M., Zhang, T., Li, H., Lin, Q., Mao, Y.-R., et al. (2019b). Inter-rater and intra-rater reliability of the Chinese version of the action research arm test in people with stroke. *Front. Neurol.* 10:540. doi: 10.3389/fneur.2019.00540

Zhou, M., Wang, H., Zeng, X., Yin, P., Zhu, J., Chen, W., et al. (2019). Mortality, morbidity, and risk factors in China and its provinces, 1990-2017: a systematic analysis for the global burden of disease study 2017. *Lancet* 394, 1145–1158. doi: 10.1016/S0140-6736(19)30427-1

frontiers | Frontiers in Neuroscience

TYPE Original Research
PUBLISHED 15 March 2024
DOI 10.3389/fnins.2024.1349059

OPEN ACCESS

EDITED BY
Vitor Engracia Valenti,
São Paulo State University, Brazil

REVIEWED BY
Hantong Hu,
Third Affiliated Hospital of Zhejiang Chinese Medical University, China
Ma Tingting,
Hospital of Chengdu University of Traditional Chinese Medicine, China

*CORRESPONDENCE
Yingjun Zhang
zhangyingjun82@163.com
Tianshu Hou
houtianshu@cdutcm.edu.cn
Min Feng
fengminfengmin@sina.com

†These authors have contributed equally to this work and share first authorship

RECEIVED 04 December 2023
ACCEPTED 05 March 2024
PUBLISHED 15 March 2024

CITATION
Liu Z, Huang J, Yan D, Liang S, Zhao S, Zhang M, Li Z, Jiang C, Yin X, Zhang Y, Hou T and Feng M (2024) Effect of "needle sensation" and the real-time changes in autonomic nervous system activity during acupuncture analgesia.
Front. Neurosci. 18:1349059.
doi: 10.3389/fnins.2024.1349059

Effect of "needle sensation" and the real-time changes in autonomic nervous system activity during acupuncture analgesia

Zehua Liu[1†], Jinglei Huang[1†], Dingshang Yan[1†], Sha Liang[1], Shatong Zhao[2], Mengzhen Zhang[1], Zhongwen Li[1], Chuliang Jiang[1], Xiang Yin[1], Yingjun Zhang[3]*, Tianshu Hou[4]* and Min Feng[1]*

[1]School of Rehabilitation Medicine and Healthcare, Hunan University of Medicine, Huaihua, China, [2]Hunan Provincial Key Laboratory of Dong Medicine, Hunan University of Medicine, Huaihua, China, [3]School of Clinical Medicine, Hunan University of Medicine, Huaihua, China, [4]Department of Preventive Traditional Chinese Medicine, Chengdu Integrated TCM and Western Medical Hospital, Chengdu, China

Introduction: Acupuncture analgesia (AA) is widely used in clinical practice. The autonomic nervous system (ANS) may be an important pathway for acupuncture signal transduction. However, real-time changes in autonomic function during AA and the effect of "needle sensation" remain unclear.

Methods: We established a human pain model in healthy adults and randomly assigned 128 participants to the model, sham acupuncture, and acupuncture groups in a 1:1:2 ratio. Heart rate variability (HRV), including total power (TP), low-frequency power (LF), high-frequency power (HF), ratio of LF to HF (LF/HF), standard deviation of the normal-normal intervals (SDNN), and root mean square of successive interval differences (RMSSD), were used to assess autonomic function. The visual analog scale (VAS) and efficiency were used to assess the analgesic effect of acupuncture. The Massachusetts General Hospital acupuncture sensation scale (MASS) was used to indicate the intensity of the needle sensation. Anxiety levels were also measured. Finally, the correlation of MASS with HRV, VAS, and anxiety levels was analyzed.

Results: VAS decreased after 10 min of needling and 5 min after needle withdrawal in the acupuncture group compared with those in the model group ($p = 0.038$, $p = 0.020$). The efficacy rates were 82.0, 50.0, and 61.3% in the acupuncture, model, and sham groups, respectively. These represent significant differences between the acupuncture group and the model and sham acupuncture groups ($p < 0.001$ in each case). No differences were observed between the model and sham acupuncture groups. HF, TP, SDNN, and RMSSD were all increased in the acupuncture group compared with those in the model group ($p = 0.045$, $p = 0.041$, $p = 0.002$, $p = 0.006$, respectively). No differences were observed in the sham acupuncture group compared to the model group ($p = 0.632$, $p = 0.542$, $p = 0.093$, $p = 0.222$, respectively). The LF and LF/HF did not differ among all three groups. A positive correlation was observed between MASS and $RMSSD_2$, LF_2, $RMSSD_4$, TP_4, VAS_5, and anxiety levels.

Conclusion: AA was associated with enhanced vagal activity. The intensity of needle sensation was positively correlated with vagal and sympathetic nerve

activities. Acupuncture is an effective means of regulating autonomic function, and needle sensation may be an important modulator.

KEYWORDS

acupuncture analgesia, needle sensation, autonomic nervous system, heart rate variability, traditional Chinese medicine, vagal activity

1 Introduction

Acupuncture is an external treatment originating from traditional Chinese medicine (TCM), which is now used in more than 183 countries and regions worldwide (Fan et al., 2020). Acupuncture is effective for multisystem disorders and associated pain (He et al., 2020). Researchers have intensively studied the mechanism of acupuncture analgesia (AA) and found that it is related to the release of endogenous analgesic substances, increased local blood flow, and improved muscle movement synergy (Qiao et al., 2020). A growing body of research suggests that the autonomic nervous system (ANS) is involved in AA (Lin and Chen, 2008; Shi et al., 2023).

The ANS includes sympathetic, parasympathetic, and enteric branches. The vagus nerve is a cranial nerve and the main component of the parasympathetic nervous system. The sympathetic and parasympathetic nerves synergize and antagonize each other in the bidirectional regulation of autonomic functions. Studies have shown that autonomic dysfunction, characterized by decreased vagal activity and increased sympathetic activity, is present in the elderly in various chronic disorders, including pain (Forte et al., 2022). As the modulation of autonomic function may reduce the incidence of related diseases, the role of the ANS in disease and health is being increasingly emphasized (Dormal et al., 2021). A biostatistical study identified six important future research directions from current trends and hotspots in acupuncture research, including "the value of acupuncture in autonomic regulation" (Xiong et al., 2022). A recent meta-analysis showed that acupuncture can regulate the ANS mainly by decreasing sympathetic activity, elevating vagal tone, and regulating their balance; this has been observed when utilizing AA (Hamvas et al., 2023). However, the real-time changes in autonomic function during AA and the effect of "needle sensation," which is considered a key factor in the efficacy of acupuncture, remain unclear. Answering these questions is important for studying the autonomic regulatory mechanisms of AA and exploring the objective indicators of needle sensation.

Heart rate variability (HRV) is the number of temporal variations between cardiac cycles and can be obtained by quantitatively describing the beat-to-beat variation in the R-R intervals on electrocardiogram (ECG) recordings. Different indicators of HRV may reflect activities of the various ANS components. The combined measurement of high-frequency power (HF), root mean square of successive interval differences (RMSSD), and standard deviation of the normal-normal intervals (SDNN) reflect vagal activity. Low-frequency power (LF) reflects sympathetic activity. The ratio of LF to HF (LF/HF) reflects the balance between the two, and total power (TP) reflects the overall activity of the ANS. Due to the sensitivity, objectivity, and noninvasiveness of HRV, it has become the most commonly used index for assessing autonomic activity in clinical and scientific research (Forte et al., 2022). Studies have shown that HRV is closely related to changes in immediate biochemical indicators in blood serum during pain, providing a real-time objective indicator for AA and changes in autonomic activity during AA (Chen et al., 2016). Therefore, this study established a pain model in healthy people using HRV as an indicator to observe the real-time changes in autonomic activity during AA and the role played by "needle sensation" to explore the autonomic regulatory effects in AA and its influencing factors.

2 Materials and methods

2.1 Study design

This was a randomized, controlled, single-blind study. In our previous study on acupuncture analgesia (AA) at the Hegu point, the Visual Analog Scale (VAS) scores were 3.6, 5.1, and 5.6 in the acupuncture, sham acupuncture, and model groups, respectively. For the current study, we conducted a sample size calculation considering a two-tailed test, 90% power, and a significance level of 0.05, with a dropout rate of 10% and a ratio of model group to sham acupuncture group to acupuncture group of 1:1:2. This resulted in a total of 128 participants across the three groups. Participants in the current study were recruited from the Hunan University of Medicine and randomly divided into model (no treatment control), sham acupuncture (placebo control), and acupuncture groups at a ratio of 1:1:2 using SPSS software and sealed envelopes that were coded sequentially. The operators were acupuncturists who received a 10-day standardized training in modeling and acupuncture methods, electrocardiogram recording, and information collection, and passed the assessment successfully. The operators were unaware of the participants' enrollment until the envelopes were opened, and the intervention was administered to the participants in strict accordance with the requirements of each group. Participants were placed in a separate room with their right hand across a cloth curtain to prevent them from seeing the intervention their right hand received. The study design is depicted in Figure 1. The study was performed in accordance with the Declaration of Helsinki, and the protocol was approved by the Ethics Committee of Hunan University of Medicine (No. 2020 [H091401]). Clinical Trial Registration Number: ChiCTR2100046699.

Abbreviations: AA, Acupuncture analgesia; ANS, Autonomic nervous system; HRV, Heart rate variability; TP, Total power; LF, Low-frequency power; HF, High-frequency power; SDNN, Standard deviation of the normal-normal intervals; RMSSD, Root mean square of successive interval differences; MASS, Massachusetts General Hospital acupuncture sensation scale.

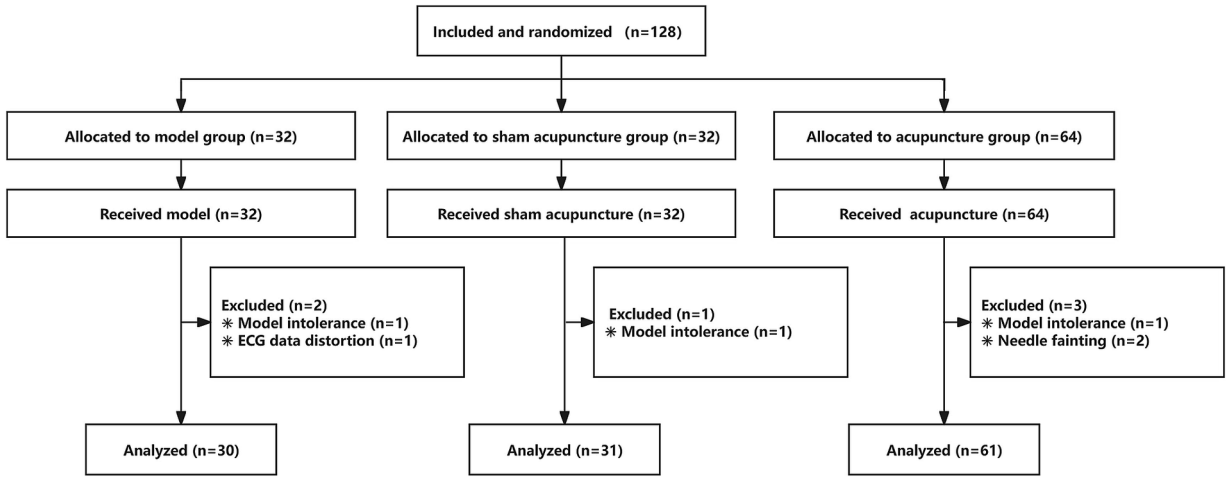

FIGURE 1
Study flow chart.

2.2 Participants

The inclusion criteria were: (1) adults aged 18–25; (2) no knowledge or prior experience of acupuncture; (3) no history of heart disease, hypertension, diabetes, neurological and/or mental health conditions, chronic pain, sensory disorders, or allergy to *Capsicum* fruit; (4) no record of treatment or medication for disease within the 2 weeks prior to the study; (5) non-smokers; and (6) voluntary participation in the study by providing signed informed consent.

The exclusion criteria were: (1) pregnant women, women preparing for pregnancy, and breastfeeding women; (2) individuals with a bleeding tendency; (3) individuals who frequently consume spicy food; (4) individuals with a history of needle-related fainting; (5) individuals suspected of having any disease; and (6) any other circumstances that could confound the results of the study. Individuals with incomplete records were automatically excluded.

2.3 Modeling method

An acute pain model was constructed by covering the participant's lower lip with a cotton patch (4 cm x 1 cm) impregnated with 0.5 mL of capsaicin (98.55%, Ruifensi, Chengdu, China) solution (0.1% solution configured with 30% alcohol) for 15 min (Fang et al., 2015).

2.4 Interventions

2.4.1 Acupoint localization

"Hegu" (LI4) is located at the midpoint of the radial side of the 2nd metacarpal bone on the dorsal aspect of the hand. The "non-acupoint" is located between the 2nd and 3rd metacarpal bones on the dorsum of the hand, the midpoint between Wailaogong (EX-UE8) and Yaotongdian (EX-UE7) (Zaslawski et al., 2003) (Figure 2).

2.4.2 Acupuncture methods

The participants were seated with their right hand exposed and extended into a cloth curtain to shield their vision. The application site was sterilized with 75% alcohol, and the intervention was carried out strictly according to the group intervention protocol by an administrator. Needling was not performed in the model group. In the sham acupuncture group, a tube needle (0.18 × 25 mm, 0.35 × 25 mm, Huatuo, Suzhou, China) was used to simulate needle insertion at a non-acupoint, touching the skin without breaking it. In the acupuncture group, the needle was inserted 0.5–0.8 inches into the Hegu point and left for 15 min. Reinforcement–reduction methods (uniform lifting and thrusting combined with twirling and rotating, 60 times/min) were performed for 30 s immediately, 4 min, 9 min, and 14 min after needle insertion (Figure 3).

2.5 Indicators

2.5.1 Indicators of analgesic effects

(1) Pain level: Paper-based VAS assessment (Delgado et al., 2018). The test uses a 10-point intensity rating scale, where the participant is asked to rate their pain between "0," indicating no pain, and "10," indicating excruciating pain. VAS values were recorded at time intervals of 1 (t1), 5 (t2), 10 (t3), and 15 min after needling (t4), and again at 5 min after needle withdrawal (t5).

(2) Effective rate: According to the pain characteristics of the capsaicin patch model, one of VAS_3, VAS_4, and $VAS_5 \geq VAS_1$ was selected as ineffective. Effective rate = (sample size - ineffective sample size)/sample size.

2.5.2 Indicators of heart rate variability (HRV)

Short-term 5-min recordings were recorded by ECG (Li C. T. et al., 2022). The night before the test, the participants were asked to get adequate sleep, avoid strenuous exercise, and consume no alcohol, tea, or coffee. Following a 10-min break, the participants were seated, and ECG data were collected with a micro-ECG recorder R211B (Healink, Bengbu, China) for 5 min before modeling, 0–5 min, 5–10 min, 10–15 min, and 15–20 min after modeling. Excessive activity was avoided during collection,

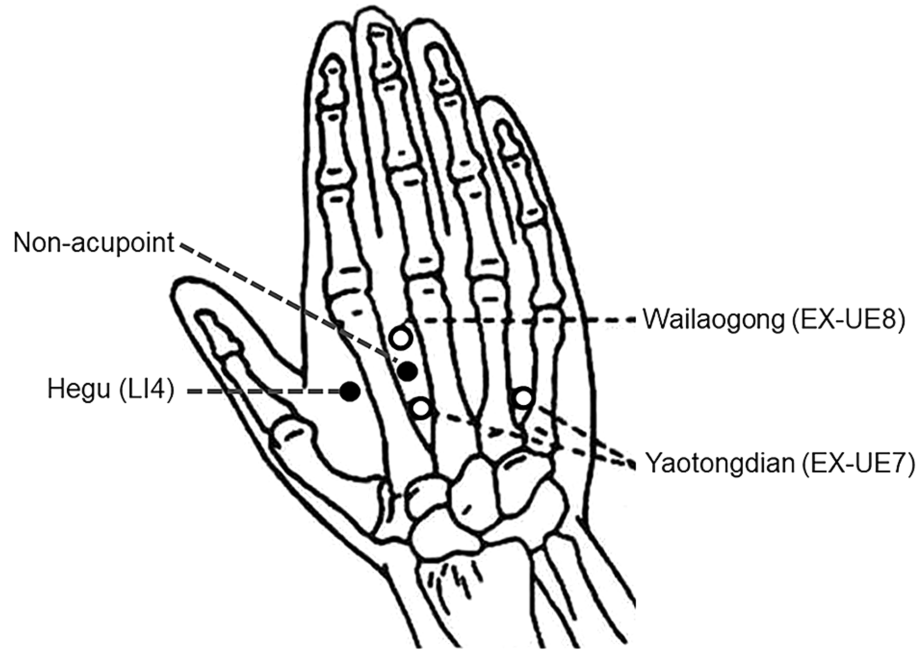

FIGURE 2
Anatomical localization of Hegu (LI4) and the "non-acupoint."

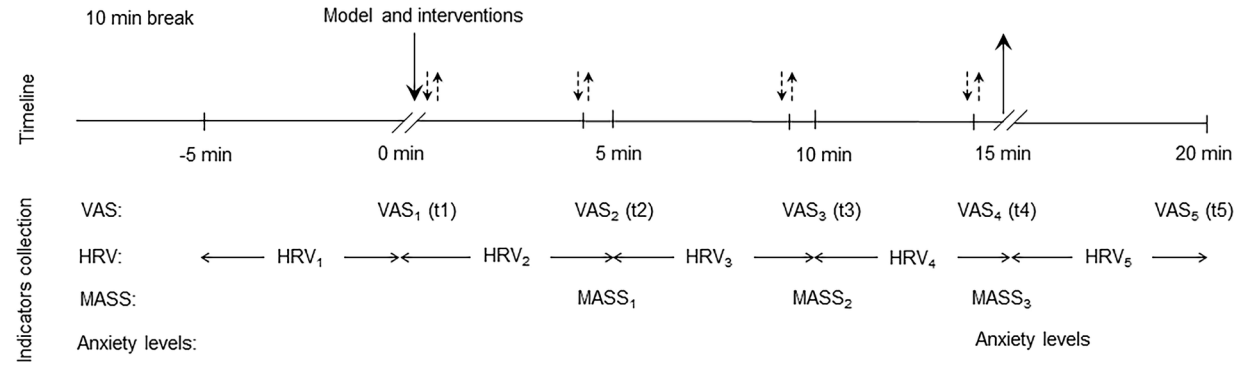

FIGURE 3
Timeline of the experimental procedure. ↓: Needle insertion; ↑: Needle withdrawal; ↓↑: Reinforcement–reduction methods.

and the environment was kept quiet and at room temperature (24 ± 1°C). TP, LF, HF, and LF/HF of the frequency domain analysis and SDNN and RMSSD of the time domain analysis were selected to assess overall HRV, vagal activity, sympathetic activity, and sympathetic-vagal balance (Wu et al., 2023). Parameter analyses were performed using the Kubios HRV version 3.1.0 software (Kubios Oy: Kuopio, Finland).

2.5.3 Indicators of sensory evaluation

At 5 min, 10 min, and the end of needling, the participants were asked whether they felt a needle sensation and its intensity, which was assessed using the Massachusetts General Hospital acupuncture sensation scale (MASS) (Li et al., 2017). The average of the three MASS scores was taken as the final intensity of the needle sensation. At the end of needling, the anxiety levels of the participants were measured using the same evaluation as the VAS (Kou et al., 2007).

2.6 Data processing

The data were entered independently by two research staff members. Statistical analyses were performed using IBM SPSS Statistics for Windows, version 23.0. An independent sample t-test was used for pre- and post-comparisons. The chi-square test and one-way analysis of variance (ANOVA) test were used for group comparisons. Repeated-measures ANOVA was used to analyze data from multiple measurements. Pearson's correlation was used for correlation analysis. A value of $p < 0.05$ was considered a statistically significant difference.

3 Results

3.1 Participants and baseline

There was no difference in age or sex between the groups (Table 1). The MASS curves and the average MASS score were significantly higher in the acupuncture group than in the sham acupuncture group, and the difference was statistically significant ($p < 0.001$, $p < 0.001$) (Figure 4).

TABLE 1 Basic characteristics of participants among groups.

	Model group ($N = 30$)	Sham acupuncture group ($N = 31$)	Acupuncture group ($N = 61$)	p
Sex				0.823
Female	22	22	41	
Male	8	9	20	
Age (year)	19.5 ± 0.7	19.5 ± 0.9	19.6 ± 0.8	0.744

Age is expressed as mean ± standard deviation.

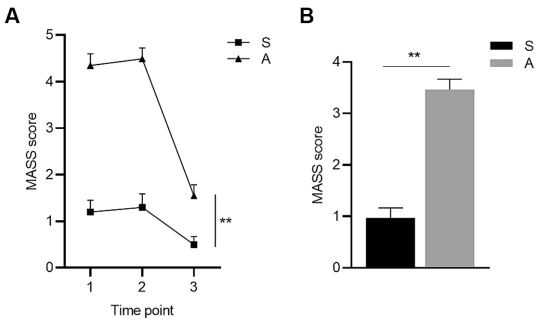

FIGURE 4
Comparison of MASS between groups. **(A)** shows the MASS curves of the sham acupuncture and the acupuncture group at three time points and **(B)** shows the comparison of average MASS scores between the two groups. * $p < 0.05$, ** $p < 0.01$. Groups: S, sham acupuncture group, $n = 31$; A, acupuncture group, $n = 61$. The error bars indicate the standard errors. Time points 1–3: 5 min (t1), 10 min (t2), and the end of needling (t3).

3.2 Analgesic effect

Compared with the baseline pain level (t1), the VAS score peaked after 5 min (t2) in the model group, and the difference was statistically significant ($p = 0.005$), while no differences were observed in the acupuncture and sham acupuncture groups ($p = 0.465$, $p = 0.500$) (Figure 5A).

Compared with that in the model group, the pain level decreased in the acupuncture group, and the difference in the VAS score was statistically significant at 10 min after needling (t3) ($p = 0.038$) and 5 min after needle withdrawal (t5) ($p = 0.020$). There were no significant differences in the sham acupuncture group ($p = 0.402$ and $p = 0.221$, respectively) (Figure 5A).

Comparing the total effective rate of each group, 82.0% in the acupuncture group was the highest, which was statistically significant compared with 50.0% in the model group ($p < 0.001$) and 61.3% in the sham acupuncture group ($p < 0.001$). No significant differences were observed between the model and sham acupuncture groups ($p = 0.370$) (Figure 5B).

3.3 Effect on heart rate variability (HRV)

3.3.1 Frequency domain indicators

Compared with that at baseline (t1), LF in the sham acupuncture group increased ($p = 0.030$) at the end of the intervention (t5) (Figure 6A), and HF in the acupuncture group increased ($p = 0.005$) from 0–5 min of the intervention (t2) (Figure 6B). During the same period, the LF/HF decreased in the model ($p = 0.001$), sham acupuncture ($p = 0.048$), and acupuncture groups ($p < 0.001$) (Figure 6D). No differences were observed in the frequency domain indicators for the remaining periods.

Compared with those in the model group, HF and TP levels increased in the acupuncture group, and the difference was statistically significant ($p = 0.045$, $p = 0.041$); no difference was observed in the sham acupuncture group ($p = 0.632$, $p = 0.542$) (Figures 6B,C). LF and LF/HF did not differ between the groups (model vs. sham, $p = 0.857$; model vs. acupuncture, $p = 0.077$; acupuncture vs. sham, $p = 0.113$) (Figures 6A,D).

3.3.2 Time domain indicators

Compared with that at baseline (t1), SDNN increased in the model, sham acupuncture, and acupuncture groups ($p = 0.018$, $p = 0.007$, $p = 0.007$) from 0–5 min of the intervention (t2) (Figure 6E), and remained elevated in the acupuncture group ($p = 0.034$) from 5–10 min of the intervention (t3). No significant differences were observed in the remaining time intervals.

Compared with those in the model group, SDNN and RMSSD increased in the acupuncture group, and the difference was statistically significant ($p = 0.002$, $p = 0.006$); no difference was observed in the sham acupuncture group (SDNN $p = 0.093$, RMSSD $p = 0.222$) (Figures 6E,F).

3.4 Correlation analysis

3.4.1 Massachusetts general hospital acupuncture sensation scale (MASS) and HRV

To understand the relationship between needle sensation and HRV, a correlation analysis bewteen average MASS scores and HRV indicators was performed in the acupuncture and sham acupuncture groups. The results revealed that the MASS was positively correlated with $RMSSD_2$, LF_2, $RMSSD_4$, and TP_4 (Table 2), and no correlation was observed with the other HRV indicators (data not shown).

3.4.2 MASS and visual analog scale (VAS)

To understand the relationship between needle sensation and acupuncture analgesia, a correlation analysis between average MASS score and VAS scores was performed in the acupuncture group. The results revealed that MASS was positively correlated with VAS_5 (Table 3), and no correlation was observed at other time points (data not shown).

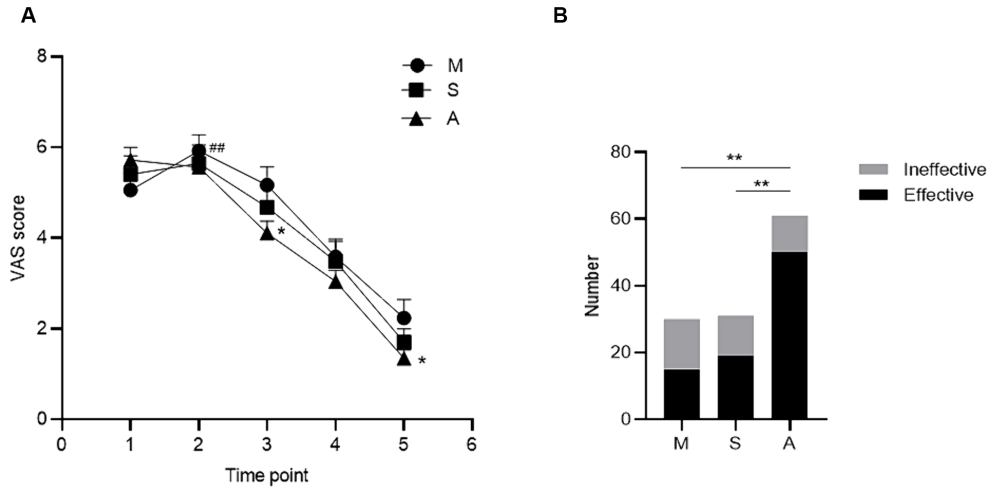

FIGURE 5
Comparison of analgesic effect among groups. **(A)** shows the VAS curves of the three groups at five time points, and **(B)** shows the comparison of the effective rates of the three groups. Compared with baseline, $^{\#}p < 0.05$, $^{\#\#}p < 0.01$; compared among groups, $^{*}p < 0.05$, $^{**}p < 0.01$. Groups: M, model group, $n = 30$; S, sham acupuncture group, $n = 31$; A, acupuncture group, $n = 61$. The error bars indicate the standard errors. VAS: visual analog scale. Time points 1–5: 1 (t1), 5 (t2), 10 (t3), and 15 min after needling (t4), and at 5 min after needle withdrawal (t5).

3.4.3 MASS and anxiety levels

There was no significant difference in anxiety levels between the acupuncture and sham acupuncture groups ($p = 0.926$, data not shown). To understand the effect of needle sensation intensity on anxiety during acupuncture, a correlation analysis between average MASS score and anxiety levels was performed in the acupuncture group, and the results showed that they were positively correlated (Table 4).

3.5 Adverse events

Each of the three groups experienced one case of excessive pain leading to intolerance, which was alleviated after halting the model and washing the affected skin. Two cases of mild fainting occurred in response to the needle in the acupuncture group, which were self-reported by the participants. It was attributed to excessive needle sensation and was resolved after stopping acupuncture and resting.

4 Discussions

This study found that AA was associated with increased vagal activity. The intensity of the "needle sensation" was positively correlated with vagal and sympathetic activity. A strong "needle sensation" may lead to higher levels of anxiety and weaken the sustained effects of AA.

In this study, a human pain model was prepared by applying capsaicin to the lower lip, which resulted in moderate-to-severe pain at 5 min and maintained mild-to-moderate pain for the next 15 min, indicating that the model was a success. Based on the pain location, we chose the Hegu (LI4) point, located on the back of the hand, as the needle acupoint. In Chinese medicine, the Hegu is connected to the face and mouth via the large intestine meridian, making it the preferred acupoint for treating facial and oral diseases (Qiao et al., 2020). From the VAS curves of the three groups, unlike the model and sham acupuncture groups, the acupuncture group experienced inhibition of the rising trend of pain and reduced pain at two subsequent time points. The efficiency in the acupuncture group was significantly higher than that in the other two groups, whereas there was no difference between the sham acupuncture and model groups. These results confirm the immediate analgesic effect of acupuncture, which is consistent with the results of several previous studies (Qiao et al., 2020; Liu et al., 2022).

We observed that HF, RMSSD, and SDNN, which reflected vagal activity, and TP, which reflected overall ANS activity, were elevated in the acupuncture group compared with those in the model group, and appeared concurrently with the analgesic effect within 5 min after acupuncture. There was no difference in the sham acupuncture group, nor was there any difference in LF, which reflected sympathetic activity. This suggests that AA is associated with increased vagal activity, which causes an increase in overall autonomic activity. Similar autonomic modulatory effects have been observed in clinical trials of acupuncture for migraine and lower back pain (Li Y. W. et al., 2022) and are consistent with the results of a recent meta-analysis (Hamvas et al., 2023). Auricular vagus nerve stimulation is an effective therapy for both chronic and acute pain (Likar et al., 2023). Studies have demonstrated that auricular acupuncture can also increase HRV and vagal activity during pain relief (Butt et al., 2020). These results suggest that the ANS is one of the targets of AA and that increasing vagal activity may be one of the mechanisms. A functional link exists between somatosensation and the ANS, and the activation of cutaneous sensory fibers can modulate disease conditions by affecting the autonomic nerves (Ma, 2020). In anti-inflammatory acupuncture studies, it was found that the dense neural distribution of myelinated Prokr2Cre fibers in the limbs may underlie the neural basis for the remote effects of limb acupoint stimulation in activating sympathetic and/or parasympathetic pathways (Ma, 2022). This study also provides insight into the autonomic regulatory basis of AA.

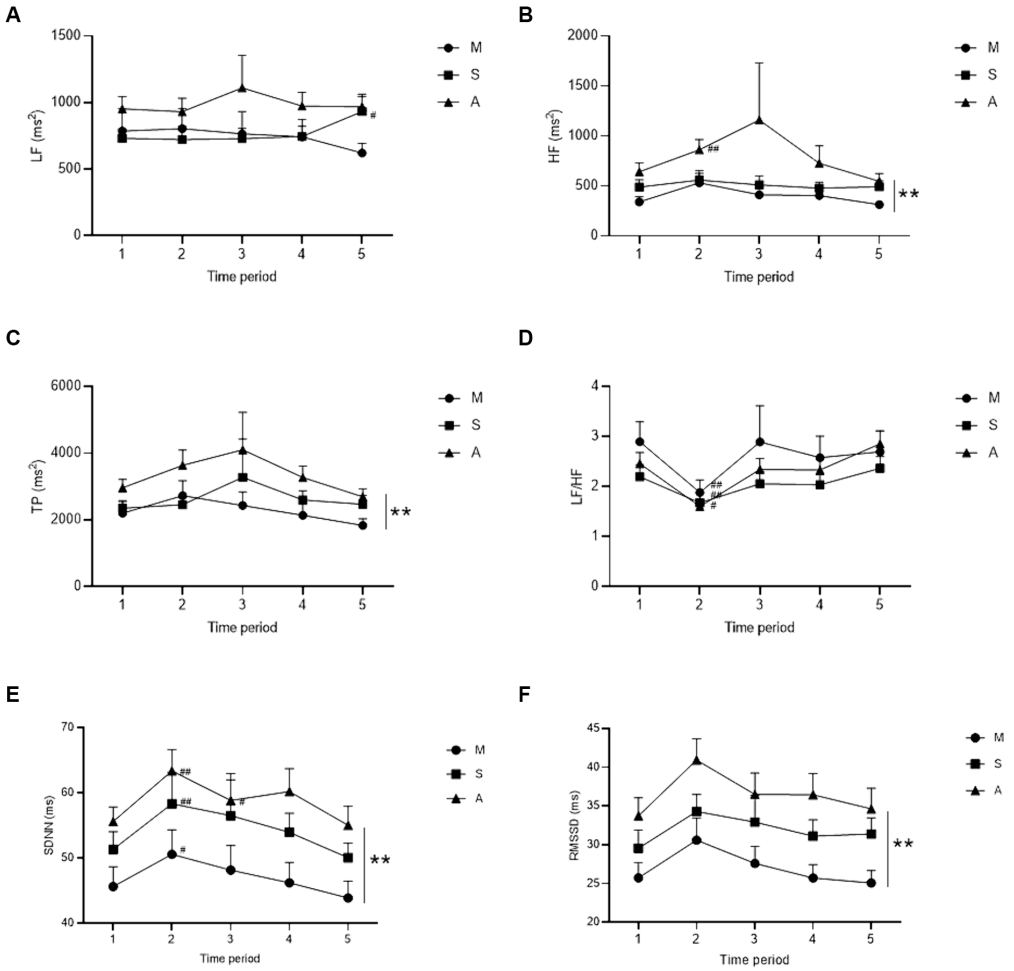

FIGURE 6
Comparison of HRV indicators for each group. **(A–D)** show the frequency domain indicators of LF, HF, TP, and LF/HF curves for the three groups at five time periods, respectively. **(E,F)** show the time domain indicators of SDNN and RMSSD curves for the three groups at five time periods, respectively. Compared with baseline, $^{\#}p < 0.05$, $^{\#\#}p < 0.01$; compared among groups, $^{*}p < 0.05$, $^{**}p < 0.01$. Groups: M, model group, $n = 30$; S, sham acupuncture group, $n = 31$; A, acupuncture group, $n = 61$. The error bars indicate the standard errors. LF: low-frequency power, HF: high-frequency power, TP: total power, and LF/HF: ratio of LF to HF. SDNN: standard deviation of the normal-normal intervals, RMSSD: root mean square of successive interval differences. Time periods 1–5: 5 min before modeling (t1), 0–5 min (t2), 5–10 min (t3), 10–15 min (t4), and 15–20 min after modeling (t5).

TABLE 2 Significant correlations between MASS and HRV indicators.

		$RMSSD_2$	LF_2	$RMSSD_4$	TP_4
MASS	Pearson Correlation	0.229	0.207	0.227	0.217
	Sig.(2-tailed)	0.028	0.047	0.029	0.038
	N	92	92	92	92

RMSSD, root mean square of successive interval differences; LF, low-frequency power; TP, total power; MASS, Massachusetts General Hospital acupuncture sensation scale.

TABLE 3 Significant correlations between MASS and VAS.

		VAS_5
MASS	Pearson Correlation	0.342
	Sig.(2-tailed)	0.007
	N	61

VAS, visual analog scale; MASS, Massachusetts General Hospital acupuncture sensation scale.

TABLE 4 Correlation between MASS and anxiety levels.

		Anxiety levels
MASS	Pearson Correlation	0.433
	Sig.(2-tailed)	0.000
	N	61

MASS, Massachusetts General Hospital acupuncture sensation scale.

Functional connectivity in the brain is altered after acute pain stimulation. Neuroimaging studies have found that acupuncture enhances the post-stimulation spatial extent of the resting brain networks, including the hypothalamus (Lin and Chen, 2008), anterior cingulate cortex, periaqueductal grey matter, amygdala, hippocampus, middle temporal gyrus, and other brain regions that are resistant to nociception, memory, and emotion (Hauck et al., 2017). In addition, several minutes after the needle was removed, the connections formed by the default mode network with the hippocampus were enhanced by the acupuncture-induced sympathetic-to-parasympathetic transfer

(Dhond et al., 2008), which may explain the continuous analgesic effect after needle withdrawal. Simultaneously, systems involved in autonomic control are strictly correlated with those involved in pain perception (Forte et al., 2022). These results confirm the role of the ANS in AA at the central level, and there may also be interactions between brain regions that allow for the integrated modulation of pain in the emotional and cognitive dimensions.

According to TCM and modern neurobiological theories, the intensity of acupuncture is an important factor influencing its effects (Ma, 2022). According to the TCM theory, needle sensation, also known as De Qi, is the sensation of soreness, numbness, heaviness, and distension experienced by participants during acupuncture, which can be transmitted through meridians and is considered the key to acupuncture efficacy. We found that needle sensation intensity was positively correlated with vagal, sympathetic, and overall autonomic activities, with the effects on vagal activity being stronger and lasting longer. Thicker myelin is associated with faster impulses, and electrophysiological recordings revealed that vagal reflexes can be driven by the activation of thinly myelinated Aδ fibers and can be further enhanced by activation of unmyelinated C fibers, whereas sympathetic reflexes may require C fiber activation (Ma, 2022). This may explain why the effects of needle sensation on the vagus nerve are more pronounced and long-lasting and why the pain score 5 min after needle withdrawal is positively correlated with needle sensation. Moderate needle sensation activates the vagus nerve to produce analgesia, whereas excessive needle sensation may activate sympathetic nerves, thereby antagonizing vagal activity and weakening the continuous effects of AA. Simultaneously, a strong needle sensation triggers higher anxiety levels, further activating sympathetic nerves (Lambert et al., 2010) and interfering with AA. Combined with the causes of needle-related fainting, this suggests that a stronger needle sensation is not better for patients during AA (Lee et al., 2014). Acupuncture is an integrative therapy that encompasses both physiological and psychological modulation. Choosing the appropriate intensity of acupuncture to achieve the best clinical outcome is worth considering. Whether HRV is an objective indicator of needle sensation requires further investigation.

Some studies have reported results contradictory to ours. One study concluded that AA was not associated with HRV (De Kooning et al., 2015). Another study found that acupuncture reduced sympathetic tone and improved vagal tone in fatigued states but not in non-fatigued states (Xiong et al., 2022). There are individual variations in HRV, and the autonomic function of an organism is related to many factors, such as age, sex, smoking, alcohol consumption, body position, respiration, and even level of education (Strüven et al., 2021), which may lead to different conclusions. The fact that acupuncture works only under pathological conditions may also be a factor (Lee et al., 2010).

This study has some limitations. First, the distribution of needle sensations was relatively concentrated; therefore, stratified analyses based on needle sensation intensity were not performed. More intuitive conclusions can be drawn by comparing the effects of different needle sensation intensities on HRV. Second, this study observed acute pain and did not examine chronic pain, which has a different mechanism and is more common in clinical settings.

In conclusion, AA was associated with enhanced vagal activity, the intensity of needle sensation was positively correlated with vagal and sympathetic activities, and excessive needle sensation may weaken the analgesic effects of acupuncture. Acupuncture is an effective means of regulating autonomic function, and needle sensation may be an important modulator, which provides a basis for an in-depth discussion of the autonomic mechanism of acupuncture. Therefore, how acupuncture can be used to treat autonomic dysfunction deserves further study.

Data availability statement

The raw data supporting the conclusions of this article will be made available by the authors, without undue reservation.

Ethics statement

The studies involving humans were approved by the Ethics Committee of Hunan University of Medicine. The studies were conducted in accordance with the local legislation and institutional requirements. The participants provided their written informed consent to participate in this study.

Author contributions

ZeL: Writing – original draft, Investigation. JH: Writing – original draft, Investigation. DY: Writing – original draft, Investigation. SL: Writing – original draft, Investigation. SZ: Writing – original draft, Data curation, Investigation. MZ: Writing – original draft, Data curation, Investigation. ZhL: Writing – original draft, Investigation. CJ: Writing – original draft, Funding acquisition, Investigation. XY: Writing – original draft, Investigation. YZ: Writing – review & editing, Formal Analysis, Methodology. TH: Writing – review & editing, Visualization, Formal Analysis, Methodology. MF: Funding acquisition, Writing – review & editing, Project administration, Conceptualization, Methodology.

Funding

The author(s) declare financial support was received for the research, authorship, and/or publication of this article. This work was supported by the National College Students' Innovation and Entrepreneurship Training Program of China (202212214005) and the Scientific Research Fund of Hunan Provincial Education Department (20B419 and HNJG-2022-1317).

Acknowledgments

We thank Professor Bo Shi for his help with the HRV data analysis. We thank Dr. Haoqing Shao for her help with the plotting.

Conflict of interest

The authors declare that the research was conducted in the absence of any commercial or financial relationships that could be construed as a potential conflict of interest.

Publisher's note

References

Butt, M. F., Albusoda, A., Farmer, A. D., and Aziz, Q. (2020). The anatomical basis for transcutaneous auricular vagus nerve stimulation. *J. Anat.* 236, 588–611. doi: 10.1111/joa.13122

Chen, Z., Zhao, Y., Wang, X., Xiang, Y., and Zhao, L. (2016). Recent research situation of heart rate variability-based analysis of the regulating effect of acupuncture on autonomic nervous function. *Shanghai J. Acupunct. Moxibustion* 35, 754–757. doi: 10.13460/j.issn.1005-0957.2016.06.0754

De Kooning, M., Tobbackx, Y., Meeus, M., Wauters, L., Ickmans, K., De Vilder, P., et al. (2015). Acupuncture-analgesia following a single treatment session in chronic whiplash is unrelated to autonomic nervous system changes: a randomized cross-over trial. *Pain Physician* 18, 527–536.

Delgado, D. A., Lambert, B. S., Boutris, N., McCulloch, P. C., Robbins, A. B., Moreno, M. R., et al. (2018). Validation of digital visual analog scale pain scoring with a traditional paper-based visual analog scale in adults. *J. Am. Acad. Orthop. Surg. Glob. Res. Rev.* 2:e088. doi: 10.5435/JAAOSGlobal-D-17-00088

Dhond, R. P., Yeh, C., Park, K., Kettner, N., and Napadow, V. (2008). Acupuncture modulates resting state connectivity in default and sensorimotor brain networks. *Pain* 136, 407–418. doi: 10.1016/j.pain.2008.01.011

Dormal, V., Vermeulen, N., and Mejias, S. (2021). Is heart rate variability biofeedback useful in children and adolescents? A systematic review. *J. Child Psychol. Psychiatry* 62, 1379–1390. doi: 10.1111/jcpp.13463

Fan, A. Y., Wei, H., Tian, H., Huang, J., and Alemi, S. F. (2020). Universities of Chinese medicine enter the global stage of best universities rankings in 2020. *Med. Acupunct.* 32, 136–142. doi: 10.1089/acu.2019.1403

Fang, Z., Jian, Z., and Dai, S. (2015). Capsaicin stimulation on autonomic nervous system in human by heart rate variability analysis. *Chin. J. Surg. Integr. Trad. West. Med.* 21, 363–365. doi: 10.3969/j.issn.1007-6948.2015.04.008

Forte, G., Troisi, G., Pazzaglia, M., Pascalis, V., and Casagrande, M. (2022). Heart rate variability and pain: a systematic review. *Brain Sci.* 12:153. doi: 10.3390/brainsci12020153

Hamvas, S., Hegyi, P., Kiss, S., Lohner, S., McQueen, D., and Havasi, M. (2023). Acupuncture increases parasympathetic tone, modulating HRV-systematic review and meta-analysis. *Complement. Ther. Med.* 72:8. doi: 10.1016/j.ctim.2022.102905

Hauck, M., Schröder, S., Meyer-Hamme, G., Lorenz, J., Friedrichs, S., Nolte, G., et al. (2017). Acupuncture analgesia involves modulation of pain-induced gamma oscillations and cortical network connectivity. *Sci. Rep.* 7:16307. doi: 10.1038/s41598-017-13633-4

He, Y., Guo, X., May, B. H., Zhang, A. L., Liu, Y., Lu, C., et al. (2020). Clinical evidence for association of acupuncture and acupressure with improved cancer pain: a systematic review and Meta-analysis. *JAMA Oncol.* 6, 271–278. doi: 10.1001/jamaoncol.2019.5233

Kou, W., Gareus, I., Bell, J. D., Goebel, M. U., Spahn, G., Pacheco-López, G., et al. (2007). Quantification of DeQi sensation by visual analog scales in healthy humans after immunostimulating acupuncture treatment. *Am. J. Chin. Med.* 35, 753–765. doi: 10.1142/S0192415X07005247

Lambert, E., Dawood, T., Straznicky, N., Sari, C., Schlaich, M., Esler, M., et al. (2010). Association between the sympathetic firing pattern and anxiety level in patients with the metabolic syndrome and elevated blood pressure. *J. Hypertens.* 28, 543–550. doi: 10.1097/HJH.0b013e3283350ea4

Lee, S., Lee, M. S., Choi, J. Y., Lee, S. W., Jeong, S. Y., and Ernst, E. (2010). Acupuncture and heart rate variability: a systematic review. *Auton. Neurosci.* 155, 5–13. doi: 10.1016/j.autneu.2010.02.003

Lee, J., Napadow, V., and Park, K. (2014). Pain and sensory detection threshold response to acupuncture is modulated by coping strategy and acupuncture sensation. *BMC Complement. Altern. Med.* 14:324. doi: 10.1186/1472-6882-14-324

Li, Y. W., Li, W., Wang, S. T., Gong, Y. N., Dou, B. M., Lyu, Z. X., et al. (2022). The autonomic nervous system: a potential link to the efficacy of acupuncture. *Front. Neurosci.* 16:1038945. doi: 10.3389/fnins.2022.1038945

Li, G., Wu, S., Zhao, H., Guan, W., Zhou, Y., and Shi, B. (2022). Non-invasive prognostic biomarker of lung cancer patients with brain metastases: recurrence quantification analysis of heart rate variability. *Front. Physiol.* 13:987835. doi: 10.3389/fphys.2022.987835

Li, M., Yuan, H., Wang, P., Xin, S., Hao, J., Liu, M., et al. (2017). Influences of De qi induced by acupuncture on immediate and accumulated analgesic effects in patients with knee osteoarthritis: study protocol for a randomized controlled trial. *Trials* 18:251. doi: 10.1186/s13063-017-1975-7

Likar, R., Perruchoud, C., Kampusch, S., Köstenberger, M., Sator, S., Stremnitzer, C., et al. (2023). Klinische Wirksamkeit der aurikulären Vagusnervstimulation in der Behandlung chronischer und akuter Schmerzen: Eine systematische Übersichtsarbeit ['clinical efficacy of auricular vagus nerve stimulation in the treatment of chronic and acute pain: a systematic review']. *Schmerz.* 1–12. doi: 10.1007/s00482-022-00686-2

Lin, J. G., and Chen, W. L. (2008). Acupuncture analgesia: a review of its mechanisms of actions. *Am. J. Chin. Med.* 36, 635–645. doi: 10.1142/S0192415X08006107

Liu, C. T., Hsieh, T. M., Wu, B. Y., Huang, Y. C., Shih, C. H., Hu, W. L., et al. (2022). Acupuncture analgesia in patients with traumatic rib fractures: a randomized-controlled trial. *Front. Med.* 9:896692. doi: 10.3389/fmed.2022.896692

Ma, Q. (2020). Somato–autonomic reflexes of acupuncture. *Med. Acupunct.* 32, 362–366. doi: 10.1089/acu.2020.1488

Ma, Q. (2022). Somatotopic organization of autonomic reflexes by acupuncture. *Curr. Opin. Neurobiol.* 76:102602. doi: 10.1016/j.conb.2022.102602

Qiao, L., Guo, M., Qian, J., Xu, B., Gu, C., and Yang, Y. (2020). Research advances on acupuncture analgesia. *Am. J. Chin. Med.* 48, 245–258. doi: 10.1142/s0192415x20500135

Shi, J., Cao, W., Zhang, X., Wan, H., Su, Y., Qu, Z., et al. (2023). Local analgesia of electroacupuncture is mediated by the recruitment of neutrophils and released β-endorphins. *Pain* 164, 1965–1975. doi: 10.1097/j.pain.0000000000002892

Strüven, A., Holzapfel, C., Stremmel, C., and Brunner, S. (2021). Obesity, nutrition and heart rate variability. *Int. J. Mol. Sci.* 22:4215. doi: 10.3390/ijms22084215

Wu, S., Li, G., Chen, M., Zhang, S., Zhou, Y., Shi, B., et al. (2023). Association of heartbeat complexity with survival in advanced non-small cell lung cancer patients. *Front. Neurosci.* 17:1113225. doi: 10.3389/fnins.2023.1113225

Xiong, J., Wang, Z., Ruan, M., Yao, H., Wei, M., Sun, R., et al. (2022). Current status of neuroimaging research on the effects of acupuncture: a bibliometric and visual analyses. *Ther. Med.* 71:102877. doi: 10.1016/j.ctim.2022.102877

Zaslawski, C. J., Cobbin, D., Lidums, E., and Petocz, P. (2003). The impact of site specificity and needle manipulation on changes to pain pressure threshold following manual acupuncture: a controlled study. *Complement. Ther. Med.* 11, 11–21. doi: 10.1016/s0965-2299(02)00116-4

Frontiers in Neuroscience

Provides a holistic understanding of brain function from genes to behavior

Part of the most cited neuroscience journal series which explores the brain - from the new eras of causation and anatomical neurosciences to neuroeconomics and neuroenergetics.

Discover the latest Research Topics

See more →

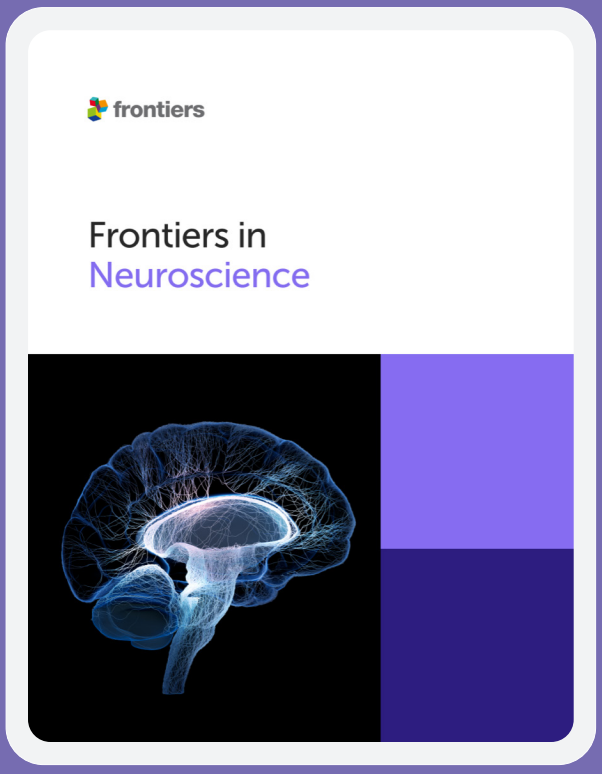

Frontiers

Avenue du Tribunal-Fédéral 34
1005 Lausanne, Switzerland
frontiersin.org

Contact us

+41 (0)21 510 17 00
frontiersin.org/about/contact